The Molecular Deconstruction of the MicroRNA160 *Auxin Response Factor 10/16/17* Expression Module in *Arabidopsis thaliana*

Kim Zimmerman

BSc (Hons.) (Newcastle)

Thesis submitted for the degree of Doctor of Philosophy
in
Biological Science
School of Environmental and Life Sciences
The University of Newcastle
New South Wales, Australia
February, 2019

This research was supported by an Australian Government
Research Training Program (RTP) Scholarship

Declaration

STATEMENT OF ORIGINALITY

I hereby certify that the work embodied in the thesis is my own work, conducted under normal supervision. The thesis contains no material which has been accepted, or is being examined, for the award of any other degree or diploma in any university or other tertiary institution and, to the best of my knowledge and belief, contains no material previously published or written by another person, except where due reference has been made. I give consent to the final version of my thesis being made available worldwide when deposited in the University's Digital Repository, subject to the provisions of the Copyright Act 1968 and any approved embargo.

Kim Zimmerman

Contents

List of figures

List of tables

Acknowledgments

To my supervisors Dr. Andy Eamens, Ass/Prof. David Collings, and Dr. Ming-bo Wang I can't express my gratitude enough. Andy as my principal supervisor, your guidance, expertise, and above all patience has meant a lot to me, I can't imagine how this process would have gone without you. David and Ming-bo as my co-supervisors, your insight at critical stages of this undertaking has helped me in so many ways. I would also like to thank the other members of the Centre for Plant Science at the University of Newcastle, Chris Grof, David McCurdy, Tina Offler, John Patrick, and Yong-ling Ruan. Your insight has been a great asset to tap into when I work presented my work, and your interest in my studies has been wholeheartedly appreciated.

To the postgraduate student cohort that has been studying alongside me, you also have my thanks. From within the Eamens' lab group, Joey Pegler and Jackson Oultram have been great lab buddies, and always a great source of assistance and support when I needed a sounding board for my ideas. Those that I have shared an office with, Jun Li and Quan Nguyen, I will miss our discussions on plant science, as well as what any particular Australian phrase means, the sushi lunches were the best times. Those outside of the Eamens' lab group, Chris Brown, Lachlan Campbell, and Evan Gibbs, your friendship has meant a great deal to me and has always provided an outlet if things got tough or if rest and relaxation was needed. Your patience dealing with my plant science ramblings will not be forgotten.

To our glasshouse technical officer Joe Enright, I have always valued your knowledge and skills in plant care. I will forever be glad that we have become close and firm friends over the years, and that we could always have a chat and solve the problems of the world in that potting shed.

To my undergraduate mates, Shawn Bourke, Mitch McDonald, Tait Nielsen, and Ben Wilson, you too share in my gratitude, for that is where we all became excited and passionate about undertaking PhDs in our career futures.

And last, but certainly not least, to my family. My mum and dad have always been the strongest supporters of whatever I have undertaken. To have you both as such proud parents has helped me to strive for better things. I could not have done this without your love.

Abstract

Small RNAs (sRNAs) form a class of regulatory molecule that is central to the control of gene expression at both the transcriptional and posttranscriptional level. In plants, sRNAs have evolved to form a number of different sRNA species, including the microRNA (miRNAs), *trans*-acting small-interfering RNA (tasiRNA), natural antisense transcript siRNA (natsiRNA) and repeat-associated siRNA (rasiRNA) species. The production of each sRNA species is mediated by a DICER-LIKE (DCL) endonuclease, acting with or without the assistance of a DOUBLE-STRANDED RNA BINDING (DRB) protein via the processing of structurally distinct, double-stranded RNA (dsRNA) precursor molecules.

In addition to sRNAs, plants also rely on hormonal signalling to control gene expression. Plant hormones fall into a diverse range of classes including the auxins, abscisic acid, brassinosteroid, cytokinins, ethylene, gibberellic acids, jasmonic acid, salicylic acid, and strigolactones. Of these, auxin is a crucial phytohormone that regulates diverse aspects of growth and development. Auxin can elicit molecular responses via multiple pathways. One example of this action is whereby auxin frees AUXIN RESPONSE FACTOR (ARF) transcription factors from their posttranslational inhibition by AUXIN/INDOLE-3-ACETIC ACID (Aux/IAA) proteins. Auxin-directed release allows the ARF to function as a classic transcription factor to either promote or repress *AUXIN RESPONSE GENE* (*ARG*) expression.

Considering that both sRNAs and auxin are demonstrated molecular regulators, it is not a surprise that, on occasion, both regulate the same developmental or adaptive response in plants. Furthermore, sRNA-directed regulation of the protein machinery central to the auxin pathway is well documented, including the miR160/*ARF10*/*ARF16*/*ARF17* and miR167/*ARF6*/*ARF8* expression modules.

To further assess sRNA-directed regulation of the auxin response pathway, a single expression module was selected for detailed molecular analysis. Initial molecular examination of the miR160/*ARF10*/*ARF16*/*ARF17* expression module in wild-type *Arabidopsis thaliana* roots, and in the knockout mutant lines, *drb1* and *drb2*, defective in DRB1 and DRB2 activity, respectively, indicated that both DRB proteins are central to the regulation of this expression module. Both DRB1 and DRB2 influence the production of the miR160 sRNA, and following miR160 production, DRB1 and DRB2 aid in the regulation of the abundance of the miR160 target transcripts, *ARF10*, *ARF16*, and *ARF17*.

Following the demonstration of the requirement for DRB1 and DRB2 for homeostatic maintenance of the miR160/*ARF10*/*ARF16*/*ARF17* expression module in *Arabidopsis* root tissues, the phenotypic and molecular consequence of synthetic auxin, (2,4-dichlorophenoxyacetic acid (2,4-D)) treatment of wild-type *Arabidopsis* plants and the *drb1*, *drb2*, and *drb12* mutants were assessed. This analysis revealed that exogenous auxin treatment had a significant impact on root architectural development in all four plant lines, with the promotion of lateral and adventitious root development. Further, at the molecular level, this experiment provided evidence that both DRB1 and DRB2 are required for mediating miR160 production, and subsequently for regulating *ARF10*, *ARF16*, and *ARF17* transcript abundance as part of the molecular response of *Arabidopsis* to exogenous auxin treatment.

To further characterise the regulatory requirement of DRB1 and DRB2 for maintenance of the miR160/*ARF10*/*ARF16*/*ARF17* expression module, miR160 resistant versions of *ARF10* and *ARF16*, under the control of their native promoters, were introduced into wild-type *Arabidopsis* plants, and the *drb1* and *drb2* mutant backgrounds. In addition, miR160 overexpression lines were also generated in these plants, via the introduction of the *MIR160B* overexpression transgene. Taken together, the phenotypic and molecular analyses stemming from this experiment revealed that in the absence of DRB1 activity, DRB2 can readily direct miR160 production in root tissues and, further, that miR160-directed regulation of *ARF10* and *ARF16* expression appeared to be predominantly mediated via a translational repression mechanism of RNA silencing in *drb1* roots. Specifically, miR160-directed translational repression of *ARF10* appeared to largely control the promotion of lateral and adventitious root growth and development.

In summary, the experimental component of this research thesis demonstrated that both DRB1 and DRB2 are required for miR160 production, and to subsequently control miR160-directed expression regulation of *ARF10*, *ARF16*, and *ARF17* target gene expression. Moreover, in addition to the well documented mRNA cleavage mechanism of *ARF10*, *ARF16*, and *ARF17* expression regulation directed by the miR160 sRNA, the findings presented here provide strong evidence that miR160-directed translational repression forms an additional layer of posttranscriptional regulatory complexity to control miR160 target gene abundance in *Arabidopsis* root tissues. This thesis has also identified a possible role for ARF16, in addition to that previously documented for ARF17, in promoting adventitious root growth and development in *Arabidopsis*.

Common abbreviations

Abbrev.	Term
2,4-D	2,4-dichlorophenoxyacetic acid
AD	activator domain
Arabidopsis	*Arabidopsis thaliana*
ARE	auxin response element
CaMV	cauliflower mosaic virus
CIAP	calf intestinal alkaline phosphatase
CTD	C-terminal dimerization domain
DBD	DNA-binding domain
DR5pro	*DR5* gene promoter
dsRBM	dsRNA binding motif
dsRNA	double-stranded RNA
eTM	endogenous target mimic
GFP	green flourescent protein
GSA	gravitropic setpoint angle
GUS	β-glucuronidase
hcsiRNA	heterochromatin siRNA
IAA	indole-3-acetic acid
mARF	micro-resistant ARF
MCS	Multiple cloning site
miRNA	microRNA
MQ-H_2O	MilliQ water
natsiRNA	natural antisense transcript siRNA
nt	nucleotide
OH	hydroxyl
p4-siRNA	PolIV generated class of siRNA
phasiRNA	phased secondary siRNA
Pi	inorganic phosphate
PolII	RNA polymerase II
PolIV	RNA polymerase IV
pre-miRNA	precursor miRNA
pri-miRNA	primary miRNA
QC	quiescent centre
RAM	root apical meristem
SAM	shoot apical meristem
siRNA	small interfering RNA
sRNA	small RNA
STL-qPCR	stem-loop RT-qPCR
tasiRNA	*trans*-acting siRNA
U	uracil
UTR	untranslated region

List of gene names

Abbreviation	Full gene name
ABP1	AUXIN BINDING PROTEIN1
AFB	AUXIN F-BOX
AGO	ARGONAUTE
ARF	AUXIN RESPONSE FACTOR
ARG	AUXIN RESPONSE GENE
ASK	ARABIDOPSIS SKIP LIKE
Aux/IAA	AUXIN/INDOLE-3-ACETIC ACID
AUX1	AUXIN INFLUX PROTEIN1
AXR	AUXIN RESISTANT
BIG	DARK OVEREXPRESSION OF CAB
Class III HD ZIP	Class III HD ZIP
CLE	CLAVATA3/ESR-related
CLV	CLAVATA
CRN	CORYNE
CUL1	CULLIN1
DCL	DICER-LIKE
DRB	dsRNA BINDING
EF1-α	ELONGATION FACTOR1-α
HAM	HAIRY MERISTEM
HEN1	HUA ENHANCER1
HST	HASTY
IBR5	INDOLE-3-BUTYRIC ACID RESPONSE
KANADI1	KANADI1
LPR1	LOW PHOSPHATE-RESISTANT ROOT1
MAPK	MITOGEN ACTIVATING PROTEIN KINASE
MIR	MICRORNA
MKK	MAPK KINASE
NRT1.1	NITRATE TRANSPORTER1.1
PIN	PIN/PINOID
POL	POLTERGEIST
RBX1	RING BOX1-H2
RDR6	RNA-DEPENDENT RNA POLYMERASE6
SCF	SKIP/CULLIN/F-BOX
SCR	SCARECROW
SE	SERRATE
SGT1b	ENHANCER OF TIR1-1 AUXIN RESISTANCE3
SHR	SHORTROOT
TIR	TRANSPORT INHIBITOR
WOX5	WUSCHEL-RELATED HOMEOBOX 5
WUS	WUSCHEL

Chapter 1

General

Introduction

1.1 *Arabidopsis thaliana*: a model to study plant small RNAs

In eukaryotes, small RNAs (sRNAs) are a class of regulatory RNA that influence gene expression at either the transcriptional or post-transcriptional level. Small RNAs are typically 21 to 24 nucleotide (nt) in length, non-protein-coding RNAs whose binding by protein complexes upon maturation determines their gene expression regulatory function (Allen et al. 2005; Gregory et al. 2005; Vaucheret 2006). In plants, five predominant sRNA species have been characterised to date that regulate gene expression (Allen et al. 2005; Axtell 2013; Borsani et al. 2005; Curtin et al. 2008; Fei et al. 2013; Jones-Rhoades and Bartel 2004; Vaucheret 2006; Vazquez et al. 2004b;). These include:

i) microRNAs (miRNAs)

ii) *trans*-acting small-interfering RNAs (tasiRNAs)

iii) natural antisense transcript siRNAs (natsiRNAs)

iv) phased secondary siRNAs (phasiRNAs), and

v) heterochromatin siRNAs (hcsiRNAs)

Each species of plant sRNA is processed from a structurally-distinct double-stranded RNA (dsRNA) template and requires the combined action of a defined set of protein machinery, namely members of two gene families, the *DICER-LIKE* (*DCL*) and *dsRNA BINDING* (*DRB*) gene families (Song et al. 2010). Different DCL/DRB functional partnerships recognise, bind and process each structurally distinct dsRNA precursor for miRNA, tasiRNA, natsiRNA, phasiRNA, and hcsiRNA production (Eamens et al. 2012a; Mallory and Vaucheret 2006; Pelissier et al. 2011; Rajagopalan et al. 2006). Upon DCL/DRB-mediated excision from the dsRNA template, the mature sRNA is loaded into a specific protein complex termed the RNA-induced silencing complex, or RISC (Carrington and Ambros 2003). An ARGONAUTE (AGO) protein forms the catalytic core of each functionally-distinct RISC, and each AGO-catalysed RISC uses a loaded sRNA as a sequence specificity guide to direct gene expression repression of highly complementary target sequences, at either the DNA (transcriptional silencing), RNA, or protein level (post-transcriptional silencing) (Brodersen et al. 2008; Carbonell et al. 2012; Carrington and Ambros 2003; Lanet et al. 2009; Yang et al. 2012).

Arabidopsis thaliana (*Arabidopsis*) is not of any agronomic importance, but has been widely utilised by the plant biology research community as a genetic model due to its relatively small sized (~150,000,000 base pairs; 150 Mb), lowly-repetitive, fully-sequenced, and extensively-annotated genome, its short stature (~20 cm at maturity), rapid life cycle (6-8 weeks from seed to seed), ease of transformation (via established and reproducible

Agrobacterium tumefaciens-mediated floral dip transformation), and extensive genetic resource collections (Alonso et al. 2003; Arabidopsis Genome 2000; Lavagi et al. 2012; Meinke et al. 1998). Much of the knowledge gained to date on sRNA production and sRNA-directed RNA silencing (sRNA action) in plants has been developed in *Arabidopsis* (Baulcombe 2004; Hamilton and Baulcombe 1999). Furthermore, the *Arabidopsis* genome encodes four DCL, five DRB, and 10 AGO protein family members, the smallest gene family member numbers amongst plants (Vazquez 2006). Together, these attributes identify *Arabidopsis* as an ideal experimental system in which to generate mutant plant lines with altered gene expression for the functional characterisation of the parallel RNA silencing pathways of plants.

1.1.1 The *Arabidopsis* microRNA pathway

Due to their ease of identification, high level of interspecies conservation, and central role in developmental gene expression regulation, miRNAs remain the best characterised class of plant sRNAs (Park et al. 2005). The majority of plant miRNAs identified to date originate from individual genomic loci, termed *MICRORNA* (*MIR*) genes (Park et al. 2002b). DNA-dependent RNA polymerase II (PolII), the same RNA polymerase responsible for protein-coding gene transcription, transcribes a primary-miRNA (pri-miRNA) transcript from each *MIR* gene. The resulting pri-miRNA is a long non-protein-coding RNA that contains a region of partial self-complementarity to allow this region of the pri-miRNA transcript to fold back onto itself to form a stem-loop structure of imperfectly paired dsRNA (Vaucheret 2006).

In the plant cell nucleus, the stem-loop structured pri-miRNA is recognised and bound by SERRATE (SE), a zinc finger protein with the capacity to bind RNA (Iwata et al. 2013). SE transports the bound pri-miRNA to specialised nuclear bodies, called nuclear Dicing bodies or D-bodies (Fang and Spector 2007). In D-bodies, the pri-miRNA is bound by DRB1, the functional partner of the RNase III-like endonuclease, DCL1 (Schauer et al. 2002; Vazquez et al. 2004a). DRB1 correctly positions DCL1 on the dsRNA stem-loop region of the pri-miRNA to ensure accurate and efficient DCL1-catalysed pri-miRNA processing (Dong et al. 2008; Szarzynska et al. 2009). This initial cleavage event produces the precursor-miRNA (pre-miRNA) which is a processing intermediate, and the pre-miRNA is further processed by the DCL1/DRB1 partnership to remove the stem and loop structured regions to liberate the miRNA/miRNA* duplex (Kurihara and Watanabe 2004). The 2′ hydroxyl (OH) group at the

3′ terminal nucleotide of each duplex strand is subsequently methylated by the sRNA-specific methyltransferase, HUA ENHANCER1 (HEN1), to prevent degradation of these sRNA sequences following duplex strand separation (Wu et al. 2007; Li et al. 2005; Yang et al. 2006; Yu et al. 2005).

The miRNA/miRNA* duplex strands are unwound from one another and the miRNA guide strand is preferentially selected over the miRNA* strand for loading into RISC, termed miRISC, by DRB1 (Carrington and Ambros 2003). AGO1 forms the catalytic core of miRISC and uses the loaded miRNA as a sequence specificity guide to direct mRNA cleavage-based RNA silencing to repress the expression of highly complementary gene transcripts. An overall schematic of the *Arabidopsis* miRNA pathway is provided in **Figure 1.1**.

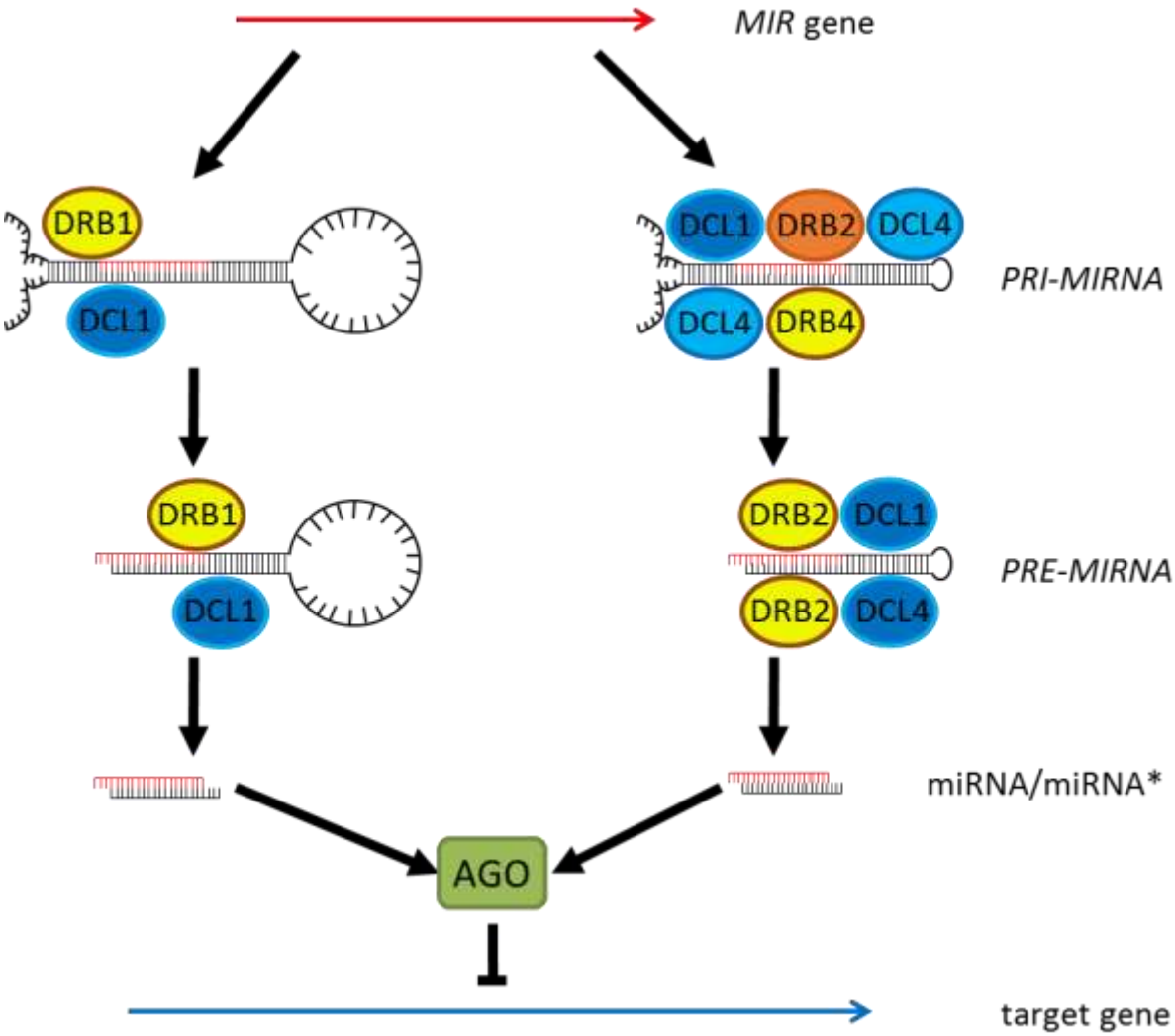

Figure 1.1. Schematic of the *Arabidopsis* miRNA pathway. RNA Pol II transcribes a long non-protein-coding RNA transcript from a *MIR* gene. The resulting transcript contains a region of partial self-complementarity allowing the transcript to fold back onto itself to form the stem-loop structure of imperfectly-paired dsRNA, processed by DRB1 (left), or near perfectly-paired dsRNA, processed by DRB2 and DRB4 (right), termed the pri-miRNA. The pri-miRNA is recognised and bound by SE in the plant cell nucleus and is transported to nuclear processing bodies, termed D-bodies. In D-bodies, the pri-miRNA is bound and processed by DCL1 in association with DRB1 or DRB2 or DCL4/DRB2/4 into the pre-miRNA intermediate, and subsequently the miRNA/miRNA* duplex. DRB1, DRB2, or DRB4 directs the preferential selection of the miRNA guide strand over the miRNA* passenger strand for RISC incorporation. AGO1 uses the loaded miRNA as a guide to direct cleavage-based RNA silencing to regulate the expression of highly complementary target gene mRNAs.

Many of the highly conserved plant miRNAs experimentally characterised to date, have been demonstrated to regulate the expression of members of transcription factor gene families, with transcription factors themselves being exceptionally important regulators of developmental gene expression (Mallory and Vaucheret 2006; Park et al. 2002b). Therefore, it is unsurprising that *Arabidopsis* plant lines harbouring T-DNA insertions that generate loss-of-function mutations in the key protein machinery of the miRNA pathway, namely *dcl1*,

drb1, and *ago1* plants (plant lines defective in DCL1, DRB1, and AGO1 activity, respectively) display a range of deleterious development phenotypes (**Figure 1.2**).

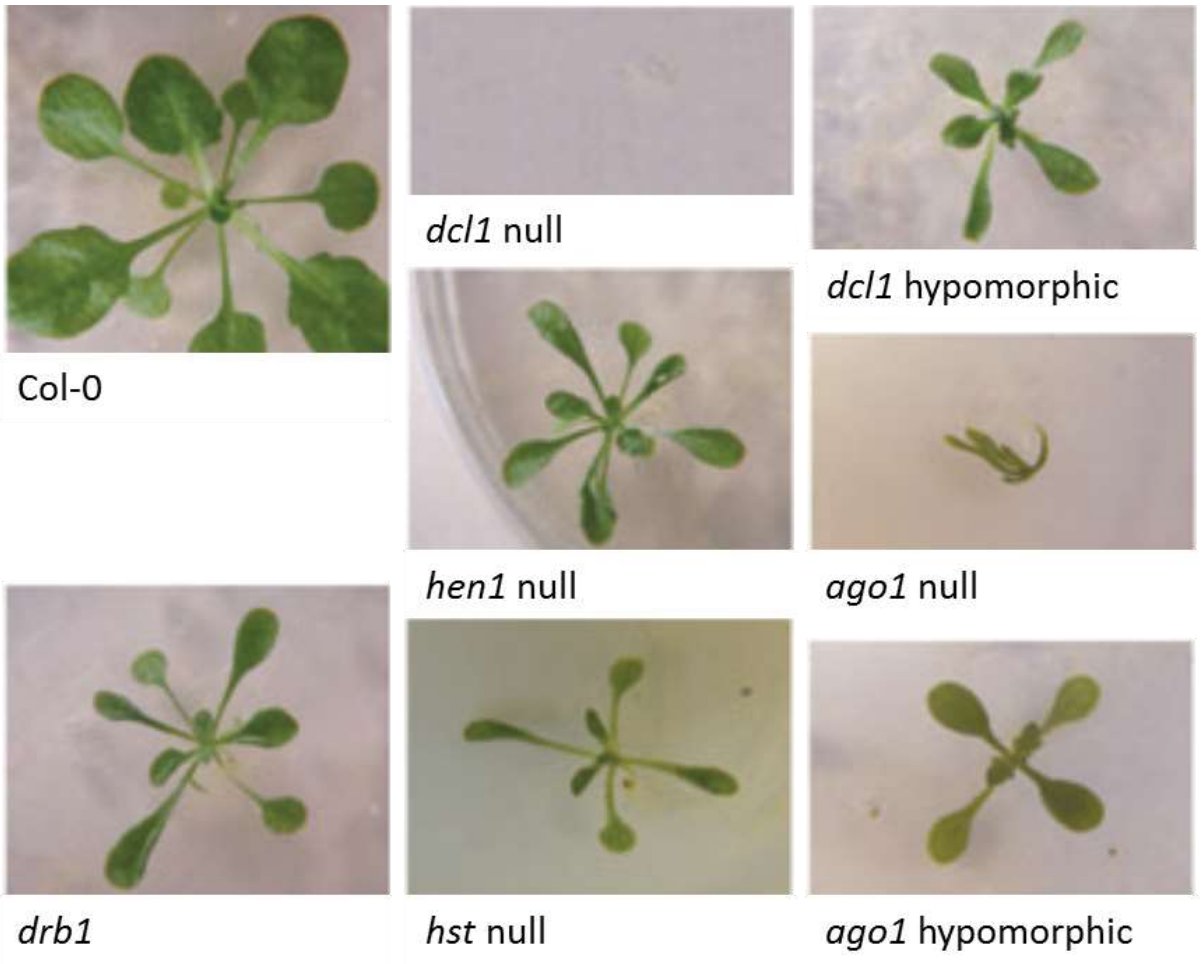

Figure 1.2. Developmental phenotypes displayed by *Arabidopsis* plant lines defective in DRB1, DCL1, and AGO1 activity. A high percentage of genes experimentally validated to be miRNA target genes encode transcription factors that are themselves important regulators of developmental gene expression. The importance of the miRNA pathway to *Arabidopsis* development is illustrated by the severe developmental phenotypes displayed by *Arabidopsis* plant lines harbouring, loss-of-function mutations in the key miRNA pathway machinery proteins. These include, DCL1 (some *dcl1* alleles are embryo lethal), DRB1, and AGO1 (some *ago1* alleles are embryo lethal; data not shown). DCL1 and AGO1 roles were assessed using hypomorphic, single allelic mutations reducing protein functionality, lines. Mutations in additional proteins HEN1 and HASTY (HST), involved in miRNA duplex and cytoplasmic export respectively, both show severe developmental phenotypes similar to *drb1*. Images modified from Mallory and Vaucheret, 2006.

1.1.2 Expanded roles for DCL, DRB and AGO proteins in the *Arabidopsis* miRNA pathway

Early research indicated that SE, DCL1, DRB1, and AGO1 were the only protein machinery required for a functional *Arabidopsis* miRNA biogenesis pathway. That is, DCL1 and DRB1, and to a lesser degree SE, function together to process the miRNA sRNA out of the much larger sized dsRNA precursor transcripts and further, upon maturation, the miRNA is loaded into miRISC for target gene expression repression via miRNA-directed AGO1-catalysed mRNA cleavage. More recently, however, additional members of the *DCL*, *DRB*, and *AGO* gene families have also been demonstrated to be involved in either the production or action stage of the *Arabidopsis* miRNA pathway.

Improvements to high throughput sequencing technology, often referred to as deep sequencing, and to the bioinformatic software used to interrogate the vast volumes of resulting sequencing data, enabled the identification of a new miRNA subclass (Fahlgren et al. 2009). Non-conserved, or species-specific miRNAs, are similar to conserved miRNAs that operate via the canonical SE/DCL1/DRB1/AGO1 miRNA pathway (**Figure 1.1**) in that only a single 21-nt miRNA is generated from a much larger sized dsRNA stem-loop structured precursor transcript (Ben Amor et al. 2009; Fahlgren et al. 2009; Rajagopalan et al. 2006; Tsuzuki et al. 2014; Zhang et al. 2010). However, the dsRNA precursor transcript encoded by a non-conserved *MIR* gene is structurally distinct to those of conserved miRNAs and their fates differ following PolII-directed transcription and pri-miRNA folding (Ben Amor et al. 2009; Qin et al. 2010; Rajagopalan et al. 2006; Tsuzuki et al. 2014). Due to extensive complementarity within these precursor transcripts, a non-conserved pri-miRNA folds to adopt a near perfect dsRNA stem-loop, composed of a long, perfectly-dsRNA stem region, and a very small loop structure containing only a handful of nucleotides (Ben Amor et al. 2009; Rajagopalan et al. 2006; Tsuzuki et al. 2014).

In the plant cell nucleus, the long, perfectly-dsRNA stem region of a non-conserved pri-miRNA is recognised by DRB4 and not by DRB1. DRB4 recognition of the precursor can occur either with or without the functional assistance of SE (Rajagopalan et al. 2006). DRB4 has been demonstrated to preferentially interact with DCL4 (Rajagopalan et al. 2006; Zhang et al. 2010), and as for the DRB1/DCL1 functional partnership in the production of conserved miRNAs (**Figure 1.1**), DRB4 ensures that DCL4 is correctly positioned on the non-conserved pri-miRNA transcript for accurate and efficient production of the non-conserved miRNA (Ben Amor et al. 2009; Rajagopalan et al. 2006). Upon DRB4/DCL4-mediated processing of the

miRNA/miRNA* duplex from the much larger sized pri-miRNA and pre-miRNA structures, the 2ˈ OH group of the 3ˈ terminal nucleotide of each duplex strand is again methylated by HEN1, the duplex strands are unwound, and the miRNA is loaded into miRISC to direct target gene expression regulation (Ben Amor et al. 2009; Rajagopalan et al. 2006; Tsuzuki et al. 2014; Zhang et al. 2010).

Non-conserved miRNAs also tend to have a 5ˈ terminal nucleotide different from uracil (U), the predominant 5ˈ terminal nucleotide of conserved miRNAs (Eamens et al. 2009). The high frequency of U at the 5ˈ terminal position of conserved miRNAs is believed to direct their preferential loading into AGO1, the catalytic core of miRISC (Montgomery et al. 2008; Zhang et al. 2010). As with the 5ˈ terminal nucleotide preference of AGO1, a number of other AGO proteins, including AGO2, AGO4, AGO5, AGO7, and AGO10, have also been demonstrated to have 5ˈ terminal nucleotide preferences, or to have a highly selective preference for only binding a specific miRNA and/or sRNA (Montgomery et al. 2008; Zhang et al. 2010). It is, therefore, reasoned that other AGOs, in addition to AGO1, could potentially play a role in miRNA target gene expression regulation once they have bound their preferred miRNA and/or sRNA payload (Ben Amor et al. 2009; Rajagopalan et al. 2006). Such preferential loading of a specific miRNA was best demonstrated by Montgomery and colleagues (2008) who showed that *Arabidopsis* AGO7 almost exclusively loads the miR390 sRNA, the miRNA required for catalysing the *TAS3* tasiRNA pathway.

In addition to potentially being loaded by an AGO protein distinct to AGO1, non-conserved miRNAs typically regulate the expression of target genes that mediate roles outside of plant development. These targets include abiotic stress adaptation, and mounting defence responses against invading pathogens (Windels and Vazquez 2011). The role of non-conserved miRNAs in pathways outside of plant development is exemplified by the mild developmental phenotypes expressed by *drb2* and *drb4* (**Figure 1.3**) plants, compared to the severe or lethal phenotypes displayed by the *dcl1*, *drb1*, and *ago1* mutants (**Figure 1.2**), when these loss-of-function plant lines are cultivated under standard growth conditions.

Figure 1.3. Phenotypes of *drb2* and *drb4* insertion mutant plant lines. *Arabidopsis* insertion knockout mutant plant lines *drb2* and *drb4* express mild developmental phenotypes when cultivated under standard growth conditions.

Small RNA production by the DCL4/DRB4 functional partnership is not limited to non-conserved miRNAs. DCL4/DRB4 are required for the production of 'in phase', 21-nt tasiRNA from the non-protein-coding *TAS3* transcript (Nakazawa et al. 2007). Initial cleavage of the *TAS3* transcript is directed by miR390, generated by DCL1/DRB1 in association with AGO7 (Nakazawa et al. 2007). miR390/AGO7-mediated cleavage of *TAS3* identifies this transcript as a template for dsRNA synthesis by RNA-DEPENDENT RNA POLYMERASE6 (RDR6), one of the six RDRs encoded by the *Arabidopsis* genome. The resulting perfectly dsRNA *TAS3* molecule is recognised and bound by DRB4, and DRB4 continually repositions DCL4 along the length of the *TAS3* dsRNA to ensure accurate 21-nt phasing of the generated, tasiRNA/tasiRNA* duplexes (Montgomery et al. 2008; Nakazawa et al. 2007). Although multiple tasiRNAs/tasiRNAs* duplexes are produced from the DCL4/DRB4-processed *TAS3* dsRNA precursor, only a small number of *TAS3* tasiRNAs are selected for incorporation in AGO1-catalysed RISC (Qu et al. 2008). *TAS3*-derived tasiRNAs are commonly referred to as tasiARFs, as they direct AGO1-mediated mRNA cleavage-based silencing of a small clade of members of the *AUXIN RESPONSE FACTOR* (*ARF*) transcription factor family (Wang et al. 2005). The importance of DRB1 and DRB4 in miRNA and tasiRNA production cannot be understated. DRB1 is absolutely essential for accurate positioning of DCL1 on conserved miRNA precursor transcripts to direct efficient miRNA production, and similarly, DCL4-catalysed dsRNA cleavage is highly inaccurate in the absence of DRB4 (Montgomery et al. 2008; Nakazawa et al. 2007; Rajagopalan et al. 2006).

The central role played by DRB proteins in miRNA and tasiRNA production was further highlighted by the recent demonstration that DRB proteins act differently in two developmentally-important *Arabidopsis* tissues, the shoot apex and reproductive organs

(i.e., the floral organs). DRB2 can be both synergistic and antagonistic to the roles played by either DRB1 or DRB4 in the miRNA or tasiRNA pathway, respectively (Eamens et al. 2012a; Pelissier et al. 2011).

DRB2 expression is restricted almost exclusively to the shoot apical meristematic region (SAM) and reproductive tissues, indicative of a pivotal role in developmental processes (Eamens et al. 2012a). Whilst *DRB2* expression is most striking in these tissue types, some expression has been detected in root tissues (Reis et al. 2015), indicating that DRB2 also has a role in root cell types. Conversely, *DRB1* expression is fairly ubiquitous throughout *Arabidopsis* tissue types (Reis et al. 2015), indicating that DRB1-directed miRNA production is the dominant form of miRNA-mediated posttranscriptional silencing in most of these tissues. Although, DRB2 expression is higher than DRB1 in both the shoot apex and reproductive tissues (Reis et al. 2015). Like *DRB1*, *DRB4* expression is of comparable levels throughout the *Arabidopsis* plant (Nakazawa et al. 2007). Whilst *DRB4* expression is still strongest in reproductive tissues, it also has been shown to be highly expressed in root tisuue types (Nakazawa et al. 2007). The overlapping spatial expression of *DRB1*, *DRB2*, and *DRB4* in *Arabidopsis* maintains the potential for both synergistic and anatagonistic interaction between these DRB family members.

Demonstration that DRB2 is involved in the miRNA and tasiRNA pathways indicates that DRB2 possesses plasticity in its two dsRNA binding motifs (dsRBMs) that each of the five members of the *Arabidopsis* DRB protein family encodes in the amino (N)-terminal half of the protein. As for the other four *Arabidopsis* DRB proteins, the two N-terminal dsRBMs would facilitate the DRB2 protein to; i) recognise and bind a specifically structured dsRNA substrate(s), and; ii) mediate interaction with other proteins, namely interaction with DCLs, DCL1 and DCL4 (Eamens et al. 2012a; Eamens et al. 2012b; Pelissier et al. 2011).

Antagonism between DRB2 and DRB1, and DRB2 and DRB4, infers that there is competition between these three DRBs to form functional partnerships with DCL1 and DCL4. A recent report is highly supportive of this, demonstrating that in the *Arabidopsis* shoot apex, to where *DRB2* expression is predominantly localised in wild-type *Arabidopsis*, the DRB2 protein represses the expression of the *DRB1* gene via an unknown mechanism (Reis et al. 2015). DRB2 suppression of DRB1 would enable DRB2 to interact with DCL1 for miRNA production in this tissue, with DRB1 previously demonstrated *in vitro* to have an interaction affinity with DCL1 that is 20 times stronger than the binding affinity of either DRB2, DRB3, DRB4, or DRB5 with DCL1 (Hiraguri et al. 2005). In the same tissues, synergism between

DRB1 and DRB2 could ensure that miRNA production remained relatively unaffected when the plant is exposed to different environmental conditions, such as exposure to abiotic stresses. Mechanistically, a miRNA could be loaded into a functionally distinct RISC to direct an alternate mechanism of miRNA-directed RNA silencing; namely translational repression. Translational repression is a less energy demanding form of miRNA-directed RNA silencing for a plant cultivated under suboptimal growth conditions, or when the plant is exposed to abiotic stress or pathogen attack (Eamens et al. 2012a; Eamens et al. 2012b; Reis et al. 2015). The mild developmental phenotype displayed by *drb2* plants (**Figure 1.3**) when this insertion knockout mutant line is grown under optimal growth conditions further supports the proposed central role for DRB2 in sRNA production during environmental challenge or pathogen attack.

1.2 Auxin: A crucial phytohormone for plant development

Auxin, indole-3-acetic acid (IAA), is a crucial phytohormone synthesised in all plants, predominantly in the shoot apical meristem (SAM), through either a tryptophan-dependent or -independent biosynthetic pathway from the precursor molecule, indole-3-acetaldoxime (Jones et al. 2010; Tao et al. 2008; Zhao 2010). Auxin is an essential hormone for plant development (Zhao 2010), due to its widely documented roles in the regulation of, but not limited to; (1) gravitropism (Rashotte et al. 2000); (2) phototropism (Stowe-Evans et al. 2001), and; (3) organ patterning (Bainbridge et al. 2008). More recently, auxin has been identified as a key regulator of floral development (Krizek 2011), and seed dormancy/germination (Liu et al. 2013; Park et al. 2011). Auxin regulates these developmental processes via a multitude of mechanisms. However, the unusual modes of transport of auxin are fundamental in eliciting auxin regulatory functions in plants.

1.2.1 Polar auxin transport and intracellular auxin perception in *Arabidopsis thaliana*

Auxin is transported throughout the plant in two ways; (1) non-polar transport through the phloem (Goldsmith et al. 1974), and (2) by the far more common mechanism of cell-to-cell polar auxin transport (Galweiler et al. 1998). Auxin can be transported passively in a polar fashion throughout the plant due to its unique chemical properties (Friml and Palme 2002). Auxin is primarily synthesised in the SAM (Vernoux et al. 2010), where auxin efflux proteins of the *PIN/PINOID* (*PIN*) gene family mediate the transport of auxin down a concentration gradient into the extracellular space (Palme and Galweiler 1999). In the extracellular space, auxin is protonated by the slightly acidic pH environment (Muller and Schier 2011), and this in turn mediates the transport of auxin back into cells via the activity of AUXIN INFLUX PROTEIN1 (AUX1) (Muller and Schier 2011; Palme and Galweiler 1999). In the plant cell cytoplasm, auxin is deprotonated by the near neutral pH (Muller and Schier 2011). As AUX1 is located in the apical plasma membrane, respective to the SAM, and PIN proteins are located in the basal plasma membrane, this creates an asymmetry in the site of auxin influx and the site of auxin efflux (Muller and Schier 2011; Palme and Galweiler 1999). It is this asymmetry in the influx-efflux protein location, coupled with the constant protonation-deprotonation cycling that passively directs auxin transport in a polarised direction throughout the plant (Gray et al. 1999; Muller and Schier 2011; Palme and Galweiler 1999).

As outlined above, the movement of auxin into and out of plant cells is mediated via the action of AUX1 and PIN proteins, respectively. However, once auxin is transported into the cytoplasm of a plant cell, a complex network of genetic cascades is required for the initial perception of auxin as well as the subsequent promotion of appropriate auxin responses (Gray et al. 1999; Gray et al. 2001; Kepinski and Leyser 2004). These responses can be described as "fast", mediated directly by changes in cell activities, and "slow", mediated by changes in gene expression (Vanderhoef and Stahl 1975).

In slow responses, intracellular auxin perception and response is primarily mediated by the activity of members of three gene families, including the; i) *AUXIN/INDOLE-3-ACETIC ACID (Aux/IAA)*; ii) *AUXIN REPONSE FACTOR* (*ARF*), and; iii) *TRANSPORT INHIBTIOR* (*TIR*) gene families (Guilfoyle and Hagen 2007; Kepinski and Leyser 2004; Reed 2001) (**Figure 1.4**). From the cytoplasm, auxin diffuses into the plant cell nucleus through non-selective nuclear pores whereupon it binds directly with the intracellular auxin perception protein, TIR1 (Kepinski and Leyser 2004). The binding of auxin to TIR1 facilitates the interaction between TIR1 and either the ARABIDOPSIS SKIP LIKE1 (ASK1) or (ASK2) protein both of which are core components of the SKIP/CULLIN/F-BOX (SCF) complex. The binding of auxin by TIR1 also recruits a cullin-like protein, CULLIN1 (CUL1), and together, these three subunits form an SCF ubiquitin E3 ligase (Gray et al. 1999; Gray et al. 2001). A number of other core components are subsequently recruited to the activated SCF complex, including the RING BOX1-H2 (RBX1) protein, a protein that binds to ASK1 (or ASK2) and recruits the ubiquitin E2 ligase, AUXIN RESISTANT1 (AXR1), a ubiquitin-related gene involved in CUL1 post-translational modifications, and ENHANCER OF TIR1-1 AUXIN RESISTANCE3 (SGT1b), a tetratricopeptide-repeat protein that interacts with CUL1 and is implicated in the turnover of the SCF complex. Together, these interacting proteins form the entirety of the auxin SCF complex (Calderon-Villalobos et al. 2010; Walsh et al. 2006).

When auxin signalling is perceived within the plant cell nucleus, ARF proteins, a family of auxin responsive transcription factors, are able to homodimerise and bind to *AUXIN RESPONSE ELEMENT*s (*ARE*s; DNA-based sequence motifs) in the promoters of *AUXIN RESPONSE GENE*s (*ARG*s). *ARG*s encode proteins that elicit an appropriate auxin response (Chapman and Estelle 2009). However, under non-auxin conditions, ARFs are present as heterodimers, bound to a specific Aux/IAA protein(s). Thus, Aux/IAA proteins are repressors of *ARG* gene expression and prevent the bound ARFs from binding to the AREs in the promoters of *ARG*s (Dharmasiri et al. 2005; Kepinski and Leyser 2004; Overvoorde et al. 2005;

Reed 2001). The SCF complex, functioning as a ubiquitin protein ligase, ubiquinates the bound Aux/IAA proteins which is a signal for their degradation by the 26S proteasome (Gray et al. 2001). Once the Aux/IAA protein is degraded, the ARF(s) that the Aux/IAA was repressing via formation of a heterodimer with the ARF, allows the now free ARF to homodimerise, and carry out its role as a transcription factor. It is important to note that the individual ARFs can be either activators or repressors of *ARG* gene expression. The process of auxin transport and intracellular auxin perception is schematically represented in **Figure 1.4**.

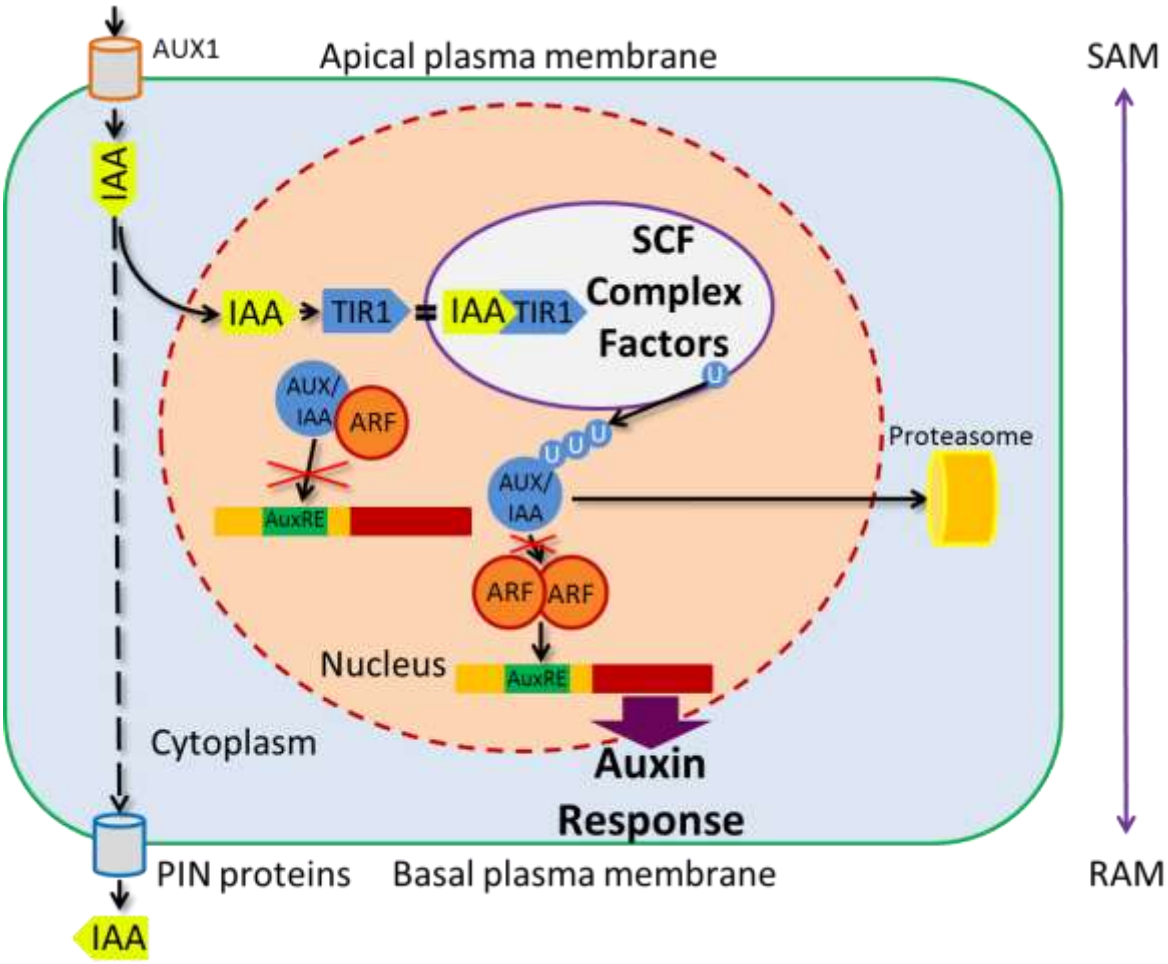

Figure 1.4. Schematic representation of polar auxin transport and intracellular auxin perception triggering genetic responses. Auxin (IAA) is passively transported into the cytoplasm of a plant cell by the transmembrane auxin influx protein, AUX1. Upon entry into the plant cell, IAA either, flows through the cytoplasm and is passively transported back into the extracellular space by an auxin efflux protein, a PIN protein, or the auxin molecule is perceived by the cell. For perception, auxin diffuses into the nucleus through non-selective nuclear pores whereupon it is bound by the auxin perception protein, TIR1. Binding auxin induces a conformational change in the TIR1 protein and this, in turn, promotes the formation of the SCF complex, a complex comprised of ASK1, CUL1, RBX1, AXR1, and SGT1b. The resulting SCF complex, an E3 protein ligase, then mediates the ubiquitination of an AUX/IAA protein, a repressor of ARF transcription factors. Following degradation of the targeted Aux/IAA protein, the now free ARF can homodimerise and bind to AREs in the promoter regions of *ARG*s, to modulate *ARG* expression in response to auxin.

Plant cells can also demonstrate "fast" responses to auxin in which changes of gene expression are not required. This alternate auxin response pathway operates independent of gene expression and was documented prior to "slow" auxin responses becoming the accepted mechanism for auxin to influence cellular changes (Vanderhoef and Stahl 1975). In this historical case, auxin was demonstrated to have an almost immediate effect on membrane potential, cell division, and cell elongation, antagonistic to cytokinin (Vanderhoef and Stahl 1975), and is too rapid to be the result of gene expression changes. However, no candidate for the mediator of this effect was identified at that time.

More recently, a candidate was postulated to mediate "fast" auxin responses. AUXIN BINDING PROTEIN1 (ABP1) was shown to interact with auxin at the plasma membrane and induce a physiological response (Leblanc et al. 1999). Furthermore, *abp1* knockout mutants were shown to be embryo lethal (Chen et al. 2001), providing evidence of a role for ABP1 in critical auxin signalling pathways. Analysis of knockdown *abp1* mutants revealed that it directly contributes to the control of plant cell expansion, and either directly or indirectly to cell division (Chen et al. 2001). Furthermore, it was postulated that ABP1 may be interacting with downstream, "slow" auxin signalling responses as part of integrated auxin signal transduction events (Chen et al. 2001; Leblanc et al. 1999). Combined, this evidence illustrates the perceived critical nature of ABP1 not only to "fast" auxin responses, but to an integration between "fast" and "slow" auxin responses throughout the plant. However, technological limitations prevented a comprehensive investigation into ABP1, and other "fast" auxin response pathways are believed to exist (Gao et al. 2015; Hemmati et al. 2017). Plasma membrane localisation seems to be of great significance in "fast" auxin responses, as would be expected as this is the site of auxin influx (**Figure 1.4**). For example, the protein INDOLE-3-BUTYRIC ACID RESPONSE5 (IBR5) is plasma membrane localised and responds to another endogenous auxin species (Strader et al. 2008). IBR5 is also the beginning of a response chain, where IBR5 quickly triggers a significant increase in MITOGEN ACTIVIATING PROTEIN KINASE (MAPK activity; specifically, MPK12 (Lee et al. 2009). MPK12, in turn, interacts with a MAPK kinase (MKK), MKK1 (Hemmati et al. 2017), which influences cell division and elongation during leaf development in response to auxin signalling modulations (Hemmati et al. 2017).

Our understanding of all forms of auxin transport, perception, and response is becoming clearer, while auxin has been demonstrated to be critical to plant development (Zhao 2010). Considering this, further in-depth investigation of auxin transport and signalling may provide significant insight into plant organ development and environmental responses.

1.2.2 Auxin and the regulation of shoot development

The pivotal developmental role directed by auxin is elegantly demonstrated by its regulation of the balance between lateral organ developmental and meristematic cell proliferation in the SAM (Sablowski 2007; Traas and Doonan 2001). During this process, PIN1 proteins orientate on the apical plasma membrane in the outer layers of the SAM, as opposed to the basal plasma membrane as illustrated in **Figure 1.4**, transporting auxin away from the site of biosynthesis. This results in auxin localising in leaf primordia, and in floral organ primordia later in development (Palme and Galweiler 1999). There is a similar inversion of the localisation of AUX1 proteins to facilitate auxin transport (Reinhardt et al. 2000). However, in the SAM AUX1 is localised to the inner layers and remains largely unpolarised in these tissues illustrating the role of AUX1 in auxin mobilisation, but not in flux direction, in the SAM (Reinhardt et al. 2003).

In the central zone of the SAM, a relatively consistent population of undifferentiated cells is maintained, and this maintenance is predominantly governed by the transcription factor WUSCHEL (WUS). WUS achieves this via disruption of hormone signalling pathways in this zone, notably the cytokinin pathway, but also the auxin pathway to a lesser extent. This prevents commitment of cells to mature identities (Gordon et al. 2009). Conversely, organ development in the peripheral zone of the SAM is governed by the CLAVATA3/ESR-related (CLE) protein family comprised of CLAVATA1 (CLV1), CLV2, and CLV3 which act to form part of a receptor ligand complex, that push cells out of a state of meristematic proliferation and into a state of organ initiation (Schoof et al. 2000). The *WUS* and *CLV* genes form a negative feedback loop, whereby WUS negatively regulates the expression of the *CLV3* locus (Mayer et al. 1998; Schoof et al. 2000). In turn, *CLV3* encodes for a polypeptide which binds to receptor kinases formed by CLV1 and CLV2, and with another protein, CORYNE (CRN) (Muller et al. 2008). These three receptor kinases repress the function of phosphatase genes, either *POLTERGEIST* (*POL*) or *POL*-like genes (Yu et al. 2003). The POL protein has been shown to enhance the expression of *WUS* (Yu et al. 2003). Either through direct repression by WUS on *CLV* gene expression, or by indirect repression by CLVs on the expression of *WUS*,

meristematic cell proliferation in the central zone or organ initiation in the peripheral zone, respectively, is maintained.

Through CLV activity, auxin is concentrated in the peripheral zone of the SAM (Schoof et al. 2000). Auxin forms specific local maxima through the selective positioning of PIN1 radially outwards from the central zone of the SAM (Benjamins et al. 2001; Vernoux et al. 2000), and these local maxima begin cell signalling to form lateral organ primordia (Benjamins et al. 2001). Primordia formed in this way start development by post-embryonic organogenesis into leaves, and later into the development of floral structures for reproduction (Aida and Tasaka 2006). Distinct leaf phyllotaxis, and thus the radial patterning observed in *Arabidopsis*, is due to lateral aerial organs formed in this fashion.

1.2.3 Auxin and the regulation of root development

Meristem maintenance and control of cell differentiation in the root is similar to the shoot. It does, however, differ both physiologically and genetically in distinct and significant ways. The root apical meristem (RAM) is located close to the root tip. The root cap forms the final epidermal cell layers at the root terminus for the protection of the root, and for soil penetration (Bengough and McKenzie 1997). Above the RAM, in the direction towards the soil surface, is the elongation zone, where cells expand under controlled conditions before entering the differentiation zone where cells adopt particular fates (Dolan et al. 1993). In *Arabidopsis*, a set of four cells sit at the centre of the RAM forming the quiescent centre (QC) which acts as an organisation hub for the surrounding stem cell initials (Dolan et al. 1993). These initials are the basis for cell lineages, which form layers in the root, to progress through the elongation and differentiation zones as they adopt the characteristics of each mature cell type (Dolan et al. 1993; van den Berg et al. 1997).

Genetically, the RAM is organised in a similar manner to the SAM, but with different genes occupying the roles described above for WUS and CLV. *SHORTROOT* (*SHR*) is transcribed in provascular tissue of the root with the mature protein transported to the QC to activate *SCARECROW* (*SCR*) gene expression (Heidstra et al. 2004). SCR is required for correct QC cell identity and is, therefore, critical to stem cell number maintenance in the RAM (Heidstra et al. 2004). As in the SAM, members of the CLE protein family are involved in controlling cell proliferation in the RAM (Casamitjana-Martinez et al. 2003; Hobe et al. 2003). CLV3, in conjunction with other CLE protein family members, CLE19 and CLE40, regulates

stem cell number (Casamitjana-Martinez et al. 2003; Hobe et al. 2003). This differs from the SAM, however, as CLE proteins control cell divisions in proto-committed cells as opposed to their role in the SAM where they determine the difference between the proliferation zone and the differentiation zone (Brand et al. 2000; Fletcher et al. 1999; Rojo et al. 2002).

Auxin signalling plays a pivotal role in the formation of root structures in early development, forming RAM cell identity, and promoting lateral organ formation (Laskowski et al. 1995). In the developing embryo, auxin synthesised in the SAM is directed to the root cells by basally localised, relative to the position of the SAM, PIN1 proteins (Galweiler et al. 1998). Elevated auxin activates the ARFs (**Figure 1.4**) in the root tissue, with the ARFs directing the expression of the gene products required for the formation of cell identity and structure in the root (Hardtke and Berleth 1998). Applications of exogenous auxin during this critical developmental stage leads to the ectopic development of the QC and the QC stem cells, revealing the role of auxin in RAM formation and cell identity in the root (Sabatini et al. 1999). Auxin accumulates at the RAM throughout plant development to maintain stem cell proliferation and orchestrate root growth.

Lateral root formation requires a balance between basipetal auxin transport to the RAM, and specific localisation of auxin within the root tissue to pericycle cells, for postembryonic organogenesis. Local auxin maxima also form at sites of lateral root development (Laskowski et al. 1995). Auxin, primarily synthesised in shoot tissue, redistributes in the root from the RAM to xylem pole pericycle cells forming local auxin maxima. The presence of higher concentrations of auxin in these cells leads to the formation of a pseudo-QC, and the associated stem cells, providing a basis of undifferentiated cells for the cell lineages required for lateral root growth to initiate. Further, in the absence of alterations to the concentration of auxin, these cells continue to develop into regular pericycle cells (Casimiro et al. 2001).

Auxin signalling has also been implicated in adaptive responses in plants to a number of abiotic stresses, including nitrogen and phosphate deficiencies, as well as drought and salt stresses (Kazan 2013). For example, in low nitrate conditions, the nitrate influxer and sensor protein, NITRATE TRANSPORTER1.1 (NRT1.1), promotes the basipetal transport of auxin, while inhibiting the accumulation of auxin in lateral root initials. Low auxin in lateral root initials represses lateral root growth while promoting primary root growth for exploration of the surrounding soil-based environment (Bouguyon et al. 2012; Gojon et al. 2011; Krouk et al. 2010). Conversely, when nitrate levels are high, NRT1.1-dependent basipetal auxin transport

is inhibited, and as such, auxin accumulates in lateral root primordia to promote their growth (Bouguyon et al. 2012; Gojon et al. 2011; Krouk et al. 2010).

Auxin is involved in other root development responses to the environment. During periods when inorganic phosphate (Pi) is deficient, referred to either as phosphate or Pi stress, primary root growth is repressed while lateral root growth is promoted, resulting in increased plant mass within the nutrient-rich rhizosphere (Lopez-Bucio et al. 2002). Promotion of lateral root growth is not simply achieved via the plant repressing primary root growth. Under Pi stress conditions, a substantial increase in both the length and number of lateral roots is observed (Lopez-Bucio et al. 2002; Perez-Torres et al. 2008; Williamson et al. 2001). This increase has been directly linked to an influx of auxin into specific pericycle cells (Lopez-Bucio et al. 2002; Perez-Torres et al. 2008). Pericycle cycle cells which accumulate auxin in this manner go on to form lateral roots, and the maintenance of auxin influx stimulates the growth of these lateral roots (Perez-Torres et al. 2008; Williamson et al. 2001). Adjacent pericycle cells that retain their nascent function experience no such auxin influx (Lopez-Bucio et al. 2002). This is thought to increase the rhizosphere area available to the plant for Pi acquisition. Auxin was shown to accumulate in pericycle cells, initiating lateral root development, in *Arabidopsis* plants harbouring the GUS reporter gene under the control of *DR5* gene promoter (*DR5*pro), an auxin receptive gene (*DR5pro*:GUS plants) (Perez-Torres et al. 2008). When the *DR5*pro:GUS plants were cultivated under Pi deprived conditions, an increase in *GUS* expression within pericycle cells was observed (Perez-Torres et al. 2008). The induction of the GUS reporter expression was further increased when auxin was applied exogenously to the *DR5*pro:GUS plants. These observations confirm that auxin accumulation in pericycle cells is directly linked to increased lateral root number in response to Pi deprivation (Perez-Torres et al. 2008).

Evidence for the role of auxin in lateral root initiation also derives from the analysis of mutants. A reduced response to Pi deprivation, in the form of a less pronounced increase in lateral root length and number, has been observed in the *axr1* and *iaa7* mutants (Perez-Torres et al. 2008; Williamson et al. 2001). AXR1 and Aux/IAA7 are both core proteins involved in SCF complex-mediated auxin perception. Related experimental evidence implicates LOW PHOSPHATE-RESISTANT ROOT1 (LPR1), a protein involved in determining root architecture by being part of the primary sensing complex in the root cap which initialises a signalling cascade reporting a low Pi environment (Svistoonoff et al. 2007). This ultimately results in a modification to overall root architecture. Loss-of-function *lpr1* mutant plants have

a reduced number and a reduced length of lateral roots under Pi deprived conditions. The *LPR1* gene is allelic to *DARK OVEREXPRESSION OF CAB* (*DOC1*, also known as *BIG*), a calossin-like gene that encodes a protein required for auxin transport (Gil et al. 2001). The exogenous application of auxin to *lpr1* mutants under Pi deprived conditions reversed the lateral root shortening and restored these plants to a near wild-type phenotype (Lopez-Bucio et al. 2005). Thus, by disrupting key components of auxin transport and signalling, the plant is unable to alter its root architecture in response to Pi deprivation (Lopez-Bucio et al. 2002; Perez-Torres et al. 2008; Williamson et al. 2001). Together, the Pi insensitive phenotypes, as well as the role of NRT1.1 in altering auxin transport under differing nitrogen availability, demonstrates the key functional role that auxin signalling plays in mediating physiological responses to abiotic stress in plants.

Auxin has also been shown to play a regulatory role in response to salt stress. Again, auxin-directed alterations to root architecture have been reported for plants grown in conditions of differing salt concentration. A reduction in lateral root growth, but an increase in lateral root number, is observed under mild salt stress. However, under high salt conditions, lateral root growth, and lateral root initiation are completely inhibited (Zolla et al. 2010). The observed changes in root architecture, and growth under increasing salt concentration, is regulated by auxin, with plants harbouring knockout mutations in the *AXR1*, *TIR1*, and *AUX1* loci (*axr1*, *tir1* and *aux1* mutant plants, respectively) all displaying a decrease in lateral root number in response to mild salt stress (Wang et al. 2009; Zolla et al. 2010). Salt stress, and the role of auxin in regulating this process, demonstrates the role that auxin plays in root adaption to abiotic stress, in addition to the established role of auxin in plant development.

1.3 Auxin, small RNAs, and the regulation of root development

There is substantial evidence indicating that sRNA-targeted auxin responsive genes may influence root architecture. *NAC* family transcription factors are most commonly associated with aerial tissue developmental processes (Souer et al. 1996). However, *NAC1* is exclusively expressed in root tissue and has been shown to influence lateral root architecture (Xie et al. 2000). Overexpression of *NAC1*, and antisense-mediated knockdown of *NAC1* expression, results in the proliferation and retardation of lateral root growth, respectively (Xie et al. 2000). Furthermore, induced perturbations in auxin signalling affect the expression of *NAC1* causing a lack of lateral root formation and development (Xie et al. 2000). The overexpression of *NAC1* in *Arabidopsis* lacking the intracellular auxin perception gene, *tir1*, rescues the defective lateral root phenotype displayed by *tir1* mutant plants, a finding that strongly indicates that *NAC1* acts downstream of TIR1 in the auxin pathway and that it is an auxin responsive gene (Xie et al. 2000). Interestingly, *NAC1* is not only auxin responsive, but is also under posttranscriptional regulation by miR164 (Guo et al. 2005). *MIR164* expression, and hence miR164 accumulation, is itself auxin-induced and combined with its role as a negative regulator of *NAC1* expression, auxin and miR164, together with NAC1, form an auto-regulated loop that controls lateral root initiation (Couzigou and Combier 2016; Guo et al. 2005).

High-throughput sequencing of the high molecular weight RNA fraction (RNA-Seq) has shown that there are many *Arabidopsis* genes whose expression is altered in response to changes in the root environment (Zhu et al. 2013a; Zhu et al. 2013b). Included in this gene cohort are members of gene families known to be involved in auxin transport and perception, or in downstream events known to be affected by changes in auxin concentration (Zhu et al. 2013a). Interestingly, some of the genes in this auxin gene cohort have previously been identified as miRNA target genes including *TIR1* and the *TIR1* family members, *AFB1*, *AFB2*, and *AFB3*, that are targeted by miR393 (Windels and Vazquez 2011), *ARF2*, *ARF3*, and *ARF4*, which are the target genes of tasiARF (Williams et al. 2005), *ARF6* and *ARF8*, that are target genes for miR167 (Kinoshita et al. 2012), and *ARF10*, *ARF16*, and *ARF17*, which are target genes of miR160 (Mallory et al. 2005).

1.3.1 The miR160/*ARF10*/*ARF16*/*ARF17* expression module

Studies examining the role of sRNA regulation in root architecture determination have found that the miR160 targets *ARF10*, *ARF16*, and *ARF17* play a critical role in responding to auxin accumulation in lateral root primordia (Wang et al. 2005). ARF10, ARF16, and ARF17 are three closely related members of the ARF transcription factor family, with ARF10 and ARF16 more closely related to each other than to ARF17 (Piya et al. 2014). ARF10, ARF16, and ARF17 act as transcriptional repressors of their target genes, a function similar to the majority of ARFs characterised to date that have also been shown to function as repressors of target gene expression (Piya et al. 2014). miR160 is known to target the *ARF10*, *ARF16*, and *ARF17* transcripts for expression repression via the mRNA cleavage-directed mechanism of RNA silencing, with the production of miR160 thought to be solely mediated by the canonical DCL1/DRB1 partnership (Eamens et al. 2009). Although the miR160 sRNA directs the regulation of auxin responsive gene expression, the three distinct loci from which miR160 precursor transcripts are transcribed, *MIR160A*, *MIR160B*, and *MIR160C*, are not themselves regulated by auxin (Mallory et al. 2005). miR160 only targets *ARF10*, *ARF16*, and *ARF17* for expression repression. The exclusive nature of this relationship indicates an absolute need in plant development for tight posttranscriptional control of this subclade of *ARF* genes.

Plants harbouring deleterious mutations in *ARF10*, *ARF16*, and *ARF17* (*arf10*, *arf16*, and *arf17* mutants respectively), or combinations thereof, exhibit root architecture phenotypes characterised by a loss of primary root gravitropic growth, loss of lateral roots, and loss of root hairs on both primary and lateral roots (Wang et al. 2005). Furthermore, the constitutive overexpression of a miR160 precursor sequence induces the expression of similar root growth architectural defects to those displayed by *arf10*, *arf16*, and/or *arf17* plants (Wang et al. 2005). The relationship between miR160, the three *ARF*s targeted by miR160 (*ARF10*, *ARF16*, and *ARF17*), and auxin accumulation was further confirmed when the m*ARF16* transgene, a miR160-resistant version of ARF16, was expressed *in planta*. In the m*ARF16* transformant line, an increase in both the numbers of lateral roots, and primary and lateral root hairs, was observed (Wang et al. 2005). While these studies primarily focused on the effects of the molecular manipulation of the miR160/*ARF10*/*ARF16*/*ARF17* expression module, a suite of genes under posttranscriptional control of a single sRNA species, a clear phenotypic consequence on lateral root development to altering this miRNA/target gene expression module is apparent.

Repeated and elegant demonstrations have been made that highlight the importance of the auxin pathway, and sRNA-directed regulation of the protein machinery that mediate functional roles in the auxin pathway, to plant organ development and responses to environmental stress. The documented interplay between sRNA-directed posttranscriptional expression regulation, and auxin transport and signalling considered thus far, shows that both pathways are integral to the adaption of plants to their changing abiotic environment, and at each stage of plant development. By studying the miR160/*ARF10*/*ARF16*/*ARF17* expression module in a range of genetic backgrounds with altered sRNA or auxin environments, it is suggested that significant advancements to our current understanding of the role of sRNA-mediated gene expression regulation and auxin signalling and transport could be made.

1.4 Study aims, objectives, and hypotheses

In plants, sRNAs have been demonstrated to regulate all aspects of development including organ shape, architecture, and polarity, as well as vegetative phase change and flowering time (Kinoshita et al. 2012; Mallory et al. 2004; Nikovics et al. 2006; Raman et al. 2008; Wang et al. 2005). These small regulatory RNAs have also been shown to mediate plant responses to hormonal signals, adaption to environmental stress, and defence against mobile endogenous or invading exogenous nucleic acids, to maintain genome integrity (Matsui et al. 2013; Navarro et al. 2006; Rand et al. 2005; Tagami et al. 2007; Windels and Vazquez 2011). Auxin is an absolutely crucial phytohormone that regulates diverse aspects of plant growth, including organ architecture and patterning, vascular development, vegetative phase change, the defence against invading pathogens, and the ability of a plant to adapt to environmental stress (Bainbridge et al. 2008; Krizek 2011; Kazan and Manners 2009; Zhao 2010). The overarching aim of this project was to characterise sRNA-directed, auxin-mediated control of organ development with a primary focus on root architecture. From preliminary analyses, the *Arabidopsis* miR160/*ARF10*/*ARF16*/*ARF17* expression module was identified as an ideal candidate to molecularly manipulate in genetic backgrounds defective in the activity of protein machinery known to be required for sRNA production, namely the molecular manipulation of the miR160/*ARF10*/*ARF16*/*ARF17* expression module in the *drb1* and *drb2* mutant backgrounds. It was hypothesised that such an approach would advance our current knowledge of auxin-mediated responses in root development.

Aim 1 - To establish the degree of small RNA-mediated regulation of the expression of auxin pathway genes.

Aim 2 - To assess the phenotypic differences, and to determine molecular changes in *ARF10*, *ARF16*, and *ARF17* gene expression and miR160 accumulation in the root tissue of wild-type *Arabidopsis* plants (ecotype, Col-0), and knockout insertion mutant lines, *drb1*, *drb2*, and *drb1 drb2* (referred to as *drb12* from herein), both in the presence and absence of exogenously applied auxin.

Aim 3 - To assess phenotypic differences, and to determine molecular profile changes in miR160 resistant version of target genes *ARF10* and *ARF16*, and in *MIR160B* precursor overexpression lines generated in wild-type *Arabidopsis* plants, and the *drb1* and *drb2* mutant backgrounds.

Aim 1: To establish the degree of small RNA-mediated regulation of the expression of auxin pathway genes.

Background

A comprehensive list of auxin pathway genes, including *ARF1* to *ARF23, Aux/IAA1* to *Aux/IAA20* and *Aux/IAA26* to *Aux/IAA34*, *TIR1* and *AFB1* to *AFB5* was compiled. In addition, a search of available literature on other auxin pathway genes, outside of these three main gene families, was conducted. This identified 12 additional 'putative' genes of interest, including *ASK1* and *ASK2*, *SGT1b*, *RBX1*, *ABP1*, *ATRMA2*, *GH3.3*, *BIG*, *PINOID*, *WAG1* and *WAG2*, and *RCN1*. Combined, these two lists comprised a total of 69 genes for initial bioinformatic investigation by degradome analysis. In this analysis, a database of truncated cleavage products of known genes can be mapped to the individual transcript nucleotides of cleavage. This data set is generated by searching for cleaved ends that map to each of these transcripts of interest. Degradome patterning can reveal the identity of the class of sRNA species potentially targeting a particular gene transcript. Subsequent assessment to map all known plant sRNA sequences to the same sequences of interest in order to determine if there was any correlation between the mapping of cleaved ends to the target sequence of a mapped sRNA.

Aim 2: To assess the phenotypic differences, and to determine molecular changes in *ARF10*, *ARF16*, and *ARF17* gene expression and miR160 accumulation in the root tissue of wild-type *Arabidopsis* plants (ecotype, Col-0), and knockout insertion mutant lines, *drb1*, *drb2*, and *drb12*, both in the presence and absence of exogenously applied auxin.

Background

Previous research by Eamens and colleagues (2012a) has shown that processing of precursor transcripts encoded by *Arabidopsis* loci *MIR160A*, *MIR160B*, and *MIR160C*, and the accumulation of the resulting sRNA, miR160, requires the activity of both DRB1 and DRB2. Furthermore, previous research has shown that *Arabidopsis* plants molecularly modified to have altered miR160 abundance, or *ARF10*, *ARF16*, and *ARF17* expression, display altered lateral root architecture (Wang et al. 2005). In addition to their involvement in miR160 production, Eamens et al. (2012) have shown that DRB1 and DRB2 are required for the production of multiple miRNA species in *Arabidopsis* and due to these significant changes in sRNA abundance, the *drb1* and *drb2* mutant plants display altered lateral root phenotypes.

Considering the importance of sRNA regulation and auxin signalling during plant development, both individually and in combination with each other, together with the findings presented in the Eamens et al. (2012) and Wang et al. (2005) studies, changes in *ARF10*, *ARF16*, and *ARF17* expression and miR160 abundance and overall shoot and root architecture of *drb1*, *drb2*, and *drb12* plants, were expected to occur upon exogenous auxin application.

Aim 3: To assess phenotypic differences, and to determine molecular profile changes in miR160 resistant version of target genes *ARF10* and *ARF16*, and in *MIR160B* precursor overexpression lines generated in wild-type *Arabidopsis* plants, and the *drb1* and *drb2* mutant backgrounds.

Background

To further experimentally validate the role(s) of *ARF10* and *ARF16*, and the targeting sRNA, miR160, during auxin-controlled shoot and root development, it was necessary to molecularly modify the expression of *ARF10* and *ARF16* via two transgene-based approaches. These were, (1) the overexpression of the *MIR160B* precursor transcript that target *ARF*s, *ARF10*, *ARF16*, and *ARF17*, and; (2) making miR160-resistant versions of *ARF10* and *ARF16* to relieve these two miR160 target genes of their expression repression by the miR160 sRNA. The resulting three transgenes were inserted into plant expression vectors and introduced into wild-type *Arabidopsis* plants and the *drb* single mutants, *drb1* and *drb2*, via standard *Agrobacterium tumefaciens*-mediated transformation. It was predicted that manipulation of *ARF10* and *ARF16* expression in these three plant lines via this approach would allow for the molecular deconstruction of the miR160/*ARF10*/*ARF16*/*ARF17* expression module. That is, (1) determination of the requirement of either DRB1 or DRB2 for miR160 liberation from the precursor transcripts, *PRI-MIR160A*, *PRI-MIR160B*, and *PRI-MIR160C*, and; (2) the mechanism of miR160-directed RNA silencing of *ARF10*, *ARF16*, and *ARF17*, mediated by either the DRB1- or DRB2-dependent pathways.

Chapter 2

Methods and Materials

2.1 Plant material

2.1.1 Plant lines

For all experimental analyses performed, *Arabidopsis* (ecotype, Columbia-0; Col-0), was used as the wild-type control. The T-DNA insertional mutants in each of the *DRB* loci assessed in this study have been described previously in Curtin et al. (2008) or Eamens et al. (2012a) and included the single mutant lines, *drb1-1* (SALK_064863), *drb2-1* (GABI_348A09), *drb3-1* (SALK_003331), *drb4-1* (SALK_000736), and *drb5-1* (SALK_031307), and the double mutant lines, generated via a standard genetic crossing approach, *drb1-1 drb2-1* (*drb12*), *drb1-1 drb4-1* (*drb14*), and *drb2-1 drb4-1* (*drb24*). In addition to Col-0 plants and the *drb* mutant lines described previously (Curtin et al. 2008; Eamens et al. 2012b), nine novel *Arabidopsis* plant lines were generated in this study to address specific experimental aims. These lines included miRNA-resistant versions of *ARF10* and *ARF16*, and a miR160 overexpression line of *MIR160B*. The expression of the miRNA resistant *ARF* (m*ARF*) transgenes and that of the *MIR160* overexpression transgene was driven by the native promoter of each *ARF* gene and the 35S promoter of the *Cauliflower mosaic virus* (CaMV), respectively. All three generated plant expression vectors were introduced into the Col-0, *drb1*, and *drb2* backgrounds via a standard *Agrobacterium tumefaciens*-mediated transformation approach (outlined in **Section 2.1.3** *below*). The homozygosity of all single and double *drb* mutants was verified via standard PCR-based genotyping, and the number of individual insertion events of each of the generated m*ARF* or *MIR160* transformant lines was determined via identifying transformant lines that segregated on selective media at the desired 3:1 ratio in the T_2 generation. All PCR primers (DNA oligonucleotides) used for transgene construction or genotyping are listed in **Appendix 1**.

2.1.2 Growth conditions

Prior to placing seeds on selective or standard plant growth media, seeds were exposed to chlorine gas ($Cl_{2(g)}$), generated by mixing 97 mL 4.2% (w/v) sodium hypochlorite bleach (WhiteKing) with 3 mL 16 M $HCl_{(aq)}$, for 100 min for surface sterilisation. After surface sterilisation, seeds were very carefully spread out onto full strength Murashige and Skoog (MS) plant growth media (for preparation see **Appendix 2**) containing 1% (w/v) sucrose and 0.8 % (w/v) agar (Becton, Dickinson and Co.) in a biosafety cabinet. Each media plate was then sealed with parafilm tape, covered with aluminium foil, and stratified at 4ºC for 48 h. Following

stratification, the plates containing the sterilised seeds were transferred to an environment-controlled growth cabinet and cultivated under long day conditions of 16 h light and 8 h dark at 100-150 µmol m^{-2} s^{-1}. Further, the day/night temperature of the environment-controlled growth cabinet was set to 22/18ºC. After 10 d cultivation under the specified conditions, seedlings were transferred to new MS media plates that were orientated vertically for all phenotypic and molecular characterisation. It is important to note, however, that for the selection of transformant lines MS media plates that contained the appropriate selective agent were cultivated in a horizontal orientation only.

Col-0, *drb1*, and *drb2* plants that were used for the *Agrobacterium*-mediated transformation procedure were sown directly onto soil and following 48 h at 4ºC for stratification, soil-grown plants were cultivated in the same environment-controlled growth cabinets and under the same growth conditions as outlined for growth of *Arabidopsis* on MS media.

2.1.2.1 Exogenous auxin treatments

Following 10 d of cultivation on full strength MS media plates, Col-0, *drb1*, *drb2*, and *drb12* seedlings were transferred to fresh MS media plates that contained either 0.0, 0.1, 1.0, or 10 µM, experimentally determined to provide the most informative concentration range for observing phenotypic and molecular changes, of the synthetic auxin 2,4-dichlorophenoxyacetic acid (2,4-D) (Sigma Aldrich). 2,4-D was selected as an appropriate synthetic auxin substitute as it is light stable. The plates were sealed with parafilm and returned to the environment-controlled growth cabinet where the plates were orientated vertically. Following exposure to the synthetic auxin for 24 h, plants were returned to fresh, standard MS media plates and cultivated vertically for an additional 12 d period under standard growth conditions.

2.1.3 *Agrobacterium tumefaciens*-mediated transformation of *Arabidopsis thaliana* via floral dipping

Forty millilitre (40 mL) cultures of *Agrobacterium tumefaciens* (*Agrobacterium*; strain GV3101), cultured at 28ºC at 180 rpm for 18 h, harbouring each plant expression vector of interest were centrifuged at 4000 rpm for 15 min at 4ºC to pellet the bacterial cells. The resulting supernatants were discarded, and the pellets resuspended in 40 mL of Milli-Q water (MQ-H_2O) with 5% (w/v) sucrose via careful pipetting. Mature *Arabidopsis* plants with

primary inflorescences that had unopened floral buds were dipped in the *Agrobacterium* resuspensions for 30 s. Each dipped plant was wrapped in cling film and incubated at room temperature in the dark for 24 h. The cling film was then removed, and the dipped plants transferred to the environment-controlled growth cabinet and cultivated under standard growth conditions to allow for the production, and subsequent collection, of putatively transformed seed.

2.1.4 Selection of plant lines harbouring introduced plant expression vectors

Seed (T_1 seed) of plant lines Col-0, *drb1*, and *drb2* putatively transformed with the generated m*ARF* or *MIR160* plant expression vectors were surface sterilised with Cl_2 gas and plated out onto solid MS media containing 5.0 µg/mL of the selective agent glufosinate ammonium (Sigma Aldrich), and 150 µg/mL of timentin (PhytoTechnology Laboritories) to remove any unwanted residual *Agrobacterium* that may have remained following surface sterilisation. Selection plates were again sealed with parafilm, covered in aluminium foil, and then stratified at 4^{o}C for 48 h. Following stratification, the selection plates were transferred to environment-controlled growth cabinets and cultivated under standard growth conditions for 14 d. The selection plates were then visually screened for seedlings that were of normal size and that developed healthy green coloured rosette leaves. Such plants were transferred back to standard MS media plates that did not contain selection and cultivated for an additional 7 to 10 d to ensure each plant had fully recovered from the selection process. At this stage, T_1 plants (**Appendix 6)** were transferred to soil and cultivated to maturity to allow for T_2 seed collection. In the T_2 generation (**Appendix 7**), a known number of seeds for each plant line were plated out on solid MS media that contained the selective agent (5.0 µg/mL glufosinate ammonium) and only plant lines returning the desired segregation ratio of 3:1 were selected for further analysis as such plant lines were assumed to harbour a single transgene insertion. Single transgene insertion lines were returned to standard MS media for a 7 to 10 d period to recover and then these plants were transferred to soil and cultivated to maturity to allow for the collection of T_3 seeds (phenotypic and molecular analyses were conducted in the T_3 generation).

2.2 Bioinformatics

2.2.1 Degradome analysis

Analysis of the *Arabidopsis* degradome was conducted using the SoMART dRNA mapper, an online tool that enables users to map RNA cleavage products onto their transcript sequences of interest to identify target genes potentially under sRNA-directed expression regulation (Li et al. 2012). For each transcript of interest analysed, the generated output was received in an appropriate format for direct importation into Microsoft Excel. This allowed for simple visualisation of the number of cleaved ends mapping, in both the sense and antisense orientation, to each nucleotide of the assessed transcript. Using the graphing tool of Microsoft Excel, mapped reads were used to graph the number of total cleaved ends at each nucleotide, against the total number of cleaved ends for the entire length of the analysed transcript. This was done to identify a putative; (1) miRNA target transcript (a single defined peak to which all aligned cleaved ends mapped); (2) siRNA target transcript (many, small cleavage peaks running along the entire length of the assessed transcript); or (3) no target transcript that is not under miRNA- or siRNA-directed expression regulation (no cleavage peaks identified for the assessed transcript).

2.2.2 sRNA mapping

Bioinformatic assessment of the global sRNA population was next assessed using the online software, PatMaN (Prufer et al. 2008). The global sRNA populations of *Arabidopsis* plant lines, Col-0, *drb1*, and *drb2* (stored online as individual datasets) were obtained from the Gene Expression Omnibus (https://www.ncbi.nlm.nih.gov/geo) and compared against transcripts of either confirmed sRNA target genes (confirmed in previous studies), or putative sRNA target genes identified in this study (*see* **Section 1.4** Aim 1). The mapping of each sRNA read was solely determined by sequence homology between the mapped sRNA and the sequence of the target gene under assessment. In addition, the number of times each sRNA read mapped to an assessed transcript was also determined using this approach, and graphically this data was presented as the total number of aligned reads against the position along the assessed transcript. Graphs were again generated using the graphing tool of Microsoft Excel.

2.2.3 Promoter analysis

In silico screening of gene promoter regions was conducted using three online programs, these being;

(1) PlantCARE (bioinformatics.psb.ugent.be/webtools/plantcare/html/);

(2) PLACE (www.dna.affic.go.jp/PLACE), and;

(3) AtcisDB (agris-knowledgebase.org/ AtcisDB/).

Further, the promoter region of a gene under assessment was defined in one of the following ways; (1) previously reported in the literature; (2) the region that lies 3.0 kilobase (kb) immediately upstream of the start codon of the assessed gene, or; (3) the immediate region upstream of the start codon of the assessed gene until the next preceding gene end was encountered, if less than 3.0 kb. The output generated by each of these three programs was next searched specifically for known '*Auxin Response Elements*' (*ARE*s), DNA based sequences known to attract DNA binding proteins that perform a functional role in the auxin response pathway.

2.3 Phenotypic assessments

2.3.1 Leaf surface area

Plant images were captured using a Canon IXUS 801S digital camera with a 4 cm^2 red calibration square included. Images with the calibration square were loaded into the software, Easy Leaf Area V2 (www.plant-image-analysis.org/software/easy-leaf-area). Easy Leaf Area V2, via use of the calibration square, subsequently determined the number of green pixels, which corresponds to leaf surface area in each image to provide a final surface area measurement in cm^2. Three biological replicates with six technical replicates per biological replicate were used for these analyses.

2.3.2 Primary root length and lateral/adventitious root number

Images captured, as per **Section 2.3.1**, of whole plants were loaded into ImageJ with length calibration included. In ImageJ, the number of pixels corresponding to 1.0 cm was determined and the 'free hand' tool used to trace the primary root of each plant. This allowed the ImageJ software to calculate a final measurement in centimetres for the primary root. The number of lateral roots, and adventitious roots, was counted manually using the same images that were loaded into ImageJ. Three biological replicates with six technical replicates per biological replicate were used for these analyses.

2.4 Molecular biology techniques

2.4.1 Genomic DNA isolation

Fresh rosette leaf material was harvested from each plant line of interest and transferred to a labelled 1.5 mL microfuge tube, the tubes were capped and immersed in liquid nitrogen. For each sample, the collected tissue was ground into a fine powder with a plastic micropestle under liquid nitrogen. Next, 250 µL of pre-warmed (65ºC) CTAB buffer was added (see **Appendix 2** for preparation), the tubes capped, and incubated at 65ºC for 30 min, with vigorous vortexing every 10 min, to assist the cell lysis process. Samples were transferred to ice and incubated for 2 min. Two hundred microliters of chloroform was added, the tubes capped, and then shaken by hand for 15 s. Tubes were incubated for 3 min and then centrifuged at 13 200 rpm for 10 min at room temperature. Two hundred microlitres of upper aqueous phase was transferred to a new, labelled 1.5 mL microfuge tube that contained 200 µL of 100% isopropanol. Samples were mixed by hand inversion (20 times) and then centrifuged at 13 200 rpm for 10 min, at room temperature. The resulting supernatants were discarded and 500 µL of 70% (v/v) ethanol added to the visible pellets. Tubes were capped, and the pellets washed via hand inversion (20 times) and centrifugation at 9000 rpm for 7 min, at room temperature. The wash was pipetted off the pellets and discarded and the pellets air-dried at RT for 20 min. The DNA pellet was resuspended in 50 µL of MQ-H_2O and samples stored at -20ºC until required for use.

2.4.2 Polymerase chain reaction (PCR)

PCR reactions typically contained 1 unit (U) of Taq DNA polymerase (NEB), 1 X ThermoPol Reaction Buffer (NEB), 200 µM of dNTP mix, 4.5 µM $MgCl_2$, 200 nM of each primer, and 1.0 µL of template DNA made to a usual final reaction volume of 10 µL. Thermal cycling conditions were as follows: Initial denaturation at 95ºC for 2 min, followed by 35 cycles of; (i) denaturation at 95ºC for 30 sec; (ii) annealing at 60ºC for 40 sec, and; (iii) elongation at 68ºC for 1 min per kilobase of DNA being amplified. A final termination cycle at 68ºC for 10 min, was also performed. Each pair of primers was designed to have an optimal annealing temperature of 60ºC. However, this was not always possible and, therefore, annealing temperatures in addition to 60ºC were also routinely used for PCR product amplification in this study.

2.4.3 Gel electrophoresis

Generally, 1% (w/v) agarose gels were prepared in 1 X Tris borate EDTA (TBE) buffer (*see* **Appendix 2** for preparation). Agarose (Bioline) gels were polymerised in the presence of 100 µg/L ethidium bromide (Sigma Aldrich) for subsequent visualisation of separated nucleic acids. Samples were loaded into the lanes of a polymerised gel after being diluted with 6 X loading dye (Bioline). Electrophoresis was carried out at approximately 10 V/cm gel. At the completion of electrophoresis, gels were visualised under UV light in a Bio-Rad Gel Doc system.

2.4.5 RNA isolation

Plant material for RNA isolation was harvested, immediately placed in aluminium foil packets, and snap frozen in liquid nitrogen. All plant material was stored at -80^{o}C until required for use. Frozen tissue was ground into a fine powder in a ceramic mortar and pestle, transferred to a pre-chilled microfuge tube, and 500 µL of TRIzol Reagent (Thermo Fisher) was added to the top of the powder. The frozen powder was allowed to thaw and dissolve into the TRIzol reagent via incubation of the capped tube at room temperature for 5 min. Once all samples had been processed, 200 µL chloroform was also added, the tubes capped and vigourously shaken by hand for 15 s. The samples were then incubated at room temperature for 3 min. After this incubation period, the tubes were centrifuged at 13 200 rpm for 10 min, at room temperature. Approximately 500 µL of the RNA containing upper aqueous phase was transferred to a new, labelled 1.5 mL microfuge tube and an additional 200 µL chloroform was added. The tubes were capped, and hand shaken for 15 s, and then incubated for 3 min at room temperature. The tubes were again centrifuged at 13 200 rpm for 10 min, at room temperature and the resulting upper aqueous phase transferred to a new, labelled 1.5 mL microfuge tube that contained 500 µL of ice-cold isopropanol. Each tube was capped and inverted by hand 20 times and then incubated at -20^{o}C for 16 h. Following the -20^{o}C incubation, sample tubes were centrifuged at 13 200 rpm for 20 min, at 4^{o}C. The resulting supernatant was carefully removed by pipetting and discarded. The RNA pellets, whether visible or not, were washed once via the addition of 500 µL of 75% (v/v) ethanol, hand inverted (20 times), and centrifuged at 9000 rpm for 7 min at room temperature. The wash solution was carefully removed via pipetting and the tubes were pulse spun to return the residual ethanol to the bottom of the tube. The residual wash was carefully removed via pipetting and the RNA pellet air-dried for exactly 5 min at room

temperature. Following air-drying, pellets were resuspended in 20 µL of RNase-free H_2O. The sample tubes were also incubated at 65ºC for 15 min, and then the RNA resuspended via careful manual pipetting. The RNA concentration of each total RNA extraction was determined using a NanoDrop spectrophotometer with absorbance measured at 260 nm. Concentration was calculated automatically by the NanoDrop using Beer Lambert's Law ($A_{260} = \varepsilon lc$); where A_{260} = absorbance at 260 nm, ε = molar absorptivity (L mol^{-1} cm^{-1}), l = path length (cm), and c = concentration (mol L^{-1}). All total RNA samples were also visualised via agarose gel analysis (**Section 2.4.3**) to ensure that each sample was free of degradation. RNA samples were stored at -20ºC until required for subsequent analysis.

2.4.6 DNase treatment and RNA clean-up

Prior to cDNA synthesis, 1.5 µg of total RNA was treated with DNase to ensure that each sample was free of genomic DNA contamination. Typically, the 1.5 µg of total RNA was diluted to 100 ng/µL in 15 µL of RNase-free H_2O (Promega) in a 1.5 mL microfuge tube. To each tube, 5 U of DNase I (New England Biolabs), 10 µL of 5 X DNase I buffer, and 1 U of RNasin (RNase Inhibitor, Murine; New England Biolabs), and the final reaction volume made up to 50 µL with RNase-free H_2O. The components of each reaction tube were carefully mixed by pipetting and then the reaction incubated at 37ºC for 40 min. The reaction was next terminated via a 10 min incubation on ice. All DNase-treated RNA (dtRNA) was then immediately purified using an RNeasy Mini Kit according to the manufacturer's instructions (QIAGEN), and the final pellet resuspended in 20 µL of RNase-free H_2O. Samples were stored at -20ºC until required for use.

2.4.7 First strand complementary DNA synthesis

First strand complementary DNA (cDNA) synthesis was carried out using ProtoScript® II reverse transcriptase (New England Biolabs) according to the manufacturer's instructions. Each reaction was comprised of: 200 U of ProtoScript® II reverse transcriptase, 1 X ProtoScript® II buffer (New England Biolabs), 10 mM DTT (New England Biolabs), 500 µM dNTPs, 5.0 µM oligo $dT_{(18)}$, 1.0 U RNasin (RNase inhibitor, Murine; New England Biolabs), and 1.0 µg of dtRNA (*see* **Section 2.4.6**). Initially, and to denature all of the nucleic acids in the cDNA synthesis reaction, the dtRNA, oligo $dT_{(18)}$, and dNTPs were mixed together

and incubated at 55ºC for 10 min, and then immediately snapped on ice and incubated for 5 min. After cooling, the remaining reaction components were added to the reaction tube, carefully mixed by pipetting, and then the final reaction mixture was incubated at 42ºC for 1 h. All reaction tubes were then transferred to and incubated on ice for 5 min. An additional 30 µL of RNase-free H_2O was added to each reaction tube, the reaction components mixed by careful pipetting and the resulting cDNA preparations stored at -20ºC until required for use.

2.4.8 Stem-loop primer complementary DNA synthesis

Stem-loop primer cDNA synthesis reactions contained the following components: 40 U of ProtoScript® II reverse transcriptase (New England Biolabs), 1 X ProtoScript® II buffer, 500 µM dNTPs, 1.0 µM stem-loop primer (primer sequence specific to the small RNA under analysis), 10 mM DTT, 1.0 U RNasin (RNase inhibitor, Murine; New England Biolabs), and 250 ng of total RNA. The final reaction volume was made up to 20 µL with RNase-free H_2O. Reactions were cycled as follows: 1 x 16ºC/30 min, 60 x 30°C/30 s, 42°C/30 s, 50°C/2 s, and 1 x 85°C/5 min. Following synthesis, all stem-loop primer cDNAs were stored at -20ºC until required for use.

2.4.9 Quantitative reverse-transcriptase PCR analysis

All RT-qPCR analyses were performed in 10 µL reaction volumes and were prepared on ice using a Rotor-Disc 100 (Qiagen) ring. Each 10 µL RT-qPCR reaction contained 1 X GoTaq® qPCR Master Mix (Promega), 200 nM of each primer (**Appendix 1**), and 110 ng of cDNA for a standard RT-qPCR run, or 75 ng of stem-loop primer synthesised cDNA for the quantification of sRNA abundance. Reactions were performed using three biological replicates and two technical replicates were performed per biological replicate. A Rotor-Gene 6000 (Qiagen) was used for all RT-qPCR assessments, and the cycling conditions were as follows: 1 x 95ºC/2 min, 40 x 95ºC/10 s, and 60ºC for 30 s. A melt cycle was performed after each amplification; starting at 72°C and increasing 1°C per cycle to 85°C. Expression fold changes were determined using the $2^{-\Delta\Delta Ct}$ method normalised to the values obtained for wild-type *Arabidopsis* (Col-0). In all RT-qPCR experiments, the *ELONGATION FACTOR1-α* (*EF1-α*; *AT5G60390*) transcript was used as the internal reference for the normalisation of the quantification of mRNA transcript abundance and the small nucleolar RNA, snoR101, was used as the internal reference to normalise the quantification of sRNA abundance. Reference gene primer sequences can be found in **Appendix 1**.

2.5 Bacterial cloning for plant expression vector construction

2.5.1 Gene of interest sequence isolation or synthesis

The DNA sequences corresponding to the precursor transcript sequences of *PRI-MIR160B* was amplified from wild-type *Arabidopsis* (Col-0) genomic DNA via a standard PCR-based approach using the GoTaq® Long PCR Master Mix (Promega) protocol. Additionally, the DNA sequences that represented the promoter regions of the miR160 target genes, *ARF10* and *ARF16*, were also amplified from wild-type *Arabidopsis* (Col-0) genomic DNA via a standard PCR-based approach using the GoTaq® Long PCR Master Mix (Promega) protocol. The promoter region sequence for *ARF10* has been reported previously (Mallory et al. 2005; Wang et al. 2005). In addition, a 2.0 kb fragment immediately upstream of the *ATG* start codon of the *ARF16* locus was selected for PCR-based amplification to represent the *ARF16* promoter region. The sequence of each primer used in these reactions is provided in **Appendix 1** and the restriction endonuclease restriction sites included at the 5' terminus of each primer are listed in **Table 2.1**.

Table 2.1. Restriction sites synthetically added to genomic sequences of *miR160B* precursors, and *ARF10* and *ARF16* promoters. Restriction endonuclease cleavage sites were synthetically added to the 5' and 3' ends of *miR160* precursor and *ARF10/16* promoter sequences isolated from Col-0 genomic DNA. These sites were subsequently used to ligate these transcripts into destination vectors.

Isolated sequence	Forward Primer restriction endonuclease site	Reverse primer restriction endonuclease site
PRI-MIR160B	*Xho*I	*Bam*HI
*ARF10*pro	*Xho*I	*Bam*HI
*ARF16*pro	*Xba*I	*Xho*I

The miR160-resistant versions of the *ARF10* and *ARF16* (termed m*ARF10* and m*ARF16*, respectively) transcripts were synthesised by the commercial supplier of synthetic nucleic acids, GenScript (sequence information see **Appendix 3**). Each m*ARF* sequence was delivered in the pUC57 bacterial vector (**Table 2.3**) Further, for subsequent bacterial cloning, each m*ARF* sequence was designed to harbour a specific restriction endonuclease site at both

the 5' and 3' terminus of the synthesised sequence (**Table 2.2**). Following restriction endonuclease cleavage to release each m*ARF* fragment, the resulting restriction fragments were cloning into the similarly digested cloning vector, pGEM®-T Easy (*see* **Table 2.3**).

Table 2.2. Restriction sites synthetically added to miR160-resistant *ARF10* and *ARF16* transcripts. Restriction endonuclease cleavage sites were synthetically added to the 5' and 3' ends of -resistant *ARF10/16* transcript sequences synthesised *in vitro*. These sites were subsequently used to ligate these transcripts into destination vectors.

miR160 target gene synthesised	**5' restriction endonuclease site**	**3' restriction endonuclease site**
m*ARF10*	*Sal*I	*Kpn*I
m*ARF16*	*Eco*RI	*Sal*I

2.5.2 Plant expression vector construction

Transgenic constructs were generated using two main techniques: (1) restriction endonuclease digestion, and (2) subsequent restriction fragment ligation. Restriction endonuclease digestions were performed using New England Biolabs restriction endonuclease under the conditions recommended by the manufacturer for each enzyme. All restriction fragments were purified by isopropanol precipitation. Isopropanol precipitation was conducted via the addition of 10 µL of 3.0 M ammonium acetate to each digestion reaction followed by the addition of 0.6 volumes of 100% isopropanol. The tubes were mixed by inversion (20 times) and DNA pelleted by centrifugation at 4ºC at 13 200 rpm for 30 min. The resulting supernatants were removed by careful pipetting and discarded. The remaining visible pellets were washed via the addition of 1.0 mL of 70% ethanol, hand inversion (20 times), and centrifugation at 13 200 rpm for 15 min at room temperature. The wash was removed and discarded, and the pellets were air-dried at room temperature for 20 min, before being resuspended in 20 µL of MQ-H_2O. In the instance of a vector backbone (destination vector) being digested with a single restriction endonuclease, the resulting vector fragment was subsequently treated with calf intestinal alkaline phosphatase (CIAP) (New England Biolabs) according to the manufacturer's instructions. Purified digest products were ligated into destination vectors using T4 DNA ligase (Promega). Digest products and destination vectors were mixed in an 8:1 (v/v) ratio and incubated at room temperature for 18 hours. Ligation products were then transformed into

either *E. coli* competent cells. Plasmids either used, or generated in this study, are presented in **Table 2.3**.

Table 2.3. Plasmid vectors used in this study.

Plasmid	Features	Reference
pGEM-T Easy	Cloning vector	Promega
pUC57	Delivery vector	Genscript
pART7	Primary cloning vector for *MIR160B* precursor manipulation, contains CaMV:35S promoter, multiple cloning region and OCS terminator. All three features can be removed with one single *NotI* digest. Has ampicillin resistance marker.	(Gleave 1992)
pBART	Binary vector for use in *Agrobacterium* transformation of plants. Contains a single *NotI* restriction site for compatibility with pART7. Has spectinomycin selectable marker for bacteria, and PPT (Basta) for *in planta* selection.	(Gleave 1992)
pORE1	Primary cloning vector for m*ARF10*, and m*ARF16* manipulation. A binary vector with multiple cloning region and OCS terminator, for use in both bacteria and *Agrobacterium* plant transformation. Has kanamycin selectable marker for bacteria, and Basta for *in planta* selection.	(Coutu et al. 2007)

pARF10prom:m*ARF10*	The *ARF10* promoter was amplified (sequence listed in **Appendix 1**) and cloned into pGEM-T Easy. It was digested from here with *XhoI* and *BamHI* and ligated into pORE1. Following promoter insertion, the synthesised m*ARF10* transcript was digested from pUC57 with *SalI* and *KpnI* and ligated into pORE1 downstream of its endogenous promoter.	This study
pARF16prom:m*ARF16*	The *ARF16* promoter was amplified (sequence listed in **Appendix 1**) and cloned into pGEM-T Easy. It was digested from here with *XbaI* and *XhoI* and ligated into pORE1. Following promoter insertion, the synthesised m*ARF16* transcript was digested from pUC57 with *EcoRI* and *SalI* and ligated into pORE1 downstream of its endogenous promoter.	This study
p35S:*PRI-MIR160B*	The *PRI-MIR160B* sequence was amplified and cloned into pGEM-T Easy. *XhoI* and *BamHI* were used to digest *PRI-MIR160B* from pGEM-T Easy and ligate into pART7. *NotI* was used to digest *PRI-MIR160B* from pART7 and ligate into pBART.	This study

2.5.3 *Escherichia coli* and *Agrobacterium* transformation techniques

Plant expression vectors (**Section 2.5.2**) that were prepared during the bacterial cloning-based construction steps were transformed into *Escherichia coli* (*E. coli*; DH5α strain) competent cells upon completion. Typically, a 2.0 µL aliquot from a 10 µL ligation reaction was incubated in the presence of a 50 µL aliquot of heat-shock competent *E. coli* cells on ice, for 30 min. At the end of this incubation period, the competent cell/ligation product mixture was incubated at 42ºC for 1 min, and then transferred back to ice and incubated for 2 min. Next, 1.0 mL of Luria-Bertani (LB) liquid media was added to each bacterial cell suspension and the suspension incubated at 37ºC on a shaking platform (at 200 rpm) for 1 h. The cell

suspensions were then spread onto solid LB media plates that contained the appropriate selection (**Table 2.4**). Following a 16 h, 37ºC incubation, resistant colonies were screened by PCR to identify positive transformants. Positive colonies were used to seed 10 mL LB liquid media cultures that were incubated for 16 h at 37ºC and post this incubation the plasmid DNA was recovered using a QIAprep Spin Miniprep kit (QIAGEN) according to the manufacturer's instructions.

Table 2.4. Selection markers for vectors used to generate transgenic plant lines. During bacterial and *in planta* positive transformants identifications processes selectable markers were utilised to assist in this identification. Listed below are the selectable markers and concentrations used, relevant to each plasmid and organism of selection.

Construct backbone	Bacterial selection	*In planta* selection
pGEM-T Easy	100 µg/mL ampicillin	N/A
pUC57	100 µg/mL ampicillin	N/A
pART7	100 µg/mL ampicillin	N/A
pBART	50 µg/mL spectinomycin	5 µg/mL glufosinate ammonium
pORE1	50 µg/mL kanamycin	5 µg/mL glufosinate ammonium

All confirmed plant expression vector preparations were transformed into *Agrobacterium tumefaciens* (*Agrobacterium*; GV3101 strain). Isolated plasmids were incubated in the presence of electro-competent *Agrobacterium* cells before being electroporated. Successfully electroporated cell suspensions were made to 1.0 mL with LB liquid media and incubated at 28ºC on a shaking platform (at 100 rpm) for 4 h. Cell suspensions were spread on solid LB media plates, containing 25 µg/mL rifampicin in addition to the selective agent appropriate to each plant expression vector (**Table 2.4**). The solid LB media plates were incubated at 28ºC for 48 h and resulting positive transformants confirmed at this time using a combination of PCR and restriction enzyme digestion. Finally, confirmed colony transformants were used to seed 40 mL LB liquid cultures for subsequent floral dip transformation of the wild-type *Arabidopsis* (Col-0) plants, and the *drb1* and *drb2* mutant lines (**Section 2.1.3**).

Chapter 3

Determining the small RNA-mediated regulation of auxin pathway gene expression

3.1 Introduction

Polar auxin transport and intracellular auxin perception are vital processes to normal plant development and stress response pathways (Galweiler et al. 1998; Gray et al. 1999; Vernoux et al. 2010; Zhao 2010). Auxin regulated developmental processes include phototropism (Stowe-Evans et al. 2001), gravitropism (Rashotte et al. 2000), and organ patterning (Bainbridge et al. 2008), while auxin signalling has been implicated in influencing drought and salt stress responses in plants (Kazan 2013), as well as protecting against biotic stresses such as those experienced during root pathogen infection (Ghanashyam and Jain 2009). There are a substantial number of genes from a variety of gene families which are either directly, or indirectly, involved in driving these essential auxin signalling processes. In particular, members of the *AUXIN RESPONSE FACTOR* (*ARF*) transcription factor and *AUXIN/INDOLE-3-ACETIC ACID* (*Aux/IAA*) transcriptional regulator gene families, as well as those of the *AUXIN F-BOX* (*AFB*) gene family which encode for proteins that bind intracellular auxin, are central contributors to the specificity of the auxin cellular response in plant cells (Gray et al. 1999; Gray et al. 2001; Ulmasov et al. 1999).

3.1.1 Auxin Response Factors

AUXIN RESPONSE FACTORs are a family of transcription factor proteins that have a range of different functions in plants. In *Arabidopsis*, there are 23 members of the *ARF* gene family, five of which have been determined to encode transcriptional activators (ARF5, ARF6, ARF7, ARF8, and ARF19), and the remainder demonstrated to be transcriptional repressors, except for one pseudo-gene (*ARF23*) (Hagen and Guilfoyle 2002). Each ARF has a specific function in *Arabidopsis* with some ARFs acting in concert with other family members to elicit their biological function. For instance, ARF1 and ARF2 are known to act together to regulate leaf senescence and floral organ abscission (Ellis et al. 2005). ARF3, however, acts in tandem with a non-ARF protein, called KANADI1, to regulate leaf polarity (Kelley et al. 2012). ARF4 has also been shown to play a role in determining organ polarity, including leaf organ polarity (Hunter et al. 2006). A further reduction in lateral organ polarity determination occurs in the *arf3 arf4* double mutant, indicating another shared role for these ARF proteins (Finet et al. 2010). ARF5 is a critical component in initial root formation and embryonic patterning (Hardtke and Berleth 1998). Additionally, ARF7 has been assigned a role in embryonic patterning and the *arf5 arf7* double mutant shows an increased disorganisation of embryonic

development (Hardtke and Berleth 1998). ARF6 and ARF8 share a close relationship, both phylogenetically and functionally, with a demonstrated redundant functional role in flower maturation (Finet et al. 2010). ARF10 and ARF16 have been demonstrated, via phenotyping of the *arf10 arf16* double mutant, to cooperatively influence lateral root formation but neither the *arf10* nor *arf16* single mutant displays this phenotype (Wang et al. 2005). ARF17 is the most closely related ARF family member to ARF10 and ARF16 and has also been shown to influence root development. However, ARF17 does not functionally cooperate with either ARF10 or ARF16 to mediate its role in root development (Wang et al. 2005). Furthermore, ARF17 is one of a sub-class of ARFs that have a truncated DNA binding domain, along with ARF3 and ARF13 (Guilfoyle and Hagen 2007). ARF19 has also been implicated in lateral root formation, similar to the demonstrated role of ARF10 and ARF16, but ARF19 is thought to mediate this role independently of all the other ARFs with the exception of ARF7 (Cho et al. 2014).

Several ARFs remain uncharacterised. No function has, as yet, been described for ARF12, although Northern blot analysis has revealed that the *ARF12* transcript is exclusively expressed in the developing seeds of *Arabidopsis* (Okushima et al. 2005). No function has yet been assigned to ARF13 either, but ARF13 is one of the three ARFs with a truncated C-terminal domain (Hagen and Guilfoyle 2002). As a whole, the *ARF12*, *ARF13*, and *ARF14* transcripts show little to no expression in most *Arabidopsis* tissues and, as such, are thought to play only very minor roles in *Arabidopsis* development under normal growth conditions (Piya et al. 2014). As with *ARF12*, *ARF13*, and *ARF14*, the *ARF20* and *ARF22* loci are not expressed to significant levels under normal growth conditions (Piya et al. 2014). Further, no functional analyses of ARF15, ARF18, or ARF21 have been conducted, and there is no information available to indicate putative biological functions for these three ARFs. Finally, the *ARF23* locus is classed as a pseudogene as this gene does not encode for the crucial domains typical of other ARFs, domains that are necessary for an ARF protein to carry out its transcription factor function (Guilfoyle and Hagen 2007).

ARF proteins function as transcription factors in a diverse range of developmental and stress response processes. Because of the nature of ARF function, it follows that critical signalling response processes must respond sensitively to their own governing regulatory pathways. ARFs must also be equally sensitive during interactions with regulatory proteins and downstream regulatory targets.

3.1.2 Aux/IAA proteins

Unlike ARF proteins, the Aux/IAAs are not transcription factors, but instead act to regulate ARF activity via protein-protein interactions with specific ARFs. The *Arabidopsis Aux/IAA* gene family consists of 29 members. Due to the fluid nature of gene function in different tissues, the Aux/IAAs may heterodimerise with different ARFs, depending on the cellular environment (Piya et al. 2014). Additionally, the expression of individual *Aux/IAA*s is modulated differently, and at specific times, via a cascade of responses to auxin perception by the SCF^{TIR1} complex, the ubiquitin E3 ligase complex formed after auxin interacts with the intracellular auxin receptor protein TIR1 (Park et al. 2002a). Furthermore, some *Aux/IAA* gene promoter regions may be bound by certain ARFs, an interaction that indicates that multiple positive and negative feedback mechanisms and regulatory networks control cellular responses to auxin (Lee et al. 2009). Aux/IAA1 and Aux/IAA2, for example, are thought to be early onset Aux/IAAs involved in constructing some of the regulatory networks present at the beginning of the auxin response induction pathway (Park et al. 2002a).

As previously mentioned, different Aux/IAAs have specific relationships with different ARFs in different tissues. ARF7 function, for example, is regulated by Aux/IAA3 in roots, but ARF7 function is controlled by Aux/IAA19 in *Arabidopsis* shoots (Chapman and Estelle 2009). Aux/IAA4, Aux/IAA5, and Aux/IAA6 also have been identified as mediating roles in the establishment of the early regulatory networks that respond to auxin (Park et al. 2002a), whereas the Aux/IAA7, Aux/IAA17, and Aux/IAA28 proteins are involved in late onset auxin responses and, as such, are highly stable proteins. Furthermore, assessment of the *aux/iaa17* single mutant phenotype implicates this Aux/IAA family member in the regulation of lateral and adventitious rooting in *Arabidopsis* (Worley et al. 2000). A significant level of redundancy occurs within the *Aux/IAA* gene family, as exhibited by the wild-type phenotypes displayed by the *aux/iaa8 aux/iaa9* and *aux/iaa10 aux/iaa11* double mutants (Overvoorde et al. 2005). Such redundancy adds a considerable challenge to attempts at the elucidation of the exact roles of individual Aux/IAA proteins when acting in concert within the cellular auxin signalling system.

Further specific indications of roles for Aux/IAAs have been reported. A documented role in embryo polarity has been assigned to Aux/IAA12 (Stowe-Evans et al. 1998), a role that aligns closely with the known roles for some members of the ARF family, namely ARF3, ARF4, and ARF7. Similarly, Aux/IAA13 is known to associate with ARF5 to influence vascular development (Hamann et al. 2002). Like Aux/IAA17, Aux/IAA14 has a documented role in controlling lateral root initiation in *Arabidopsis* (Vanneste et al. 2005). The *Aux/IAA15*

locus is expressed at a very low level in almost all tissues and, further, was once considered to be a pseudogene (Abel et al. 1995), while this classification has since been overturned, the function of Aux/IAA15 remains unknown (Overvoorde et al. 2005). An *aux/iaa16* gain-of-function mutant displays an altered root phenotype like those displayed by the *aux/iaa14* and *aux/iaa17* single mutants, yet to a lesser degree. Considering that Aux/IAA16 is closely related to both Aux/IAA14 and Aux/IAA17, it has been suggested that these three Aux/IAAs may share a degree of functional redundancy (Rinaldi et al. 2012). Another gain-of-function mutant, the *aux/iaa18* mutant, develops misplaced cotyledons, a phenotype that suggests that Aux/IAA18 is required for early vegetative development in *Arabidopsis* (Ploense et al. 2009). The Aux/IAA proteins, Aux/IAA20 and Aux/IAA30, are unusual when compared to other members of the *Aux/IAA* gene family, as both proteins lack the domain that directs rapid Aux/IAA protein degradation through polyubiquination (Sato and Yamamoto 2008), and further, the overexpression of the loci encoding for these two atypically stable Aux/IAAs, results in the collapse of the root cap (Sato and Yamamoto 2008).

In conclusion, Aux/IAA proteins regulate a diverse range of developmental and stress response processes, shaped through their interactions with ARF proteins. Each Aux/IAA protein may interact with several different ARFs under different conditions, and while not transcription factors themselves, indirectly influence genetic auxin responses by acting as regulators of transcriptional regulatory proteins. The critical intermediary role which Aux/IAAs occupy underlines the necessity for tight, multi-tiered control during active biological processes.

3.1.3 AUXIN F-BOX proteins

AUXIN F-BOX (AFB) proteins, including the well characterised intracellular auxin perception protein, TRANSPORT INHIBITOR RESPONSE1 (TIR1), are intermediaries in the intracellular auxin signalling pathway. They form a central component of the SCF complex and regulate Aux/IAA protein stability. As previously outlined, once auxin is bound by TIR1, TIR1 recruits the other members of the SCF^{TIR1} complex to make a ubiquitin E3 ligase complex that mediates the intracellular auxin response (Kepinski and Leyser 2004).

Additionally, AFB1, AFB2, and AFB3, characterised after TIR1 and later found to be part of the same gene family (Parry et al. 2009), have been shown to have redundant function throughout the plant (Dharmasiri et al. 2005). However, there is experimental evidence to suggest that TIR1 and AFB2 may interact more readily with specific Aux/IAA proteins, such

as Aux/IAA7 (Parry et al. 2009), than do AFB1 and AFB3. AFB4 has also been shown to be responsive to intracellular auxin and can mediate the formation of an SCF^{AFB4} complex (Prigge et al. 2016). AFB5 is also auxin responsive, although AFB5 responds to the picloram class of auxinic herbicides, as opposed to the more prevalent indole class of auxin. Furthermore, AFB5 has not been shown to be involved in the formation of a SCF complex (Prigge et al. 2016). *BIG*, originally identified as *TIR3*, is also a member of the *AUXIN F-BOX* gene family. The BIG protein has been shown to be critical for normal auxin efflux during polar auxin transport. BIG targets and interacts with intracellular auxin transport vesicles to mediate their passage to transmembrane auxin efflux proteins, PIN proteins (Gil et al. 2001; Lopez-Bucio et al. 2005).

Ultimately, AFB proteins govern the distinction between an auxin-elicited genetic response or the simple movement of auxin through the cytoplasm towards *trans*-membrane efflux proteins. However, several other proteins not residing within the ARF, Aux/IAA, or AFB families also facilitate genetic auxin responses.

3.1.4 Other auxin response proteins

The SCF complexes specific to the auxin pathway are composed of several key members. Firstly, ASK1 or ASK2 are recruited to the nuclear located TIR1/AFB followed by the cullin-like protein, CUL1. Together, the interaction of these proteins forms an SCF ubiquitin E3 ligase (Gray et al. 1999; Gray et al. 2001). Subsequently, RBX1 binds to ASK1 (or ASK2), and recruits the ubiquitin E2 ligase, AXR1, and the protein, SGT1b. Together, these interacting proteins form the entirety of the SCF complex (Calderon-Villalobos et al. 2010; Walsh et al. 2006). The role of SCF complexes is to respond to changes induced in AFB proteins through the binding of auxin. Subsequently, they directly regulate Aux/IAA function, and indirectly ARFs, and, as such, are critical to genetic auxin responses in *Arabidopsis*.

Polar auxin transport is also mediated by a suite of genes. *AUX1* encodes a *trans*-membrane protein which is responsible for auxin influx (Reinhardt et al. 2003), whilst the AXR4 protein localises to the intracellular plasma membrane interface and positions AUX1 appropriately for auxin influx (Dharmasiri et al. 2006).

3.1.5 Small RNA directed expression control of auxin signalling

All of the genes/proteins outlined thus far are involved in intracellular auxin perception or polar auxin transport, processes which regulate many diverse aspects of plant growth and development, from tropic responses (Rashotte et al. 2000; Stowe-Evans et al. 1998) through to organ patterning and floral development (Bainbridge et al. 2008; Krizek 2011). However, this hormonal regulatory network is itself controlled, in part, by a different regulatory network, the sRNA-directed gene expression regulatory network.

The global sRNA population of any plant cell is composed of a multitude of individual species from multiple sRNA classes. Research has shown that of primary importance to the auxin signalling pathway are the sRNA classes; the miRNAs (Mallory and Vaucheret 2006) and the tasiRNAs, a plant-specific siRNA class (Guilfoyle and Hagen 2007; Marin et al. 2010). These sRNA classes require complex molecular machinery for their production. Specifically, these are the DCL1/DRB1 functional partnership for miRNA production (Eamens et al. 2009), and the DCL4/DRB4 functional partnership for tasiRNA production (Montgomery et al. 2008; Nakazawa et al. 2007; Qu et al. 2008). Additional research has indicated other possible DCL/DRB partnerships may potentially be required for miRNA and tasiRNA production in *Arabidopsis*, including the proposed DCL1/DRB2 partnership for miRNA production (Eamens et al. 2012a) and the proposed DCL4/DRB2 partnership for tasiRNA production (Pelissier et al. 2011).

There are a number of examples where the expression of auxin pathway genes has been shown to be under sRNA-directed posttranscriptional regulation. For instance, *TIR1* is under miR393-directed expression regulation (Windels and Vazquez 2011). Critical to intracellular auxin perception, multi-tiered regulation of *TIR1* allows tight control of a key mediator in the auxin response. On one level, TIR1 is indirectly under auxin regulation, as it is the first protein to respond to intracellular auxin signals and interacts directly with auxin (Kepinski and Leyser 2004). At a second level, recent experimental evidence suggests that the *TIR1* promoter is targeted by AGAMOUS-LIKE15 (AGL15), a MADS box transcription factor identified as an orthologue to a protein known to be involved in somatic embryogenesis from soybean (Zheng et al. 2016). Identification of AGL15 is a demonstration of conventional expression regulation of the *TIR1* gene transcription in *Arabidopsis*. However, in addition to hormonal and transcriptional regulation, *TIR1* is also under posttranscriptional regulation, as the *TIR1* transcript is a known target of miR393 (Navarro et al. 2006; Windels and Vazquez 2011). For example, reduced *TIR1* transcript abundance was observed in response to elevated miR393

accumulation, with elevated miR393 levels induced by the flg22 peptide, a peptide derived from eubacterial flagella (Navarro et al. 2006). miR393-directed expression regulation of *TIR1* has subsequently been demonstrated in a number of critical plant processes, including root architecture modifications to increase nitrate uptake (Vidal et al. 2010), secondary metabolite synthesis (Robert-Seilaniantz et al. 2011), embryogenic transition (Wojcik and Gaj 2016), and auxin homeostasis (Windels et al. 2014).

The ARF transcription factors, ARF6 and ARF8, are also under multi-tiered expression regulation. Posttranslational repression of ARF6 and ARF8 is governed by Aux/IAA protein family members, whose activity in turn is regulated by the formation of the SCF^{TIR1} complex in response to auxin (Gray et al. 2001; Ulmasov et al. 1997). Other than a key role in hormonal response to intracellular auxin signals, the abundance of the *ARF6* and *ARF8* transcripts is also regulated by the miRNA, miR167 (Wu et al. 2006). Overexpression experiments of the miR167 precursor transcript correlates with elevated miR167 abundance and a reduction in *ARF6* and *ARF8* mRNA levels in *Arabidopsis* floral tissues (Wu et al. 2006). In addition, miR167-directed expression regulation of the *ARF6* and *ARF8* transcripts has been shown to influence root architecture via modifications to jasmonic acid signalling (Kinoshita et al. 2012). Posttranscriptional regulation of *ARF6* and *ARF8* is important to a number of other plant processes including, but not limited to, male and female reproductive organ patterning (Wu et al. 2006), hypocotyl cell elongation (Oh et al. 2014), and adventitious root formation and development (Gutierrez et al. 2009).

ARF10, *ARF16*, and *ARF17* are another example of a multi-tiered regulatory expression module. Like other ARFs, ARF10, ARF16, and ARF17 are under posttranslational control mediated by ARF-Aux/IAA protein-protein interactions (Gray et al. 2001; Ulmasov et al. 1997). Additionally, *ARF10*, *ARF16*, and *ARF17* transcript abundance is posttranscriptionally regulated by miR160 (Mallory et al. 2005). ARF10, ARF16, and ARF17 have known roles in root cap development and lateral root primordia formation in *Arabidopsis* (Mallory et al. 2005; Wang et al. 2005). Furthermore, overexpression of the precursor transcript, *PRI-MIR160C*, leads to a reduction in the abundance of *ARF10*, *ARF16*, and *ARF17* in *Arabidopsis* root tissue. In these same experiments, modification of the *ARF16* transcript to uncouple the transcript from miR160-directed posttranscriptional regulation resulted in complementation of *arf10 arf16* double mutant and *PRI-MIR160C* overexpression phenotypes back to wild-type-like phenotypes (Wang et al. 2005). The complexity of this multi-tiered regulatory expression module is further exemplified in the existence of *e*ndogenous *t*arget *m*imics (eTMs)

for miR160 (*eTM160-1* and *eTM160-2*) (Wu et al. 2013). eTMs are long non-coding RNA transcripts originating from genomic loci defined as intergenic regions. eTMs function in sequestering mature miRNAs by containing a non-cleavable miRNA target sequence within the eTM transcript. The eTM target sequences maintain sufficient homology to cleavable miRNA binding sites but are rendered non-cleavable by the presence of mismatches in the 5' 9th to 11th nucleotides in binding site (Wu et al. 2013). In this fashion, miRNAs may bind eTMs but are unable to be released from these transcripts due to the absence of cleavage, thus preventing these same miRNAs from binding and cleaving legitimate target mRNA transcripts. In *Arabidopsis*, two eTM loci are currently known for miR160, *eTM160-1* and *eTM160-2* (Wu et al. 2013). This work elegantly illustrates the importance of ARF10, ARF16, and ARF17, their miR160-directed posttranscriptional regulation, and regulation of miR160 activity by eTMs, in root development.

Expression of other members of the *ARF* transcription factor family is also controlled by multiple regulatory networks. As with ARF6 and ARF8, ARF2, ARF3, and ARF4 all participate in repressive protein-protein interactions with Aux/IAA proteins (Gray et al. 2001; Ulmasov et al. 1997). However, *ARF2*, *ARF3*, and *ARF4* are all under posttranscriptional regulation directed by a different class of sRNA species, the tasiRNAs (Williams et al. 2005). This posttranscriptional regulatory network is more complex than simple targeting of complementary sequences in the target gene mRNA by a single miRNA species, as described above for the miR393/*TIR1*, miR167/*ARF6*/*ARF8*, and miR160/*ARF10*/*ARF16*/*ARF17* expression modules. A miRNA is still, however, required to initiate the tasiRNA-directed target gene expression repression pathway. For target genes, *ARF2*, *ARF3*, and *ARF4*, the first step in the tasiRNA pathway is miR390-directed, AGO7-mediated cleavage of the miR390 target sequence harboured in the non-protein-coding RNA transcript, *TAS3* (Nakazawa et al. 2007). The *TAS3* transcript harbours two miR390 binding sites. However, AGO7 only catalyses cleavage at one site, and this cleavage event promotes RDR6-mediated synthesis of a *TAS3* dsRNA molecule, which is in turn, processed by DCL4/DRB4 to produce a population of phased 21-nt siRNAs. One such phased siRNA, termed tasiARF, is loaded by AGO1, with AGO1 using the loaded tasiARF sRNA to direct cleavage-based silencing of the *ARF2*, *ARF3*, and *ARF4* transcripts, three *ARF* transcripts that harbour complementary tasiARF binding sites, to regulate the expression of these transcripts (Montgomery et al. 2008; Nakazawa et al. 2007). Unsurprisingly, ARF2, ARF3, and ARF4 play important roles in plant development, sufficient to warrant this extensive multi-tiered regulation, including plant wide developmental timing

and patterning (Fahlgren et al. 2006), heteroblasty (Hunter et al. 2006), and lateral root patterning and elongation (Meng et al. 2010).

3.1.6 Identifying sRNA targets

Identification, and the subsequent experimental validation of potential sRNA target genes, can prove to be a very long and laborious endeavour. However, a number of high-throughput tools exist that facilitate the identification of potential sRNA targets, and which allow the development of downstream investigative avenues. These approaches include utilising degradome and sRNA mapping analysis strategies.

Degradome analysis utilises degradome sequencing techniques, whereby the number of 3' cleaved ends are detected for each gene transcript of interest, and the repeat-normalised abundance of each degradome product transcript is calculated. The normalised total is then compared to the predicted expression abundance of each transcript to give a relative degradome product value. The relative number of cleaved ends at a given transcript nucleotide is an indication of the number of degradome products: cleaved end reads can occur either by normal transcript degradation or by targeted transcript cleavage directed by a sRNA (Addo-Quaye et al. 2009). Transcript cleavage directed by different sRNA species have indicative cleavage patterns (Addo-Quaye et al. 2009; Llave et al. 2002), and via careful examination of these patterns the mode of posttranscriptional expression regulation of the assessed transcript can be predicted. For example, when cleaved ends at each individual nucleotide are visualised on an X-Y plot, a single, predominant degradome peak mapping to a specific nucleotide of a transcript is indicative of miRNA-directed posttranscriptional regulation (Addo-Quaye et al. 2009; Llave et al. 2002). Conversely, siRNA-directed expression regulation is indicated by a larger peak at a specific nucleotide, together with many numerous smaller sized peaks in the 5' and/or 3' direction. Individually, such small sized peaks would not significantly influence target transcript abundance. Cumulatively, however, this population of mapped cleaved ends would have a major regulatory impact on the expression of the targeted transcript (Zhang et al. 2014). In this way, degradome analysis can provide insight into the class of sRNA that may be targeting a specific gene transcript for expression regulation.

sRNA mapping analysis, when overlaid with degradome analysis, can assist in the accuracy of a predicted sRNA species targeting a gene transcript. Like degradome profiles, sRNA mapping profiles can be visualised by plotting the normalised number of a sRNA

sequence to the corresponding nucleotides at which the sRNA is predicted to bind (Bousios et al. 2017; Johnson et al. 2016). The number of reads of a mapped sRNA species is then expressed relative to the total number of sRNA reads of the global population, and to the relative abundance of target gene transcript levels (Bousios et al. 2017; Johnson et al. 2016). A distinct advantage that sRNA mapping profiles have over degradome profiles is that they provide a sequence for the sRNA species mapping to the complementary region within the target gene transcript. However, sRNA mapping is most powerful when conducted in conjunction with degradome data to provide predictions of target gene transcript nucleotides of interest from two different sources. Together, degradome data and sRNA mapping data also provide an indication of both the class of sRNA species to which a predicted sRNA sequence may belong, as well as predicting the gene transcript under sRNA-mediated posttranscriptional regulation. In this study, both degradome data analysis and sRNA mapping data analysis have been utilised as powerful, if simple, bioinformatic tools to examine the potential for auxin pathway genes to be under sRNA-mediated posttranscriptional regulation.

3.1.7 Aims and objectives in this chapter

Polar auxin transport and intracellular perception are key developmental and stress response processes in *Arabidopsis*. It is understandable that such vital processes would need specific and sensitive control mechanisms to ensure normal biological function. For control to be both specific and sensitive, a multi-tiered regulatory network is required that allows for multiple control checkpoints and ascending levels of acuteness resulting in the formation of unique regulatory networks between targets and regulators.

In this instance, factors affecting polar auxin transport and intracellular auxin perception form one level by which the cell responds to the presence or absence of auxin, while Aux/IAA proteins form another level of regulation of ARFs, while responding to the current local auxin environment. The ARFs also form another level of regulation, as they are regulators themselves, promoting or inhibiting the transcription of auxin response genes, ultimately leading to developmental or stress responses. Small RNA regulation adds yet another level to this regulatory network allowing for greater control specificity and sensitivity. Small RNA biogenesis is itself complex, as multiple pathways can be taken, and multiple classes of sRNA may exhibit regulation over suites of related genes.

Considering this situation, this chapter aims to:

- Identify known and unknown sRNA regulators of auxin pathway genes, and to explore the interaction between the auxin pathway and sRNA regulatory networks.
- Examine the effects of manipulating sRNA biogenesis on the identified auxin pathway/sRNA regulator interactions in order to investigate the role of different sRNA classes in auxin pathway regulation.
- Analyse the miR160/*ARF10*/*ARF16*/*ARF17* expression module, a suite of genes (*ARF10*, *ARF16*, and *ARF17*) under posttranscriptional control directed by a single sRNA species, miR160. Analysis of a single expression module provides an opportunity to deepen our understanding of interactions between auxin signalling, sRNA biogenesis, and sRNA regulation.

3.2 Results

3.2.1 Degradome analysis of known and novel sRNA targeted auxin pathway gene transcripts

To determine the extent to which the transcripts that encode the protein machinery of the auxin pathway are under sRNA-mediated posttranscriptional regulation, degradome analysis was conducted. *Arabidopsis* degradome databases from floral tissues were screened for degradome products mapping to a total of 71 genes. These genes were *ARF1* to *ARF23, Aux/IAA1* to *Aux/IAA20* and *Aux/IAA26* to *Aux/IAA34*, *TIR1*, *AFB1* to *AFB5*, *ASK1* and *ASK2*, *SGT1b*, *RBX1*, *ABP1*, *ATRMA2*, *GH3.3*, *BIG*, *PINOID*, *WAG1* and *WAG2*, and *RCN1*. The assessed transcripts either belong to the three main auxin pathway gene families (*ARF*, *Aux/IAA*, and *TIR* (*AFB*) families), or encode a protein that comprises a crucial part of the intracellular auxin response pathway.

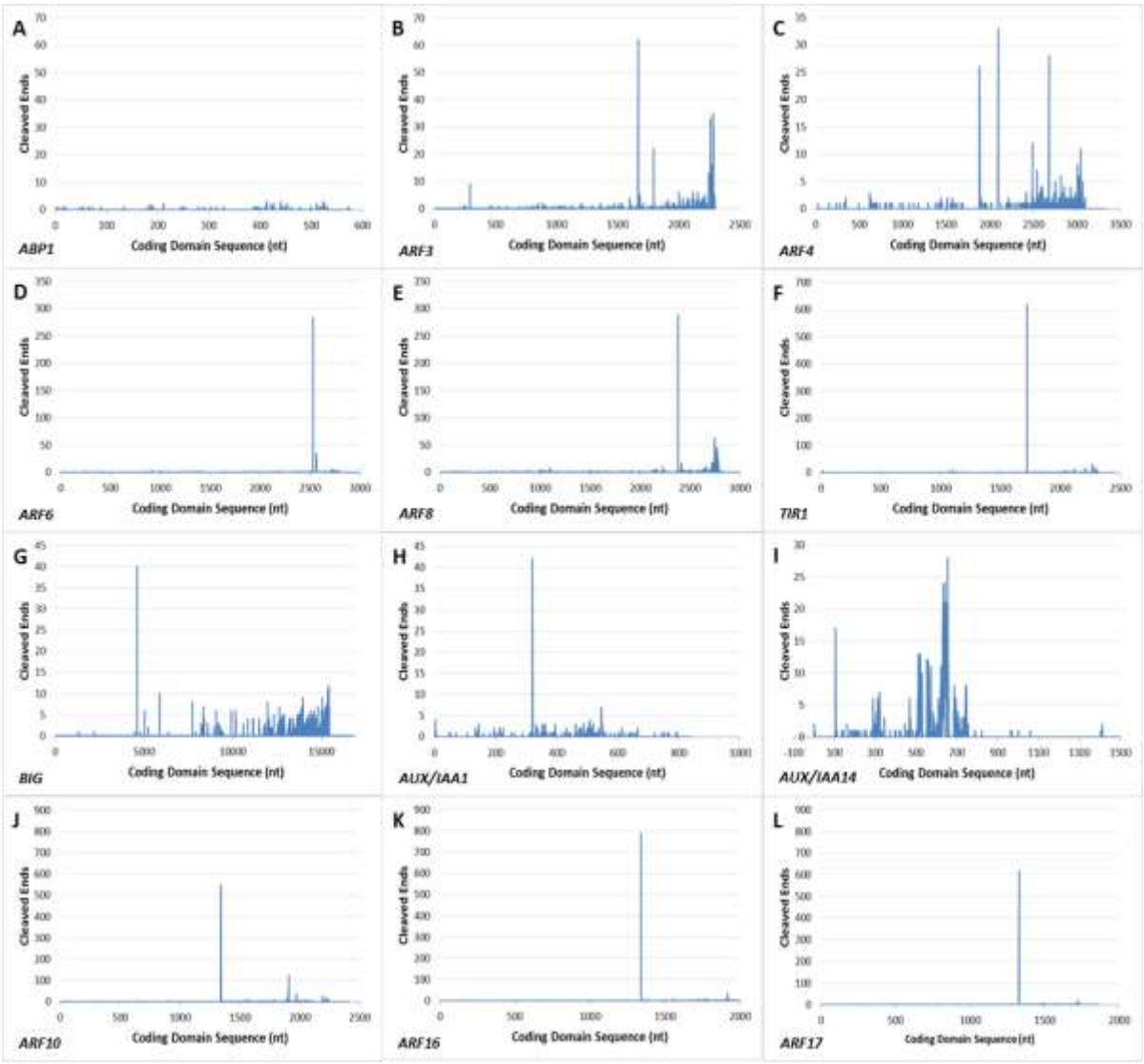

Figure 3.1. Degradome analysis of potential sRNA-targeted auxin responsive gene transcripts. Col-0 (blue) coding domain sequences of auxin responsive genes *ABP1* (A), *ARF3* (B), *ARF4* (C), *ARF6* (D), *ARF8* (E), *TIR1* (F), *BIG* (G), *Aux/IAA1* (H), *Aux/IAA14* (I), *ARF10* (J), *ARF16* (K), and *ARF17* (L) were analysed in floral tissue for degradome cleaved end products. A relatively large number of cleaved ends at a single nucleotide is indicative of miRNA-directed AGO-catalysed transcript cleavage. Small cleavage peaks mapped across multiple nucleotide positions within the assessed transcript is indicative of siRNA-directed AGO-catalysed transcript cleavage. Lowly abundant (small sized peaks), regardless of their number across the length of an assessed transcript, is indicative of an absence of either miRNA-directed or siRNA-directed AGO-catalysed transcript cleavage. Additional degradome analyses for a further 65 genes appear in **Appendix 4**.

Auxin pathway gene transcripts were degradome analysed using this method, and a selection of the most striking results are presented in **Figure 3.1**. ABP1 has previously been identified as a "fast" auxin response factor (Leblanc et al. 1999), but no demonstration of sRNA-mediated posttranscriptional regulation has been observed for the *ABP1* transcript. Degradome analysis showed no significant accumulation of degradome products for *ABP1* at

any transcript nucleotide, and this provided a baseline to compare degradome product profiling for other auxin responsive genes (**Figure 3.1A**). *ABP1*, therefore, is an ideal candidate to use a negative control to compare with the degradome profiles of other auxin response genes.

ARF3 and *ARF4* transcripts are under posttranscriptional regulation by the tasiRNA class of sRNA in *Arabidopsis* (Williams et al. 2005). Due to the phased production of tasiRNAs, it is not uncommon for targeted transcripts to have multiple peaks of relatively high abundance, as opposed to a large number of lowly abundant cleavage peaks that spread across the coding sequence. *ARF3* and *ARF4* show three cleavage peaks at nucleotides, 293, 1669, and 1795, and 1885, 2095, and 2682, respectively. These peaks ranged in abundance from ~10 to 60 cleaved ends per mapped transcript nucleotide (**Figure 3.1B** and **C**). This supports that both the *ARF3* and *ARF4* transcripts are under tasiRNA-directed expression regulation in *Arabidopsis* floral tissues.

ARF6 and *ARF8* are both known targets of miR167-directed RNA silencing (Kinoshita et al. 2012) and show abundance peaks of ~300 cleaved ends at transcript nucleotide positions, 2531 and 2258, respectively. A cleavage product peak of this magnitude at a single nucleotide, relative to the normalised expression of the gene, is highly indicative of miRNA-directed AGO1-catalysed target transcript cleavage (Addo-Quaye et al. 2008; Addo-Quaye et al. 2009; Jeong et al. 2011). As both *ARF6* and *ARF8* are experimentally validated targets of miR167, this degradome analysis is unsurprising. However, multiple smaller peaks were also present downstream from the miR167 cleavage site on the *ARF8* transcript (**Figure 3.1D** and **E**). Such a profile could be indicative of additional siRNA-directed expression regulation for *ARF8* in *Arabidopsis* floral tissues, or it potentially provides demonstration of the transitive spread of the secondary silencing signal post initial miR167-directed cleavage of the *ARF8* transcript, as has been demonstrated for other miRNA target transcripts in *Arabidopsis* (Boutet et al. 2003; Martinez de Alba et al. 2011; Parent et al. 2015).

The *TIR1* transcript is a well-documented miR393 target (Windels and Vazquez 2011). As with *ARF6* and *ARF8*, a predominant peak of ~600 cleaved ends at nucleotide position 1722 was observed for *TIR1* (**Figure 3.1F**). This result is highly indicative of miRNA-directed target transcript cleavage by the miR393 sRNA. Another *TIR* gene family member, *BIG,* returned a curious degradome profile. A predominant peak of ~40 cleaved ends was found at a single nucleotide (position 4618) in addition to numerous smaller peaks mapping between nucleotides 7724 and 15119. When these smaller peaks are summed, they return a total of greater than ~600 cleaved ends mapping to within this region (**Figure 3.1G**). Such a profile is indicative

that the *BIG* transcript may be under both miRNA- and siRNA-directed gene expression regulation.

Only two of the 29 *Aux/IAA* gene family members analysed returned degradome profiles strongly suggestive of sRNA-directed gene expression regulation. The *Aux/IAA1* transcript had a defined cleavage peak of ~40 cleaved ends at nucleotide 321 (**Figure 3.1H**) which suggests that *Aux*/*IAA1* may be under miRNA-directed expression regulation. However, no miRNA that could potentially target the *Aux/IAA1* transcript for cleavage-based RNA silencing has been identified in *Arabidopsis*. Further, this predominant peak at nucleotide position 321 is surrounded by numerous lowly abundant peaks, in both the 5' and 3' direction of the putative miRNA target site, along the *Aux*/*IAA1* transcript (**Figure 3.1H**), suggestive of siRNA-directed posttranscriptional regulation. The *Aux/IAA14* transcript might also be a target of sRNA-directed gene expression repression. The siRNA class of sRNA appears the most likely regulator targeting the *Aux/IAA14* transcript with a readily apparent cleavage '*hot spot*' identified via the mapping of ~750 cleaved ends between nucleotides 468 and 749 (**Figure 3.1I**). However, a locus that could encode a dsRNA precursor from which this pool of *Aux*/*IAA14* targeting siRNAs could be generated remains to be identified.

The *ARF* gene family members, *ARF10*, *ARF16*, and *ARF17*, are all experimentally validated targets of miR160-directed expression regulation (Mallory et al. 2005). Degradome assessment of the *ARF10*, *ARF16*, and *ARF17* transcripts revealed single cleavage peaks of ~600, ~800, and ~600 cleaved ends at nucleotide positions 1340, 1340, and 1328, respectively (**Figure 3.1J**-**L**). This result confirms that *ARF10*, *ARF16*, and *ARF17* are indeed targets of miR160, and that miR160 regulates the expression of its three target genes via an AGO1-catalysed mRNA cleavage mode of RNA silencing. As documented for *ARF8*, multiple smaller peaks were mapped further downstream of the miR160 cleavage site on the *ARF10* transcript (**Figure 3.1J**). Such a profile is most likely to result from siRNA-directed RNA silencing of the *ARF10* transcript, siRNAs generated as part of the transitive spread of the secondary sRNA silencing signal post initial miR160-directed cleavage of the *ARF10* transcript.

The degradome analysis presented here shows the most striking results, and therefore most likely candidates, of sRNA-directed posttranscriptional regulation of auxin pathway genes. Degradome profiles of an additional 65 *ARF*, *Aux/IAA*, *AFB*, and polar auxin transport associated transcripts were analysed and presented in **Appendix 4**. Many degradome profiles indicated that auxin pathway genes may be under miRNA- and/or siRNA-directed regulation. From these, *ARF2*, *Aux/IAA7*, *Aux/IAA17*, *AUX1*, *ASK1*, and *SGT1b* degradome profiles

indicated the most striking potential siRNA regulation, while *AFB2*, *AXR1*, *AXR4*, and *RCN1* degradome profiles indicated potential miRNA regulation. These transcripts, in addition to those presented in **Figure 3.1**, were mapped against sRNA sequence alignments. Degradome analysis of several other transcripts also showed potential miRNA and/or siRNA regulation, namely; *ARF3*, *ARF7*, *ARF9*, *Aux/IAA2-4*, *Aux/IAA8-13*, *Aux/IAA16*, *Aux/IAA18*, *Aux/IAA19*, *Aux/IAA26-30*, *AFB1*, *AFB3*, and *ASK2*. However, these profiles were either closely related to or not as striking as those presented in **Figure 3.1**, and as such were presented in **Appendix 4**. The remaining 33 auxin pathway gene transcripts returned degradome profiles showing no clear indication of sRNA-directed posttranscriptional regulation.

3.2.2 Small RNA mapping to auxin pathway gene transcripts

Degradome analysis is useful in determining the site(s) of potential sRNA-directed, AGO1-catalysed target transcript cleavage. Based on the cleavage patterns observed, the generated profiles are also useful for predicting the sRNA species directing the mapped target transcript cleavage events. For example, a single, predominant peak mapping to a specific transcript nucleotide is strongly suggestive of a miRNA-directed cleavage event, whereas multiple peaks mapping across all of the nucleotides within a specific region of the transcript, or the entire length of the transcript, indicates siRNA-directed target transcript cleavage (Addo-Quaye et al. 2008; Addo-Quaye et al. 2009; Branscheid et al. 2015).

Although degradome mapping data suggests that the analysed transcript is under sRNA-directed expression regulation and can indicate the likely class of sRNA directing transcript cleavage-based silencing of the transcript, it cannot be used on its own to definitively identify the causative sRNA class directing transcript cleavage. Thus, sRNA mapping was employed to gain further insight to the identification of auxin pathway genes whose expression is under sRNA-directed regulation, and the class(es) of sRNA directing this expression regulation. Therefore, sRNA sequencing datasets (unpublished Eamens' lab data) were used for this analysis with each dataset derived from the floral tissues of unique genetic backgrounds. These were wild-type *Arabidopsis* (ecotype, Col-0, the same background and tissue type from which the degradome sequencing database was generated), and the *drb1* and *drb2* single mutant backgrounds. These two mutant backgrounds were selected for sRNA mapping as each is defective in the activity of central piece of protein machinery required for sRNA production with DRB1 required by DCL1 for efficient miRNA production (Dong et al. 2008; Szarzynska et al. 2009), and DRB2 thought to form a functional partnership with either DCL1 or DCL4

for miRNA and siRNA production, respectively (Eamens et al. 2012a; Pelissier et al. 2011). To demonstrate the power of the sRNA mapping approach, all 22 auxin pathway gene transcripts whose analysis is described in **Section 3.2.1** were aligned with sRNA sequencing datasets from the Col-0, *drb1*, and *drb2* floral tissue libraries using PatMaN analysis software. However, only the auxin pathway gene transcripts presented in **Figure 3.1** are presented in **Figure 3.2**, with analyses of the remaining 10 genes presented in **Appendix 5**.

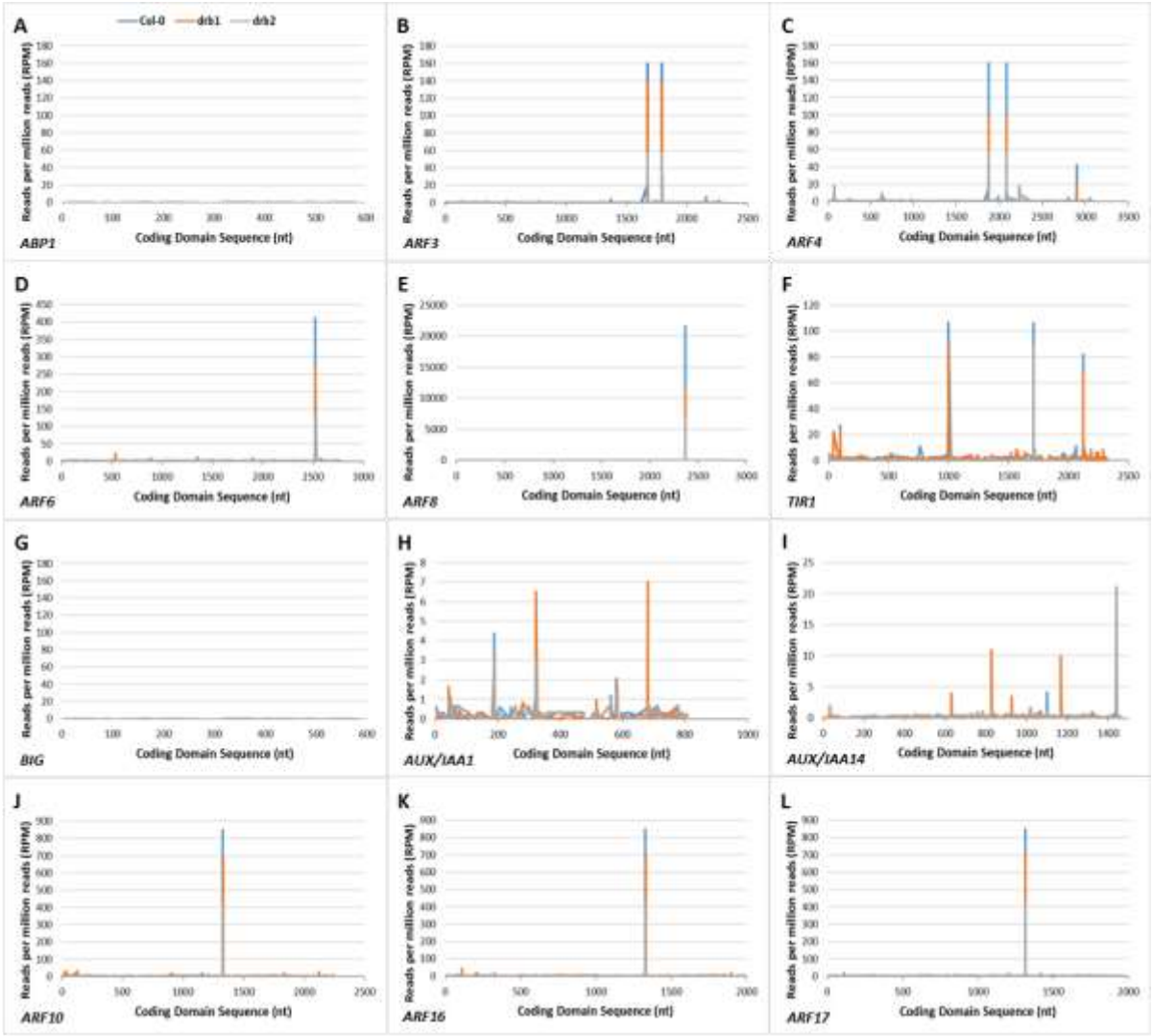

Figure 3.2. sRNA mapping analysis of potential sRNA-targeted auxin responsive gene transcripts. Coding domain sequences of auxin responsive genes *ABP1* (A), *ARF3* (B), *ARF4* (C), *ARF6* (D), *ARF8* (E), *TIR1* (F), *BIG* (G), *Aux/IAA1* (H), *Aux/IAA14* (I), *ARF10* (J), *ARF16* (K), and *ARF17* were mapped against the three available sRNA libraries from Col-0 (blue), *drb1* (orange), and *drb2* (grey) floral tissue. Peaks indicate proportion of sRNA sequence identities mapping to complementary target transcript sequences, with the sRNA cleavage position at the transcript nucleotide shown. Additional sRNA mapping analyses for another ten genes appear in **Appendix 5**.

As with the degradome analysis, the *ABP1* transcript provides an excellent baseline for sRNA-mapped target comparison. No cleavage product formation was observed in degradome analysis of the *ABP1* transcript (**Figure 3.1A**), and no abundant sRNA read was mapped to any region of the *ABP1* transcript from either the Col-0, *drb1*, or *drb2* floral tissue libraries (**Figure 3.2A**). Taken together, the degradome and sRNA mapping results for *ABP1* readily indicate that this transcript is free from sRNA-directed expression regulation in *Arabidopsis* floral tissues.

ARF3 and *ARF4* are known targets of tasiARF-directed posttranscriptional expression regulation (Williams et al. 2005). Two of the three degradome peaks that mapped to transcript nucleotide positions 1669 and 1795 had sRNA read peaks mapping to the same *ARF3* transcript positions (**Figure 3.2B**). However, no sRNA read peak mapped to the *ARF3* transcript at nucleotide 293 (**Figure 3.2B**), the nucleotide at which a small, but distinct, degradome peak was observed (**Figure 3.1B**). This observation suggests that if this *ARF3* degradome peak does result from sRNA-directed transcript cleavage, then the causative sRNA is not of sufficient abundance to be detected by sRNA sequencing of Col-0, *drb1*, or *drb2* floral tissues. Furthermore, read abundance for both mapped peaks were highest in the Col-0 background, at ~160 reads (**Figure 3.2B**). There was a reduction in the abundance peak of mapped reads in the *drb1* background to ~140 reads, and a further reduction in the *drb2* background to ~60 reads (**Figure 3.2B**). Three sRNA sequence peaks were mapped to the *ARF4* transcript at nucleotide positions 1885, 2095, and 2903, respectively (**Figure 3.2C**). The peaks aligning to nucleotides 1885 and 2095 correspond to the two peaks identified via the *ARF4* degradome analysis (**Figure 3.1C**), with the highest number of reads (~160 reads) observed in the Col-0 background for both peaks (**Figure 3.2C**). Interestingly, the read abundance mapping to these two peaks dropped to ~100 reads in the *drb1* background, and ~60 aligned reads in the *drb2* background (**Figure 3.2C**).

The reduced abundance of the two mapped sRNAs aligned to both the *ARF3* and *ARF4* transcripts in the *drb* mutants was not surprising considering the roles DRB1 and DRB2 play at different steps within the tasiRNA production pathway. DRB1, together with DCL1, is required for production of the miRNA, miR390, which directs the first cleavage event of the *TAS3* transcript that triggers the tasiARF production pathway (Montgomery et al. 2008; Nakazawa et al. 2007). DRB2 has been demonstrated to act synergistically with DRB4, presumably via functional interaction with DCL4, to process the *TAS3* dsRNA precursor for tasiRNA production (Eamens et al. 2012a; Pelissier et al. 2011). The more significant reduction

in the *drb1* background in aligned sequence reads mapped to the *ARF4* transcript compared to the *ARF3* transcript is suggestive of a more prominent role for DRB1 directing biogenesis of sRNAs involved in *ARF4* posttranscriptional regulation, than for *ARF3*. Further, the more drastic reduction in mapped sRNA reads to both the *ARF3* and *ARF4* transcripts in the *drb2* background, compared to the *drb1* background, also indicates that DRB2 plays a more central role in the tasiARF pathway than DRB1.

ARF6 and *ARF8* posttranscriptional regulation differs from that of *ARF3* and *ARF4*, as it is directed by a miRNA, specifically miR167 (Kinoshita et al. 2012). For *ARF6* and *ARF8*, a single predominant peak was mapped to transcript nucleotide positions 2531 and 2258, respectively (**Figure 3.2D** and **E**). The identity of this single mapped sRNA species was determined to be miR167, the known regulator of *ARF6* and *ARF8* gene expression (Kinoshita et al. 2012). **Figure 3.2D** reveals that miR167-directed expression regulation of *ARF6* returned a maximum of ~400 sRNA reads in the Col-0 background mapping to nucleotide 2531 of the targeted transcript. As miRNA biogenesis is unperturbed in the Col-0 background, it was unsurprising that the highest number of mapped sRNA reads to the miR167 target site occurred in this genetic background. It was also unsurprising that there was a drop in sRNA read abundance mapping to the miR167 target site (~275 reads) in the *drb1* floral tissue library, with DRB1 previously demonstrated to be required by DCL1 for accurate and efficient miRNA production in *Arabidopsis* (Eamens et al. 2009). It was, however, surprising to observe a greater reduction in miR167 read numbers (to ~140) mapping to the *ARF6* target site in the *drb2* background. DRB1 and DRB2 function both synergistically and antagonistically with one another in miRNA biogenesis (Eamens et al. 2012b; Pelissier et al. 2011), a demonstration that explains the observed reductions to miR167 abundance in both the *drb1* and *drb2* backgrounds. Alternatively, this surprise result may imply that in *Arabidopsis* floral tissues, DRB2 (presumably via interaction with DCL1), and not DRB1, is the primary DRB protein required for miR167 production.

For *ARF8*, Col-0 returned the maximum number of reads (~20,000 reads) mapped to the miR167 target site of the *ARF8* transcript (**Figure 3.2E**). Again, that the highest read numbers were observed in Col-0 was not an unexpected result as wild-type *Arabidopsis* has a fully functional miRNA pathway. And as demonstrated for *ARF6*, the *drb1* background returned the next highest number of miR167 reads mapping to the *ARF8* miR167 target site (~12,000 reads) (**Figure 3.2E**). This 40% reduction in miR167 read numbers for the *drb1* background was expected due to the well documented role of DRB1 in DCL1-catalysed

miRNA production (Eamens et al. 2009). The largest reduction to miR167 reads mapping to the *ARF8* transcript was again observed in the *drb2* background, with only ~6,000 miR167 reads mapping to the miR167 target site coordinates of the *ARF8* transcript in the *drb2* floral tissue sRNA library (**Figure 3.2E**). This 70% reduction in miR167 reads mapping to the *ARF8* transcript in *drb2* plants taken together with the miR167/*ARF6* profiling, strongly indicates that DRB2 is the primary DRB required for miR167 production in *Arabidopsis* flowers.

Comparison of the degradome analysis of the *TIR1* transcript to the sRNA mapping for *TIR1* is considerably more complicated than the relationships observed for miR167 and its target transcripts, *ARF6* and *ARF8*. **Figure 3.2F** reveals a clear peak at *TIR1* nucleotide position 1722, the same transcript position to which the only significant degradome peak was mapped (**Figure 3.1F)**. The sRNA mapped to this position corresponds to the miR393 sRNA, a known regulator of *TIR1* gene expression (Windels and Vazquez 2011). It was also unsurprising that the highest sRNA read number for miR393 (~110 sRNA reads) was in the Col-0 background (**Figure 3.2F**). Further, the complete absence of any sRNA reads mapping to the *TIR1* miR393 target site in the *drb1* background, in combination with only mild reductions to the number of miR393 reads mapping to this position in the *drb2* background, strongly indicates that DRB1 is the sole DRB protein involved in miR393-directed expression regulation of *TIR1* in *Arabidopsis* floral tissues.

However, two additional mapped sRNA peaks were observed for *TIR1* at transcript positions, 999 and 2126 (**Figure 3.2F**), with neither of these sRNA read peaks having a corresponding degradome cleavage peak (**Figure 3.1F**). Both of these sRNA peaks were only recorded in the Col-0 and *drb1* datasets (**Figure 3.2F**), with no sRNA mapping to either peak in *drb2* plants. The sRNA sequence that mapped to the 2126 nucleotide peak did not align with any known plant miRNA, and the 24-nt length of the aligned sequence mapping to *TIR1* nucleotide position 2126 is an unusual size for a 'typical' *Arabidopsis* miRNA. The sequence of the sRNA mapping to *TIR1* transcript position 999, although of the expected length at 21-nt, also does not match the mature sRNA sequence of any known *Arabidopsis* miRNA. The absence of corresponding degradome peaks at the mapped position of the *TIR1* transcript, coupled with the unknown identity of the sRNAs mapping to these positions, suggests that another sRNA class, distinct from the miRNA class might be placing additional expression regulation onto the *TIR1* transcript. The obvious requirement for DRB2 in the production of these unknown sRNAs, identified in these floral tissue-specific sequencing libraries, suggests the RNA polymerase IV (PolIV)-generated class of siRNAs (p4-siRNAs) as the most likely

candidates, as DRB2 is required for the specific accumulation of p4-siRNAs, and not other classes of siRNAs or miRNAs (Pelissier et al. 2011).

Degradome analysis indicated that *BIG* may be under both miRNA and siRNA regulation. However, sRNA mapping analysis aligned sequences along the entire length of the *BIG* transcript (**Figure 3.2G**). Furthermore, the highest read numbers for the mapped sRNAs were observed in either the wild-type library, or the sRNA library generated from *drb2* floral tissues. DRB2 has been demonstrated to be antagonistic to DRB4 in the production of numerous classes of siRNA in *Arabidopsis* (Pelissier et al. 2011). Therefore, high read numbers in the plant line defective in DRB2 activity suggests that the expression of the *BIG* transcript is indeed under siRNA-directed regulation, most likely the p4-siRNA class of sRNA.

The first *Aux/IAA* transcription factor presented here, *Aux/IAA1*, showed three peaks aligned with sRNA mapped sequences at nucleotides 189, 321, and 681, respectively (**Figure 3.2H**). The aligned sequence peak at nucleotide 321 corresponds to the only notable cleavage product peak from the degradome analysis (**Figure 3.1H**) with the other two other sRNA mapping identified peaks having no corresponding degradome peak. The mapped sRNA sequence peak at nucleotide 321 is highest in the *drb1* background at ~7 reads (**Figure 3.2H**). While this is a low number of reads compared to the transcript expression levels, it could be significant. Furthermore, the highest number of mapped reads was present in the *drb1* background, which suggests that an alternate DRB protein (either DRB2 or DRB4) is the primary mediator of the production of this 'potential' sRNA regulator of *Aux/IAA1* expression. Interestingly, the sRNA sequence that mapped to *Aux/IAA1* at nucleotide position 321 was determined to have significant homology with the wheat miRNA, miR1134. However, no homologs of the miR1134 sRNA have been documented in *Arabidopsis* and, additionally, miR1134 remains to be experimentally verified in wheat. The next highest number of aligned reads at nucleotide 321 is in the Col-0 background with this peak further reduced in the *drb2* background (**Figure 3.2H**). The mapped sRNA sequence peak at nucleotide 189 is highest in the Col-0 background (~5 reads) and present in the *drb2* background, but absent in *drb1* background (**Figure 3.2H**).

The complete absence of a mappable sRNA to this transcript position in the *drb1* background suggests that the DRB1/DCL1 functional partnership might be required for the production of this sRNA from its precursor transcript. However, no experimentally validated miRNA sequence corresponds precisely to the aligned sequence peak at nucleotide *Aux*/*IAA1* nucleotide, although the mapped sRNA returned partial identity to *Arabidopsis* miRNA,

miR5021. The third sRNA peak (~7 reads) mapped to the *Aux*/*IAA1* transcript at nucleotide position, 681, was only detected in the *drb1* floral tissue library. Again, no known miRNA from any plant species shared any significant homology to the mapped sRNA. Due to the mapped sRNA only being detected in one of three sequencing libraries, together with its low abundance, and failure of the degradome analysis to identify a cleavage peak, this peak may well represent a false positive and might not be indicative of sRNA-directed regulation of *Aux/IAA1* at this transcript position.

Three notable sRNA peaks mapped to the *Aux/IAA14* transcript at nucleotide positions 827, 1169, and 1441 (**Figure 3.2I**). These three sRNA mapped peaks sit within a sRNA mapping '*hotspot*' on the *Aux*/*IAA14* transcript and are positioned in the 3' half of the transcript. This is distinct from the cleaved end '*hotspot*' in the 5' half of the *Aux*/*IAA14* transcript identified by the degradome analysis (**Figure 3.1I**). Taken together, the degradome and sRNA mapping analysis of the *Aux*/*IAA14* transcript strongly suggest that subsequent to the initial siRNA-directed cleavage of the 5' portion of *Aux*/*IAA14*, the 3' cleavage product is being used as a template for secondary siRNA production. This would amplify the silencing signal that is directing expression repression of *Aux*/*IAA14*, and of any other *Aux*/*IAA* gene family members that share significant sequence homology to the *Aux*/*IAA14* transcript (Boutet et al. 2003; Martinez de Alba et al. 2011; Parent et al. 2015).

The sRNA mapping analysis revealed a single mapped sequence peak for the *ARF10*, *ARF16*, and *ARF17* expression module transcripts at nucleotides 1340, 1340, and 1328, respectively, in *Arabidopsis* floral tissues (**Figure 3.2J-L**). The highest number of aligned reads of ~850 reads for *ARF10*, *ARF16*, and *ARF17* was observed in the Col-0 background (**Figure 3.2J-L**) and this was expected as *ARF10*, *ARF16*, and *ARF17* are all known miR160 targets (Mallory et al. 2005). A reduction in the number of miR160 reads to ~700 reads that aligned to the miR160 target sites of *ARF10*, *ARF16*, and *ARF17* was observed in the *drb1* background (**Figure 3.2J-L**). Interestingly, further reductions in miR160 read abundance was observed for the *ARF10*, *ARF16*, and *ARF17* transcripts in the *drb2* background. The ~400 mapped reads represents a more than 50% decrease in abundance of mapped miR160 in *drb2* floral tissues compared to miR160 abundance in wild-type flowers. Based on the degree of reduction of mapped miR160 read numbers alone, sRNA mapping suggested that DRB2, and not DRB1, is the primary DRB protein required for miR160 production in *Arabidopsis* floral tissues.

The sRNA sequence alignment analysis presented here shows the most striking results, and therefore most likely candidates, of sRNA-directed posttranscriptional regulation of auxin pathway genes. Small RNA sequence alignment analysis of *Aux/IAA7*, *Aux/IAA17*, *AUX1*, *ASK1*, and *SGT1b*, degradome profiles indicated potential siRNA regulation, and *AFB2*, *AXR1*, *AXR4*, and RCN1, degradome profiles indicated potential miRNA regulation, are presented in **Appendix 5**. Apart from those presented in **Figure 3.2**, only *AFB2* returned any significant sRNA mapping sequence alignment results.

Considering the cumulative results from both the degradome and sRNA sequence mapping analysis, it is clear that several auxin pathway genes are under sRNA-directed posttranscriptional regulation. In deconstructing a multi-tiered regulatory network involving posttranscriptional regulation it is important to examine the biogenesis pathways through which these sRNA classes are produced. By examining auxin pathway sRNA targeted transcripts, in mutant backgrounds deficient in the activity of sRNA processing machinery proteins, it is possible to gain insight into the sRNA biogenesis pathways at play in these multi-tiered regulatory networks.

3.2.3 Semi-quantitative assessment of auxin responsive transcript levels in *drb* mutant background

The computationally generated analyses presented in **Figures 3.1** (degradome profiling) and **3.2** (sRNA mapping) of auxin pathway gene transcripts provided numerous insights into the nature and degree of the sRNA-directed regulatory environment that controls the expression of many auxin pathway genes.

To gain further insight into sRNA-directed regulation of auxin pathway gene expression, transcript abundance was assessed via a semi-quantitative RT-PCR approach in four *Arabidopsis* lines, comparing Col-0 wild-type to the T-DNA insertion knockout mutant plant lines, *drb1*, *drb2*, and *drb12* (the *drb1 drb2* double mutant). The single and double *drb* mutant combinations used in this study were selected based on previous demonstrations that DRB1 and DRB2 are required in the production stages of both the *Arabidopsis* miRNA and siRNA pathways (Dong et al. 2008; Eamens et al. 2012a; Eamens et al. 2012b; Pelissier et al. 2011; Szarzynska et al. 2009). The computational analyses presented in **Figures 3.1** and **3.2** further focused the list of auxin pathway genes that required additional investigation. To this end, semi-quantitative RT-PCR was used to document transcript abundance for the 12 genes

shown in **Figures 3.1** and **3.2**, namely *ABP1*, *ARF3*, *ARF4*, *ARF6*, *ARF8*, *TIR1*, *BIG*, *Aux/IAA1*, *Aux/IAA14*, *ARF10*, *ARF16*, and *ARF17*, across the four genetically distinct *Arabidopsis* backgrounds. Inflorescence tissue from 4-week-old plants was used to generate cDNA templates for the semi-quantitative RT-PCR based expression analyses.

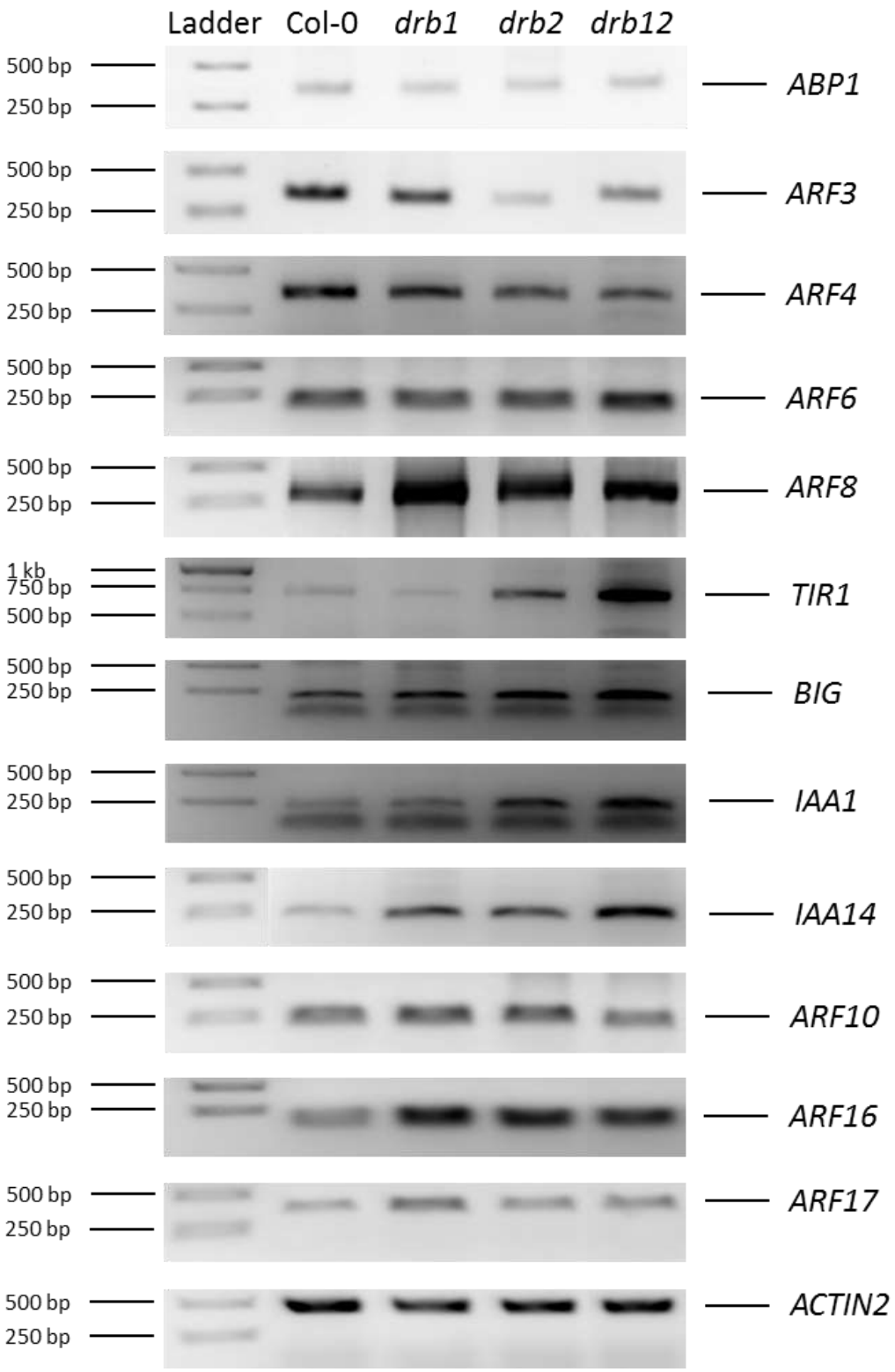

Figure 3.3. Semi-quantitative RT-PCR analysis of auxin responsive genes in Col-0 and *drb* mutant backgrounds. The expression of 12 auxin responsive genes was semi-quantitatively analysed with RT-PCR. Expression analyses were conducted using an equal concentration of cDNA template synthesised from equal concentrations of total RNA extracted from 4-week old Col-0, *drb1*, *drb2*, and *drb12* inflorescence tissue. All target gene expression analyses were compared to the house keeping control gene, A*CTIN2*.

In silico analyses of *ABP1* showed no indication of sRNA-directed posttranscriptional regulation (**Figure 3.1A** and **3.2A**). It was, therefore, expected that *ABP1* expression would remain constant in Col-0, *drb1*, *drb2*, and *drb12* inflorescence tissues. Accordingly, semi-quantitative RT-PCR analysis of *ABP1* transcript abundance showed that *ABP1* expression did not change in *drb1*, *drb2*, or *drb12* mutant backgrounds compared to Col-0 (**Figure 3.3**).

ARF3 and *ARF4* are known targets of the tasiRNA post transcriptional regulatory pathway (Williams et al. 2005). Considering this, it was surprising to observe a slight reduction in *ARF4* transcript abundance in the *drb1* single mutant background, but no such change for *ARF3* (**Figure 3.3**), as a loss in the abundance of the triggering miRNA, miR390, for tasiARF production would be expected to result in reduced tasiARF sRNA production and, therefore, released expression repression of *ARF3* and *ARF4*. It was not, however, surprising to detect a decrease in *ARF3* and *ARF4* expression in the *drb2* single mutant background, and in the *drb12* double mutant background (**Figure 3.3**). As DRB4 is the primary DRB protein involved in tasiRNA-mediated production, and that DRB2 acts antagonistically to DRB4 (Pelissier et al. 2011), expression changes observed in DRB2 deficient backgrounds is believed to be the result of elevated tasiARF abundance due to enhanced DRB4/DCL4 activity.

ARF6 and *ARF8* have been previously shown to be under miR167-directed expression regulation (Kinoshita et al. 2012), and this was further confirmed through the degradome (**Figure 3.1D** and **E**) and sRNA mapping (**Figure 3.2D** and **E**) analyses. However, sRNA mapping to the *ARF6* transcript indicated that more than one DRB protein is potentially required for miR167 production and/or miR167-directed *ARF6* expression regulation with the largest reduction to the mapped miR167 peak for the *ARF6* transcript observed in the *drb2* floral tissue library. This suggested that DRB2 is the primary DRB required for miR167-directed *ARF6* expression regulation in this tissue. Surprisingly, however, no change in *ARF6* transcript abundance was revealed by RT-PCR analysis of *drb2* plants (**Figure 3.3**). It was also curious that no change was detected in *ARF6* transcript abundance in the *drb1* background (**Figure 3.3**), the mutant plant line known defective in DRB1-mediated, DCL1-catalysed miRNA production. Elevated transcript abundance in the *drb12* background did (**Figure 3.3**), however, further suggest that both DRB1 and DRB2 are required to maintain miR167 production and miR167-directed expression regulation of *ARF6*.

RT-PCR analysis of *ARF8* transcript abundance across the suite of *drb* mutant lines also revealed surprising results. Compared to *ARF8* expression in Col-0 plants, the greatest degree of expression elevation was observed in *drb1* plants (**Figure 3.3**). This was a surprise result as

sRNA mapping revealed that miR167 abundance was only reduced by 40% in the *drb1* floral tissue library, compared to a 70% reduction in sRNA reads in *drb2* floral tissues. However, RT-PCR revealed that *ARF8* expression was not deregulated to the same degree in either the *drb2* single mutant or the *drb12* double mutant (**Figure 3.3**). This unexpected result is most likely due to target transcript cleavage-based silencing being completely defective in the *drb1* mutant background, and translational repression-based silencing being lost in the *drb2* and *drb12* mutants, a defective mechanism of miR167-directed *ARF8* expression repression that cannot be assessed accurately by RT-PCR-based expression analysis. Considering the close evolutionary and functional relationship between *ARF6* and *ARF8*, RT-PCR analysis of *ARF8* expression helps clarify the expression trends in the *drb1* and *drb2* genetic backgrounds for *ARF6*. It is likely that the synergistic relationship between DRB1 and DRB2 is required for efficient miR167 production.

TIR1 and other *AFB* gene family members are known targets of miR393 (Windels and Vazquez 2011). As such, changes in *TIR1* transcript abundance might be anticipated in the assessed *drb* mutant backgrounds. However, no change in *TIR1* expression was observed between Col-0 and *drb1* plants (**Figure 3.3**). Furthermore, a significant increase in *TIR1* transcript abundance was observed in *drb2*, an expression change that was even more pronounced in *drb12* (**Figure 3.3**). That the largest expression change was observed in the *drb12* double mutant background, implies a role for both DRB1 and DRB2 in miR393 production and/or miR393-directed expression repression of *TIR1* expression. Alternatively, DRB1 may exclusively direct miR393 biogenesis, targeting *TIR1* transcripts, and DRB2 direct the biogenesis of unknown sRNAs showing mapped sequence alignment to the *TIR1* transcript at nucleotides 999 and 2126 (**Figure 3.2F**). This would add further support for p4-siRNAs as strong candidates for additional posttranscriptional regulation of *TIR1*.

RT-PCR analysis of another F-box gene, *BIG*, related to *TIR1*, showed increased in expression in all three assessed *drb* backgrounds (**Figure 3.3**). Such increases in transcript abundance strongly implies that both DRB1 and DRB2 are required for the posttranscriptional regulation of *BIG* gene expression. The degradome profile of the *BIG* transcript (**Figure 3.1G**) indicated that siRNAs, rather than miRNAs, may regulate *BIG* expression. Indeed, as *BIG* transcript abundance was highest in DRB2 deficient genetic backgrounds (**Figure 3.3**), and that DRB2 is known to act antagonistically with DRB4 in p4-siRNA production (Pelissier et al. 2011), the class of siRNA is most likely directing *BIG* posttranscriptional regulation.

Two *Aux/IAA* genes, *Aux/IAA1* and *Aux/IAA14*, showed degradome profiles (**Figure 3.1H** and **I**) and sRNA mapping alignments (**Figure 3.2H** and **I**) indicative of 'potential' siRNA-directed posttranscriptional regulation. RT-PCR analysis showed that *Aux/IAA1* expression increased in the *drb2* genetic background, and an additional mild increase in the *drb12* genetic background was also observed (**Figure 3.3**). No increase in *Aux/IAA1* expression was observed in the *drb1* single mutant genetic background (**Figure 3.3**) implying that DRB1 is not involved in posttranscriptional regulation of *Aux/IAA1* expression. The absence of DRB1 liberates DRB2 from DRB1-mediated antagonistic effects (Eamens et al. 2012a), an effect indicated by the sRNA pool targeting the *Aux/IAA1* transcript having the highest abundance in the *drb1* background (**Figure 3.2H**). Taken in conjunction with expression of *Aux/IAA1* increasing in the absence of DRB2 activity (**Figure 3.3**), this result further supports a primary role for DRB2-mediated posttranscriptional regulation of *Aux/IAA1* gene expression.

Aux/IAA14 also shows a widespread increase in expression across the different *drb* mutant backgrounds, with increases in expression observed in the *drb1* and *drb2* single mutant backgrounds, and further gains in transcript abundance in the *drb12* double mutant (**Figure 3.3**). The observed increase in *Aux/IAA14* expression across all three assessed *drb* mutants firmly implies a role for both DRB1 and DRB2 in targeting *Aux/IAA14* for expression regulation. Considering that degradome profiling (**Figure 3.1I**) and sRNA mapping (**Figure 3.2I**) identified different regulatory '*hotspots*' on the *Aux/IAA14* transcript, it may be that DRB1-mediated miRNA cleavage occurs in the 5' portion of the *Aux/IAA14* transcript, followed by a proliferation of the siRNA silencing signal, mediated by DRB2, in the 3' portion of the *Aux/IAA14* transcript.

Finally, RT-PCR analysis of *ARF10*¸ *ARF16*, and *ARF17* transcript levels revealed a diverse range of expression changes across the assessed *drb* mutants. *ARF10* expression increased in the *drb1* and *drb2* single mutants but no change in transcript abundance was observed in the *drb12* double mutant (**Figure 3.3**). As expression changes were observed in only single mutant backgrounds and considering that DRB1 and DRB2 have been shown to act antagonistically to each other (Eamens et al. 2012b), this suggests that both DRB1 and DBR2 are required for miR160 production and/or miR160-directed expression regulation of *ARF10*. The *ARF16* transcript showed a significant increase in abundance in all three *drb* mutant backgrounds analysed (**Figure 3.3**). This observation further supports the requirement for both DRB1 and DRB2 in miR160-directed expression regulation of *ARF16*, and as demonstrated for *ARF10*. The *ARF17* transcript only appeared to significantly increase in expression in the

drb1 single mutant. However, subtle changes in transcript abundance were observed in the *drb2* and *drb12* backgrounds (**Figure 3.3**). Taken together, the curious expression changes observed for the *ARF10*, *ARF16*, and *ARF17* transcripts via RT-PCR strongly suggested that both DRB1 and DRB2 play functional roles in miR160-directed expression regulation of these three target genes. This finding warranted further experimental characterisation.

3.2.4 Phenotypic assessment of Col-0, *drb1*, *drb2*, and *drb12* shoot and root development

From preliminary semi-quantitative RT-PCR analyses of inflorescence tissue (**Figure 3.3**), it is apparent that many changes to the sRNA environment result from modified sRNA biogenesis pathways in the *drb* mutant backgrounds. To examine the effects of disrupting sRNA biogenesis on plant development, shoot and root phenotypes were assessed in 23-day-old Col-0, *drb1*, *drb2*, and *drb12* plants.

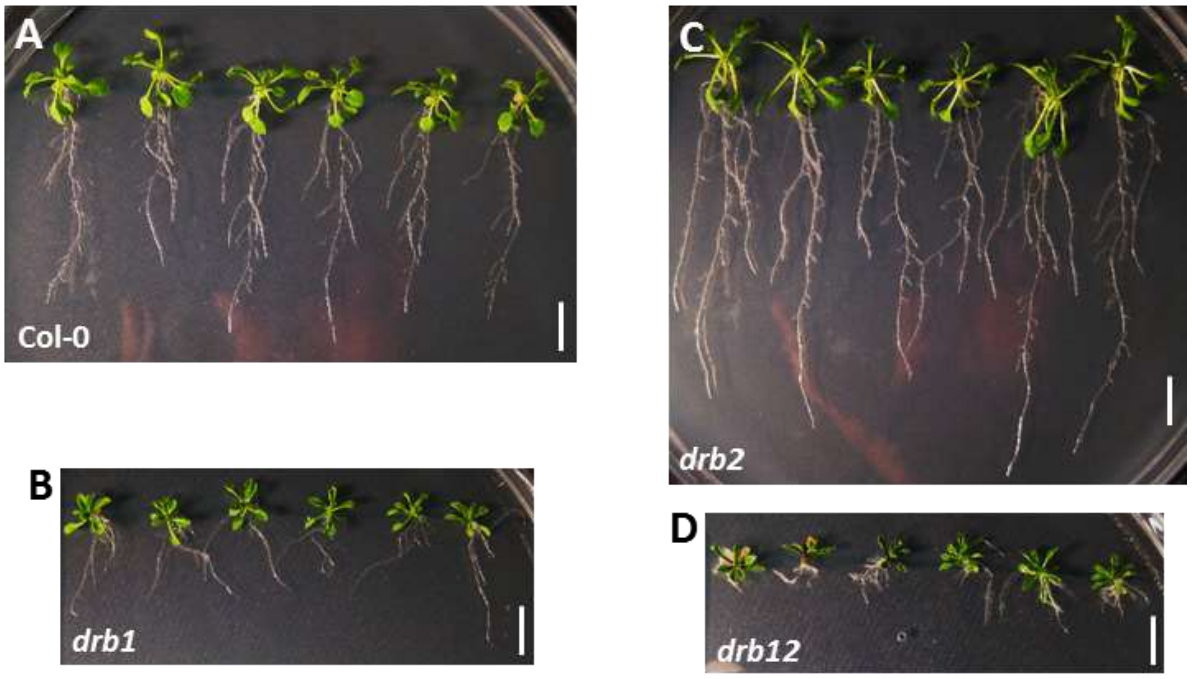

Figure 3.4. Representative phenotypes of vertically grown Col-0, *drb1*, *drb2*, and *drb12* *Arabidopsis* plant lines. Col-0 (A), *drb1* (B), *drb2* (C), and *drb12* (D) plants were germinated and cultivated on horizontally orientated MS media plates under standard growth conditions for 10 d, before being transferred to new MS media plates that were orientated vertically for an additional 13 d of growth. Photographic images were used for phenotypic analyses of primary root length, lateral root number, adventitious root number, and rosette surface area. The root and shoot material from the same plants was collected and used for subsequent molecular analyses. Scale bars represent 1 cm.

The phenotypes displayed by the *drb1*, *drb2*, and *drb12* mutant lines demonstrated the importance of DRB1 and DRB2 for plant development. The previously reported phenotype of *drb1* plants (Curtin et al. 2008; Mallory and Vaucheret 2006) was confirmed, and included upward rosette leaf curling (hyponasty), altered temporal vegetative phase change, and overall stunted growth. In addition, the root phenotypes displayed by *drb1* plants, including reduced primary root length, and an increase in root spreading adjacent to aerial tissue (**Figure 3.4B**) further demonstrated the impact of loss of DRB1 activity on subterranean development. As DRB1 is thought to be the primary DRB protein family member required for miRNA production in *Arabidopsis*, the root phenotype of *drb1* plants suggests that modification of the miRNA production pathway negatively influences root architecture.

drb2 plants have been reported to develop a more pronounced epinastic shoot architecture, rosette leaf margin serration, and more ovoid shaped rosette leaves compared to Col-0 plants (Curtin et al. 2008). A similar phenotype was also observed here (**Figure 3.4C**) and, further, *drb2* plants also showed an increase in primary root length, a larger aerial tissue biomass, and a proliferation of lateral root development (**Figure 3.4C**), compared to wild-type Col-0 plants. As DRB2 is implicated in both miRNA, and varying classes of siRNA biogenesis (Eamens et al. 2012a; Eamens et al. 2012b; Pelissier et al. 2011), it is difficult to attribute these preliminary observations of modified root development to a specific portion of the global sRNA population of *Arabidopsis* root cells. The *drb12* double mutant plant displays a compounded deleterious effect on root and shoot development (**Figure 3.4D**). However, as most features are similar to the *drb1* single mutant phenotype, this suggests that DRB1 has a more profound influence on both shoot and root development than DRB2, as noted previously (Curtin et al. 2008; Eamens et al. 2012a). The compounded phenotypic effects in *drb12* double mutant plants suggests that both DRB1 and DRB2 influence root architecture during plant development, and that these roles differ. To gain further insight into the phenotypic effects, particularly those associated with root development, of disrupting DRB1 and DRB2 function, key aspects of phenotypic development were quantified in the *drb1*, *drb2*, and *drb12* mutant backgrounds for comparison to Col-0 plants.

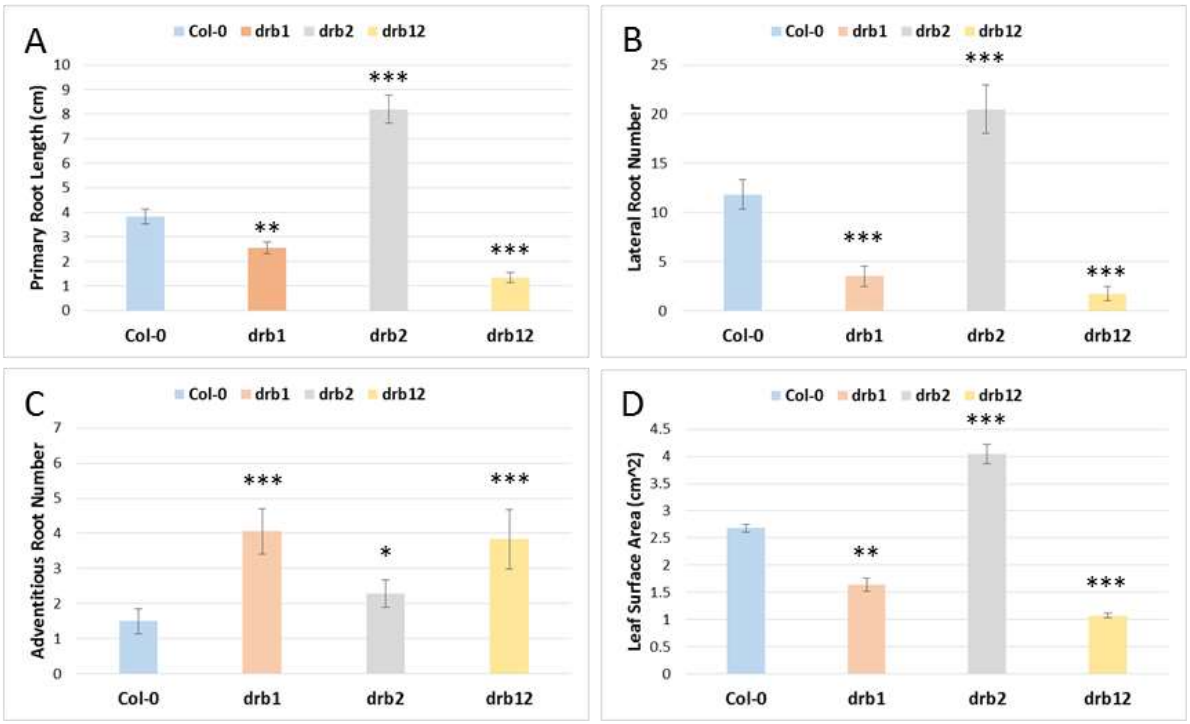

Figure 3.5. Phenotypic analysis of primary root length, lateral root number, adventitious root number, and rosette leaf surface area in Col-0, *drb1*, *drb2*, and *drb12* genetic backgrounds. Primary root length (A), lateral root number (B), adventitious root number (C), and rosette surface area (D) of Col-0 (blue), *drb1* (orange), *drb2* (grey), and *drb12* (yellow) plants lines were measured after 23 d of growth using ImageJ. Averages of *drb1*, *drb2*, and *drb12* were compared to Col-0 with a two-tailed t-test. n = 18. Error bars represent SEM. *** $p \leq 0.001$, ** $p \leq 0.01$, * $p \leq 0.05$.

Primary root length is a strong indicator of overall plant development, and alterations in primary root length confirm the pronounced developmental impact of disrupted DRB-mediated sRNA production. As qualitatively observed (**Figure 3.4**), *drb1* plants show a reduced primary root length compared to Col-0 (**Figure 3.5A**). This reduction indicates that DRB1 plays a major role in primary root development in *Arabidopsis*. In *drb2* plants, a significant increase in primary root length is observed, compared to Col-0 plants (**Figure 3.5A**). Considering the synergistic and antagonistic relationships between DRB1 and DRB2 (Eamens et al. 2012a; Pelissier et al. 2011), and the opposite effects that manipulating DRB1 and DRB2 function have on primary root length, it is clear that interactions between DRB1 and DRB2 and their effect on the sRNA environment play a major role in normal root development. Furthermore, a further decrease, compared to Col-0, in primary root length occurred in the *drb12* double mutant (**Figure 3.5A**). This observation provides further evidence of a need for both functional DRB1 and DRB2 for normal root development.

Similar trends to those observed for primary root length are present in lateral root number in the *drb1*, *drb2*, and *drb12* mutant backgrounds. A decrease in the number of lateral

roots by ~75% was observed in *drb1* plants when compared to Col-0, an effect more pronounced than the changes to primary root length. As with primary root length, there was a significant, ~60% increase, in lateral root number in *drb2* plants compared to Col-0 plants. However, the magnitude of this change in lateral root number was less than that on primary root length in *drb2* plants (**Figure 3.5B**). The opposing effects of manipulating DRB1 and DRB2 function on lateral root number further suggests a pivotal role for both DRB1 and DRB2 in controlling development of root architecture in *Arabidopsis* and is consistent with the 85% reduction in lateral root number observed in the *drb12* double mutant background (**Figure 3.5B**).

A different trend was observed across the Col-0, *drb1*, and *drb2* backgrounds when quantitatively assessing adventitious root number. Adventitious root number increased by ~160% in *drb1* plants when compared to Col-0 plants (**Figure 3.5C**). This increase in adventitious root number is inverse to the primary root and lateral root phenotypes and suggests that DRB1 is a major player throughout plant root development. Adventitious root number in *drb2* plants also displayed a different trend to that observed in *drb1* plants, with *drb2* plants still showing an approximate 50% increase in adventitious root number compared to Col-0 plants (**Figure 3.5C**). The increase in adventitious root number in both *drb1* and *drb2* genetic backgrounds indicates a similar role for DRB1 and DRB2 in controlling adventitious root development, instead of opposing roles observed for primary root length and lateral root number. However, an increase in adventitious root number in *drb12* plants compared to Col-0 of approximately 160% (**Figure 3.5C**), an increase equivalent to that observed in the *drb1* single mutant background, indicates that DRB1 is dominant over DRB2 function in determining adventitious root structure.

To fully understand the role played by DRB1 and DRB2 in root development, examination of the phenotypic effects of manipulating DRB1 and DRB2 function on aerial structures was analysed by measuring rosette leaf surface area. Leaf areas of *drb1* and *drb2* plants conform to the trends observed when examining primary root length and lateral root number, with a decrease in rosette leaf surface area of ~40% in *drb1* compared to Col-0 plants and an increase in *drb2* of ~60% (**Figure 3.5D**). This decrease in *drb1* is equivalent to that of the primary root length in the *drb1* background, potentially implying a link between these two phenotypic characteristics while the increase in *drb2* is equivalent in magnitude to the increase observed in lateral root number, again potentially indicating a link between these two phenotypic characteristics. The *drb12* double mutant plants show a compounded effect, with a

significant, ~60%, reduction in rosette leaf surface area compared to Col-0 (**Figure 3.5D**). As with primary root length and lateral root number, a more substantial decrease in rosette leaf surface area in the *drb12* double mutant background is indicative of the requirement for both DRB1 and DRB2 function for normal shoot development. However, examination of the relationships between these phenotypic characteristics has revealed that phenotypic changes in different aspects of root development, influenced by manipulating either DRB1 and DRB2 function, may cause changes in shoot development, and *vice versa*.

3.2.5 Molecular assessment of the miR160/*ARF10*/*ARF16*/*ARF17* expression module in Col-0, *drb1*, *drb2*, and *drb12* root tissue

To enable a comprehensive study of the effects of modifying the sRNA environment using *drb* mutant plant lines; an expression module, where a suite of genes is under posttranscriptional control directed by a single sRNA species, was selected for further analysis. From the degradome, sRNA mapping, and RT-PCR analyses two strong expression module candidates were presented; the miR167/*ARF6*/*ARF8* and miR160/*ARF10*/*ARF16*/*ARF17* expression modules. To gain the greatest depth of understanding only one expression module candidate was selected for further analysis. To this end, an examination of the miR160/*ARF10*/*ARF16*/*ARF17* expression module was conducted in Col-0, *drb1*, *drb2*, and *drb12* root tissue to elucidate the molecular mechanisms involved in directing the *drb1*, *drb2*, and *drb12* root architectural changes. This analysis should provide insight into the specific interaction between an example of a miRNA-targeted gene expression module, miRNA production machinery, and the role of DRBs in root development.

Figure 3.6. RT-qPCR analysis of the miR160/*ARF10*/*ARF16*/*ARF17* expression module. Analysed in root tissue of the Col-0 (blue), *drb1* (orange), *drb2* (grey), and *drb12* (yellow) genetic backgrounds were *PRI-MIR160A/B/C* precursor genes (A,B, and C), *eTM160-1* and *eTM160-2* miR160 endogenous target mimic (E and F), *ARF10/16/17* miR160 target genes (G, H, and I), and *DRB1* (J), *DRB2* (K), and *DRB4* (L) expression, and STL-qPCR analysis of miR160 accumulation (D). Fold changes were determined by the ΔΔCt method, with three biological replicates, and normalised to Col-0. Averages of expression fold change in *drb1*, *drb2*, and *drb12* genetic backgrounds were compared to Col-0 by a standard two-tailed t-test. Error bars represent SEM. *** $p \leq 0.001$, ** p- ≤ 0.01, * $p \leq 0.05$.

RT-qPCR examination of the miR160/*ARF10*/*ARF16*/*ARF17* expression module revealed the complexity of the DRB1/DRB2 relationship to the posttranscriptional regulation of this expression module. A large accumulation in precursor transcripts, *PRI-MIR160A*, *PRI-MIR160B*, and *PRI-MIR160C*, was observed in *drb1* root tissue when compared to their levels in Col-0 roots (**Figure 3.6A-C**). As DRB1 plays a pivotal role in the production of miR160 (Eamens et al. 2009), an increase in the accumulation of all miR160 precursors was expected in *drb1* mutant plants due to the inefficient precursor transcript processing in the absence of DRB1 activity. Were this the case, stem-loop RT-qPCR (STL-qPCR) should show a reduction in accumulation of mature miR160 compared to Col-0. This was confirmed for *drb1* plants with a significant reduction observed in the amount of mature miR160 that accumulated (**Figure 3.6D**).

In *drb2* plants, however, the inverse trend was not observed. While a significant increase in the accumulation of both *PRI-MIR160A* and *PRI-MIR160C* precursors was determined (**Figure 3.6A** and **C**), a decrease in the accumulation of *PRI-MIR160B* precursor transcript was also observed in *drb2* roots compared to its abundance in Col-0 roots (**Figure 3.6B**). Furthermore, there was only a mild elevation in mature miR160 abundance in *drb2* roots compared to Col-0 roots (**Figure 3.6D**). In *drb12* double mutant plants, a further increase in *PRI-MIR160A* and *PRI-MIR160C* precursor transcript accumulation was observed although no significant change was observed for the *PRI-MIR160B* precursor (**Figure 3.6A-C**). From this observation, it might be expected that a decrease in mature miR160 accumulation would be observed, similar to that in the *drb1* single mutant background. Surprisingly, however, a substantial increase in mature miR160 accumulation was observed compared to Col-0 (**Figure 3.6D**). This increase in miR160 production could be attributed to the unchanged accumulation of *PRI-MIR160B* precursor transcripts in *drb12* plants compared to Col-0. This would indicate potential role(s) for other miRNA biogenesis machinery proteins in the processing of *MIR160* precursor transcripts to produce mature miR160 in the absence of DRB1 and DRB2 activity.

Apart from conventional transcriptional control through regulating precursor expression, miR160 levels are also modulated through eTM-mediated sequestration (Boer et al. 2014). Examination of *eTM160-1* and *eTM160-2* abundance in *drb1* plants revealed a reduction in the levels of both transcripts compared to Col-0 (**Figure 3.6E** and **F**) suggesting that *eTM160* levels scale to the levels of mature miR160 sRNA that these two non-protein-coding RNAs sequester. Further evidence for this is evident as *eTM160-1* and *eTM160-2* levels both significantly increase in *drb12* plants compared to Col-0, corresponding to the observed

abundance increase in mature miR160 levels in the *drb12* background. However, observations of *eTM160-1* and *eTM160-2* levels in *drb2* plants showed an increase, for *eTM160-1*, and a decrease, for *eTM160-2*, compared to their levels in Col-0 plants (**Figure 3.6E** and **F**). Considering that mature miR160 levels are unchanged compared to Col-0 in *drb2* plants, *eTM160-1* and *eTM160-2* could be working in concert with each other to further fine-tune mature miR160 abundance in *drb2* roots.

Examining miR160 production and regulation in distinct *drb* mutant backgrounds provides a framework for analysing changes in expression of the miR160 target genes, *ARF10*, *ARF16*, and *ARF17*. If miR160 is directing posttranscriptional regulation via transcript cleavage, then increasing or decreasing levels of the mature miR160 should display an inverse abundance trend to those of its targeted transcripts, *ARF10*, *ARF16*, and *ARF17*. When *ARF10*, *ARF16*, and *ARF17* expression was measured in *drb1* plants, an increase in target gene expression was observed that was inversely proportional to the decreased abundance of mature miR160 (**Figure 3.6D**, **G-I**). When observing target gene expression in *drb2* plants, the same trend, of conforming to mature miR160 levels, holds true for *ARF10* and *ARF17*, as both transcripts showed only a very mild elevation in expression (**Figure 3.6G** and **I**). However, an increase in expression compared to Col-0 was observed for *ARF16* (**Figure 3.6H**), despite mature miR160 levels remaining unchanged in this genetic background. Target gene expression either remained unchanged, *ARF10*, or increased, *ARF16* and *ARF17*, in *drb12* plants compared to Col-0 plants (**Figure 3.6G-I**). This increase in target gene expression is contrary to the inversely proportional expression trend expected, with both *ARF* transcripts scaling in increased abundance along with mature miR160 accumulation in *drb12* root tissue. Only *PRI-MIR160B* precursor transcript accumulation remained unchanged in *drb12* plants, suggesting a regulatory link between mature miR160 produced from *PRI-MIR160B* precursors targeting *ARF10*, as they display the same expression trend in *drb12* root tissue.

Further exploration of the interaction between miRNA biogenesis machinery was conducted to identify the role for different DRB proteins in miR160 production. Analysing *DRB1* expression in *drb1*, *drb2*, and *drb12* root tissue showed, the expected complete absence of expression in *drb1* and *drb12* plants consistent with these lines being null knockouts for DRB1. However, *DRB1* expression did increase in *drb2* root tissue compared to Col-0 roots (**Figure 3.6J**). Again, this result is not surprising as the antagonistic role between DRB1 and DRB2 is well documented (Eamens et al. 2012a; Eamens et al. 2012b; Reis et al. 2015). When analysing *DRB2* expression, no expression, as expected, was detected in the *drb2* and *drb12*

mutants (**Figure 3.6K**). No increase in *DRB2* expression was observed in *drb1* roots compared to Col-0 roots, a finding that indicates that in *Arabidopsis* roots, elevated *DRB2* gene activity does not occur in order to compensate for loss of DRB1 activity (**Figure 3.6J** and **K**).

DRB4 expression was also tested in the lines because an antagonistic relationship between DRB2 and DRB4 has been reported previously (Pelissier et al. 2011). *DRB4* expression increases in both *drb2* and *drb12* root tissue compared to Col-0 roots consistent with this proposed antagonistic relationship (**Figure 3.6L**). However, no change in *DRB4* expression was observed in *drb1* root tissue although a compounded effect was present in the *drb12* double mutant, as shown by a significantly larger increase in *DRB4* expression in the double mutant than the single *drb2* mutant background. This suggests that in the absence of both DRB1 and DRB2 activity, DRB4 may facilitate processing of a proportion of the miR160 precursor transcripts that over-accumulate.

3.3 Discussion

3.3.1 Predicting sRNA-directed regulation of auxin pathway gene expression from degradome and sRNA mapping analyses

There are several demonstrated examples of sRNA-mediated posttranscriptional regulation of auxin pathway genes, including, but not limited to *ARF3*, *ARF4* (Williams et al. 2005), *ARF6*, *ARF8* (Kinoshita et al. 2012), *ARF10*, *ARF16*, *ARF17* (Mallory et al. 2005), and *TIR1* (Windels and Vazquez 2011). These demonstrations show that *ARF6* and *ARF8* are under miR167-mediated posttranscriptional regulation (Kinoshita et al. 2012), *ARF10*, *ARF16*, and *ARF17* are under miR160-mediated posttranscriptional regulation (Mallory et al. 2005), and *TIR1* is under miR393-mediated posttranscriptional regulation (Windels and Vazquez 2011), while *ARF3* and *ARF4* are under tasiARF-mediated posttranscriptional regulation (Williams et al. 2005). Each of these forms an expression module, a suite of genes under posttranscriptional control directed by a single sRNA species.

sRNA sequence mapping and degradome profiling analyses, techniques not previously utilised to examine such a comprehensive set of auxin pathway genes, confirmed these previously demonstrated examples of sRNA-directed auxin pathway gene expression regulation at the posttranscriptional level. The appearance of multiple degradome peaks along both the *ARF3* and *ARF4* transcripts (**Figure 3.1B** and **C**) is indicative of the phased production of secondary siRNAs following the initial cleavage of the *ARF3* and *ARF4* transcripts by the targeting sRNA, tasiARF (Montgomery et al. 2008; Nakazawa et al. 2007). Similar degradome profiling of the *ARF6* and *ARF8* transcripts shows a single primary cleavage peak (**Figure 3.1D** and **E**) indicative of miRNA-mediated posttranscriptional regulation and confirmed that the primary contributor to these single peaks on the *ARF6* and *ARF8* transcripts is miR167 (**Figure 3.2D** and **E**) (Kinoshita et al. 2012). miR160 was also identified as the primary contributor to the major, and single cleavage peak mapped to the *ARF10*, *ARF16*, and *ARF17* transcripts. A finding that again confirmed the role of miR160 in the posttranscriptional regulation of *ARF10*, *ARF16*, and *ARF17* gene expression (Mallory et al. 2005). Such analyses also support the miR393-directed posttranscriptional regulation of the *TIR1* transcript (**Figure 3.1F**). The single cleavage peak in the degradome profile of the *TIR1* transcript, and the identity of the sRNA sequence aligning to the same transcript position (**Figure 3.2F**) confirmed the role of miR393 in targeting *TIR1* transcripts in posttranscriptional repression.

The reproducibility of degradome profiling and sRNA sequence alignment data in confirming the role of these known sRNA regulators provides strong supportive evidence for the putative identification of potentially novel sRNA-mediated posttranscriptional regulatory relationships with auxin pathway genes. Three such auxin pathway genes, *BIG*, *Aux/IAA1*, and *Aux/IAA14*, have been putatively identified here as also being under sRNA-directed expression regulation (**Figure 3.1G-I** and **3.2G-I**).

For *Aux/IAA1*, the only peak to align in both the degradome and sRNA sequence mapping analyses shares significant sequence homology with a wheat miRNA, miR1134. However, in wheat, miR1134 has been shown to have highest abundance in leaf tissue (Pandey et al. 2013), whilst *Aux/IAA1* has a low abundance in *Arabidopsis* leaves (Yang et al. 2004). Small RNA sequence mapping analyses indicated that aligned unknown sRNA sequences require DRB1, and either DRB2 or DRB4 for their production. RT-PCR analysis of *Aux/IAA1* transcript abundance further supported the requirement for DRB2 in the production of these sRNA species that aligned to the *Aux/IAA1* transcript.

Conversely, *Aux/IAA14* presents as a stronger candidate for sRNA-directed posttranscriptional regulation. A significant number of cleavage products, forming a cleavage '*hotspot*', are observed in the 5' region of the *Aux/IAA14* transcript (**Figure 3.1I**). This is indicative of siRNA regulation, but most sRNA mapped sequences align to the 3' region of the *Aux/IAA14* transcript, forming a second cleavage '*hotspot*' (**Figure 3.2I**). The potential exists for cleavage products from the 5' cleavage '*hotspot*' to act as an amplifier of the siRNA signal, targeting *Aux/IAA14* (in the 3' region) and other related genes with sequence homology to *Aux*/*IAA14*. Additionally, DRB2 was implicated in mediating the production of putative siRNA species, as most sequence alignment peaks were absent in the *drb2* background (**Figure 3.2I**). The requirement for DRB2 in mediating the biogenesis of these siRNA species was further supported by the increase in *Aux/IAA14* transcript abundance in the absence of DRB2. The irregular spacing of these cleavage points along the transcript is indicative of *cis*-natsiRNA (Martinez de Alba et al. 2011; Parent et al. 2015), adding support to the argument that *Aux/IAA14* may act as a template for siRNA production going on to target closely related *Aux/IAA* gene in posttranscriptional gene silencing pathways.

BIG acts differently to Aux/IAA1 and Aux/IAA14 in auxin transport by chaperoning intracellular auxin transport vesicles to PIN proteins for auxin efflux (Gil et al. 2001; Lopez-Bucio et al. 2005). The *BIG* transcript shows a predominant cleavage peak at the 5' end of the transcript, followed by numerous smaller sized cleavage peaks in the 5' to 3' direction (**Figure**

3.1G), suggestive of a single miRNA cleavage site with siRNA silencing signals stemming from that initial point of cleavage. However, while sRNA sequence mapping shows sRNA alignments in the 5' region before the typical miRNA peak, the high number of reads in the *drb2* background, with DRB2 antagonistic to DRB4, suggests siRNA-mediated posttranscriptional regulation (**Figure 3.2G**). The cleavage pattern of a large cleavage peak, from targeted miRNA-directed cleavage, followed by numerous smaller cleavage peaks along the transcript length, from specific siRNA-directed targeting, is indicative of phasiRNA activity (Fei et al. 2013). Increases in *BIG* transcript abundance in *drb1*, *drb2*, and *drb12* mutants indicates that both DRB1 and DRB2 are required to produce these sRNAs species. This suggests that DRB1 and/or DRB2 are required for production of this unknown miRNA, most likely triggering production of siRNAs from the *BIG* transcript mediated by DRB4. Such a posttranscriptional regulatory relationship is present in two other auxin pathway genes, *ARF3* and *ARF4*, that are targeted by tasiARFs (Williams et al. 2005).

While the *TIR1* transcript is known to be under miR393-mediated posttranscriptional regulation (Windels and Vazquez 2011), evidence presented in this study suggests that other posttranscriptional regulatory pathways may be important for *TIR1* expression control. Two additional peaks present in the sRNA sequence mapping analysis of the *TIR1* transcript indicate that other miRNAs, additional to miR393, may target the *TIR1* transcript (**Figure 3.2F**). This finding is supported by the significant increase in *TIR1* transcript abundance in the absence of DRB2. However, the length of one of these sRNA sequences is 24-nt, differing from the 21-nt length of a typical miRNA. This length, the absence of corresponding degradome peaks, and the lowest sRNA sequence reads being observed in the *drb2* background, all suggest p4-siRNAs as potential candidate regulators of *TIR1* expression. p4-siRNAs are a class of siRNA which are dependent on RNA polymerase IV (PolIV) transcriptional activity (Mosher et al. 2008). p4-siRNAs are known to form by random cleavage initiated within p4-siRNA producing genetic loci, leading to irregular alignment patterns within those regions (Mosher et al. 2008). DRB2 and DRB4 are both required for the proper accumulation of p4-siRNAs in *Arabidopsis* (Pelissier et al. 2011), and as such, the absence of both miR393-mediated (DRB1) and p4-siRNA-mediated (DRB2) posttranscriptional regulation of *TIR1* transcripts in the *drb12* background results in deregulation of *TIR1* expression.

DRB2 appears to play a role in directing biogenesis of some of the putative sRNAs targeting auxin pathway gene transcripts, specifically *Aux/IAA14*, *BIG*, and *TIR1*. The action of DRB2 in this process may either be direct, in mediating sRNA biogenesis, or indirect,

through antagonism with either DRB1 or DRB4 function (Eamens et al. 2012a; Pelissier et al. 2011). Furthermore, established miRNA regulated auxin pathway modules, such as *ARF6* and *ARF8* targeted by miR167 (Kinoshita et al. 2012), and *ARF10*, *ARF16*, and *ARF17* targeted by miR160 (Mallory et al. 2005), show significant reductions in miRNA sequences aligning to the target site in the *drb2* background. Such an observation indicates a role for DRB2 in mediating the biogenesis of miR167 and miR160 independent of DRB1.

3.3.2 Analysis of auxin pathway gene transcripts in *drb* mutant backgrounds delivers insight into sRNA production machinery interactions with the sRNA environment

In *Arabidopsis*, the three main DRB proteins that form functional partnerships with DCL proteins, are thought to regulate related, yet distinct sRNA biogenesis pathways. DRB1 is the functional partner of DCL1, a partnership that is thought to exclusively mediate miRNA production (Han et al. 2004; Vazquez et al. 2004a). DRB4 forms a functional partnership with DCL4 to direct siRNA biogenesis (Adenot et al. 2006), while DRB2 can potentially interact with either DCL1 or DCL4 and is required for both miRNA biogenesis (Eamens et al. 2012a) and siRNA production (Pelissier et al. 2011).

sRNA sequence mapping analysis suggested a role for DRB2 in two previously established posttranscriptional miRNA-mediated auxin pathway gene regulatory modules, the miR167/*ARF6*/*ARF8* and miR160/*ARF10*/*ARF16*/*ARF17* modules (**Figure 3.2**). The closely related *ARF6* and *ARF8* genes have previously been identified as being under miR167-mediated posttranscriptional regulation (Kinoshita et al. 2012), and miR167 production has been shown to be directed by the DRB1/DCL1 functional partnership (Eamens et al. 2009). RT-PCR analysis of the *ARF8* transcript indicated that DRB1 is required for miRNA biogenesis for correct miR167-directed *ARF8* regulation (**Figure 3.3**). However, the lack of a change in *ARF6* transcript levels in the *drb1* single mutant background indicates that this may not be the case for *ARF6*. RT-PCR examination of *ARF8* also showed a comparable increase in *ARF8* transcript abundance in the *drb2* background where DRB1 is still functional (**Figure 3.3**). This observation, coupled with the fact that the only apparent increase in *ARF6* transcript abundance occurred in the *drb12* double mutant background, suggests that DRB1 and DRB2 are required for miR167 production for targeting of the *ARF8* transcript to correctly regulate its expression. For miR167-directed expression regulation of *ARF6*, either DRB1 or DRB2 is required to

produce the miR167 sRNA, but these two DRBs are not necessarily acting together when performing this role.

A similar sRNA sequence mapping profile indicates a role for DRB2 in miR160 control of *ARF10*, *ARF16*, and *ARF17* expression (**Figure 3.2**). *ARF10*, *ARF16*, and *ARF17* are known targets of miR160 (Mallory et al. 2005), and miR160 production is thought to be mediated by the DRB1/DCL1 functional partnership (Eamens et al. 2009). RT-PCR analysis of *ARF10* and *ARF16* show higher transcript abundance in both the *drb1* and *drb2* single mutant backgrounds, supporting the established role of DRB1, but adding DRB2 as a candidate in further regulating the miR160/*ARF10*/*ARF16*/*ARF17* expression module (**Figure 3.3**). *ARF16* continues to demonstrate this increase in the *drb12* double mutant, while *ARF10* abundance appears to return to wild-type levels in the double mutant, providing a preliminary demonstration of mechanistic differences in the regulation of *ARF10* and *ARF16*. However, *ARF17* transcript abundance only increased in the *drb1* background (**Figure 3.3**). The absence of a similar increase in the *drb12* background indicates that, in the absence of both DRB1 and DRB2, alternative pathways may exist to regulate *ARF17* transcript abundance. These findings suggest that both DRB1 and DRB2 are required for miR160-directed expression regulation of *ARF16*. While miR160 biogenesis to target *ARF10* for expression regulation appears to also require both DRB1 and DRB2 and, further, in the absence of both of these DRBs, alternative pathways exist to ensure *ARF10* transcript abundance remains at wild-type levels. Alternative pathways regulating *ARF17* expression must also exist, potentially overlapping with regulatory pathways for *ARF10* in the absence of both DRB1 and DRB2. Such a novel role for DRB2 in mediating miRNA production in established auxin pathway gene regulatory modules encourages the examination of the specific role that DRB2 plays in influencing the sRNA environment, while interacting with established DRB1-mediated pathways.

3.3.3 The miR160/*ARF10/ARF16/ARF17* expression module provides a model system with which to study miRNA biogenesis-auxin signalling interactions

From the sRNA sequence mapping analysis (**Figure 3.2**) and semi quantitative RT-PCR assessment (**Figure 3.3**), DRB proteins other than DRB1 appear to play a potential role in sRNA biogenesis, ultimately mediating posttranscriptional regulation of auxin pathway genes. Two strong expression module candidates in this endeavour were presented, the miR167/*ARF6*/*ARF8* and miR160/*ARF10*/*ARF16*/*ARF17* expression modules. Only one

expression module, the miR160/*ARF10/ARF16/ARF17* module, was selected for further in-depth analysis of the phenotypic and molecular consequences of manipulating DRB1 and DRB2 activity.

The miR160/*ARF10/ARF16/ARF17* expression module has been described in the literature as influencing the development of root architecture in *Arabidopsis*. ARF10 and ARF16 have a demonstrated role in maintaining the maintenance of the distal stem cell population in the root cap (Ding and Friml 2010), thereby ensuring normal primary root elongation. ARF16 and ARF17 have been shown to repress lateral root primordia formation (Couzigou and Combier 2016; Mallory et al. 2005; Wang et al. 2005), while ARF10 and ARF16 have a demonstrated role in determining the gravitropic setpoint angle (GSA) in developing lateral roots (Roychoudhry et al. 2013). Further, ARF17 has also been shown to repress adventitious root formation independent of ARF10 and ARF16 (Mallory et al. 2005).

Considering these documented roles, it was unsurprising to see a decrease in lateral root number in the *drb1* and *drb12* backgrounds (**Figure 3.4B**). As DRB1 is the primary DRB protein involved in miR160 biogenesis (Eamens et al. 2009), it is expected that *ARF10*, *ARF16*, and *ARF17* abundance would increase in plants deficient in DRB1-mediated miR160 production. Indeed, this is the case: RT-qPCR analysis showed a significant reduction in mature miR160 abundance (**Figure 3.5D**), a result of inefficient precursor processing as demonstrated by the over-accumulation of the *PRI-MIR160A*, *PRI-MIR160B*, and *PRI-MIR160C* precursor transcripts in the *drb1* background (**Figure 3.5A-C**). Following on from this, *ARF10*, *ARF16*, and *ARF17* transcript abundance increased in *drb1* root tissue because of the disrupted posttranscriptional regulation by miR160. However, primary root length decreases, and adventitious root number increases, in the *drb1* background (**Figure 3.4A** and **C**). Primary root elongation was expected to be disrupted in the root cap with elevated *ARF10* and *ARF16* abundance, as this would decrease the distal stem cell population leading to a reduction in primary root length (Ding and Friml 2010). However, increased *ARF17* transcript abundance might have been expected to lead to a reduction in the number of adventitious roots, as ARF17 represses adventitious root formation (Mallory et al. 2005).

These apparently contradicting phenotypic and molecular data may be partially resolved by considering the role of DRB2-mediated sRNA production in the miR160/*ARF10*/*ARF16*/*ARF17* expression module. Primary root length, and lateral and adventitious root number, all substantially increase in the *drb2* background (**Figure 3.4A-C**). In the established model, these phenotypes would suggest that *ARF10*, *ARF16*, and *ARF17*

expression would be significantly reduced in the *drb2* background. Examination of *ARF10*, *ARF16*, and *ARF17* transcript abundance showed that only *ARF16* expression increases, with no change in either *ARF10* or *ARF17* expression observed in *drb2* root tissue (**Figure 3.5G-I**). Furthermore, mature miR160 abundance remains unchanged, while *PRI-MIR160A* and *PRI-MIR160C* accumulation is slightly elevated, and *PRI-MIR160B* precursor transcript levels are decreased in *drb2* root tissue (**Figure 3.5A-D**). From this, it can be proposed that normal processing of *PRI-MIR160A* and *PRI-MIR160C* requires DRB2, and the absence of efficient processing of these precursors leads to deregulation of *ARF16* expression by loss of miR160-mediated posttranscriptional silencing. Not only is the most significant increase in *ARF16* transcript abundance observed in DRB2 deficient genetic backgrounds, but there is no increase in *ARF16* transcript levels between the *drb2* and *drb12* backgrounds despite a substantial increase in mature miR160 abundance. This relationship between *ARF16* and DRB2 implies translational repression. DRB2 is known mediate the biogenesis of miRNAs that direct posttranscriptional silencing roles via translational repression, as opposed to transcript cleavage (Reis et al. 2015). Translational repression is a relatively common posttranscriptional gene silencing mechanism in plants (Beauclair et al. 2010; Mallory and Bouche 2008), but there is no documented role for miR160 participating in translational repression. Nevertheless, the involvement of DRB2 in mediating miRNA biogenesis that goes on to target genes for translational repression, coupled with the increase in *ARF16* transcript abundance in the *drb2* background, suggests this may the case.

The primary, lateral, and adventitious root phenotypes of *drb12* plants resemble *drb1* plants more closely than the *drb2* mutant, with decreases in primary root length and lateral root number, and an increase in adventitious root number (**Figure 3.4A-C**). However, the molecular profile of *drb12* roots does not match the molecular profile of *drb1* root tissue. While *PRI-MIR160A* and *PRI-MIR160C* precursor transcript accumulation remained elevated, *PRI-MIR160B* precursor levels did not change compared to their levels in wild-type roots (**Figure 3.5A-C**). More surprisingly, mature miR160 abundance is significantly increased in *drb12* root tissue (**Figure 3.5D**). Such an increase would be expected to repress the expression of *ARF10*, *ARF16*, and *ARF17* resulting in the observed phenotypic changes displayed by *drb12* plants. However, no change in *ARF10*, *ARF16*, or *ARF17* transcript abundance was observed in the double mutant. Instead, increases in both *ARF16* and *ARF17* expression were detected by RT-qPCR, although the alterations to *ARF16* and *ARF17* transcript levels did not differ in the *drb12* double mutant compared to either the *drb2* or the *drb1* single mutant

backgrounds (**Figure 3.5H** and **I**). Such expression trends indicate that *ARF16* may be under miR160-directed translational repression (DRB2) with *ARF17* under miR160-directed transcript cleavage repression (DRB1).

Intriguingly, *ARF10* transcript abundance returns to wild-type levels in the *drb12* background, previously having shown an increase in abundance in the *drb1* background (**Figure 3.5G**). This is further suggestive of the role that additional DRB proteins may play in the biogenesis of miR160 to regulate *ARF10*, *ARF16*, and *ARF17* expression in *Arabidopsis* root tissue. However, an additional regulatory mediator does exist in the miR160/*ARF10*/*ARF16*/*ARF17* expression module. The existence of *e*ndogenous *t*arget *m*imics (eTMs) for miR160 (*eTM160-1* and *eTM160-2*) (Wu et al. 2013), allows for posttranscriptional regulation of the posttranscriptional regulator. It is possible that even though mature miR160 abundance and *MIR160* precursor transcript processing changes are evident across the *drb* backgrounds, *eTM160-1* and *eTM160-2* moderate the impact of these changes in *Arabidopsis* root tissue. Both *eTM160-1* and *eTM160-2* abundance decreases in the *drb1* background indicating that both *eTM160-1* and *eTM160-2* scale with mature miR160 levels. However, in *drb2* root tissue, *eTM160-1* abundance increased while *eTM160-2* abundance remains reduced (**Figure 3.5E** and **F**). This is indicative of distinct roles for *eTM160-1* and *eTM160-2* from each other, possibly that *eTM160-1* is a target for miR160-directed transcript cleavage regulation, while *eTM160-2* is a target for miR160-directed translational repression mediated regulation. In either case, both *eTM160-1* and *eTM160-2* abundance responds to the dramatic increase in mature miR160 abundance in *drb12* root tissue, again illustrating the ability for both *eTM160-1* and *eTM160-2* to scale to miR160 levels.

3.3.4 Conclusions

It appears that in *Arabidopsis* root tissue that DRB1-mediated biogenesis of miR160 leads to posttranscriptional regulation of *ARF10*, *ARF16*, and *ARF17* expression. While this appears to be the exclusive situation for *ARF17*, DRB2-mediated miR160 biogenesis may direct translational repression of the *ARF16* transcript additional to classic transcript cleavage posttranscriptional regulation. DRB2 appears to have no direct role in mediating miR160 biogenesis targeting *ARF10*, but in the absence of both DRB1 and DRB2, some alternate posttranscriptional regulatory pathway seems to exist whereby *ARF10* expression can still be moderated. In addition, *eTM160-1* and *eTM1602* appear to respond differently to mature miR160 produced through either a DRB1- or DRB2-mediated biogenesis pathway. Consequently, the role of DRB2, and therefore the role of translational repression, in the miR160/*ARF10/ARF16/ARF17* expression module warrants further exploration. This subject will form the basis of the following two chapters.

Chapter 4

The effect of exogenous auxin application on the *Arabidopsis thaliana* miR160/ *ARF10*/*ARF16*/*ARF17* expression module

4.1 Introduction

AUXIN RESPONSE FACTORs (ARFs) are one of the three main gene families that drive plant genetic responses to auxin signalling and intracellular auxin perception (Guilfoyle and Hagen 2007; Kepinski and Leyser 2004; Reed 2001). These ARFs form the basis of this genetic response to auxin, because their functional repression in the absence of auxin is mediated by interactions with Aux/IAA proteins (Guilfoyle and Hagen 2007; Kepinski and Leyser 2004; Overvoorde et al. 2005; Reed 2001).

There are 23 members of the *Arabidopsis ARF* gene family, including five transcriptional activators, 18 transcriptional repressors, three truncated transcripts, and one pseudogene (Guilfoyle and Hagen 2007). ARF function is determined by three main regions within each ARF protein, namely the N-terminal located DNA-binding domain (DBD), a middle region which functions either as an activator domain (AD) or a repressor domain (RD), and the C-terminal located dimerization domain (CTD) (Guilfoyle 2001; Tiwari et al. 2003). It is the CTD that facilitates the formation of ARF:Aux/IAA heterodimers, as well as the formation of ARF:ARF dimerisation necessary for transcription factor function of each ARF (Boer et al. 2014; Guilfoyle 2001; Tiwari et al. 2003). The DBD facilitates the interaction between the ARF protein dimers and the promoter region of each target gene, but it is the AD and RD that locate the auxin response elements (*ARE*s) harboured within the *ARG* promoter regions that direct either transcriptional activation or repression based on the functionality of the bound ARF (Guilfoyle 2001; Tiwari et al. 2003).

ARFs have numerous and diverse functions in plant growth and development. For example, ARF5 and ARF7, both transcriptional activators, have been identified as major players in embryonic patterning (Hardtke and Berleth 1998). Indeed, ARF5 and ARF7 are only partially functionally redundant, as embryonic patterning is disrupted to a greater degree in the *arf5 arf7* double mutant than in either the *arf5* or *arf7* single mutant (Hardtke and Berleth 1998). ARF5 independent of ARF7, has a demonstrated role in root initiation (Hamann et al. 2002). This underlines the importance of ARFs in early development, as embryonic patterning is crucial to plant development, and the primary root radical is the first observed plant structure to develop outside of the embryonic stages. ARF1 and ARF2 exemplify the importance of ARF-directed gene expression regulation during later development, as ARF1 and ARF2 have been demonstrated to act together to regulate leaf senescence and floral organ abscission (Ellis et al. 2005), processes important for vegetative phase change and, ultimately, plant

reproduction. Further, due to their demonstrated role as central transcriptional regulators in plant auxin responses, it is unsurprising that collectively the ARFs control almost all aspects of plant development at nearly every stage. During leaf development and determination of leaf polarity, ARF3 functions in conjunction with the transcription factor KANADI1 to establish a developmental gradient (Kelley et al. 2012) which later leads to boundary definition of organs in those regions based on placement of those cellular groups (developing organs) during leaf development. It is interesting in this case that ARF3, one of the *ARF* genes with a truncated coding region (Ckurshumova et al. 2012), is involved in such a critical plant developmental process.

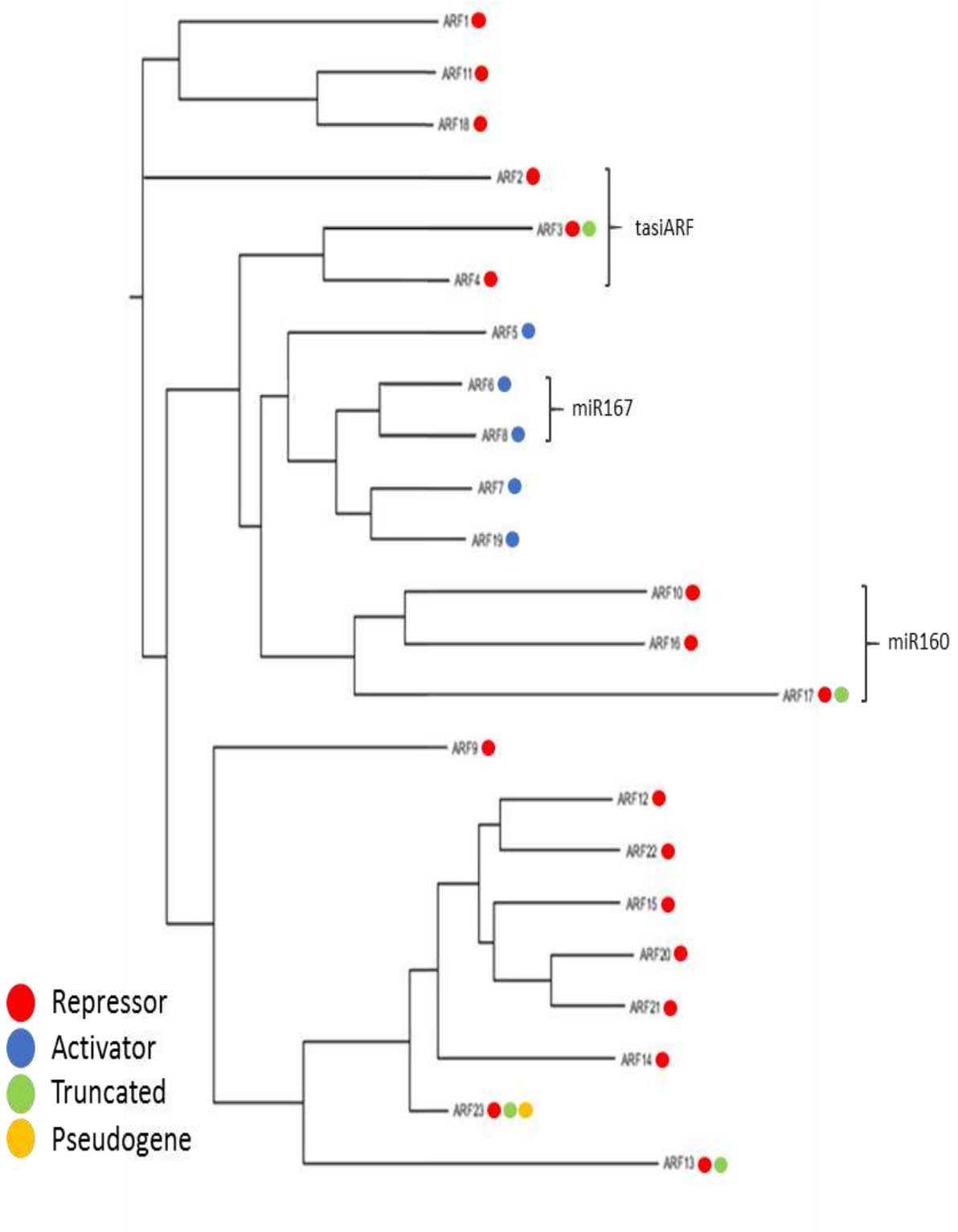

Figure 4.1. A phylogenetic tree showing the evolutionary relationship between all 23 *ARF* transcription factor family members in *Arabidopsis*. Amino acid sequence, obtained from the TAIR website, similarity between all 23 ARF transcription factor family members was compared using the Bootleg alignment function of Figtree v1.3.1. Each ARF family member has been marked based on function as either a transcriptional repressor (red) or a transcriptional activator (blue). *ARF* genes missing at least one of the three hallmark regions has been marked as truncated (green). ARFs showing high sequence similarity, but possess no transcription factor function, are pseudogenes (yellow).

In **Chapter 3**, it was shown that several suites of *ARF* genes are under sRNA-directed posttranscriptional regulation, notably (1) miR167-directed *ARF6* and *ARF8* regulation (Kinoshita et al. 2012), (2) miR160-directed *ARF10*, *ARF16*, and *ARF17* regulation (Mallory et al. 2005), and (3) tasiRNA-directed *ARF2*, *ARF3*, and *ARF4* regulation (Williams et al. 2005), each forming a unique expression module. Each suite of genes, regulated by a specific sRNA, forms a distinct sub-clade within the ARF family (**Figure 4.1**). Posttranscriptional regulation of each of these sub-clades through one sRNA-mediated regulatory pathway is significant not only because of the close phylogenetic relationship between each of the regulated groups of *ARF*s, but because of the closely related function of the ARFs within each sub-clade. For example, ARF2, ARF3, and ARF4 all function to determine the polarity of leaves or other organs (Ellis et al. 2005; Hunter et al. 2006; Kelley et al. 2012). Two additional family members, ARF6 and ARF8, have an even closer relationship, functioning redundantly in regulating flower maturation (Finet et al. 2010), and the miR160 targets, ARF10, ARF16, and ARF17, have been noted for their role in regulating root cap development and lateral root primordia formation and subsequent root growth (Mallory et al. 2005; Wang et al. 2005). The ARF10 and ARF16 proteins have a particularly close relationship to one another, functioning either in concert or redundantly, in their root development regulatory roles (Wang et al. 2005). It is not surprising that ARF10 and ARF16 function is more closely related to each other, than to the function of ARF17. ARF17 is one of the three family members that is truncated at its CTD (**Figure 4.1**) (Guilfoyle and Hagen 2007), setting ARF17 apart from ARF10 and ARF16, and from the ARF family members as a whole.

Not only is it of interest that each of these three ARF sub-clades are posttranscriptionally regulated by a single sRNA species, but that some of these sRNA regulatory species are produced through functionally distinct biogenesis pathways. miR167 biogenesis, the miRNA targeting *ARF6* and *ARF8* for expression regulation, is thought to be predominantly mediated by DRB1 (Eamens et al. 2009). DRB1 directs the selection of the miR167 guide strand, as opposed to the miR167 passenger strand, when the duplex is loaded into AGO1, thereby miR167 mediates posttranscriptional regulation via mRNA cleavage of the *ARF6* and *ARF8* target transcripts (Eamens et al. 2009). miR160, which targets *ARF10*, *ARF16*, and *ARF17* for expression repression, is also thought to be produced in a DRB1-dependent fashion, illustrated by a reduction in mature miR160 abundance, and an increase in *ARF10*, *ARF16*, and *ARF17* transcript abundance in the *drb1* mutant (**Figure 3.6**) (Eamens et al. 2009; Vazquez et al. 2004a; Wu et al. 2007). tasiRNA-directed posttranscriptional

regulation of *ARF2*, *ARF3*, and *ARF4* involves more processing steps than either the miR167 or miR160 production pathways. miR390, which is produced through a DRB1-dependent biogenesis pathway (Nakazawa et al. 2007), directs AGO7-mediated cleavage of the *TAS3* precursor transcript (Nakazawa et al. 2007). A molecule of dsRNA is then synthesised from the cleaved *TAS3* template and is processed by the DRB4/DCL4 functional partnerships to produce a population of in-phase 21-nt tasiRNAs (Nakazawa et al. 2007). Liberated tasiRNAs are subsequently loaded into AGO1, with AGO1 using a single loaded tasiRNA, the tasiARF sRNA, to target the *ARF2*, *ARF3*, and *ARF4* transcripts for mRNA cleavage-based expression repression (Montgomery et al. 2008; Nakazawa et al. 2007). Therefore, the tasiARF pathway requires two distinct DRB/DCL functional partnerships and two functionally distinct AGO proteins. Together, the miR167/*ARF6*/*ARF8*, miR160/*ARF10*/*ARF16*/*ARF17*, and tasiRNA/*ARF2*/*ARF3*/*ARF4* expression modules illustrate the intimate relationship between auxin signalling and sRNA-mediated posttranscriptional regulation of *ARF* gene expression.

4.1.1 The miR160/ARF10/ARF16/ARF17 expression module

Each of these expression modules exhibit responses to both auxin signalling and sRNA-directed transcript regulation, the miR160/*ARF10/ARF16/ARF17* expression module holds particular interest to this program of research. In **Chapter 3**, lateral root phenotypic responses were demonstrated in the *drb2* genetic background (**Figure 3.5B** and **C**), along with changes in miR160 processing and miR160 target gene expression (**Figure 3.6**). This indicates that a molecularly distinct miR160 pathway may exist in *Arabidopsis* roots. Considering this, the miR160/*ARF10*/*ARF16*/*ARF17* expression module provides a potentially unique demonstration of:

i) miRNA-directed posttranscriptional gene expression regulation;
ii) auxin-induced gene expression regulation;
iii) posttranscriptional regulation, via *eTM160* expression, of a posttranscriptional regulator (miR160), and;
iv) potential tissue-specific, DRB-mediated regulation of miR160 production.

Taken together, these possibilities make the miR160/*ARF10/ARF16/ARF17* expression module an excellent model for investigating the complex relationship between auxin signalling, post-production control of a posttranscriptional regulator, and the determination of the mechanism of miRNA-directed RNA silencing mediated by a single miRNA to regulate the expression of its targeted genes in developmentally distinct tissues. Furthermore, obtaining additional understanding into this complex gene expression regulatory module should enhance our current knowledge on plant root growth and development.

4.1.2 Aims and objectives in this chapter

This chapter aims to deconstruct this complex relationship between auxin signalling and the miR160/*ARF10*/*ARF16*/*ARF17* expression module.

Specifically, this chapter aims to:

- Examine the phenotypic and molecular consequences of exogenous auxin treatment on the miR160/*ARF10*/*ARF16*/*ARF17* expression module in Col-0, *drb1*, *drb2*, and *drb12* roots.
- Investigate the relationship between DRB1, DRB2, and DRB4, and their respective roles in miR160 production and/or miR160-directedposttranscriptional regulation of *ARF10*, *ARF16*, and *ARF17* expression.

4.2 Results

4.2.1 Phenotypic assessment of synthetic auxin treated Col-0, *drb1*, *drb2*, and *drb12* shoot and root development

Phenotypic changes resulting from modifications in DRB-mediated miRNA production pathways demonstrated the pivotal roles played by DRB proteins in the efficient and accurate processing of miRNAs, with these processing events required for the normal development of root structures (*see* **Section 3.2.4**). The molecular assessment of the miR160/*ARF10*/*ARF16*/*ARF17* expression module in *drb* mutant roots further confirmed the role of at least one specific expression module under miRNA-mediated posttranscriptional regulation, the miR160/*ARF10*/*ARF16*/*ARF17* module. This expression module also forms part of the SCF^{TIR1}-mediated intracellular auxin response pathway (Mallory et al. 2005). This initial analysis, therefore, identified the miR160/*ARF10*/*ARF16*/*ARF17* expression module as an excellent system to study the complex interaction between miRNA-mediated regulation of *ARF* gene expression, the auxin signalling pathway, and *Arabidopsis* root development. Towards this end, varying concentrations of a synthetic auxin, 2,4-dichlorophenoxyacetic acid (2,4-D), were applied to wild-type *Arabidopsis* (Col-0) plants, and to the *drb1*, *drb2*, and *drb12* mutant lines via direct root contact. This exposure was limited to a 24 h treatment, and the phenotypic changes dependent on auxin concentrations and genetic background were observed 12 days later to assess the relationship between modifying auxin signalling and miRNA-directed posttranscriptional gene expression regulation.

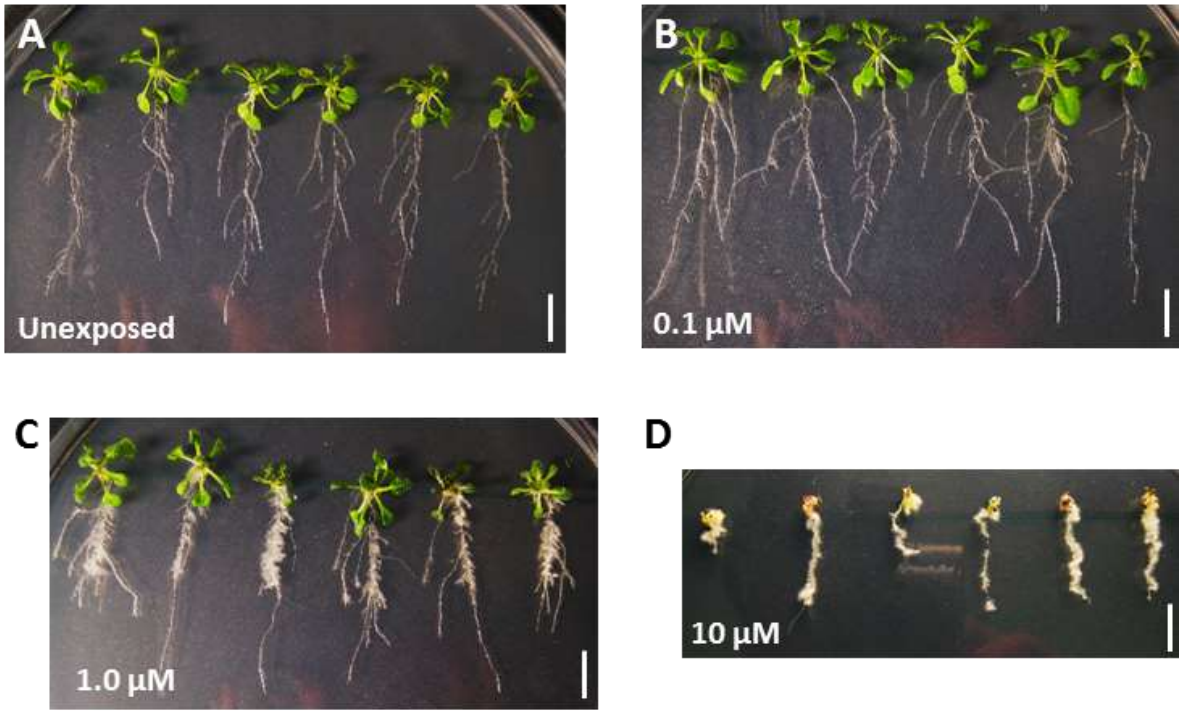

Figure 4.2. Representative phenotypes of vertically grown Col-0 plants exposed to 0.1, 1.0, and 10 µM exogenously applied synthetic auxin. Col-0 plants were germinated and grown on horizontally-orientated MS media plates under standard growth conditions for 10 d, before being transferred to vertically orientated MS media plates containing 0.0 (unexposed) (A), 0.1 (B), 1.0 (C), and 10 µM (D) 2,4-D for 24 h. Following treatment, Col-0 plants were transferred to new MS media plates orientated vertically, with no 2,4-D present in the growth media, for an additional 12 d of cultivation. Plants were phenotyped by measuring primary root length, lateral root number, adventitious root number, and rosette surface area. Root material was collected for subsequent molecular analyses. Scale bars = 1.0 cm.

Exogenously applied 2,4-D induced dramatic changes in both shoot and root structure development in Col-0 plants (**Figure 4.2**). A proliferation of lateral roots was observed after exposing Col-0 plants to the lowest concentration of 2,4-D (0.1 µM), without any apparent effect on primary root length or the development of aerial structures (**Figure 4.2B**). This effect was compounded when the 2,4-D concentration was increased to 1.0 µM with a readily apparent increase in the number of adventitious roots, shortening of the primary root length, and a small decrease in leaf surface area (**Figure 4.2C**), presumably as a result of leaf epinasty, a common effect of exposure to high 2,4-D concentrations (Rodriguez-Serrano et al. 2014). At the maximum concentration of 2,4-D (10 µM), wild-type plants displayed a severe retardation of growth, a phenotype that was consistent with an *Arabidopsis* plant near death. All root and shoot growth was retarded, and primary root length, lateral and adventitious root number, and rosette size had decreased. Rosette leaves were often discoloured, being brown, yellow, or even white in colouration (**Figure 4.2D**). This demonstrated that for wild-type *Arabidopsis*,

application of 2,4-D at 10 µM stops 2,4-D from acting as an endogenous auxin mimic, and fully transitions to the alternate role as an auxinic herbicide resulting in plant death (Smith 1989).

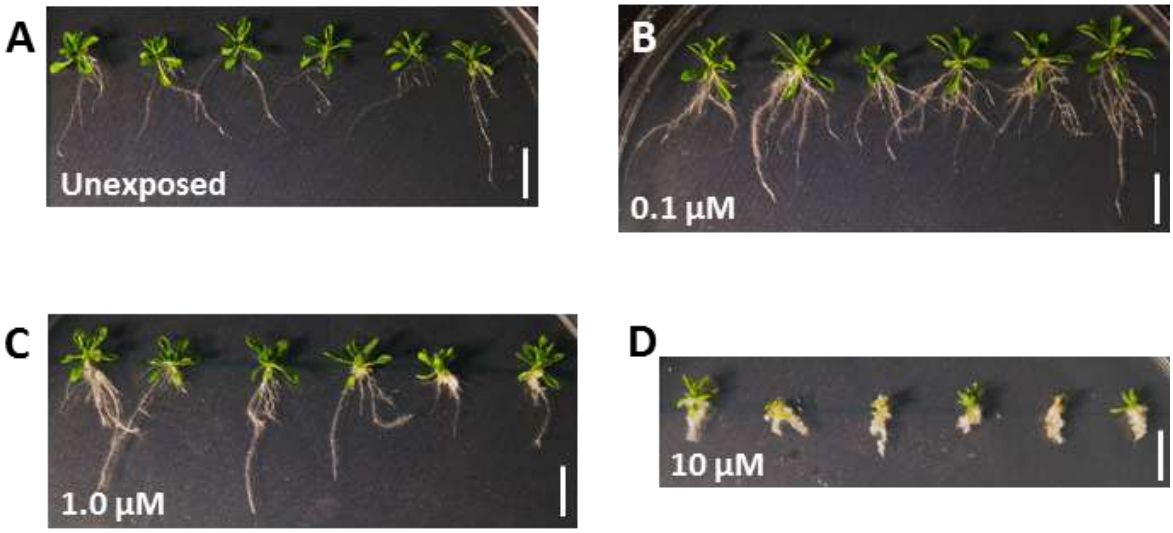

Figure 4.3. Representative phenotypes of vertically grown *drb1* plants exposed to 0.1, 1.0, and 10 µM exogenously applied synthetic auxin. *drb1* plants were germinated and grown on horizontally-orientated MS media plates under standard growth conditions for 10 d, before being transferred to vertically-orientated MS media plates containing 0.0 (unexposed) (A), 0.1 (B), 1.0 (C), and 10 µM (D) 2,4-D for a treatment period of 24 h. Following treatment, *drb1* plants were transferred to new MS media plates orientated vertically, with no 2,4-D present in the growth media, for an additional 12 d of cultivation. Plants were phenotyped by measuring primary root length, lateral root number, adventitious root number, and rosette surface area. Root material was also collected from the *drb1* plants and used for subsequent molecular analyses. Scale bars = 1.0 cm.

The application of 0.1 µM 2,4-D had a more dramatic effect on *drb1* plants than on Col-0 plants (**Figure 4.2**). Prolific growth of lateral roots was induced in *drb1* plants treated with 0.1 µM 2,4-D (**Figure 4.3B**), as was the case for Col-0 plants, but treatments had the added effect of increasing primary root length and rosette leaf surface area (**Figure 4.3A** and **D**). The drop-off in root elongation was initiated at a lower 2,4-D concentration in *drb1* plants than Col-0 plants, with a reduction in primary root length observed upon 1.0 µM 2,4-D treatment (**Figure 4.3C**) while *drb1* plants appeared more resistant to the deleterious effects of 10 µM 2,4-D than Col-0 plants (**Figure 4.3D**). Although primary root length, lateral and adventitious root number, and rosette leaf surface area were all reduced, the leaf tissues remained greener than the Col-0 plants treated with the same concentration of 2,4-D. Furthermore, hyponastic leaves, a defining feature of the *drb1* mutant, continue to develop on

10 µM 2,4-D treated *drb1* plants (**Figure 4.3D**), despite the epinastic inducing properties of at this concentration.

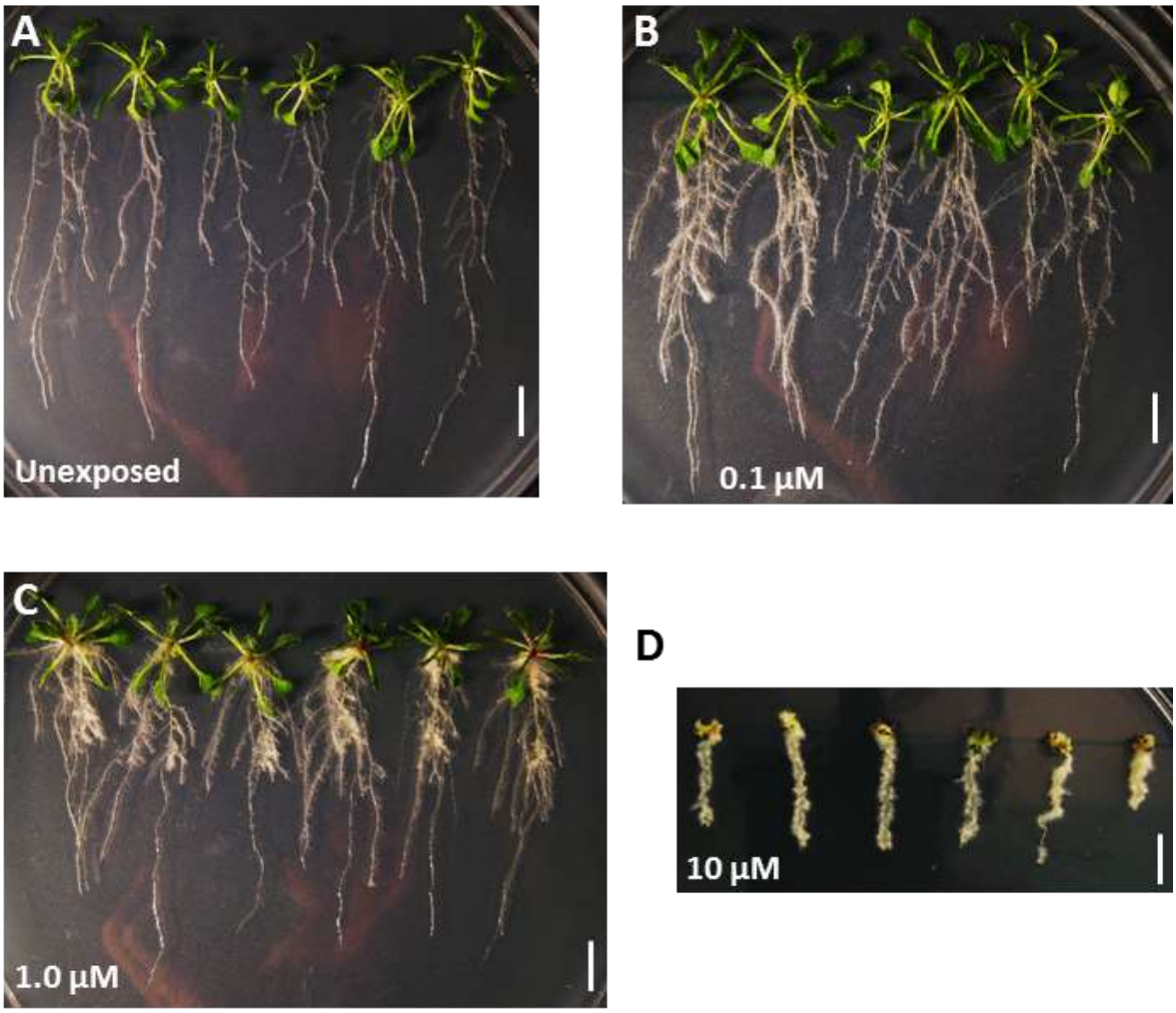

Figure 4.4. Representative phenotypes of vertically grown *drb2* plants exposed to 0.1, 1.0, and 10 µM exogenously applied synthetic auxin. *drb2* plants were germinated and grown on horizontally-orientated MS media plates under standard growth conditions for 10 d, before being transferred to vertically-orientated MS media plates containing 0.0 (unexposed) (A), 0.1 (B), 1.0 (C), and 10 µM (D) 2,4-D for 24 h. Following treatment, *drb2* plants were transferred to new MS media plates orientated vertically, with no 2,4-D present in the growth media, for an additional 12 d of cultivation. Plants were phenotyped by measuring primary root length, lateral root number, adventitious root number, and rosette surface area. Root material was also collected and used for subsequent molecular analyses. Scale bars = 1.0 cm.

Auxin treatments had a more dramatic effect on *drb2* plants than wild-type. As observed in both the Col-0 and *drb1* backgrounds, *drb2* plants treated with 0.1 µM 2,4-D produced many more lateral roots than non-treated *drb2* plants (**Figure 4.4B**). As observed in the *drb1* mutant background, the application of 2,4-D at 1.0 µM resulted in a shortening of the

primary root length of *drb2* plants and a reduction in rosette leaf surface area. In addition, there was a further increase in the number of lateral roots, particularly in the upper portion of the root structure when compared to 0.1 µM 2,4-D treated *drb2* plants. This increase in lateral root growth also coincided with a substantial increase in the development of adventitious roots (**Figure 4.4C**), a development not seen in either Col-0 or *drb1* plants treated with 1.0 µM 2,4-D. However, *drb2* plants treated with 10 µM 2,4-D developed a phenotype similar to that of 10 µM 2,4-D treated Col-0 plants, characterised by a significant reduction in the size and complexity of all root and shoot structures, coupled with leaf epinasty (**Figure 4.4D**).

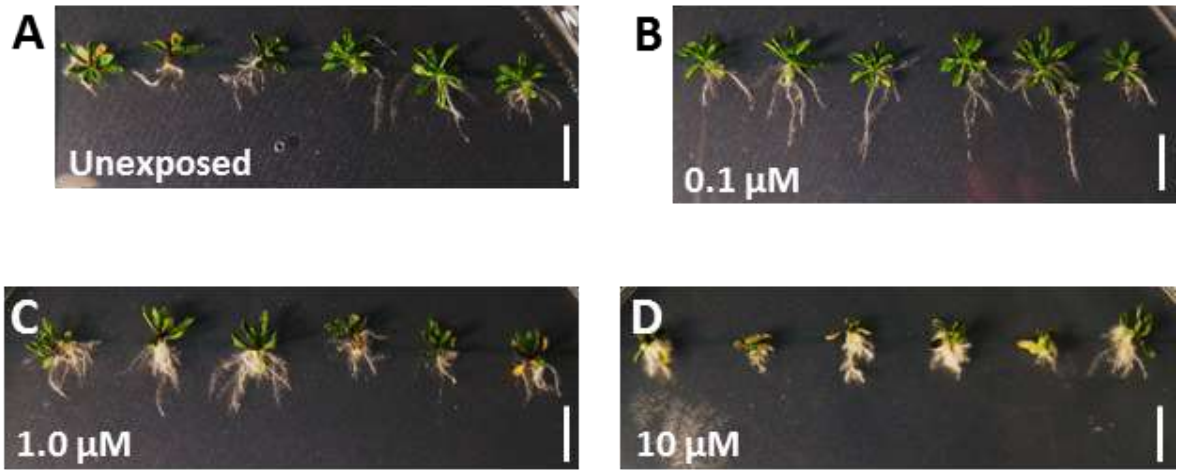

Figure 4.5. Representative phenotypes of vertically grown *drb12* plants exposed to 0.1, 1.0, and 10 µM exogenously applied synthetic auxin. *drb12* plants depicted here were germinated and grown on horizontally-orientated MS media plates under standard growth conditions for 10 d, before being transferred to vertically-orientated MS media plates containing 0.0 (unexposed) (A), 0.1 (B), 1.0 (C), and 10 µM (D) 2,4-D for 24 h. Following treatment, *drb12* plants were transferred to new MS media plates orientated vertically, with no 2,4-D present in the growth media, for an additional 12 d of cultivation Plants were phenotyped by measuring primary root length, lateral root number, adventitious root number, and rosette surface area. Root material was also collected and used for subsequent molecular analyses. Scale bars = 1.0 cm.

From all assessed plant lines, *drb12* plants show the least change across the synthetic auxin treatments compared to the untreated *drb12* control plants, in part because the untreated plants themselves display such a drastic phenotype. No appreciable phenotypic change was apparent in *drb12* plants treated with 0.1 µM 2,4-D (**Figure 4.5B**). Further, when treated with 1.0 µM 2,4-D, only a substantial increase in adventitious root formation, coupled with a marginal reduction to the development of aerial tissues of *drb12* plants was apparent (**Figure 4.5C**). *drb12* plants treated with 10 µM 2,4-D developed a phenotype like that of the *drb1*

single mutant with a reduced primary root length and a smaller sized rosette. However, these plants developed some of the extended adventitious root network displayed by 1.0 µM treated *drb12* plants, a phenotype that was not observed for the *drb1* single mutant following exposure to 1.0 µM 2,4-D. Rosette leaf health was slightly compromised in 10 µM 2,4-D treated *drb12* plants (**Figure 4.5D**), compared to the apparent resistance of *drb1* aerial tissues to the auxinic herbicide effects of 2,4-D. This compromised rosette health is still appreciable compared to Col-0 and *drb2* plants treated with the same concentration of 2,4-D, suggesting that this 'resistance' phenotype is at least partially maintained in the *drb12* background.

To fully determine the impact of treating plants for 24 h with exogenously applied synthetic auxin, it was necessary to quantify the impact that these treatments had on the phenotype. To assess this impact, primary root length, lateral root number, adventitious root number, and rosette leaf surface area were measured 12 d after the end of the synthetic auxin treatment.

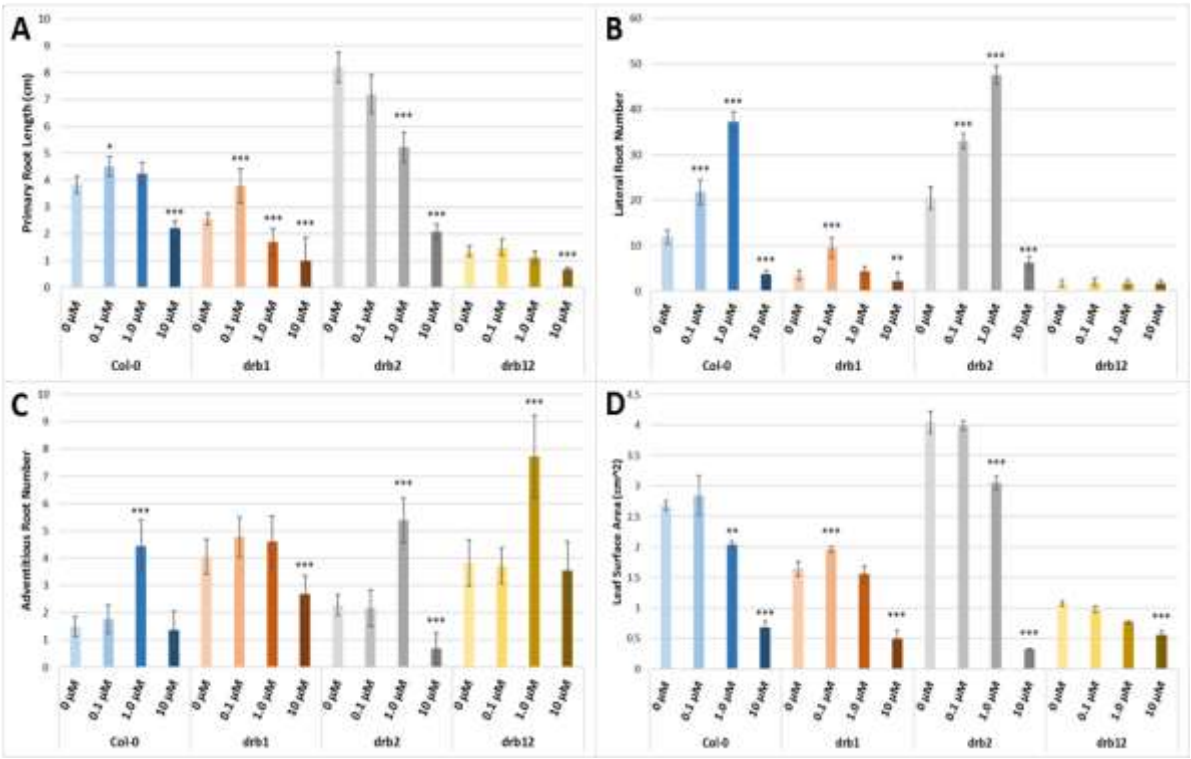

Figure 4.6. Phenotypic analysis of primary root length lateral root number, adventitious root number, and rosette leaf surface area in Col-0, *drb1*, *drb2*, and *drb12* plants exposed to exogenously applied 2,4-D. Primary root length (A), lateral root number (B), adventitious root number (C), and rosette surface area (D) of Col-0 (blue), *drb1* (orange), *drb2* (grey), and *drb12* (yellow) plants after 23 d of growth, which comprised of 10 d horizontal plate growth, followed by 24 h vertically orientated plate growth unexposed, or exposed to 0.1 µM, 1.0 µM, and 10 µM 2,4-D, and then 12 d of vertically-orientated plate growth in the absence of 2,4-D, were measured using ImageJ. Average in each distinct genetic background were compared to unexposed plants for that background by a standard two-tailed t-test. n = 18. Error bars represent SEM. *** $p \leq 0.001$, * $p \leq 0.05$.

Primary root growth is one of the major developmental processes regulated by auxin (Overvoorde et al. 2010). As such, analysing changes in primary root length in response to the exogenous application of different concentrations of 2,4-D provided valuable insight into the degree that the auxin response pathway was disrupted in each mutant line compared to wild-type *Arabidopsis* (**Figure 4.6**). In Col-0 plants, treatment with 2,4-D at 0.1 and 1.0 μM had little effect on primary root length but a significant decrease was observed on exposure to 10 μM exogenous 2,4-D, presumably as part of the auxinic herbicide effects contributing to root death at high concentrations of 2,4-D.

Compared to wild-type plants, primary root elongation of the *drb1* mutant was more responsive to all concentrations of 2,4-D applied with a significant increase in primary root length observed in *drb1* plants treated with 0.1 μM 2,4-D. However, following treatment with 1.0 μM 2,4-D, there was a large decrease in primary root length of *drb1* plants, and the degree of retardation to primary root elongation increased further when *drb1* plants were treated with 10 μM 2,4-D (**Figure 4.6A**).

The *drb2* mutant only responded to higher concentrations of 2,4-D, with primary root length in plants treated with 1.0 μM and 10 μM 2,4-D showing incrementally larger reductions (**Figure 4.6A**). The *drb12* double mutant showed little response in its primary root elongation when exposed to exogenously applied 2,4-D. Only at a concentration of 10 μM 2,4-D was any change to primary root length observed, and this was only a mild reduction (**Figure 4.6A**). Taken together, analysis of primary root length showed that activity of both DRB1 and DRB2 are required normal auxin responses contributing to primary root growth.

Measurements were also made of lateral root number (**Figure 4.6B**). In Col-0, changes to lateral root development were more pronounced than those observed for primary root growth with an ~100% increase in lateral roots following treatments with 0.1 μM 2,4-D, and with an ~200% increase application of 1.0 μM 2,4-D (**Figure 4.6B**). This dramatic promotion of lateral root development, however, was completely abolished when Col-0 plants were treated with 10 μM 2,4-D. This phenotypic effect was assumed to be another example of the auxinic herbicide effects of 2,4-D at high concentration.

In the *drb1* mutant, the number of lateral roots also increased following treatment with 0.1 μM 2,4-D, but an increase was not observed with 1.0 μM 2,4-D treatment where plants developed approximately the same number of lateral roots as untreated plants. The number of

lateral roots formed on *drb1* plants did, however, decrease by ~50% when treated with 10 µM 2,4-D (**Figure 4.6B**).

The *drb2* mutant exhibited dramatic changes in lateral root development in response to 2,4-D treatment, with an almost 50% increase in lateral root number at 0.1 µM 2,4-D, and a 150% increase when treated with 1.0 µM 2,4-D. The 10 µM 2,4-D treatment, however, induced an opposing phenotypic response, with a near 75% decrease in lateral root number observed in the *drb2* mutant, an identical degree of reduction observed for primary root development. Curiously, little change to lateral root development was observed in the *drb12* double mutant treated with any of the assessed concentrations of 2,4-D (**Figure 4.6B**).

In summary, both primary root length and lateral root number showed the greatest degree of promotion at 0.1 and 1.0 µM in the *drb1* and *drb2* mutant backgrounds, respectively, an observation that suggests that these two different aspects of root system development are differentially affected by the application of exogenous auxin in the absence of DRB1 and DRB2 activity.

Different responses were seen when adventitious roots were quantified (**Figure 4.6C**). Unlike lateral root development, adventitious root number only changed in Col-0 plants in response to treatment with 1.0 µM 2,4-D, exhibiting a 120% increase at this concentration. Adventitious rooting in *drb1* plants seems to be largely unresponsive to 2,4-D treatment, except for a 50% reduction when treated with 10 µM 2,4-D. Again, however, the reduction in adventitious roots observed for *drb1* plants treated with 10 µM 2,4-D is most likely due to the auxinic herbicide effects of 2,4-D at higher concentrations. As observed for Col-0 plants, the *drb2* mutant only showed a significant increase in adventitious root number when treated with 1.0 µM 2,4-D. Interestingly, however, a near 75% reduction in the number of adventitious roots was observed in *drb2* plants when treated with 10 µM 2,4-D (**Figure 4.6C**). At each assessed concentration of exogenously applied auxin, the contribution of loss of function of either DRB1 or DRB2 to the response of the *Arabidopsis* root system is readily apparent. That is, no significant change to adventitious root number at either the 0.1 or 10 µM application regimes and a 100% increase in adventitious root number when the *drb2* and *drb12* mutant was treated with 1.0 µM 2,4-D.

The phenotype displayed by the rosette aerial tissue is also an excellent indicator of the overall *Arabidopsis* plant health, and of the communication between root and shoot in response to the external environment. Therefore, rosette surface area was also quantified. Trends in the

response of rosette leaf surface area to varying concentrations followed the trends reported for alteration of primary root length (**Figure 4.6D**).

In Col-0 plants, no change in rosette leaf surface area was observed following the application of 0.1 μM 2,4-D. (**Figure 4.6D**), but a 20% reduction in rosette area was observed following the application of 1.0 μM 2,4-D as well as a large reduction in Col-0 rosette area after 10 μM 2,4-D treatment (**Figure 4.6D**). A similar reduction was observed at both of these 2,4-D concentrations in Col-0 primary root length. Taken together, Col-0 primary root length and rosette area data suggest communication is maintained between the root and shoot system of wild-type *Arabidopsis* plants regardless of the detrimental effects of higher concentrations of exogenously applied auxin.

In the *drb1* background, an increase, ~30%, in rosette area was observed following 0.1 μM 2,4-D treatment (**Figure 4.6D**), a finding that followed the observed 50% increase in primary root length of *drb1* following exposure to the same concentration of 2,4-D. However, a 75% decrease in rosette area was recorded in 10 μM 2,4-D treated *drb1* plants. Again, these two rosette area alterations closely followed the changes in primary root length observed for *drb1* plants following their exposure to these two higher concentrations of 2,4-D. These findings suggest that loss of DRB1 activity does not disrupt root to shoot auxin signalling in the *drb1* mutant background.

As with Col-0 and *drb1* plants, similarities were also present between changes in primary root length and an altered rosette area for the *drb2* mutant. No change in rosette area was observed for *drb2* plants treated with 0.1 μM 2,4-D. However, an ~25% decrease, and a further ~95% reduction in rosette area, was observed for the *drb2* mutant post treatment with 1.0 μM and 10 μM 2,4-D, respectively (**Figure 4.6D**).

A similarity in trends between altered rosette area and primary root length was also established for the *drb12* double mutant. No change in rosette area was observed after treatment with either 0.1 μM or 1.0 μM applications of 2,4-D, and a decrease in rosette leaf surface area of nearly 50% when the double mutant was treated with 10 μM 2,4-D (**Figure 4.6D**).

Taken together, comparison of the rosette area data to the measured changes in primary root length across the three mutant backgrounds assessed here suggests that loss of either DRB1 or DRB2 function does not interfere with auxin shoot to root signalling. This is a somewhat surprising observation considering the documented degree to which the regulation of central pieces of protein machinery of the auxin signalling pathway are under sRNA-directed

expression control. However, the disjoint in the degree of response in lateral organ phenotype, as well as the concentration of exogenous auxin at which these differing phenotypic responses were observed to occur, suggests that an even more complex auxin pathway exists in the root system of *Arabidopsis*, a pathway that requires both DRB1 and DRB2.

4.2.2 Molecular assessment of the miR160/*ARF10*/*ARF16*/*ARF17* expression module in synthetic auxin treated Col-0, *drb1*, *drb2*, and *drb12* roots

It is clear from the molecular analysis of the miR160/*ARF10*/*ARF16*/*ARF17* expression module in Col-0, *drb1*, *drb2*, and *drb12* roots (*see* **Section 3.2.5**), that dramatic changes to this expression module can be induced by modulating DRB-mediated production of miR160. Such changes elegantly portray the dynamic nature of DRB interaction with miRNA precursor transcripts, and how stringent the control of the sRNA environment is, in order for the plant to ensure that normal development is maintained.

Interactions between the sRNA-directed posttranscriptional regulatory and the auxin signalling pathways were demonstrated by the different ways in which the *drb* mutants reacted to the varied exogenous auxin concentrations. To explain the observed phenotypic changes, it was important to first determine which genes contributing to this miR160/*ARF10*/*ARF16*/*ARF17* expression module directly interact with other auxin response proteins. Therefore, the identification of auxin response elements (AREs) in the promoter regions of expression module encoding genes, *MIR160A*, *MIR160B*, *MIR160C*, *ARF10*, *ARF16*, *ARF17*, *eTM160-1*, *eTM160-2*, *DRB1*, and *DRB2*, provides a preliminary understanding of the way in which auxin interacts with and influences this expression module. The promoter region of the *DRB4* locus was also included in this assessment as the DRB4/DCL4 functional partnership is well documented as being essential for tasiARF production (Nakazawa et al. 2007), a sRNA-directed regulatory pathway known responsive to auxin.

Table 4.1. Summary of auxin response elements found in the promoter region of genes contributing to the miR160/*ARF10*/*ARF16*/*ARF17* expression module. Auxin response element (TGTCTC, GAGACA AGAAACAT, AGAAACAA, NGATT) sequence alignment was conducted using PlantCARE, PLACE, and AtcisDB. All promoters identified as containing auxin response elements are defined as responsive, blank boxes indicate no response elements identified, and N/A indicates that these promoter sequences are not available in the relevant promoter analysis database.

Gene Promoter	PlantCARE	PLACE	AtcisDB
PRI-MIR160A		Responsive	N/A
PRI-MIR160B	Responsive	Responsive	N/A
PRI-MIR160C	Responsive		N/A
eTM160-1		Responsive	N/A
eTM160-2		Responsive	N/A
ARF10	Responsive	Responsive	Responsive
ARF16		Responsive	Responsive
ARF17	Responsive		Responsive
DRB1		Responsive	
DRB2	Responsive		
DRB4		Responsive	Responsive

To identify potential *ARE*s in miR160/*ARF10*/*ARF16*/*ARF17* expression module gene promoter regions, three different online programs PlantCARE (bioinformatics.psb.ugent.be/ webtools/plantcare/html/) (Lescot et al. 2002), PLACE (www.dna.affic.go.jp/ PLACE) (Higo et al. 1999), and AtcisDB (agris-knowledgebase.org/ AtcisDB/) (Davuluri et al. 2003) were used to assess the landscape of the promoter regions of miR160/*ARF10*/*ARF16*/*ARF17* expression module encoding genes. Each program used different parameters to determine the presence or absence of *ARE*s. Therefore, utilising multiple programs was considered the best strategy to obtain a comprehensive overview of the *ARE cis*-element landscape of the promoter region of each gene.

Table 4.1 shows that at least one of the three programs identified the presence of a conserved *ARE* sequence in the promoter region of each assessed gene. Identification of an *ARE* sequence by more than one of the online search programs was believed to more confidently indicate a role of the analysed gene in auxin signalling. It was, therefore, unsurprising that all three programs identified an *ARE* in the *ARF10* promoter, while two out of three programs confirmed the presence of an *ARE* in the promoter regions of *ARF16* and *ARF17*. In addition to the *ARF16* and *ARF17* loci, two out of the three online search programs

also identified the presence of an *ARE* in the *MIR160B* gene promoter, a finding that strongly implies that the activity of this miR160 encoding gene is response to auxin. The *MIR160A, MIR160C*, *eTM160-1 eTM160-2*, *DRB1*, *DRB2*, and *DRB4* loci, were all determined by one of the three online programs to also harbour an *ARE* in their promoter regions (**Table 4.1**). Unfortunately, the AtcisDB program does not allow for the interrogation of promoter regions of non-protein coding loci, so the full extent of the *ARE* landscape of the promoter regions of assessed genes, *MIR160A*, *MIR160B*, *MIR160C*, *eTM160-1*, and *eTM160-2*, remains incomplete.

As all miR160/*ARF10*/*ARF16*/*ARF17* expression module genes, as well as the three assessed *DRB* genes, possess one or more *ARE cis*-elements in their respective promoter regions, molecular analysis of the miR160/*ARF10*/*16*/*17* expression module, and of *DRB* gene expression, under varying exogenously applied synthetic auxin concentration was performed to provide further insight into the molecular-driven phenotypic responses. Molecular analysis of this expression module was conducted in root tissue, as the documented roles of ARF10, ARF16, and ARF17 appear to contribute most significantly to overall root phenotype in *Arabidopsis*.

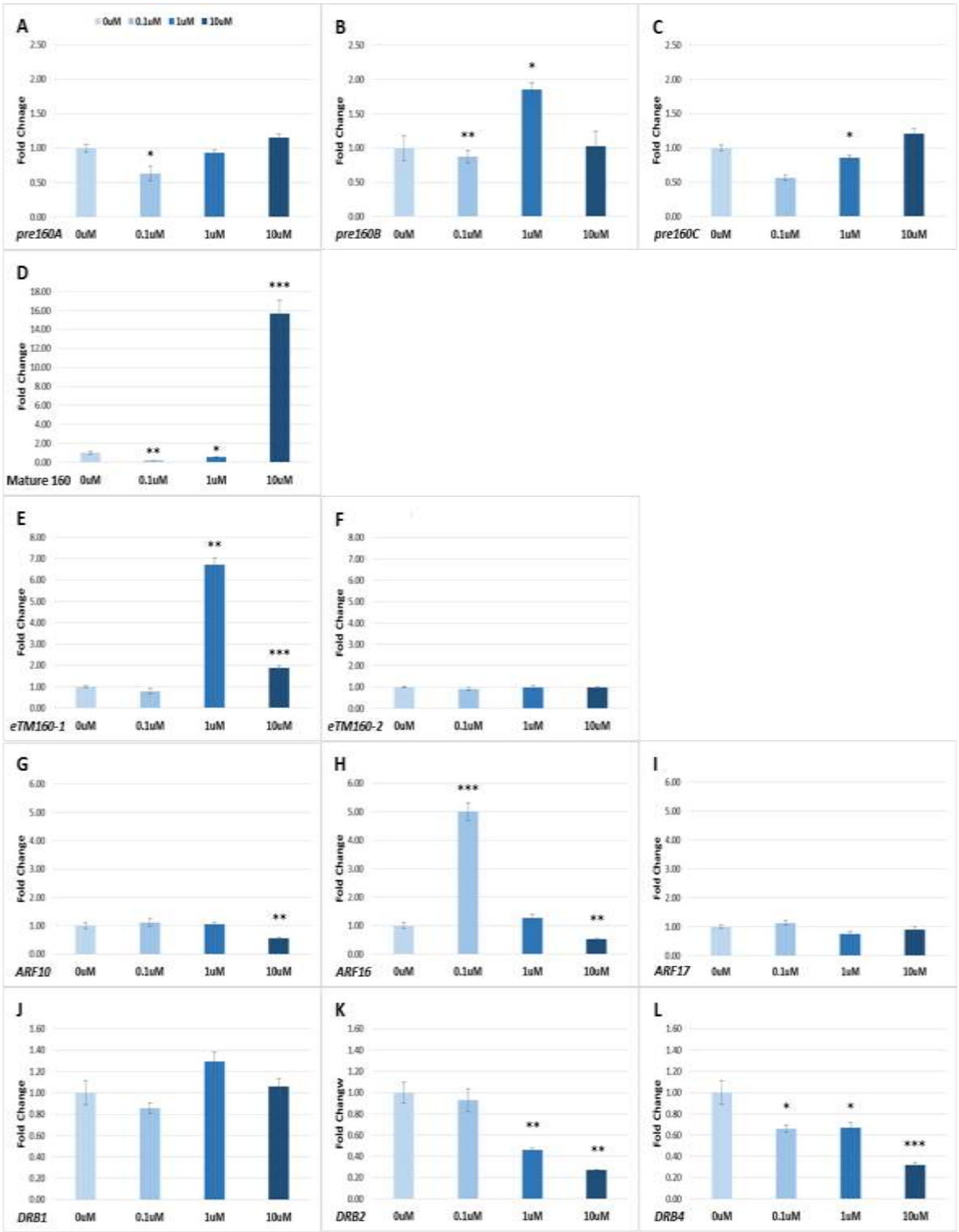

Figure 4.7. RT-qPCR analysis of the miR160/*ARF10*/*ARF16*/*ARF17* expression module in root tissue of Col-0 plants exposed to 2,4-D. Analysed in root tissue of Col-0 unexposed (lighter blue), and 0.1 µM (light blue), 1.0 µM (dark blue), and 10 µM (darker blue) 2,4-D exposed root tissue were *PRI-MIR160A/B/C* precursor genes (A,B, and C), *eTM160-1* and *eTM160-2* miR160 endogenous target mimic (E and F), *ARF10/16/17* miR160 target genes (G, H, and I), and *DRB1* (J), *DRB2* (K), and *DRB4* (L) expression, and STL-qPCR analysis of miR160 accumulation (D). Fold changes were determined by the ΔΔCt method, with three biological replicates, and normalised to unexposed Col-0. Averages of expression fold change in the 2,4-D exposed samples were compared to unexposed Col-0 by a standard two-tailed t-test. Error bars represent SEM. *** $p \leq 0.001$, ** $p- \leq 0.01$, * $p \leq 0.05$.

To understand the impact of exogenously applied synthetic auxin, each auxin concentration was compared to unexposed plants within each distinct genetic background. There was a nearly 50% reduction in the accumulation of both *PRI-MIR160A* and *PRI-MIR160C* precursors, but no change in *PRI-MIR160B* accumulation, in plants treated with 0.1 µM 2,4-D which resulted in a proportional decrease in mature miR160 accumulation in Col-0 roots treated with 0.1 µM 2,4-D (**Figure 4.7A-D**). No change in *eTM160-1* or *eTM160-2* expression (**Figure 4.7E** and **F**) indicates that their involvement in regulating miR160 levels does not change in roots treated with 0.1 µM 2,4-D. Furthermore, only *ARF16* showed a 5.0-fold increase in expression, with no change in *ARF10* or *ARF17* transcript abundance observed in 0.1 µM 2,4-D treated Col-0 roots (**Figure 4.7G-I**). Surprisingly, this increase in *ARF16* expression was concurrent with an increase in both primary root length (**Figure 4.6**) and lateral root number (**Figure 4.6B**). The observed increase in *ARF16* transcript abundance is understandable given the decrease in mature miR160 accumulation. However, no change was observed in either *DRB1* or *DRB2* expression in 0.1 µM treated Col-0 roots (**Figure 4.7J** and **K**), a finding that suggests that the observed reduction in miR160 abundance in 0.1 µM treated Col-0 roots was due to reduced *MIR160* gene expression, and not due to changes in DRB1 and/or DRB2 activity. It is of interest to note that *DRB4* expression showed a 40% reduction (**Figure 4.7L**), a finding that suggests that *DRB4* gene expression is negatively regulated by exogenously applied auxin.

Examination of 1.0 µM 2,4-D treated Col-0 roots showed no change in *PRI-MIR160A* accumulation, a decrease (~20%) in *PRI-MIR160C* expression, and an increase in *PRI-MIR160B* precursor transcript abundance (**Figure 4.7A-C**). However, stem-loop qPCR (STL-qPCR) analysis showed that mature miR160 levels were greatly reduced (**Figure 4.7D**) which might be explained by the significant, 6.0-fold, increase in *eTM160-1* expression in 1.0 µM 2,4-D treated Col-0 roots (**Figure 4.7E**). *eTM160-2* still appeared to be unresponsive to 2,4-D treatment as no change was observed in the abundance of this non-protein-coding RNA following treatment of Col-0 roots with 1.0 µM 2,4-D (**Figure 4.7F**). Interestingly, no changes were observed in *ARF10*, *ARF16*, or *ARF17* expression in 1.0 µM 2,4-D treated Col-0 roots (**Figure 4.7G-I**), suggesting that changes in posttranscriptional regulation are insufficient to change their expression. Further, this implies that phenotypic changes observed for Col-0 plants treated with 1.0 µM 2,4-D cannot be attributed to changes in the miR160/*ARF10*/*ARF16*/*ARF17* expression module. However, decreased expression of *DRB2* by 60%, and *DRB4* by 40%, but not *DRB1* (**Figure 4.7J-L**), suggests that changes to other

sRNA regulatory modules could potentially contribute to root architectural modifications in Col-0 plants.

In 10 μM 2,4-D treated Col-0 roots, no change was observed in *PRI-MIR160A*, *PRI-MIR160B*, or *PRI-MIR160C* transcript abundance (**Figure 4.7A-C**), but mature miR160 abundance was elevated by approximately 16-fold (**Figure 4.7D**). Furthermore, *eTM160-1* expression also increased by approximately 2.0-fold (**Figure 4.7E**), potentially disguising a further increase in mature miR160 abundance. This elevated accumulation of miR160 led to a 50% reduction in *ARF10* and *ARF16* expression, but no change in *ARF17* expression was observed (**Figure 4.7G-I**). *DRB2* and *DRB4* expression were both reduced, while no change in *DRB1* expression was observed (**Figure 4.7J-L**). By lowering antagonism between DRB1 and DRB2, and/or DRB4, DRB1 has greater *PRI-MIR160* precursor transcript access and this could potentially explain the substantial increase in mature miR160 abundance despite no change in precursor levels. Col-0 roots treated with 10 μM 2,4-D showed molecular changes inverse to those observed in 0.1 μM 2,4-D treated roots (**Figure 4.7**). Unsurprisingly, this translated to an opposing change in root architecture in 10 μM 2,4-D treated roots, opposed to 0.1 μM 2,4-D treated roots. However, *ARF10* and *ARF16* have been previously documented to promote, or at least maintain, primary root growth, while *ARF16* and *ARF17* both repress lateral and adventitious root initiation and growth (Couzigou and Combier 2016; Mallory et al. 2005; Wang et al. 2005). While the molecular data in **Figure 4.7** correlates with the reported function of *ARF16* in primary root development, the opposite effect on lateral and adventitious root development was observed. Such observations strengthen the case raised by the molecular data from 1.0 μM 2,4-D treated roots that exogenous auxin application, and subsequent changes in DRB sRNA processing, may alter root architecture by modifying sRNA regulatory modules additional to the miR160/*ARF10*/*ARF16*/*ARF17* expression module that was assessed here.

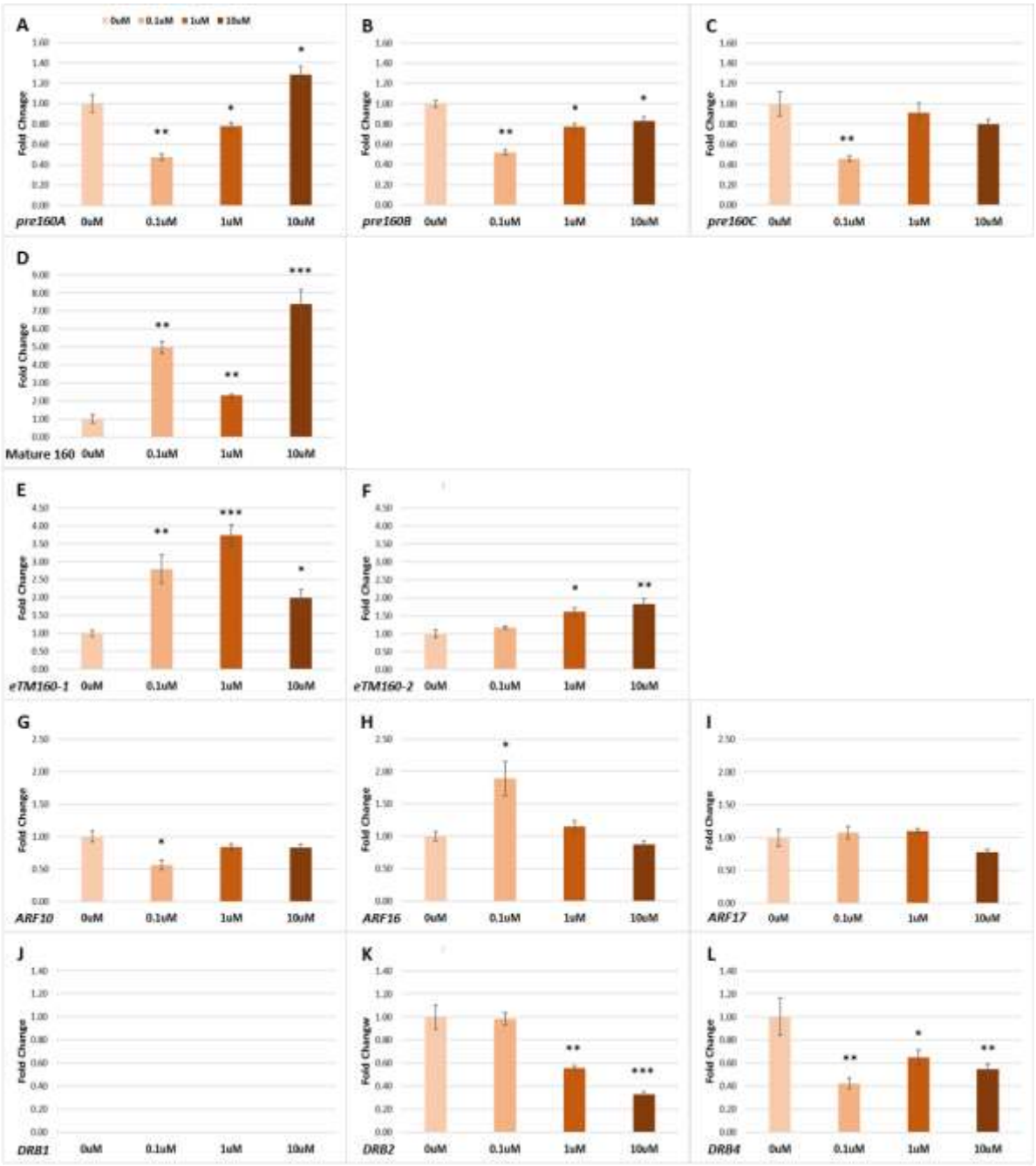

Figure 4.8. RT-qPCR analysis of the miR160/*ARF10*/*ARF16*/*ARF17* expression module in root tissue of *drb1* plants exposed to 2,4-D. Analysed in root tissue of *drb1* unexposed (lighter orange), and 0.1 µM (light orange), 1.0 µM (dark orange), and 10 µM (darker orange) 2,4-D exposed root tissue were *PRI-MIR160A/B/C* precursor genes (A,B, and C), *eTM160-1* and *eTM160-2* miR160 endogenous target mimic (E and F), *ARF10/16/17* miR160 target genes (G, H, and I), and *DRB1* (J), *DRB2* (K), and *DRB4* (L) expression, and STL-qPCR analysis of miR160 accumulation (D). Fold changes were determined by the ΔΔCt method, with three biological replicates, and normalised to unexposed *drb1*. Averages of expression fold change in the 2,4-D exposed samples were compared to unexposed *drb1* by a standard two-tailed t-test. Error bars represent SEM. *** $p \leq 0.001$, ** $p- \leq 0.01$, * $p \leq 0.05$.

As observed for Col-0 roots, *drb1* roots treated with 0.1 µM 2,4-D showed an ~50% reduction in the accumulation of *PRI-MIR160A*, *PRI-MIR160B*, and *PRI-MIR160C* precursor

transcripts (**Figure 4.8A-C**). Reduced precursor accumulation, indicative of more efficient precursor transcript processing, contributed to a 5.0-fold increase in mature miR160 abundance (**Figure 4.8D**). In response, *eTM160-1* expression also increased in *drb1* roots treated with 0.1 µM 2,4-D (**Figure 4.8E**), possibly leading to the sequestration of additional molecules of mature miR160. *ARF17* expression remained unchanged in 0.1 µM 2,4-D treated *drb1* roots despite the observed increased in mature miR160 abundance (**Figure 4.8I**). *ARF10* expression decreased, 50%, while *ARF16* expression increased, 2.0-fold (**Figure 4.8G** and **H**), suggesting that in 0.1 µM 2,4-D treated *drb1* roots, miR160 directs posttranscriptional regulation of *ARF10* via transcript cleavage, while *ARF16* is posttranscriptionally regulated via translational repression. In the absence of DRB1, *DRB2* expression remained unchanged in roots treated with 0.1 µM 2,4-D, while *DRB4* expression decreased by 60% (**Figure 4.8J-L**). As DRB2 is the dominant DRB protein for processing of the miR160 precursor transcripts in this scenario, and that DRB4 repression of DRB2 is alleviated, the argument for translational repression of *ARF16* being the dominant form of posttranscriptional regulation is strengthened.

In 1.0 µM 2,4-D treated *drb1* roots, only *PRI-MIR160A* and *PRI-MIR160B* show slight reductions, while *PRI-MIR160C* showed no change (**Figure 4.8A-C**). Mature miR160 abundance, however, still increased by 2.0-fold (**Figure 4.8D**), indicating that miR160 processing is less efficient in 1.0 µM 2,4-D treated *drb1* roots compared to the 0.1 µM 2,4-D treatment, but was more efficient than it is in untreated roots. Both the expression of *eTM160-1* and *eTM160-2* increased in 0.1 µM 2,4-D treated *drb1* roots (**Figure 4.8E** and **F**), possibly disguising the actual abundance of mature miR160. Considering that *eTM160-1* and *eTM160-2* could be preventing miR160 from going on to target the *ARF* for expression regulation, it is unsurprising that no changes in *ARF10*, *ARF16*, or *ARF17* expression were observed (**Figure 4.8G-I**). Taken together, these findings indicate that at 1.0 µM 2,4-D treatment, and in the absence of DRB1 activity, miR160 appears more likely to direct posttranscriptional regulation of *ARF10*/*ARF16*/*ARF17* via translational repression than by transcript cleavage.

Molecular analysis of 10 µM 2,4-D treated *drb1* roots showed that *PRI-MIR160A* abundance decreased slightly, while *PRI-MIR160B* levels increased slightly, and the *PRI-MIR160C* transcript remained unchanged (**Figure 4.8A-C**), leaving the total abundance of the *PRI-MIR160* precursor transcript pool, largely unaltered. Col-0 roots treated with the same concentration of 2,4-D showed a similar trend, suggesting that miR160 precursor processing, or *MIR160* gene expression responses, may be decoupled from cellular requirements at this

concentration of 2,4-D. 10 µM 2,4-D treated *drb1* roots showed a significant increase, 7.0-fold, in mature miR160 abundance (**Figure 4.8D**). But unlike Col-0, 10 µM 2,4-D treated *drb1* roots showed an increase, 2.0-fold, in *eTM160-1* and *eTM160-2* expression (**Figure 4.8E** and **F**), again potentially obscuring true miR160 abundance. Like 1.0 µM, 10 µM 2,4-D treatment showed no change in *ARF10*, *ARF16*, or *ARF17* expression in *drb1* roots (**Figure 4.8G-I**), while *DRB2* and *DRB4* expression were both reduced, ~70% and 50%, respectively (**Figure 4.8K** and **L**). Increased mature miR160 abundance, coupled with no change in *ARF10*/*ARF16*/*ARF17* transcript abundance, strengthens the argument postulated for 1.0 µM 2,4-D treated roots that, in the absence of functional DRB1, miR160 posttranscriptionally regulates *ARF10*/*ARF16*/*ARF17* expression via a translational repression mechanism of RNA silencing.

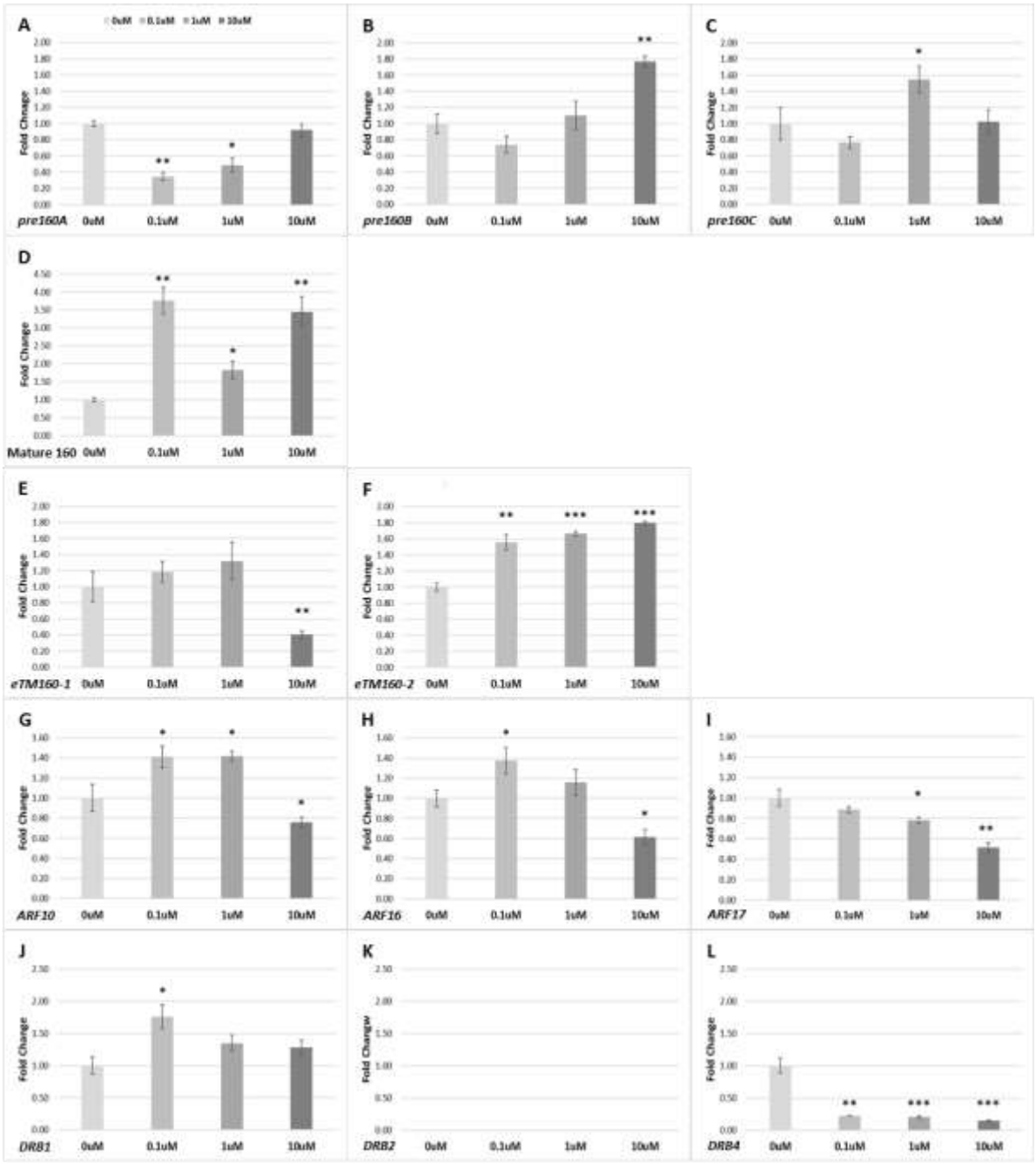

Figure 4.9. RT-qPCR analysis of the miR160/*ARF10*/*ARF16*/*ARF17* expression module in root tissue of *drb2* plants exposed to 2,4-D. Analysed in root tissue of *drb2* unexposed (lighter grey), and 0.1 µM (light grey), 1.0 µM (dark grey), and 10 µM (darker grey) 2,4-D exposed root tissue were *PRI-MIR160A/B/C* precursor genes (A,B, and C), *eTM160-1* and *eTM160-2* miR160 endogenous target mimic (E and F), *ARF10/16/17* miR160 target genes (G, H, and I), and *DRB1* (J), *DRB2* (K), and *DRB4* (L) expression, and STL-qPCR analysis of miR160 accumulation (D). Fold changes were determined by the ΔΔCt method, with three biological replicates, and normalised to unexposed *drb2*. Averages of expression fold change in the 2,4-D exposed samples were compared to unexposed *drb2* by a standard two-tailed t-test. Error bars represent SEM. *** $p \leq 0.001$, ** $p- \leq 0.01$, * $p \leq 0.05$.

It appeared that in *drb2* roots treated with 0.1 µM 2,4-D, the processing efficiency of *PRI-MIR160A* is increased, with *PRI-MIR160A* abundance reduced by 60%, although no change was observed in the abundance of either *PRI-MIR160B* or *PRI-MIR160C* (**Figure 4.9A-C**). This correlates to a 3.5-fold increase in mature miR160 accumulation (**Figure 4.9D**). Unlike in the roots of Col-0 or *drb1* plants, *drb2* roots treated with 0.1 µM 2,4-D showed no change in *eTM160-1* expression, and only a slight increase in *eTM160-2* expression (**Figure 4.9E** and **F**), implying little change in the role of either eTM between 0.1 µM 2,4-D exposed and unexposed *drb2* roots. *ARF10* and *ARF16* expression increased despite an increase in mature miR160 accumulation (**Figure 4.9G-H**). This coupled with the upregulation of *DRB1* expression, presumably due to the absence of DRB2 activity, and the downregulation of *DRB4* expression (**Figure 4.9J** and **L**), suggests that *ARF10* and *ARF16* are under translational repression posttranscriptional regulation as miR160 abundance has scaled in parallel with the observed increased in *ARF10* and *ARF16* abundance, while *ARF17* transcript levels remain unchanged.

In 1.0 µM 2,4-D treated *drb2* roots, *PRI-MIR160A* accumulation is reduced while *PRI-MIR160B* levels remained unchanged. However, *PRI-MIR160C* abundance increased by the same proportion that *PRI-MIR160A* decreased (**Figure 4.9A-C**), which led to a relatively mild increase in mature miR160 abundance (**Figure 4.9D**). In the 1.0 µM 2,4-D treatment, *eTM160-1* and *eTM160-2* expression remained at their documented levels (**Figure 4.9E** and **F**), a finding which implies little alteration to the *eTM160* regulatory role in *drb2* roots. *ARF16* expression increased, while *ARF17* expression decreased, and *ARF10* levels did not change in 1.0 µM 2,4-D treated *drb2* roots (**Figure 4.9G-I**). However, all observed expression changes were minor, suggesting that root phenotypic changes in 1.0 µM 2,4-D treated *drb2* roots are largely influenced by other expression modules. *DRB4* expression is also decreased (**Figure 4.9L**), a finding that further suggests that *DRB4* expression directly responds to auxin signalling.

In 10 µM 2,4-D treated *drb2* roots, only *PRI-MIR160B* abundance changed, a 3.0-fold increase (**Figure 4.9B**). As this is the only differentially expressed *MIR160* gene, the observed 3.5-fold increase in mature miR160 abundance (**Figure 4.9D**) is presumably a direct result of *PRI-MIR160B* expression induction. The expression of *eTM160-2* increased by almost 2.0-fold while the expression of *eTM160-1* decreased by 60% (**Figure 4.9E** and **F**), opposing changes in *eTM160* abundance potentially result in a null effect of *eTM160* facilitated sequestration of miR160. Mature miR160 appeared to be directing targeting of *ARF10*, *ARF16*, and *ARF17* as

the expression of each target is decreased by approximately 30%, 40%, and 50%, respectively (**Figure 4.9G-I**). As DRB2 was non-functional, and *DRB4* expression was significantly decreased (**Figure 4.9L**), all miR160 processing is mediated by DRB1, evidenced by the obvious detection of posttranscriptional regulation of *ARF10*, *ARF16*, and *ARF17* expression by miR160-directed transcript cleavage.

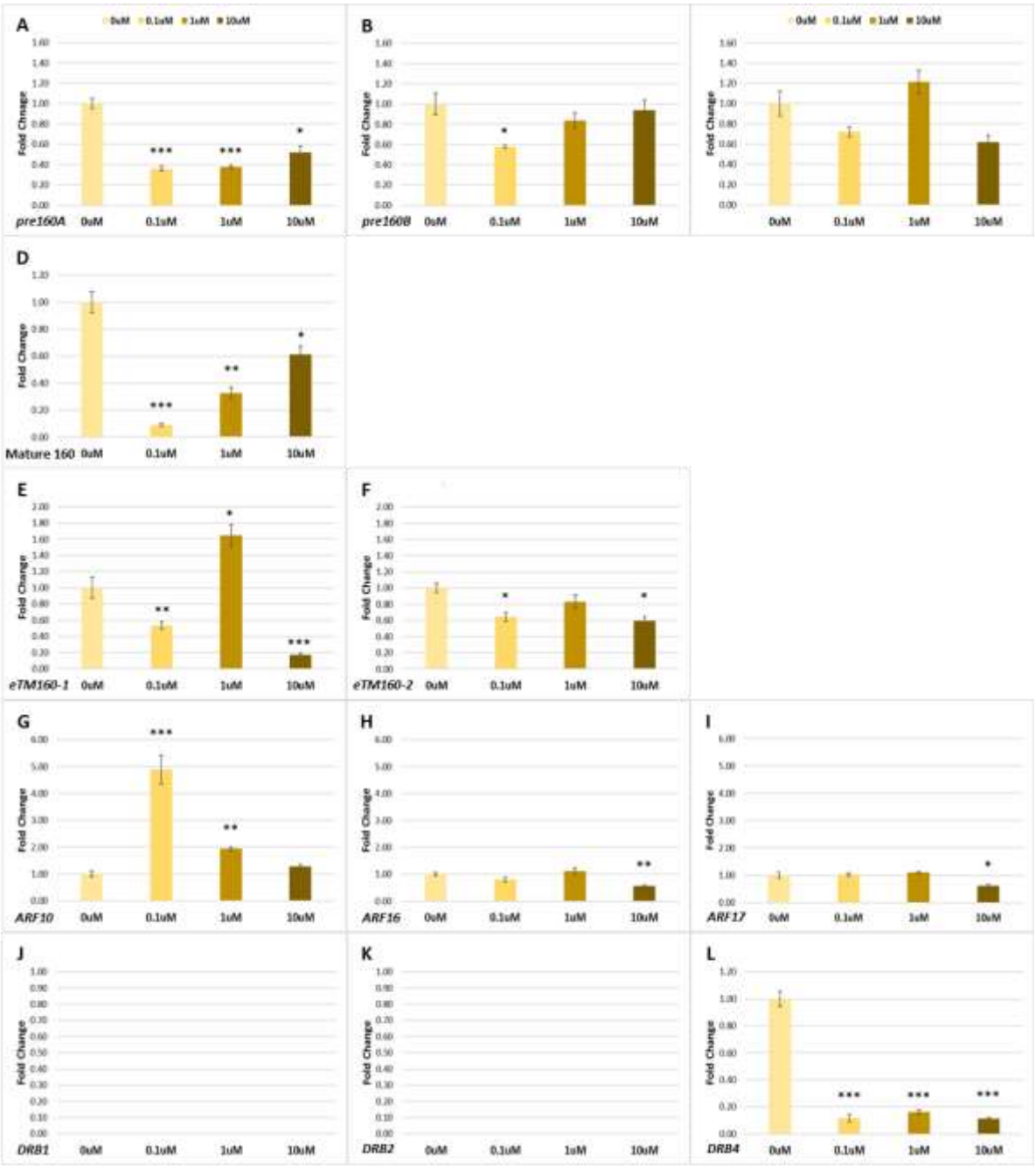

Figure 4.10. RT-qPCR analysis of the miR160/*ARF10*/*ARF16*/*ARF17* expression module in root tissue of *drb12* plants exposed to 2,4-D. Analysed in root tissue of *drb12* unexposed (lighter yellow), and 0.1 µM (light yellow), 1.0 µM (dark yellow), and 10 µM (darker yellow) 2,4-D exposed root tissue were *PRI-MIR160A/B/C* precursor genes (A,B, and C), *eTM160-1* and *eTM160-2* miR160 endogenous target mimic (E and F), *ARF10/16/17* miR160 target genes (G, H, and I), and *DRB1* (J), *DRB2* (K), and *DRB4* (L) expression, and STL-qPCR analysis of miR160 accumulation (D). Fold changes were determined by the ΔΔCt method, with three biological replicates, and normalised to unexposed *drb12*. Averages of expression fold change in the 2,4-D exposed samples were compared to unexposed *drb12* by a standard two-tailed t-test. Error bars represent SEM. *** $p \leq 0.001$, ** $p- \leq 0.01$, * $p \leq 0.05$.

In the absence of both DRB1 and DRB2 activity, *PRI-MIR160A*, *PRI-MIR160B*, and *PRI-MIR160C* abundance, was reduced in *drb12* roots treated with 0.1 µM 2,4-D (**Figure 4.10A-C**), leading to a nearly 80% reduction in mature miR160 abundance (**Figure 4.10D**). Also, both *eTM160-1* and *eTM160-2* expression were reduced by approximately 50% and 40%, respectively (**Figure 4.10E** and **F**), a response that appeared to scale with the reduced levels of mature miR160 abundance. *ARF10* expression responded to very low miR160 levels and increased 5.0-fold (**Figure 4.10G**), due to the near absence of miR160-directed transcript cleavage, although, no change in *ARF16* or *ARF17* expression was observed (**Figure 4.10H** and **I**). In the absence of both DRB1 and DRB2, *DRB4* expression was decreased upon 0.1 µM 2,4-D treatment (**Figure 4.10L**), similar to the expression trends observed in Col-0, *drb1*, and *drb2* roots for *DRB4* treated with the same concentration. It appears that exogenous auxin treatment represses *DRB4* expression irrespective of the sRNA environment and, as such, mature miR160 levels could not be restored in the absence of both DRB1 and DRB2.

PRI-MIR160A accumulation remained reduced (**Figure 4.10A**), while *PRI-MIR160B* and *PRI-MIR160C* accumulation was unchanged from unexposed in 1.0 µM 2,4-D treated *drb12* roots (**Figure 4.10B** and **C**). The decrease in *PRI-MIR160A* accumulation likely led to the observed decrease in mature miR160 abundance (**Figure 4.10D**). Interestingly, *eTM160-1* expression increased (**Figure 4.10E**) in accordance with the decreased abundance of miR160, while *eTM160-2* expression was unchanged (**Figure 4.10F**). *ARF10* expression increased by 2.0-fold in response to reduced miR160-directed transcript cleavage (**Figure 4.10G**). Again, *ARF16* and *ARF17* expression remained unchanged (**Figure 4.10H** and **I**). As in 0.1 µM 2,4-D treated roots, *DRB4* expression was significantly reduced in response to treatment with 1.0 µM 2,4-D (**Figure 4.10L**). In the absence of DRB1 and DRB2 activity, it is presumed that miR160 levels were less significantly decreased in 1.0 µM than in 0.1 µM 2,4-D treated roots due to the restoration of unexposed *drb12* root levels of *PRI-MIR160B* and *PRI-MIR160C* precursor transcript accumulation.

PRI-MIR160A and *PRI-MIR160C* accumulation was reduced in 10 µM 2,4-D treated *drb12* roots, while *PRI-MIR160B* accumulation was unchanged (**Figure 4.10A-C**), again this likely led to the decrease in mature miR160 abundance (**Figure 4.10D**), although, this reduction was not as significant as in 0.1 µM or 1.0 µM 2,4-D treated *drb12* roots. This less significant reduction could be explained by the more significant reduction in *eTM160-1* expression (**Figure 4.10E**) and a reduction in *eTM160-2* expression (**Figure 4.10F**), like that observed for 0.1 µM 2,4-D treated roots. Also, due to the less significant reduction in miR160

abundance, *ARF10* expression is unchanged compared to unexposed *drb12* roots (**Figure 4.10G**). However, both *ARF16* and *ARF17* expression was reduced in 10 µM 2,4-D treated *drb12* roots (**Figure 4.10H** and **I**), a reduction thought to be a result of reduced gene expression rather than a result of modified miR160-directed posttranscriptional regulation. As with 0.1 µM and 1.0 µM 2,4-D treatments, 10 µM 2,4-D treated *drb12* roots showed a reduction in *DRB4* expression (**Figure 4.10L**), again, supporting the direct relationship between exogenous auxin treatment and *DRB4* expression.

Based on the phenotypic observations of this study (*see* **Section 4.2.1**) it appears that the root structures of Col-0 and *drb2* plants are most responsive to 1.0 µM 2,4-D treatments, while *drb1* plants are most responsive to 0.1 µM 2,4-D treatment. As the miR160/*ARF10*/*ARF16*/*ARF17* expression module has a major impact on root development (Wang et al. 2005), it would be expected that *ARF10*/*16*/*17* expression would also change to reflect the changes in root phenotype at these concentrations. However, *ARF10*, *ARF16*, and *ARF17* expression changes are mild compared to the dramatic changes in root phenotypes across the varying concentrations of 2,4-D treatment and *drb* mutant backgrounds. *ARF10* and *ARF16* expression does, however, consistently modulate at 0.1 µM 2,4-D treatment in all *drb* mutant backgrounds, inferring that ARF10 and ARF16 exhibit the most significant control over the development of these root phenotypic structures in response to 2,4-D treatment.

4.2.3 Phenotypic assessment of Col-0, *drb4*, *drb14*, and *drb24* shoot and root development

Phenotypic and molecular examination of Col-0, *drb1*, *drb2*, and *drb12* plants, under both unexposed (*see* **Section 3.2.4** and **Section 3.2.5**) and exogenous auxin exposed (*see* **Section 4.2.1** and **Section 4.2.2**) revealed a number of anomalous instances where the demonstrated relationship between DRB1 and DRB2 in miRNA biogenesis is insufficient to explain the impacts on root development. These anomalies suggest that other factors may be acting on the auxin signalling pathway. Aside from DRB1 and DRB2, DRB4 is the other DRB family member demonstrated capable of processing sRNA precursor transcripts to produce mature sRNA molecules (Pelissier et al. 2011; Qu et al. 2008). As such, investigation of mutant lines deficient in DRB4 function, alone and in combination with plant lines also deficient in DRB1 and DRB2 activity, may provide insight into the contributions made by DRB1 and DRB2 to the sRNA environment governing root development. Phenotypic and molecular

examination of *drb4*, *drb14*, and *drb24* plants was, therefore, undertaken in an attempt to resolve some of these instances. These experiments were aimed at shedding additional light on the complex relationship between DRB1, DRB2, and DRB4, and their influence on the miR160/*ARF10*/*ARF16*/*ARF17* expression module, in controlling root development in *Arabidopsis*.

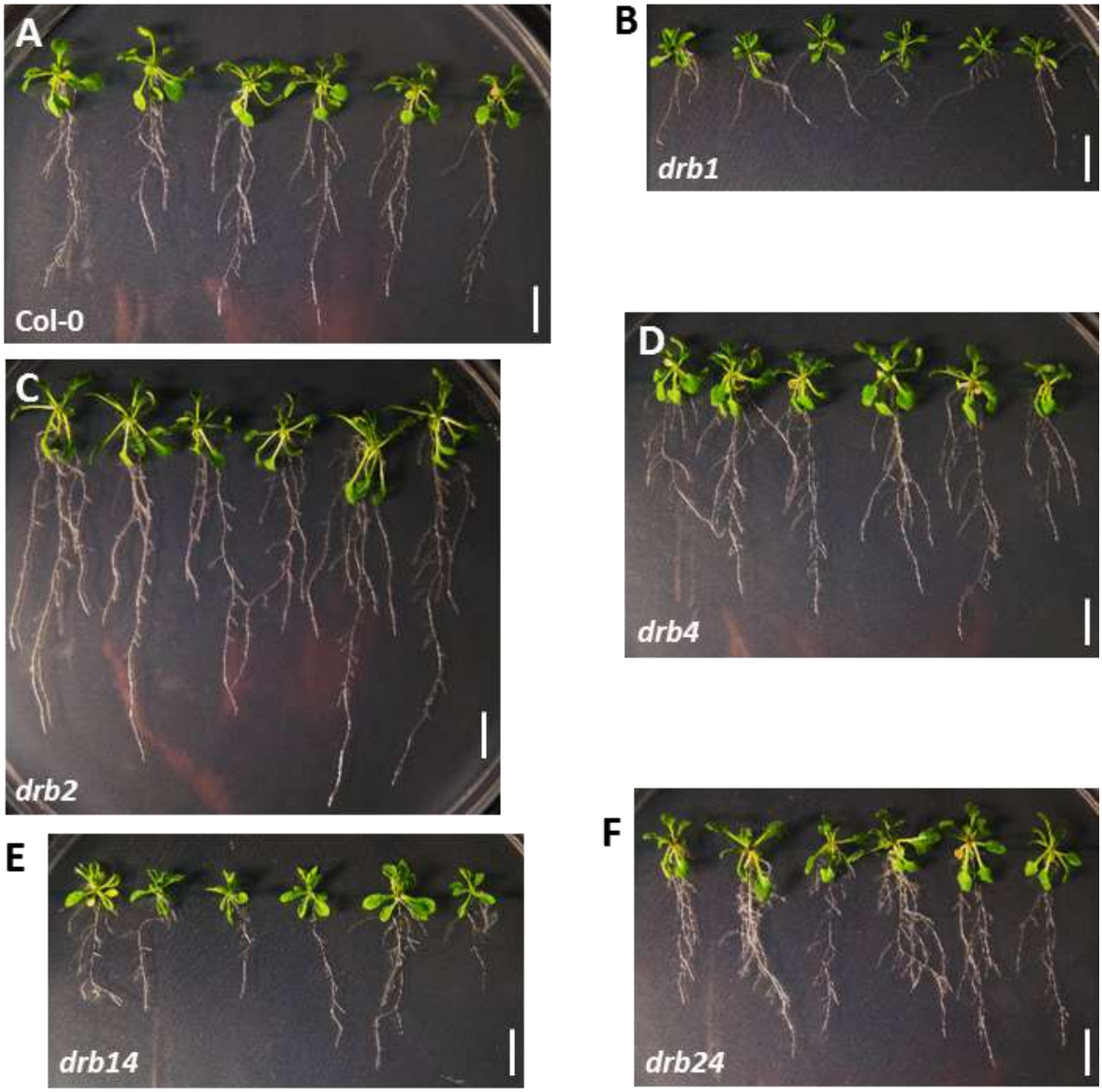

Figure 4.11. Representative phenotypes of vertically grown Col-0, *drb1*, *drb2*, *drb4*, *drb14*, and *drb24* Arabidopsis plant lines. Col-0 (A), *drb1* (B), *drb2* (C) from **Figure 3.4**, *drb4* (D), *drb14* (E), and *drb24* (F) plants depicted here were germinated and grown on horizontally-orientated MS growth plates under standard growth conditions for 10 d, before being transferred to new MS growth plates orientated vertically for an additional 13 d. Plants grown in this manner, and images taken, were used for phenotypic analyses; specifically primary root length, lateral root number, adventitious root number, and leaf surface area. Tissue from the same plants was collected and used for subsequent molecular analyses. Image scale bars represent 1 cm.

Comparison of *drb4*, *drb14*, and *drb24* plants to Col-0 showed very different trends to those observed when comparing *drb1*, *drb2*, and *drb12* to Col-0 plants. The *drb4* mutant only exhibited subtle changes compared to Col-0 although some proliferation of lateral and adventitious rooting was apparent (**Figure 4.11**), but not to the extent witnessed in *drb2* plants. Primary root length and rosette leaf phenotype were also similar (**Figure 4.11**). The only observable differences in the rosette leaf phenotype was the extent of the downward curling of the leaves and a slight elongation of the already elongated shape of mature *Arabidopsis* leaves (**Figure 4.11**), a phenotype consistent with previous aerial phenotypic observations of *drb4* plants (Adenot et al. 2006; Nakazawa et al. 2007).

Removing the activity of both DRB4 and DRB2 in *drb24* plants gave a phenotype different to both the *drb2* and *drb4* single mutant phenotypes. *drb2* plants showed an increase in the extension of primary roots compared to Col-0 plants (**Figure 3.4C**), however, no such extension was visible in *drb24* plants (**Figure 4.11C**). The extent of lateral and adventitious rooting was intermediate between the *drb2* and *drb4* single mutant phenotypes, but the *drb24* double mutant showed no change in leaf rosette phenotype compared to that of the *drb2* single mutant (**Figure 4.11D**). It appeared that neither loss of DRB2 nor DRB4 was more dominant in the *drb24* double mutant, as each contributed different morphologies to the overall phenotype.

The *drb1* single mutant phenotype is dominant over the *drb4* single mutant phenotype, with *drb14* plants displaying the distinct leaf morphology of *drb1* single mutant plants (**Figure 4.11B** and **C**). This rosette phenotype completely counteracts the downward curling leaves of *drb4* single mutant plants and though leaf shape was intermediate, compromised to a more globular, but slightly elongated version of *drb1* leaves, a noticeable trait in *drb4* single mutant plants. The root phenotype of *drb14* plants, however, is dominated by the loss of DRB1 activity with shortened primary roots, as well as a substantial increase in adventitious rooting, a phenotype not observed in the *drb4* single mutant (**Figure 4.11B**). Both of these phenotypic differences are hallmarks of the *drb1* single mutant (**Figure 3.4B**). However, the lateral root phenotype of *drb1* plants does appear to be rescued in the absence of DRB4 (**Figure 4.11**), illustrating that the relationship between DRB1 and DRB4 does have an impact on *Arabidopsis* root development.

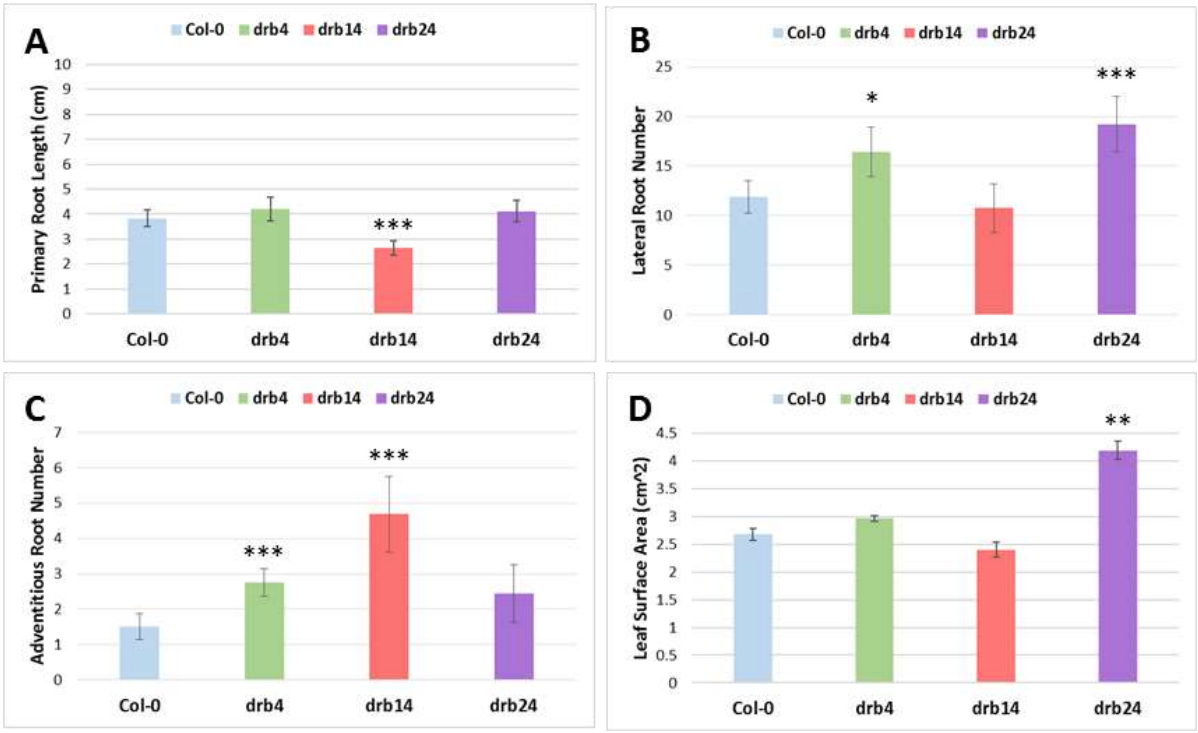

Figure 4.12. Phenotypic analysis of primary root length, lateral root number, adventitious root number, and rosette leaf surface area in Col-0, *drb4*, *drb14*, and *drb24* genetic backgrounds. Primary root length (A), lateral root number (B), adventitious root number (C), and rosette leaf surface area (D) of Col-0 (blue), *drb4* (green), *drb14* (pink), and *drb24* (purple) plant lines of 18 individual plants per line after 23 d of growth, comprised of 10 d horizontal plate growth followed by 13 d of vertical plate growth, was measured using ImageJ. Averages of *drb4*, *drb14*, and *drb24* primary root length were compared to Col-0 by a standard two-tailed t-test. Error bars represent SEM. *** $p \leq 0.001$, ** $p \leq 0.01$, * $p \leq 0.05$.

Any understanding of the developmental impact of disrupting DRB1, DRB2, and DRB4 activity is enhanced by a quantitative assessment of the phenotype. As before, this quantitative assessment included calculating the primary root length, lateral and adventitious root number, and rosette leaf surface area of *drb4*, *drb14*, and *drb24*, for comparison to wild-type plants. Regarding primary root length, only *drb14* plants showed any significant difference compared to Col-0 plants, demonstrating a reduction in primary root length (**Figure 4.12A**). This is almost the same reduction witnessed in *drb1* single mutant plants (**Figure 3.5A**). Primary root length changes apparent in the absence of either DRB1 or DRB2 activity appear to be nullified in the *drb24* mutant line, as no change in primary root length was observed (**Figure 4.12A**).

Lateral root number showed an increase of 40% and 60% in *drb4* and *drb24* plants, respectively (**Figure 4.12B**). An increase of 20% between the single mutant *drb4*, and the *drb24* double mutant, indicates an involvement of sRNAs produced through DRB2- and DRB4-mediated sRNA production pathways. However, the observation that *drb24* lateral root

number increased to the same level as *drb2* single mutant plants (**Figure 3.5B**) indicates that DRB2-mediated pathways dominate this relationship.

Adventitious rooting increased by 85% and 225% in *drb4* and *drb14* plants, respectively (**Figure 4.12C**), which demonstrated an additive effect resulting from the loss of both DRB1 and DRB4 activity. Also, unlike *drb2* and *drb4*, a compounded effect on adventitious root development was apparent by the observed increase in the number of adventitious roots in *drb14* plants above that of *drb1* single mutant plants, even though DRB1 appeared to be the dominant DRB in this relationship. The lack of a change in *drb24* adventitious root number (**Figure 4.12C**) indicated that DRB2 had little to no effect on adventitious root development.

DRB4 had minimal effect on rosette leaf surface area, as no change in either *drb4* or *drb14* genetic backgrounds was observed (**Figure 4.12D**). A significant increase in the rosette leaf surface area was observed in *drb24* mutant plants (**Figure 4.12D**), which was equal to the change observed in *drb2* single mutant plants (**Figure 3.5D**). The absence of DRB4 activity, in the *drb14* double mutant, did restore rosette leaf surface area equivalent to wild-type (**Figure 4.12D**), however, the leaf morphology of *drb14* plants remains severely altered (**Figure 4.11E**). Together, these phenotypic analyses demonstrate the dynamic nature of the interactions between DRB1, DRB2, and DRB4 in directing sRNA pathways that control a wide range of developmental processes in *Arabidopsis*.

Examining the most dramatic changes, it appears that DRB2 and DRB4 mediated sRNA pathways repress lateral root growth and development, as demonstrated by the proliferation of lateral roots in both the *drb4* and *drb24* genetic backgrounds. Similarly, DRB1 and DRB4 mediated sRNA pathways appear to repress adventitious root formation, and thus the proliferation of adventitious roots in the *drb4* and *drb14* genetic backgrounds. For example, adventitious root development in *Arabidopsis* may more heavily depend on either the tasiRNA pathway or the miR167/*ARF6*/*ARF8* expression module, than on the miR160/*ARF10*/*ARF16*/*ARF17* expression module.

4.2.4 Molecular assessment of the miR160/*ARF10*/*ARF16*/*ARF17* expression module in Col-0, *drb4*, *drb14*, and *drb24* roots

Investigating the miR160/*ARF10*/*ARF16*/*ARF17* expression module in Col-0, *drb1*, *drb2*, and *drb12* unexposed roots (*see* **Section 3.2.5**) suggested a potential role for DRB4 in the miR160 production pathway. This suggestion stemmed from the observations that mature miR160 abundance increased significantly in the absence of both DRB1 and DRB2 activity, and *DRB4* expression was elevated in the roots of the *drb12* double mutant. This, alongside the apparent relationship between DRB4 and auxin, warranted further investigation into the role of DRB4 in miR160 production, and the interaction between DRB1, DRB2, and DRB4 in *Arabidopsis* roots. To provide some insight into these relationships, RT-qPCR analysis of the miR160/*ARF10*/*ARF16*/*ARF17* expression module was conducted in the roots of the *drb4* single mutant, and the *drb14* and *drb24* double mutant genetic backgrounds.

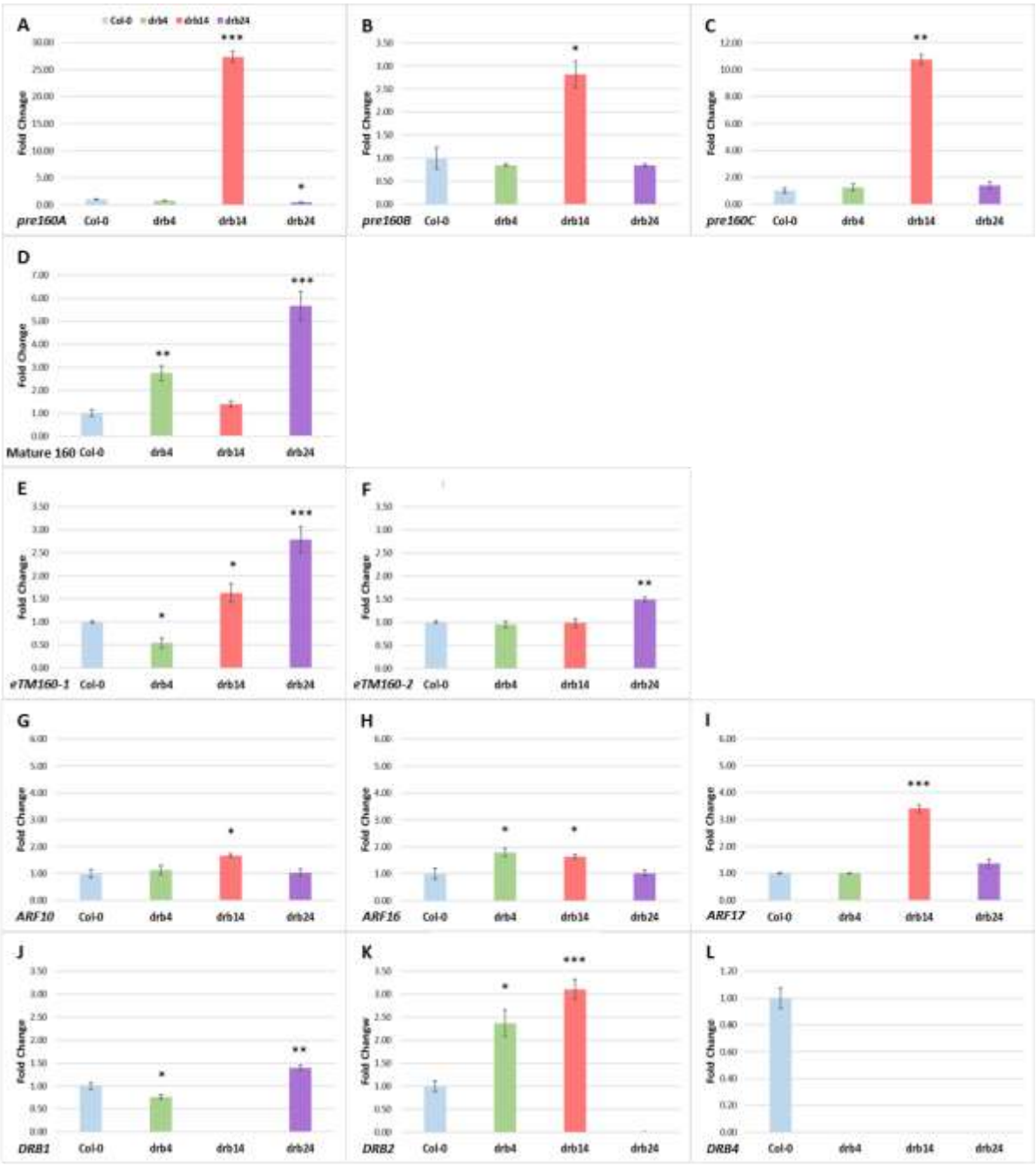

Figure 4.13. RT-qPCR analysis of the miR160/*ARF10*/*ARF16*/*ARF17* expression module. Analysed in root tissue of the Col-0 (blue), *drb4* (green), *drb14* (pink), and *drb24* (purple) genetic backgrounds were *PRI-MIR160A/B/C* precursor genes (A,B, and C), *eTM160-1* and *eTM160-2* miR160 endogenous target mimic (E and F), *ARF10/16/17* miR160 target genes (G, H, and I), and *DRB1* (J), *DRB2* (K), and *DRB4* (L) expression, and STL-qPCR analysis of miR160 accumulation (D). Fold changes were determined by the ΔΔCt method, with three biological replicates, and normalised to Col-0. Averages of expression fold change in *drb1*, *drb2*, and *drb12* genetic backgrounds were compared to Col-0 by a standard two-tailed t-test. Error bars represent SEM. *** $p \leq 0.001$, ** $p- \leq 0.01$, * $p \leq 0.05$.

The abundance of the three *MIR160* precursor transcripts showed a dramatic increase in the *drb14* double mutant but not in the *drb4* single mutant (**Figure 4.13A-C**). However, there was no change in mature miR160 abundance in *drb14* roots compared to miR160 abundance in Col-0 roots (**Figure 4.13D**). The absence of any change in the abundance of miR160 in *drb14* roots, strongly suggests that in the absence of DRB1 and DRB4 activity, DRB2 is able to mediate miR160 production. There was an approximately 3.0-fold increase in mature miR160 transcript abundance in *drb4* roots (**Figure 4.13D**) without an apparent change in precursor transcript abundance. Additionally, a near 6.0-fold increase in mature miR160 abundance was observed in *drb24* roots, coupled with a decrease in *PRI-MIR160A* precursor transcript abundance, and no change in the levels of either *PRI-MIR160B* or *PRI-MIR160C* (**Figure 4.13A-C**). This suggests an increase in processing efficiency of the *PRI-MIR160A* precursor transcript by DRB1 in the absence of DRB2 and DRB4 to produce higher levels of miR160. The dramatic increase in mature miR160 abundance in *drb24* roots is supportive of DRB1 as the primary DRB protein involved in miR160 biogenesis, as antagonism from DRB2 and DRB4 is absent in this mutant background. The increase in miR160 abundance in *drb4* roots further supports this, again due to the removal of DRB4 antagonism of either DRB1 or DRB2 activity.

In *drb4* roots, a decrease in *eTM160-1* expression by 50% (**Figure 4.13E**) could explain the increase in miR160 abundance without apparent changes in *MIR160* precursor transcript abundance. In *drb14* roots, it appears that *eTM160-1* expression scales with precursor transcript accumulation to ensure that miR160 levels are maintained, as evidenced by a 50% increase in *eTM160-1* expression (**Figure 4.13E**), while no change in mature miR160 abundance was apparent. An increase in *eTM160-1* and *eTM160-2* expression, of 175% and 50%, respectively, was observed in *drb24* roots (**Figure 4.13E** and **F**), presumably in response to the 6.0-fold increase in mature miR160 abundance in this same tissue. It is clear, that both *eTM160-1* and *eTM160-2* respond proportionally to mature miR160 abundance in *drb24* roots and, as such, appear to be acting as sequesters of miR160 activity in this tissue of the double mutant. This sequestration role of *eTM160-1* and *eTM160-2* in *drb24* roots is further supported by the wild-type-like expression of the three assessed miR160 target genes, *ARF10*, *ARF16*, and *ARF17* (**Figure 4.13G-I**).

In *drb14* roots, however, a significant increase in *ARF10*, *ARF16*, and *ARF17* expression was observed (**Figure 4.13G-I**). Of note is the 3.5-fold increase in *ARF17* expression, considering that throughout the exogenous 2,4-D application experiment, *ARF17*

expression remained largely unchanged. Also, of note was the observed increase in *ARF16* expression in *drb4* single mutant roots (**Figure 4.13H**), a result confirming that *ARF10*, *ARF16*, and *ARF17* are all under miR160-directed mRNA cleavage posttranscriptional regulation. However, it is also supportive of miR160-directed translational repression of *ARF10* and *ARF16* as a secondary posttranscriptional regulatory pathway.

DRB1 and *DRB2* expression varied greatly in *drb4*, *drb14*, and *drb24* roots. *DRB1* expression showed a decrease in *drb4* roots (**Figure 4.13J**), most likely due to higher levels of DRB2 protein presumably present in this tissue in the absence of DRB4 activity. While, *DRB1* expression increased in *drb24* roots (**Figure 4.13**), in response to DRB1 being the sole mediator of miRNA biogenesis in this genetic background. *DRB2* expression, however, increased by 2.5- and 3.0-fold, in *drb4* and *drb14* roots, respectively (**Figure 4.13K**). This was an unsurprising observation, as DRB4 has previously been demonstrated antagonistic to both DRB1 and DRB2. The central requirement for DRB2 in miR160 production was elegantly demonstrated by this set of experimental analyses. The elevated accumulation of miR160 in both the *drb4* and *drb24* genetic backgrounds showed this, by the removal of antagonism from DRB4 on either DRB1 or DRB2, in conjugation with the wild-type accumulation of miR160 in the roots of the *drb14* double mutant, where only DRB2 is functionally active.

4.3 Discussion

4.3.1 Exogenous auxin treatment affects ARF10, ARF16, and ARF17 activity, directly and indirectly, through modulating DRB-mediated miRNA biogenesis

Understanding the relationship between *ARF10*, *ARF16*, and *ARF17* function and DRB-mediated miR160 production requires an understanding of the role of ARF10, ARF16, and ARF17, both individually and collectively, in *Arabidopsis* root growth and development. ARF10, ARF16, and ARF17 have a demonstrated role in root cap formation (Wang et al. 2005) and exhibit regulatory activity in establishing lateral root primordia (Mallory et al. 2005; Wang et al. 2005). ARF10 and ARF16 repress *WUSCHEL-RELATED HOMEOBOX 5* (*WOX5*) gene transcription in distal stem cells at the root tip (Ding and Friml 2010). WOX5 itself is part of the *WUS* gene family (Bienvenut et al. 2012), with members of this gene family responsible for undifferentiated stem cell maintenance in the quiescent centre at the root tip (Gordon et al. 2009). The *arf10 arf16* double mutant not only shows a loss in gravitropic responses (Wang et al. 2005), but also a reduced primary root sensitivity to auxin (Ding and Friml 2010). In the presence of auxin, *WOX5* transcription decreases, mediated through the posttranslational activation of ARF10 and ARF16, increasing transcriptional repression of *WOX5* at the root tip (Ding and Friml 2010). In the absence of functional ARF10 and ARF16, this repression event does not occur in the presence of increased auxin concentrations, resulting in no change to WOX5 levels and, therefore, no change in distal stem cell activity (Ding and Friml 2010).

In the initiation and development of lateral roots, ARF10 has been demonstrated to mediate the auxin response, with local auxin maxima defining the location of lateral root initials (Wang et al. 2005). However, ARF16 acting in conjunction with ARF17 has been demonstrated to have a negative effect on auxin directed lateral root formation (Couzigou and Combier 2016; Mallory et al. 2005; Wang et al. 2005). ARF10 and ARF16 not only determine the location of lateral root formation, but later influence lateral root growth by determining gravitropic setpoint angles (GSAs) (Roychoudhry et al. 2013). Here, ARF10 and ARF16 act as positive regulators of antigravitropic offset responses, rather than functioning as negative regulators of gravitropic responses (Roychoudhry et al. 2013). Through both of these processes, ARF10 and ARF16 regulate both primary and lateral root growth and development.

As previously mentioned (*see* **Section 4.1** and **Figure 4.1**), ARF17 is unusual amongst the ARF protein family as it has a truncated CTD, the domain responsible for mediating interaction with its specific Aux/IAA(s), and for the formation of homodimers once its

interaction with its repressing Aux/IAA(s) is broken (Hagen and Guilfoyle 2002; Ulmasov et al. 1999; Ulmasov et al. 1997). Like ARF10 and ARF16, modifications to *ARF17* expression in *Arabidopsis* result in an altered primary and lateral root phenotype (Mallory et al. 2005; Wang et al. 2005). However, unlike ARF10 and ARF16, ARF17 negatively regulates primary and lateral root elongation (Mallory et al. 2005). Evidence for this exists, in that the *in planta* expression of a miR160-resistant version of *ARF17*, the m*ARF17* transgene, which essentially acts as an *ARF17* overexpressor, results in m*ARF17* plants developing a shorter primary root and a reduced lateral root number, as well as the lateral roots which form being reduced in length (Wang et al. 2005). Additionally, ARF17, acting a transcriptional repressor, negatively regulates *GH3*-like gene expression (Mallory et al. 2005). In turn, GH3-like proteins are auxin responsive, and have a positive regulatory role in primary root elongation, establishing lateral root initials, and subsequently driving lateral root elongation (Nakazawa et al. 2001; Takase et al. 2004). In this sense, modification to ARF17 abundance has the opposite effect on primary root elongation, lateral root primordia formation, and lateral root growth, to that of ARF10 and ARF16. However, it is important to note that the correct function of all three miR160-targeted ARFs, ARF10, ARF16, and ARF17, is an essential requirement for normal primary and lateral root development (Overvoorde et al. 2010; Zhao 2010), with abnormally perceived auxin concentrations, in most cases, resulting in the perturbation of primary root growth and fewer incidents of lateral root primordia formation (Leyser 2002; Overvoorde et al. 2010; Zhao 2010).

As miR160 is a known posttranscriptional regulator of *ARF10*, *ARF16*, and *ARF17* gene expression (Mallory et al. 2005), it too has a significant impact on root growth and development (Mallory et al. 2005; Wang et al. 2005). Currently, the molecular and phenotypic effects of manipulating miR160 abundance, and the resulting changes in auxin responses, are primarily thought to be an indirect result of such modifications via altered ARF10-, ARF16-, and/or ARF17-mediated transduction (Mallory et al. 2005; Wang et al. 2005). However, promoter analysis of the three *MIR160* encoding genes (**Table 4.1**), suggests that the expression of these three genes, and therefore miR160 abundance, may respond directly to auxin signalling, presumably through the classical genetic auxin response pathway. This finding, therefore, indicates an alternate pathway where phenotypic responses to miR160 modifications may be the result of direct changes in miR160 production, as opposed to indirect consequences of miR160-directed posttranscriptional regulation of *ARF10*, *ARF16*, and *ARF17* expression. An added level of complexity to this relationship is the existence of endogenous target mimics (eTMs) for miR160 (*eTM160-1* and *eTM160-2*) (Wu et al. 2013). These two non-cleavable

eTMs regulate the abundance of the miR160 sRNA in cells were *eTM160-1* and *eTM160-2* are expressed, sequestering miR160 to prevent miR160-directed expression regulation of *ARF10*, *ARF16*, and *ARF17* (Wu et al. 2013). In summary, ARF10 and ARF16 promote primary root elongation, the formation of lateral root primordia and, subsequently, lateral root growth, while ARF17 is demonstrated to repress these developmental processes. Furthermore, miR160 negatively regulates the expression of *ARF10*, *ARF16* and *ARF17* while, itself, being under negative regulation by *eTM160-1* and *eTM160-2*.

The DRB1/DCL1 functional partnership is thought to be the primary mediator of miR160 biogenesis in *Arabidopsis* (Eamens et al. 2009). However, molecular analysis of miR160 production, and subsequently on the effect of the miR160 sRNA on target gene expression (*see* **Section 3.2.5**), indicates a role for DRB2 in directing miR160 biogenesis and/or mediating the regulation of miR160 target gene expression. Considering this apparent relationship, determining the significance of auxin, and using exogenously applied auxin to molecularly deconstruct the relationship between DRB1, DRB2, and the miR160/*ARF10*/*ARF16*/*ARF17* expression module, was attempted here to further our current understanding of the role that the miR160/*ARF10*/*ARF16*/*ARF17* expression module plays in *Arabidopsis* root development.

Treating Col-0 plants with varying concentrations of 2,4-D for 24 h revealed that primary root length was largely unaffected by the exogenous application of synthetic auxin, except at the 10 μM concentration (**Figure 4.6**). The severely retarded development displayed by wild-type *Arabidopsis* following exposure to 10 μM 2,4-D was believed partly due to the auxinic herbicide effects of this synthetic auxin (Rodriguez-Serrano et al. 2014), but also resulting from the shifting of local auxin maxima to such a degree that it becomes catastrophic to primary root elongation (Leyser 2002). Contrary to this was the observed increase in primary root length of the *drb1* mutant following treatment with 0.1 μM 2,4-D (**Figure 4.6**). In previous reports, *drb1* plants exhibited reduced sensitivity to exogenous auxin treatment (Han et al. 2004). While exogenous auxin treatment only has a mild effect on primary root length in Col-0 plants (**Figure 4.6**), *drb1* plants respond in a different way to low concentrations of exogenous auxin treatment. This is in keeping with the expectation that miR160 abundance should be reduced in *drb1* plants (Eamens et al. 2009), alleviating miR160-directed repression of *ARF10* and *ARF16* expression. However, when compared to unexposed *drb1* roots, miR160 abundance increased at all concentrations of exogenously applied 2,4-D (**Figure 4.8D**). Such an observation may result from miR160 abundance scaling to the increased abundance of its

ARF10 and *ARF16* targets, or as shown in **Table 4.1**, altered miR160 abundance may simply be the result of altered *MIR160* gene expression if the promoter regions of either the *MIR160A*, *MIR160B*, or *MIR160C* loci are directly responsive to altered auxin homeostasis. Further, the significance of *eTM160-1* cannot be ignored in this situation, as even though mature miR160 abundance increases in *drb1* roots treated with 0.1 µM 2,4-D (**Figure 4.8D**), *eTM160-1* expression also increases significantly (**Figure 4.8E**). As *eTM160-1* is a known sequester of miR160 activity, thereby reducing its activity (Wu et al. 2013), altered *ARF10* and *ARF16* expression is likely to have a muted response to increased miR160 abundance when *eTM160-1* transcript abundance is also increased. *ARF16* expression itself showed a dramatic increase in *drb1* roots treated with 0.1 µM 2,4-D (**Figure 4.8H**), lending credence to the contribution of ARF16 activity in promoting primary root elongation in 0.1 µM 2,4-D treated *drb1* roots.

The primary root length of *drb2* plants did not show an increase in response to the exogenous application of 2,4-D (**Figure 4.6**). The observed decreases at both the 1.0 and 10 µM 2.4-D treatments is reflective of the response of Col-0 roots to these applied concentrations of 2,4-D, whereby primary root elongation is perturbed. Furthermore, miR160 levels were elevated in the roots of *drb2* plants at all concentrations of 2,4-D applied (**Figure 4.9D**), a similar trend to that observed in the *drb1* background (**Figure 4.8D**). Curiously, *ARF10* and *ARF16* expression was also elevated following treatment with 0.1, 1.0, and 10 µM 2,4-D (**Figure 4.9G** and **H**). This surprise observation suggests that miR160-directed expression repression of *ARF10* and *ARF16* could potentially become defective in *drb2* roots upon exogenous application of auxin. Alternatively, miRNAs that require DRB2, together with DCL1 for their production, instead of the canonical DRB1/DCL1 partnership, have been demonstrated to regulate target gene expression via a translational repression mode of silencing. Therefore, the observed increase in the abundance of the *ARF10* and *ARF16* transcripts along with enhanced miR160 accumulation, indicates that these two miR160 target genes are under DRB2-mediated, miR160-directed translational repression posttranscriptional regulation in *Arabidopsis* roots. Unlike *ARF10* and *ARF16*, *ARF17* expression is incrementally repressed following exogenous auxin application, a finding that suggests that this miR160 target gene is regulated via the canonical miR160-directed mRNA cleavage mechanism of silencing. Reduced *ARF17* abundance corresponds to the observed reductions to primary root length of *drb2* plants treated with 1.0 µM and 10 µM 2,4-D (**Figures 4.6** and **4.9I**).

Lateral and adventitious root phenotypes respond differently to the primary roots of *Arabidopsis* plants to exogenous auxin treatment. Increases in the number of lateral roots in Col-0 and *drb2* plants treated with 0.1 and 1.0 µM 2,4-D indicate a positive effect for exogenous auxin application in these plant lines (**Figure 4.6B**). However, increases in *ARF16* expression in 0.1 µM 2,4-D treated Col-0 roots (**Figure 4.7H**), in addition to the observed enhancement of *ARF10* expression in 0.1 and 1.0 µM 2,4-D treated *drb2* roots (**Figure 4.9G**), are counterintuitive to the repressor role that both ARF16 and ARF17 play in lateral root formation (Couzigou and Combier 2016; Mallory et al. 2005; Wang et al. 2005). Lateral root number was also increased in *drb1* plants following treatment with 0.1 µM 2,4-D (**Figure 4.6B**) and, further, *ARF16* expression was also elevated at the same concentration (**Figure 4.8H**). Considering that the *arf10 arf16* double mutant line showed an increase in the number of lateral roots (Wang et al. 2005), and that the m*ARF17* plant line displayed a decrease in lateral root number (Mallory et al. 2005), such expression increases in *ARF10* and *ARF16* would be expected to repress lateral root initiation. Indeed, mature miR160 abundance increased in roots Col-0, *drb1*, and *drb2* plants treated with these concentrations of 2,4-D, concurrent with the observed increases in *eTM160-1* and *eTM160-2* expression (**Figures 4.7D-F**, **8D-F**, and **9D-F**). Taken together, these findings indicate that in the roots of Col-0, *drb1*, and *drb2* plants, increases in *ARF* target gene expression lead to the enhancement of miR160 abundance, and the subsequent promotion of *eTM160* expression, in an attempt to maintain the miR160/*ARF10*/*ARF16*/*ARF17* expression module in a homeostatic state. Interestingly, although miR160 abundance is elevated in both *drb1* and *drb2* roots, this does not appear to result in the same phenotypic outcome in these two mutant backgrounds. This suggests that there are many additional factors that further contribute to the response of *drb1* and *drb2* plants to exogenous auxin application outside of the assessed miR160/*ARF10*/*ARF16*/*ARF17* expression module.

This observed increase in lateral root numbers, despite increases in *ARF10* and *ARF16* expression, warrants consideration of alternate auxin responsive pathways. Three genes have been implicated in positively regulating lateral root formation, and these are also auxin responsive. HAIRY MERISTEM (HAM) proteins promote the initial formation of lateral organs in *Arabidopsis*, including lateral root primordia (Engstrom 2012). In this case, it is thought that HAM may promote the functional activity of CLV3, to aid in the definition of primordial boundaries in developing lateral meristematic zones (Engstrom 2012). Furthermore, *HAM* genes are known targets of miR171 (Llave et al. 2002). The second protein is IAR3, a

known target of miR167 (Kinoshita et al. 2012), which also positively regulates lateral root formation and is auxin responsive (Couzigou and Combier 2016; Kinoshita et al. 2012). Two separate knockout mutants, *iar3-5* and *iar3-6*, both show dramatic reductions in the number of lateral roots (Kinoshita et al. 2012). Finally, Class III HD ZIPs, in conjunction with KANADI1, are demonstrated positive regulators of lateral root formation (Hawker and Bowman 2004). Interestingly, KANADI1 has been shown to interact with ARF3 (Kelley et al. 2012), a truncated ARF like ARF17 (Guilfoyle and Hagen 2007), and further, *ARF3* expression is regulated posttranscriptionally by tasiARFs (Williams et al. 2005). Although ARF3 has a demonstrated role in repressing lateral root formation (Yoon et al. 2010), the potential association between a transcriptional repressor and a transcriptional activator in lateral root formation is intriguing. There is an undeniable relationship between these positive regulatory pathways, auxin responses, and DRB-mediated sRNA production, and numerous miRNA/target gene expression modules. Further consideration of this complex relationship network may offer an alternate explanation to the upregulation of miR160 production and *ARF* transcription, and the apparently paradoxical increases in lateral root formation in Col-0, *drb1*, and *drb2* genetic backgrounds.

Interestingly, increases in adventitious root number were only observed in the Col-0, *drb2*, and *drb12* backgrounds that had been treated with 1.0 μM 2,4-D (**Figures 4.5**, **4.6B** and **C**). No change in adventitious root number in *drb1* plants, indicates that DRB2 potentially plays a role in normal adventitious root development, presumably via its documented role in miRNA production. Of the three miR160 targeted *ARF* genes, only ARF17 has a documented role in adventitious root formation (Couzigou and Combier 2016; Mallory et al. 2005). Only a slight reduction in *ARF17* expression was observed in *drb2* roots following treatment with 1.0 μM 2,4-D (**Figure 4.9I**), but no such change in *ARF17* transcript abundance was observed in Col-0 plants following treatment with any concentration of 2,4-D (**Figures 4.7I** and **8I**). The lack of change in *ARF17* abundance, in spite of significant alterations to miR160 levels in the roots of 0.1, 1.0, and 10 μM 2,4-D treated Col-0 roots, suggests that in wild-type roots *ARF17*/ARF17 abundance is likely regulated via a DRB2-mediated, miR160-directed translational repression mode of silencing. The observed reduction in *ARF17* expression in *drb2* roots explains the increase in adventitious root number with ARF17 having been previously demonstrated to repress adventitious root formation (Couzigou and Combier 2016; Mallory et al. 2005).

ARF6 and ARF8, known targets of miR167 (Kinoshita et al. 2012), are also positive regulators of adventitious root formation (Gutierrez et al. 2009). The similarities apparent between the miR167/*ARF6*/*ARF8* and miR160/*ARF10*/*ARF16*/*ARF17* expression modules in regulating adventitious root formation offers an explanation for the increase in adventitious rooting observed in 1.0 µM 2,4-D treated Col-0 roots (**Figure 4.6C**). However, no such increase was observed in *drb1* roots at any 2,4-D treatment concentration (**Figure 4.6C**). It would be expected that although no change in *ARF17* expression was observed (**Figure 4.8I**), disruption of miR167-directed repression of *ARF6* and *ARF8* expression would result in an increase in adventitious rooting. Considering that *ARF6*, *ARF8*, and *ARF17* are all miRNA targets, taken together with the observed increases in adventitious rooting of Col-0 and *drb2* plants (**Figure 4.6C**), adventitious root regulation may potentially require synergism between DRB1 and DRB2. Although, a similar increase in adventitious rooting was observed in *drb12* roots (**Figure 4.6C**), no change in *ARF17* expression was documented (**Figure 4.10I**). Such an observation suggests that although DRB1 and DRB2 synergism, directing miR160 biogenesis, is influential in regulating adventitious root formation, DRB-mediated miRNA biogenesis may also involve other DRB proteins in adventitious root initials.

From the findings reported here, it is clear that changes to root architecture, induced by exogenous auxin treatment, in different *drb* genetic backgrounds, may influence several other miRNA expression modules in addition to the miR160/*ARF10*/*ARF16*/*ARF17* module assessed here. However, questions remain regarding the relationship between miRNA-directed mRNA transcript cleavage and translational repression as modes of posttranscriptional regulation of the miR160/*ARF10*/*ARF16*/*ARF17* expression module.

4.3.2 DRB1 and DRB2 are required for miR160 production in *Arabidopsis* roots

miR160 production is a DRB-mediated process (Eamens et al. 2009). Further evidence for this has been presented in this study, with miR160 abundance changes documented in *drb1*, *drb2*, and *drb12* plants, and across the assessed 2,4-D treatment concentrations. In *drb1* roots, mature miR160 abundance is reduced compared to its accumulation in Col-0 roots across the 2,4-D treatments (**Figure 3.6D**). DRB2-mediated production of miRNAs has been demonstrated (Eamens et al. 2012a) and leads to posttranscriptional regulation via translational repression (Reis et al. 2015), rather than transcript cleavage. It appears that in the absence of DRB1 activity, DRB2 is capable of processing *PRI-MIR160* precursor transcripts to produce

mature miR160 in both unexposed and 2,4-D treated *Arabidopsis* roots. It is also apparent that *DRB4* expression responds to exogenous auxin treatment and that the antagonistic relationship of DRB4, to both DRB1 and DRB2, additionally influences the efficiency of miR160 production.

PRI-MIR160 precursor transcripts only appear to over-accumulate in *drb14* root tissue (**Figure 4.13A-C**), suggesting that efficient precursor transcript processing requires either DRB1 or DRB4. DRB1 was previously shown to be required for miR160 production (**Figure 3.6D**) (Eamens et al. 2009), and miR160 abundance decreased in *drb14* roots (**Figure 4.13D**), while *ARF10*, *ARF16*, and *ARF17* expression all increased (**Figure 4.13G-I**), conclusively demonstrating that DRB1 is required for efficient miR160 production. However, in the absence of both DRB1 and DRB4, DRB2 appears to be capable of maintaining mature miR160 levels (**Figure 4.13D**). The absence of both DRB1 and DRB4 activity significantly reduces the degree of antagonism on DRB2, leading to a significant increase in *DRB2* expression (**Figure 4.13K**), showing that DRB2 is capable of processing *PRI-MIR160* precursors, although this process is inefficient as demonstrated by the significant accumulation of *PRI-MIR160* precursor transcripts in *drb14* roots (**Figure 4.13A-C**). It would be expected that DRB2-mediated miR160 production would lead to posttranscriptional regulation by translational repression. Indeed, this appears to be the case as only very mild increases in *ARF10* and *ARF16* transcript abundance were observed in *drb14* roots (**Figure 4.13G** and **H**). However, the dramatic increase in *ARF17* expression (**Figure 4.13I**), an increase comparable to the increases observed in *drb1* and *drb12* roots (**Figure 3.6I**), indicates that *ARF17* is not under the translational repression mode of posttranscriptional silencing.

Despite the significant increase in *ARF17* expression, no change in lateral root initiation was observed in *drb14* roots (**Figure 4.12B**). This was surprising, as ARF17 has been recognised as inhibiting lateral root initiation (Couzigou and Combier 2016). However, it is possible that *eTM160-1* is acting as a target for miR160-directed translational repression and this would be expected to limit the degree of translational repression, if any, targeting *ARF17* for expression regulation. This would account for the observed changes in miR160 abundance, *eTM160* levels, and *ARF17* expression, but does not address the apparent contradictory role of ARF17 in lateral root development in *drb14* plants. Decreased primary root length in the *drb14* genetic background is consistent with the role of ARF10 and ARF16 promoting primary root elongation (Ding and Friml 2010). The observed changes in *ARF10* and *ARF16* expression after exogenous auxin treatment and in unexposed *drb14* roots suggests that DRB-mediated

miR160 production targeting *ARF10* and *ARF16* influences primary root development to a greater extent than lateral root development, shaping *Arabidopsis* root architecture.

Adventitious rooting increased substantially in the *drb14* genetic background (**Figure 4.12C**) in conjunction with a significant increase in *ARF17* expression (**Figure 4.13I**). This conflicts with observations of ARF17 function in adventitious rooting (Couzigou and Combier 2016; Mallory et al. 2005), similar to Col-0, *drb2*, and *drb12* 1.0 µM 2,4-D treated roots (**Figure 4.6C**). This supports the idea that DRB2, in the absence of DRB1 and DRB4 activity, may direct miRNA biogenesis, leading to translational repression mediated silencing, not only for the miR160 targets, but also for the miR167 targets, ARF6 and ARF8, known positive regulators of adventitious root initiation (Gutierrez et al. 2009). This is significant, as DRB2 would modulate ARF6, ARF8, and ARF17 activity via miR160- and/or miR167-directed translational repression. Alternatively, ARF17 may respond directly, and therefore may function differently, in response to exogenous auxin treatment.

In *drb4* and *drb24* roots, molecular responses of the miR160/*ARF10*/*ARF16*/*ARF17* expression module are largely the same (**Figure 4.13**), leading to similar phenotypic outcomes (**Figure 4.12**). Lateral root number increased in the *drb24* mutant (**Figure 4.12B**), and tasiARFs are known repressors of lateral root initiation (Couzigou and Combier 2016). tasiARF production is a DRB4-mediated biogenesis pathway (Yoon et al. 2010) and, therefore, in *drb4* knockout mutant lines, lateral root repression would be expected to be alleviated. Indeed, this is the case, ad an increase in lateral root proliferation was observed (**Figure 4.12B**). This suggests that both DRB2 and DRB4 are required for normal lateral root initiation and development in *Arabidopsis*.

Adventitious rooting, on the other hand, increased in both the *drb4* and *drb14* genetic backgrounds, with a compounded effect apparent in *drb14* roots (**Figure 4.12C**). *ARF10*, *ARF16*, and *ARF17* expression, all increased in *drb14* (**Figure 4.13G-I**) and, further, *ARF16* expression increased in *drb4* root tissue along with mature miR160 abundance (**Figure 4.13D** and **H**). Increased adventitious root initiation could be attributed to the miR167/*ARF6*/*ARF8* expression module. This expression module promotes adventitious root initiation (Couzigou and Combier 2016) and miR167 production requires DRB1 (Eamens et al. 2009). However, DRB2 could also be a promoter of adventitious root initiation, as no change was observed in *drb24* roots (**Figure 4.13C**). The involvement of DRB2 could be either indirectly, from the antagonistic relationships between DRB2 and DRB1 (Eamens et al. 2012a) and DRB2 and

DRB4 (Pelissier et al. 2011), or directly, by mediating miR160 and/or miR167 production leading to translational repression of target mRNA transcripts.

4.3.3 Conclusions

These findings indicate that DRB1-mediated miR160 production leads to target gene transcript cleavage as previously reported (Mallory et al. 2005), the predominant posttranscriptional regulatory pathway governing *ARF10* and *ARF16* activity in the root tip. DRB2-mediated miR160 production directs translational repression of *ARF10* and *ARF16*, most notably in the absence of DRB4, with a compounded effect in the absence of both DRB1 and DRB4. But DRB2 does not appear to mediate miR160 production targeting *ARF17* via translational repression. Additionally, DRB1- and/or DRB4-mediated sRNA biogenesis appears to influence lateral root phenotypes to a greater extent than DRB2-mediated sRNA production, and sRNA participants in such posttranscriptional regulatory pathways could account for lateral and adventitious root proliferation, despite miR160 abundance fluctuations in 2,4-D treated Col-0, *drb1*, and *drb2* roots. It is clear that a strong relationship between DRB1 and DRB2 is required for normal miR160 production and function. However, the circumstances under which DRB1- or DRB2-mediated miR160 production, leading to either mRNA transcript cleavage or translational repression, respectively, as the dominant posttranscriptional regulatory pathway remains unclear.

In the next part of this study, phenotypic and molecular characterisation of miR160-resistant *ARF10* and *ARF16* transgene expression, as well as the overexpression of the *MIR160B* transgene in Col-0, *drb1*, and *drb2* plants will be undertaken. Examination of the phenotypic and molecular consequences in these transformant lines aims to further deconstruct the miR160/*ARF10*/*ARF16*/*ARF17* expression module to provide more conclusive evidence of the role of ARF10 and ARF16 in root architectural development and the posttranscriptional regulatory pathways which control this module.

Chapter 5

Examining the consequence of miRNA-resistant *ARF10* and *ARF16* expression, and *MIR160B* overexpression in *Arabidopsis thaliana*

5.1 Introduction

A complete understanding of how and when DRB1- and DRB2-mediated miR160 production directs mRNA transcript cleavage and translational repression as respective modes of posttranscriptional regulation requires examination. Previously, this study has examined the phenotypic and molecular consequences of disrupting sRNA biogenesis in general utilising the well described *drb* mutant backgrounds (**Chapter 3**). In addition, the effects of exogenous auxin treatment on the miR160/*ARF10*/*ARF16*/*ARF17* expression module was also assessed (**Chapter 4**). From these analyses, it is evident that by manipulating aspects of posttranscriptional regulation of the miR160/*ARF10*/*ARF16*/*ARF17* expression module, both DRB1 and DRB2 are required for normal root architectural development in *Arabidopsis*.

The strong indication that miR160-directed translational repression of *ARF10* and *ARF16* transcripts is a possible posttranscriptional mechanism is a significant finding. However, the phenotypic consequences of translational repression in this expression module have not been fully addressed. This is especially important, as some phenotypic and molecular changes observed in *drb1* and *drb2* mutant lines (**Figure 3.5** and **3.6**) were counter to expected changes given our current understanding of the role of ARF10, ARF16, and ARF17 in root development.

At present, ARF10 and ARF16 are known to be involved in maintaining the population of undifferentiated stem cells in the quiescent centre of the root tip by mediating a response to increased auxin concentration in this tissue (Ding and Friml 2010). ARF10 has also been shown to play a role in defining lateral root initial locations in response to local auxin maxima (Wang et al. 2005), while ARF16 and ARF17 are known to repress other aspects of lateral root formation (Couzigou and Combier 2016; Mallory et al. 2005; Wang et al. 2005), although ARF16 does have a dual role in directing lateral root growth, by acting in conjunction with ARF10 later in development, to determine gravitropic setpoint angles (Roychoudhry et al. 2013). ARF17, however, is a known repressor of lateral and adventitious root growth (Couzigou and Combier 2016; Mallory et al. 2005; Wang et al. 2005). miR160 acts as a posttranscriptional regulator of *ARF10*, *ARF16*, and *ARF17* expression (Mallory et al. 2005), and, as such, has the potential to exert considerable influence over root developmental processes affected by ARF10, ARF16, and ARF17 activity. By extension, the biogenesis pathway mediating miR160 production also plays a role in root development.

One experimental approach that might resolve these differences would be to observe the molecular changes resulting from, and subsequent phenotypic consequences of, introducing miR160-resistant *ARF* (m*ARF*) and *MIR160* overexpression transgenes into Col-0 plants and the *drb1* and *drb2* mutant backgrounds. miRNA-resistant transcripts are an effective way of decoupling miRNA production and miRNA target transcript repression (Bishop 2003). miRNA-resistant transcripts are made by introducing silent mutations into the coding region of the target gene sequence, rendering the miRNA binding site, in this case the miR160 binding site, unrecognisable by the targeting miRNA (Bishop 2003). Further, previous work has suggested that at least six mismatches must be present to make a target binding site unrecognisable to the targeting miRNA (Mallory et al. 2005).

Previous introduction of m*ARF17* and *ARF17* overexpression transgenes into Col-0 plants, showed that miR160 responds to increased expression of *ARF17*, as shown by increased cleavage product accumulation from *ARF17* transcripts (Mallory et al. 2005). Further, m*ARF17* transgenic lines showed an increase in *ARF17* transcript abundance, and a reduction in both primary root length and lateral root number (Mallory et al. 2005), similar to the root phenotype of *drb1* plants. Similarities of the m*ARF17* line to *drb1* plants extended to the aerial tissues, with both plant lines showing reduced leaf rosette size and extended leaf petioles (Mallory et al. 2005). Also pertinent was the report that m*ARF17* plants displayed severe leaf edge serration (Mallory et al. 2005), a hallmark aerial tissue phenotype displayed by *drb2* plants. This suggests a role for both DRB1 and DRB2 in production of miR160 targeting *ARF17*.

Assessment of m*ARF10*, m*ARF16*, and *MIR160C* overexpression transgenic plants has also been reported with *PRI-MIR160C* overexpression plants showing increased transcript cleavage of *ARF10*, *ARF16*, and *ARF17* (Wang et al. 2005). Increased transcript cleavage, and thus decreased expression of *ARF10* and *ARF16*, caused a shift in stem cell differentiation and root cap patterning, ultimately leading to the loss of the root gravitropic response. However, individual introduction of m*ARF10* and m*ARF16* transgenes into plants overexpressing *PRI-MIR160C* was able to rescue this deleterious phenotype and restore primary root development to a near wild-type state (Wang et al. 2005).

Considering these successful approaches, a novel modification to these experimental strategies would be to utilise similar transgenes and observe the phenotypic and molecular responses in genetic backgrounds deficient in the function of the protein machinery central to miRNA production. The m*ARF10* and m*ARF16* transgenes were selected for assessment here as *ARF10* and *ARF16* presented as the most likely candidates under miR160-directed

translational repression (**Chapter 3** and **Chapter 4**). The *MIR160B* precursor transcript was selected as the overexpression candidate most likely to assist in elucidating the contribution of miR160-directed translational repression in determining root architecture, as it gave an expression profile across the assessed *drb* mutant lines most indicative of DRB involvement in the production of miR160 directing this posttranscriptional regulatory mechanism.

5.1.1 Aims and objectives in this chapter

This chapter aims to provide further evidence addressing the possibility of translational repression as a posttranscriptional regulatory mechanism controlling *ARF10* and *ARF16* expression in *Arabidopsis* roots, and the contributions made to root growth and development of DRB1- and DRB2-mediated miR160 production governing the miR160/*ARF10*/*ARF16*/*ARF17* expression module.

Specifically, this chapter aims to:

- Examine the phenotypic and molecular consequences of introducing the m*ARF10*, m*ARF16* and *MIR160B* transgenes into Col-0, *drb1*, and *drb2* plants.
- Investigate whether miR160-directed *ARF10, ARF16*, and *ARF17* transcript cleavage and translational repression are alternate, or parallel, posttranscriptional regulatory mechanisms used to maintain the miR160/*ARF10*/*ARF16*/*ARF17* expression module in a homeostatic state.

5.2 Results

5.2.1 Phenotypic assessment of m*ARF10*, m*ARF16*, and *MIR160B* transgene expression in Col-0, *drb1*, and *drb2* plants

From the analyses presented in **Chapter 3** and **Chapter 4**, the most dramatic changes in the miR160/*ARF10*/*ARF16*/*ARF17* expression module, contributing to root architectural modifications, appeared to be due to changes in mature miR160 abundance, resulting from changes in *PRI-MIR160B* precursor transcript expression and processing. *ARF10* and *ARF16* expression was also differentially regulated via DRB1-mediated miR160-directed *ARF* transcript cleavage and/or DRB2-mediated miR160-directed translational repression.

Deconstruction and investigation of which posttranscriptional regulatory pathway may be dominant in controlling the miR160/*ARF10*/*ARF16*/*ARF17* expression module and, therefore, influence root growth and development, is most directly achieved by analysing the consequence of decoupling miR160-directed posttranscriptional regulation of *ARF10* and *ARF16* expression, and by determining how the overproduction of miR160 from the *PRI-MIR160B* precursor transcript modulates *ARF10*, *ARF16*, and *ARF17* expression. To accomplish this, transgenes harbouring miRNA-resistant versions of *ARF10* (m*ARF10*) and *ARF16* (m*ARF16*), along with *PRI-MIR160B* encoding sequences were introduced into Col-0, *drb1*, and *drb2* plants (**Figure 5.1**).

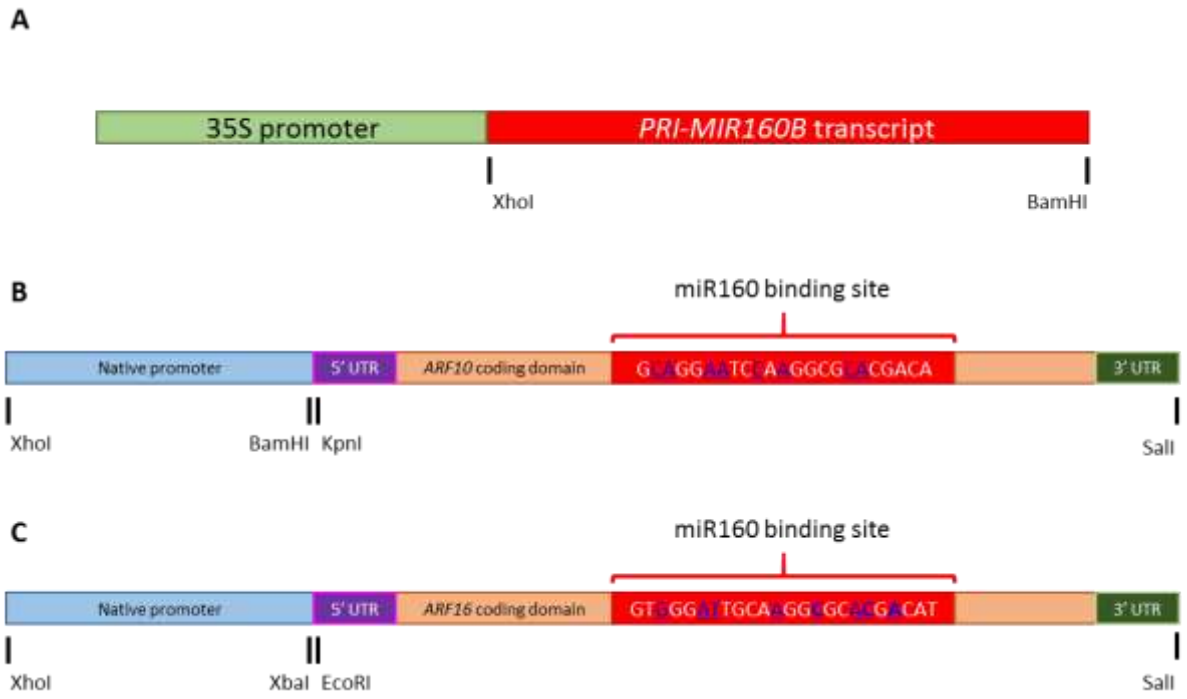

Figure 5.1. Schematic representation of *PRI-MIR160B* overexpression and miR160-resistant *ARF10* and *ARF16* transgenes. The precursor transcript for *PRI-MIR160B* was amplified from Col-0 *Arabidopsis* genomic DNA and inserted into the multiple cloning site (MCS) of pBART using *XhoI* and *BamHI* restriction sites (A), the CaMV 35S ubiquitous promoter was located within the pBART plasmid backbone. A 3 kb fragment upstream of the described 5' UTR for *ARF10* (B) and a 2 kb fragment upstream fragment for *ARF16* (C) was amplified from Col-0 *Arabidopsis* genomic DNA and inserted into the MCS of pORE1 using *XhoI* and *BamHI*, and *XhoI* and *XbaI* restriction sites for *ARF10* and *ARF16* promoter sequence, respectively. mRNA sequences for miR160-resistant versions of *ARF10* (B) and *ARF16* (C) were synthesised with eight mismatches in the miR160 binding site for both *ARF10* and *ARF16*. These synthesised fragments were inserted into the MCS of pORE1 downstream of the native promoter sequences using *KpnI* and *SalI*, and *EcoRI* and *SalI* restriction sites for *ARF10* and *ARF16*, respectively.

All reported analyses were conducted on T3 transformant plants, with T1 (**Appendix 6**) and T2 (**Appendix 7**) plant phenotypes also scored for severity. Genotypic confirmation of T3 plants was conducted to demonstrate that T3 plants harboured the introduced m*ARF10*, m*ARF16*, and *MIR160B* transgenes (**Appendix 8**). Specifically, T3 plants from Col-0/*mARF10* 17-2, Col-0/*mARF16* 5-4, Col-0/*MIR160B* 19-1, *drb1*/*mARF10* 3-2, *drb1*/*mARF16* 4-4, *drb1*/*MIR160B* 9-4, *drb2*/*mARF10* 2-3, *drb2*/*mARF16* 3-1, and *drb2*/*MIR160B* 11-1 were used for this analysis.

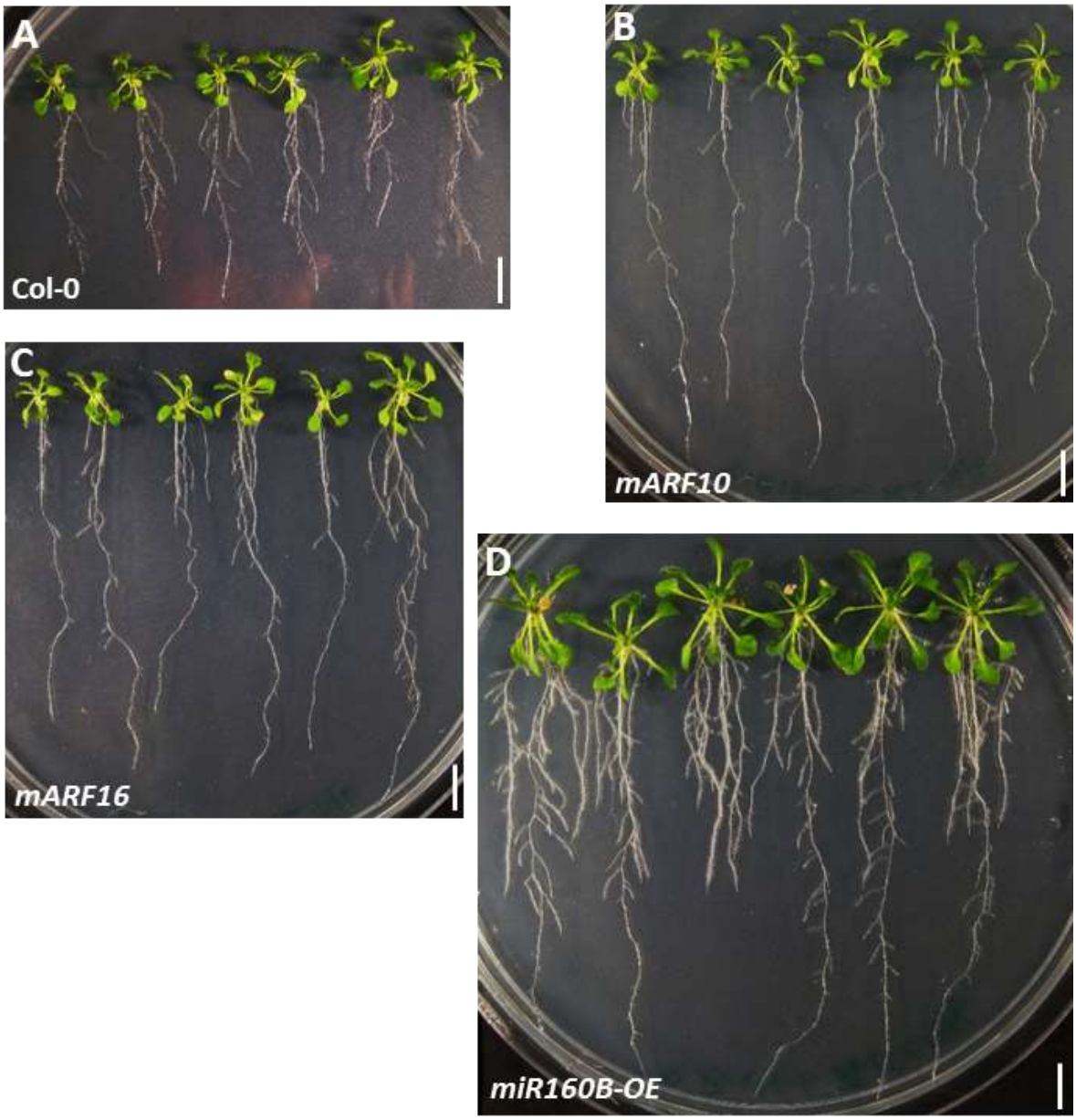

Figure 5.2. Representative phenotypes displayed by vertically grown Col-0, Col-0/m*ARF10* and Col-0/m*ARF16*, and Col-0/*MIR160B Arabidopsis* plant lines. Col-0 (A), *mARF10* (B), *mARF16* (C), and *PRI-MIR160B* overexpression (D) plants were germinated and cultivated on horizontally orientated MS media plates under standard growth conditions for 10 d, before being transferred to new MS media plates that were orientated vertically for an additional 13 d of growth. Phenotypic analyses were conducted, and root material collected for subsequent molecular analyses. Scale bars represent 1 cm.

Changes in the miR160/*ARF10*/ARF16/*ARF17* expression module, even in the presence of fully functional miRNA processing machinery, resulted in alterations in both shoot and root structures. The introduction of m*ARF10* and m*ARF16* transgenes into the Col-0 background seemed to most strongly influence primary root growth (**Figure 5.2B** and **C**), with a dramatic increase in the length of both of these transformant lines. However, little effect on lateral and adventitious root growth and development was observed (**Figure 5.2B** and **C**). This

could likely be attributed to the activity of ARF10 and ARF16 being most pronounced in the primary root cap (Ding and Friml 2010). In the aerial tissues, the rosettes of Col-0/m*ARF10* plants appeared smaller (**Figure 5.2B**), while Col-0/m*ARF16* plants appeared to have a smaller rosette size (**Figure 5.2C**).

Examination of the Col-0*/MIR160B* overexpression line, however, showed more dramatic alterations in development. Compared to Col-0 plants, overexpression of the *PRI-MIR160B* precursor transcript resulted in increased primary root growth. Further, lateral and adventitious root proliferation was also readily apparent in Col-0/*MIR160B* plants (**Figure 5.2D**). The increase in lateral and adventitious rooting in Col-0*/MIR160B* plants is surprising considering that adventitious rooting increased in *drb1* plants, while lateral rooting increased in *drb2* plants, both genetic backgrounds deficient in sRNA processing machinery contributing to altered miR160 production. Leaf rosettes also dramatically increased in size, coupled with an increase in petiole length of those leaves (**Figure 5.2D**), a phenotype similar to that displayed by *drb2* plants.

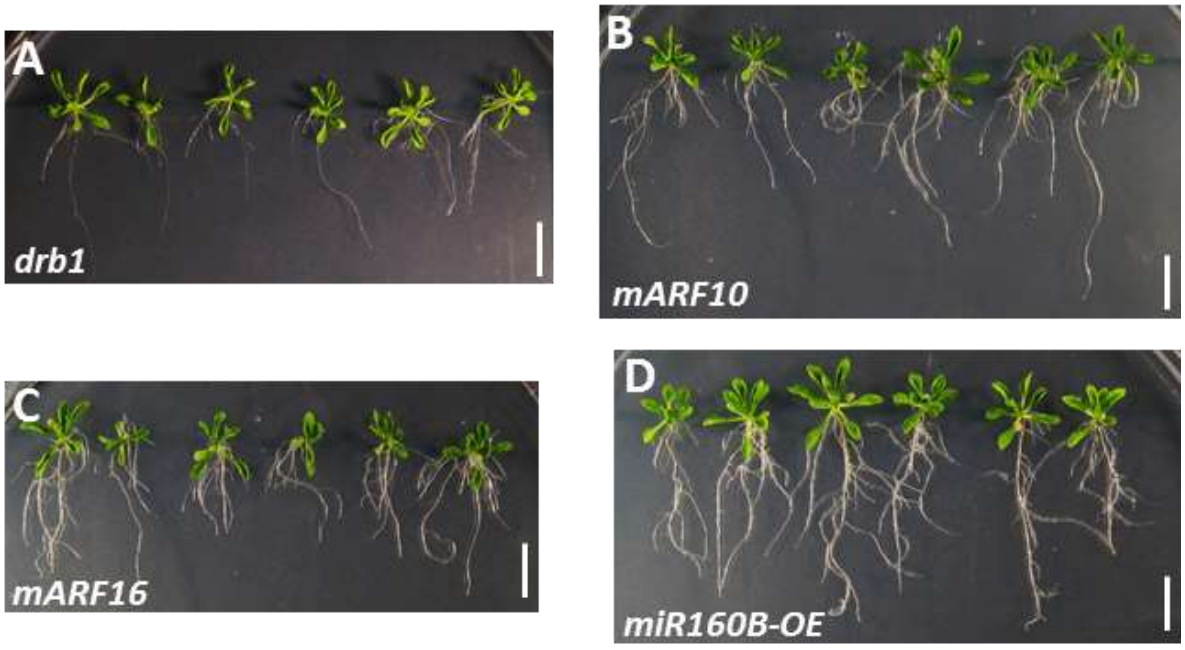

Figure 5.3. Representative phenotypes displayed by vertically grown *drb1*, *drb1*/m*ARF10* *drb1*/m*ARF16*, and *drb1*/*MIR160B* *Arabidopsis* plant lines. *drb1* (A), m*ARF10* (B), m*ARF16* (C), and *PRI-MIR160B* overexpression (D) plants were germinated and cultivated on horizontally orientated MS media plates under standard growth conditions for 10 d, before being transferred to new MS media plates that were orientated vertically for an additional 13 d of growth. Phenotypic analyses were conducted, and root material collected for subsequent molecular analyses. Scale bars represent 1 cm.

Transformation of *drb1* with the m*ARF10*, m*ARF16*, and *MIR160B* transgenes elicited different phenotypic responses to those displayed by the corresponding Col-0 plant lines. Unlike in Col-0, where m*ARF10* and m*ARF16* transgene expression resulted in primary root length extension, no increase in primary root length was apparent in *drb1*/m*ARF10* or *drb1*/m*ARF16* plants (**Figure 5.3B** and **C**). However, an increase in the number of lateral and adventitious roots in *drb1*/m*ARF10* plants was observed (**Figure 5.3B**). Excessive development of adventitious roots in *drb1*/m*ARF10* transformants is notable considering that adventitious rooting is already prevalent in the *drb1* background. Nevertheless, there was no apparent increase in adventitious rooting in *drb1*/m*ARF16* plants (**Figure 5.3C**). The increase in lateral rooting in both *drb1*/m*ARF10* and *drb1*/m*ARF16* transformant plants was an additional opposing phenotype to that expressed by unmodified *drb1* plants which displayed decreased lateral root development.

In aerial tissues, *drb1*/m*ARF10* transformants appeared to display an increase in leaf hyponasty (**Figure 5.3B**), a notable phenotypic change as *drb1* plants already exhibit this trait. No such increase in leaf hyponasty was observed in either the *drb1*/m*ARF16* or *drb1*/*MIR160B* lines (**Figure 5.3C** and **D**). The overexpression of *PRI-MIR160B* in *drb1* only appeared to result in an increase in the number of lateral roots that developed in *drb1*/*MIR160B* plants (**Figure 5.3D**), a similar phenotypic effect of *PRI-MIR160B* overexpression in Col-0 plants (**Figure 5.2D**). This suggests that overexpression of the *PRI-MIR160B* precursor transcript leads to the repression of *ARF* targets, presumably *ARF16* and/or *ARF17*, ultimately resulting in the release of lateral root developmental suppression, even in the absence of functional DRB1.

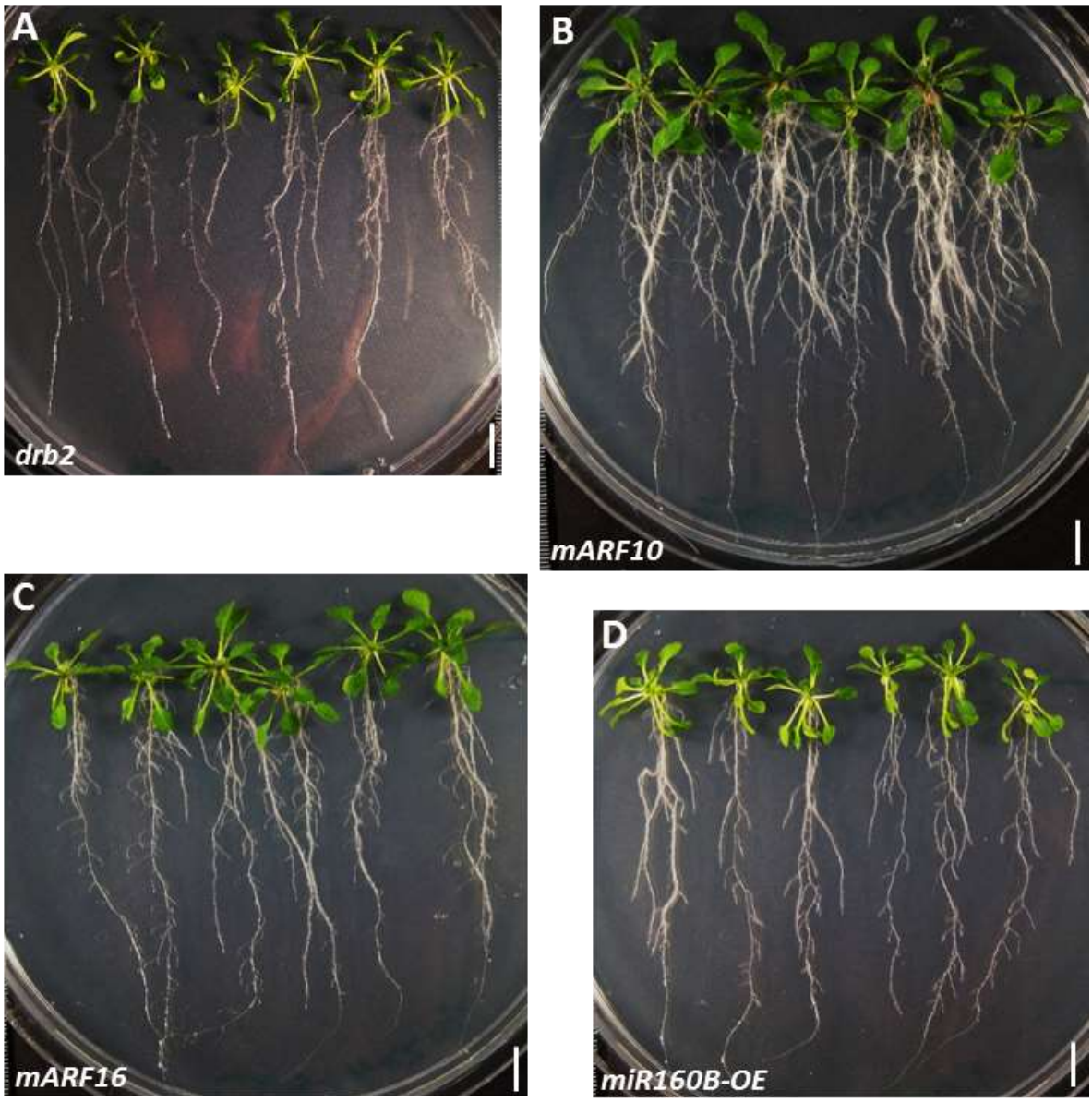

Figure 5.4. Representative phenotypes displayed by vertically grown *drb2*, *drb2*/m*ARF10* *drb2*/m*ARF16*, and *drb2*/*MIR160B* *Arabidopsis* plant lines. *drb2* (A), m*ARF10* (B), m*ARF16* (C), and *PRI-MIR160B* overexpression (D) plants were germinated and cultivated on horizontally orientated MS media plates under standard growth conditions for 10 d, before being transferred to new MS media plates that were orientated vertically for an additional 13 d of growth. Phenotypic analyses were conducted, and root material collected for subsequent molecular analyses. Scale bars represent 1 cm.

Phenotypic examination of *drb2/*m*ARF10*, *drb2/*m*ARF16*, and *drb2/MIR160B* transformants, again showed different changes in root and shoot development. It appeared that m*ARF10* transgene expression had the most profound effect in the *drb2* genetic background (**Figure 5.4B**), with increases primary root elongation, as well as promotion of lateral and adventitious rooting also readily evident. This same lateral root phenotype was observed in *drb2*/m*ARF16* plants, but to a lesser extent, and there was no increase in primary root length

or adventitious rooting (**Figure 5.4C**). The rosettes of both *drb2*/m*ARF10* and *drb2*/m*ARF16* plants appeared to be flatter than those of unmodified *drb2* plants (**Figure 5.4B** and **C**), although *drb2*/m*ARF16* transformants appeared to have a smaller rosette overall (**Figure 5.4C**).

Overexpression of the *PRI-MIR160B* transcript in *drb2*/*MIR160B* plants showed the fewest phenotypic differences from unmodified *drb2* plants. No dramatic changes in root architecture were observed although lateral roots did appear slightly longer in *drb2*/*MIR160B* plants (**Figure 5.4D**), possibly due to an earlier onset of lateral root initiation. Leaf rosettes of the *drb2*/*MIR160B* plants did appear to be smaller than those of unmodified *drb2* plants, and even smaller than those of *drb2*/m*ARF16* plants (**Figure 5.4D**). There was also a slight increase in leaf epinasty (**Figure 5.4D**), possibly contributing to the appearance of smaller leaf rosettes.

Quantification of basic phenotypic characteristics has previously revealed important information regarding the growth and development of these plant lines under different conditions (**Chapter 3** and **Chapter 4**). The same phenotypic parameters were assessed here to gain insight into the phenotypic consequences of expression of m*ARF10*, m*ARF16*, and *MIR160B* transgenes in the Col-0, *drb1*, and *drb2* backgrounds.

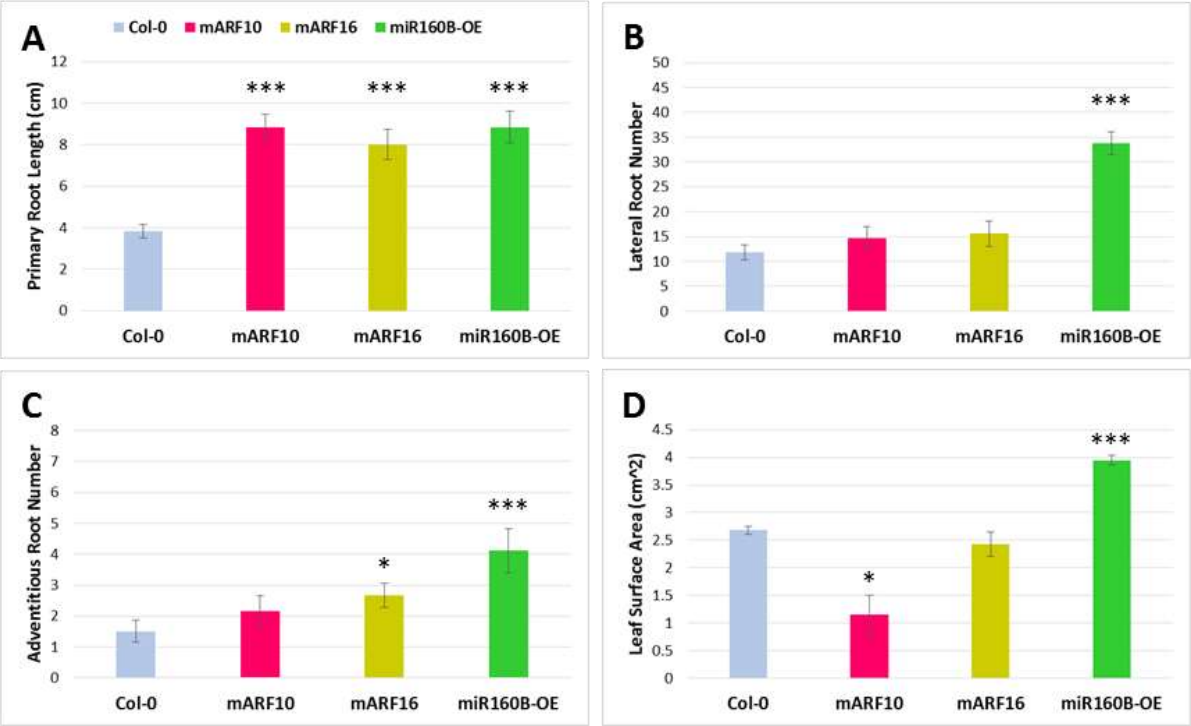

Figure 5.5. Phenotypic analysis of primary root length, lateral root number, adventitious root number, and rosette leaf surface area in Col-0, Col-0/m*ARF10*, Col-0/m*ARF16*, and Col-0/*MIR160B* plants. Primary root length (A), lateral root number (B), adventitious root number (C), and rosette surface area (D) of Col-0 (blue), Col-0/m*ARF10* (pink), Col-0/m*ARF16* (yellow), and Col-0/*MIR160B* overexpression (green) plants were measured after 23 d of growth using ImageJ. Averages for 18 plants of Col-0/m*ARF10*, Col-0/m*ARF16*, and Col-0/*MIR160B* were compared to Col-0 with a two-tailed t-test. Error bars represent SEM. *** $p \leq 0.001$, * $p \leq 0.05$.

Transformation of the m*ARF10*, m*ARF16*, and *MIR160B* transgenes into Col-0 plants resulted in significant changes in root and shoot phenotypes. The increased primary root length, common across all three transformant lines (**Figure 5.5A**), was a somewhat surprising result, as decoupling *ARF10* and *ARF16* posttranscriptional regulation from miR160 control, would be expected to cause opposing phenotypic changes compared with miR160 over-accumulation in Col-0/*MIR160B* plants. Only the Col-0/*MIR160B* transformant line showed an increase (~250%) in lateral root number (**Figure 5.5B**), indicating that by increasing miR160-directed posttranscriptional regulation of *ARF10*, *ARF16*, and *ARF17*, the suppression of lateral root initiation is released. Similarly, an increase in adventitious root number in the Col-0/*MIR160B* transformant line (**Figure 5.5C**) could potentially result from a similar mechanism. However, the Col-0/m*ARF16* transformant line also showed a slight increase in adventitious root number (**Figure 5.5C**), indicating that ARF16 may promote adventitious root formation.

As with all assessed phenotypic parameters, the Col-0/*MIR160B* transformant line showed an increase, ~60%, in rosette surface area (**Figure 5.5D**), whereas Col-0/m*ARF10*

plants showed a nearly 50% decrease in rosette size (**Figure 5.5D**), indicating that miR160-directed posttranscriptional regulation of *ARF10*/ARF10 abundance is required for normal leaf growth and development. The lack of change in Col-0/m*ARF16* plants suggests that ARF16 has no role in determining leaf size in *Arabidopsis*.

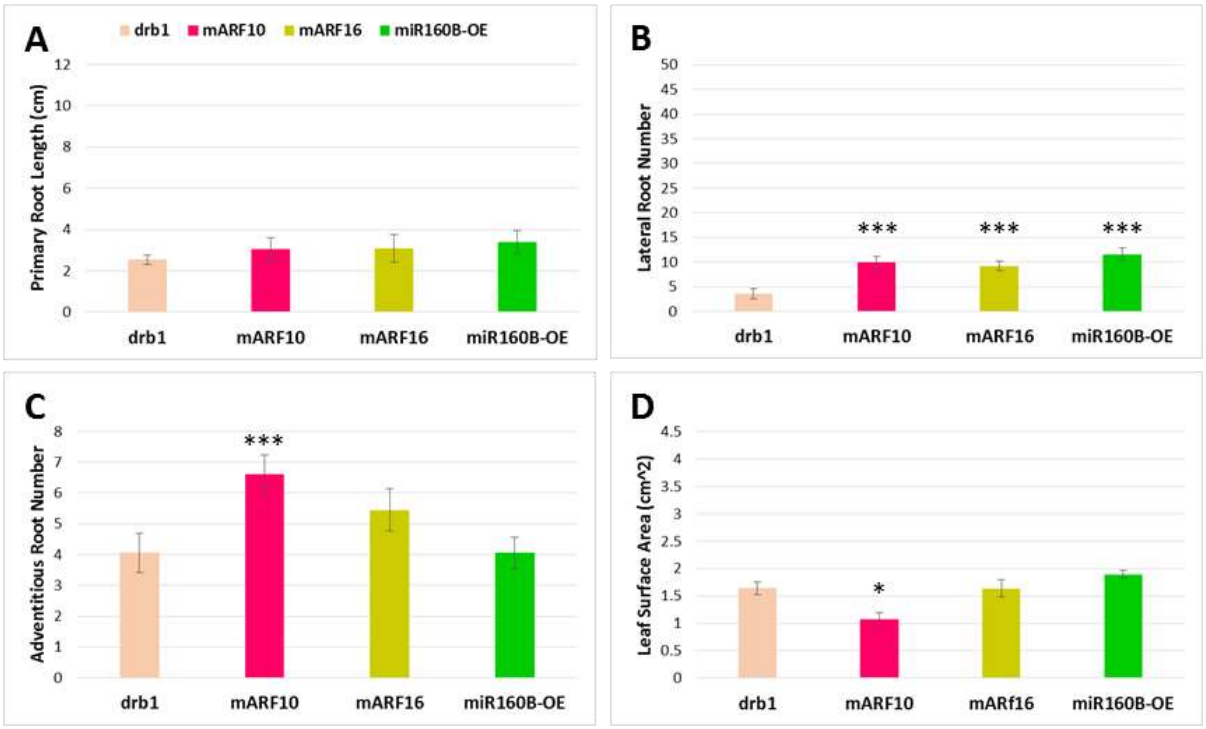

Figure 5.6. Phenotypic analysis of primary root length, lateral root number, adventitious root number, and rosette leaf surface area in *drb1*, *drb1*/m*ARF10*, *drb1*/m*ARF16*, and *drb1*/*MIR160B* plants. Primary root length (A), lateral root number (B), adventitious root number (C), and rosette surface area (D) of *drb1* (orange), *drb1*/m*ARF10* (pink), *drb1*/m*ARF16* (yellow), and *drb1*/*MIR160B* overexpression (green) plants were measured after 23 d of growth using ImageJ. Averages for 18 plants of *drb1*/m*ARF10*, *drb1*/m*ARF16*, and *drb1*/*MIR160B* were compared to *drb1* with a two-tailed t-test. Error bars represent SEM. *** $p \leq 0.001$, * $p \leq 0.05$.

Unlike Col-0 plants, m*ARF10* and m*ARF16* expression, and the overexpression of *MIR160B*, resulted in no change in primary root length in the *drb1* background (**Figure 5.6A**). This suggests that DRB1 is required for processing of miR160 from the *PRI-MIR160B* precursor to target *ARF10*, *ARF16*, and/or *ARF17* in the root tip for expression regulation. However, decoupling *ARF10* and *ARF16* from miR160-directed posttranscriptional regulation does not change primary root development in the absence of DRB1 (**Figure 5.6A**), suggesting that removing posttranscriptional regulation of *ARF10* and *ARF16* is insufficient to rescue the deleterious *drb1* primary root phenotype.

Expressing m*ARF10* and m*ARF16* and overexpressing the *MIR160B* transgenes in *drb1* plants resulted in an increase in lateral root number (**Figure 5.6B**). As with primary root length in Col-0 plants, the observed increase in all three transformant lines is surprising, as opposing phenotypic consequences of expressing m*ARF10* and m*ARF16* transgenes, to overexpressing the *MIR160B* transgene were expected. Also, a surprise observation was the increase in adventitious root number in the *drb1/*m*ARF10* transformant line, but no change in either the *drb1/*m*ARF16* or *drb1/MIR160B* transformants (**Figure 5.6C**), this could indicate an undescribed role for ARF10 in adventitious root initiation. As was the case in Col-0*/*m*ARF10* plants, only the *drb1/*m*ARF10* transformant line showed a decrease in rosette surface area (**Figure 5.6D**). Again, this implied a role for ARF10 in regulating rosette leaf development and furthered this role description by demonstrating that expressing the m*ARF10* transgene caused this change independent of a requirement for DRB1.

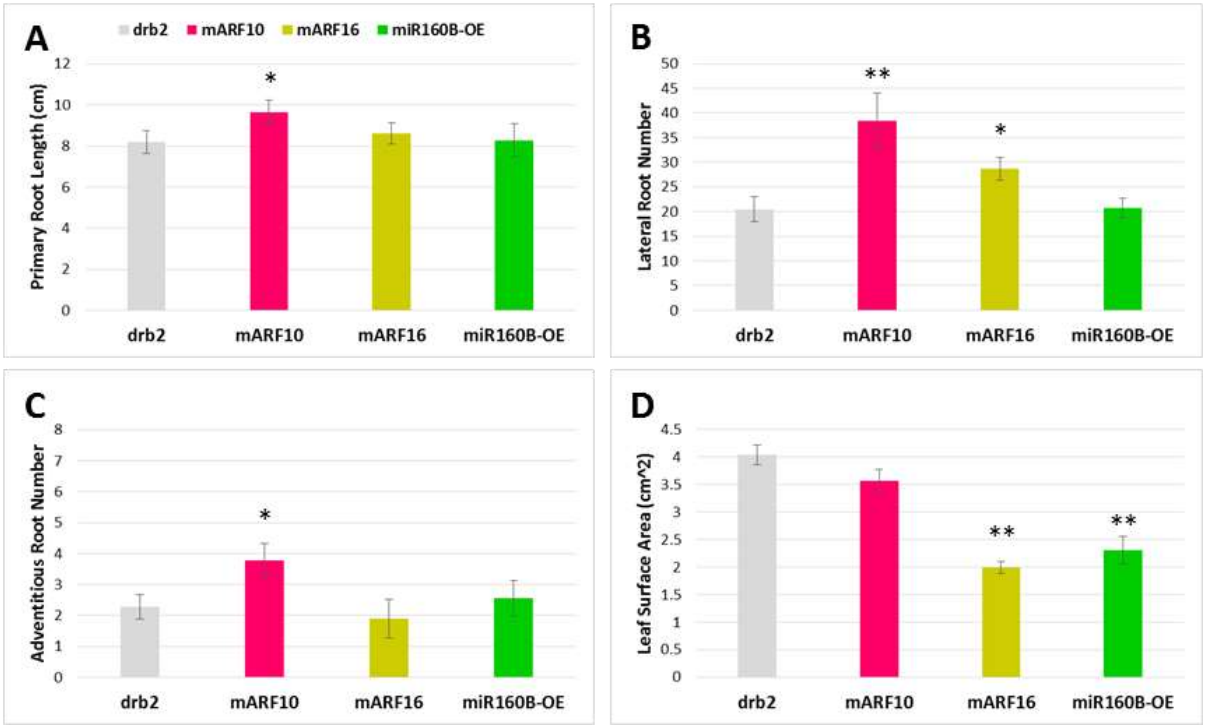

Figure 5.7. Phenotypic analysis of primary root length, lateral root number, adventitious root number, and rosette leaf surface area in *drb2*, *drb2*/m*ARF10*, *drb2*/m*ARF16*, and *drb2*/*MIR160B* plants. Primary root length (A), lateral root number (B), adventitious root number (C), and rosette surface area (D) of *drb2* (grey), *drb2*/m*ARF10* (pink), *drb2*/m*ARF16* (yellow), and *drb2*/*MIR160B* overexpression (green) plants were measured after 23 d of growth using ImageJ. Averages for 18 plants of *drb2*/m*ARF10*, *drb2*/m*ARF16*, and *drb2*/*MIR160B* were compared to *drb2* with a two-tailed t-test. Error bars represent SEM. ** $p \leq 0.01$, * $p \leq 0.05$.

The m*ARF10* transgene gave the most consistent changes in the *drb2* background with *drb2*/m*ARF10* plants showing significantly increased primary root length (**Figure 5.7A**), lateral root number (**Figure 5.7B**), and adventitious root number (**Figure 5.7C**). This indicates that DRB1 is required for *Arabidopsis* plants expressing the m*ARF10* transgene to exhibit increased primary root length, while both DRB1 and DRB2 are required for promotion of lateral and adventitious rooting.

Only the *drb2*/m*ARF16* background exhibited an increase in lateral root number (**Figure 5.7B**), similar in magnitude to the increase observed in the *drb1* background (**Figure 5.6B**), indicating that both DRB1 and DRB2 are required for this phenotype to be displayed. No change was observed in *drb2*/*MIR160B* plants, apart from a decrease in rosette surface area (**Figure 5.7D**), a surprising result as antagonism between DRB2 and DRB1 is absent in the *drb2* background. Furthermore, *drb2*/m*ARF16* plants showed a comparable decrease in rosette surface area similar to *drb2*/*MIR160B* plants (**Figure 5.7B**), again, a surprising result as these two transgenes would be expected to produce opposing phenotypic effects.

Taken together, the phenotypic characterisation of m*ARF10*, m*ARF16*, and *MIR160B* transgene expression in the Col-0, *drb1*, and *drb2* backgrounds showed that individually manipulating posttranscriptional regulation of *ARF10* and *ARF16* and expression control of *PRI-MIR160B* affected *Arabidopsis* shoot and root growth and development. It appeared that processing of the *PRI-MIR160B* precursor transcript was most efficient in the presence of both DRB1 and DRB2, while phenotypic changes due to m*ARF10* transgene expression were most readily apparent when either DRB1 or DRB2 was non-functional.

5.2.2 Molecular assessment of the miR160/*ARF10*/*ARF16*/*ARF17* expression module in Col-0, *drb1*, and *drb2* plants expressing the m*ARF10*, m*ARF16*, and *MIR160B* transgenes

Molecular examination of the miR160/*ARF10*/*ARF16*/*ARF17* expression module in Col-0, *drb1*, and *drb2* genetic backgrounds in unexposed (**Chapter 3**) and auxin treated (**Chapter 4**) conditions indicated that posttranscriptional regulation of *ARF10* and *ARF16* transcripts via translational repression contributed to root phenotypic changes. Molecular examination of *drb14* roots (**Chapter 4**) provided further experimental evidence supporting translational repression as a posttranscriptional regulatory mechanism.

In Section **5.2.1**, clear phenotypic changes were observed for primary root elongation and lateral and adventitious root development following introduction of the m*ARF10*, m*ARF16*, and *MIR160B* transgenes into Col-0, *drb1*, and *drb2* genetic backgrounds. Molecular assessment of the miR160/*ARF10*/*ARF16*/*ARF17* expression module was, therefore, undertaken to identify the primary molecular drivers of these phenotypic changes. This analysis should further deconstruct this expression module and determine the extent of its influence in controlling root development in *Arabidopsis*.

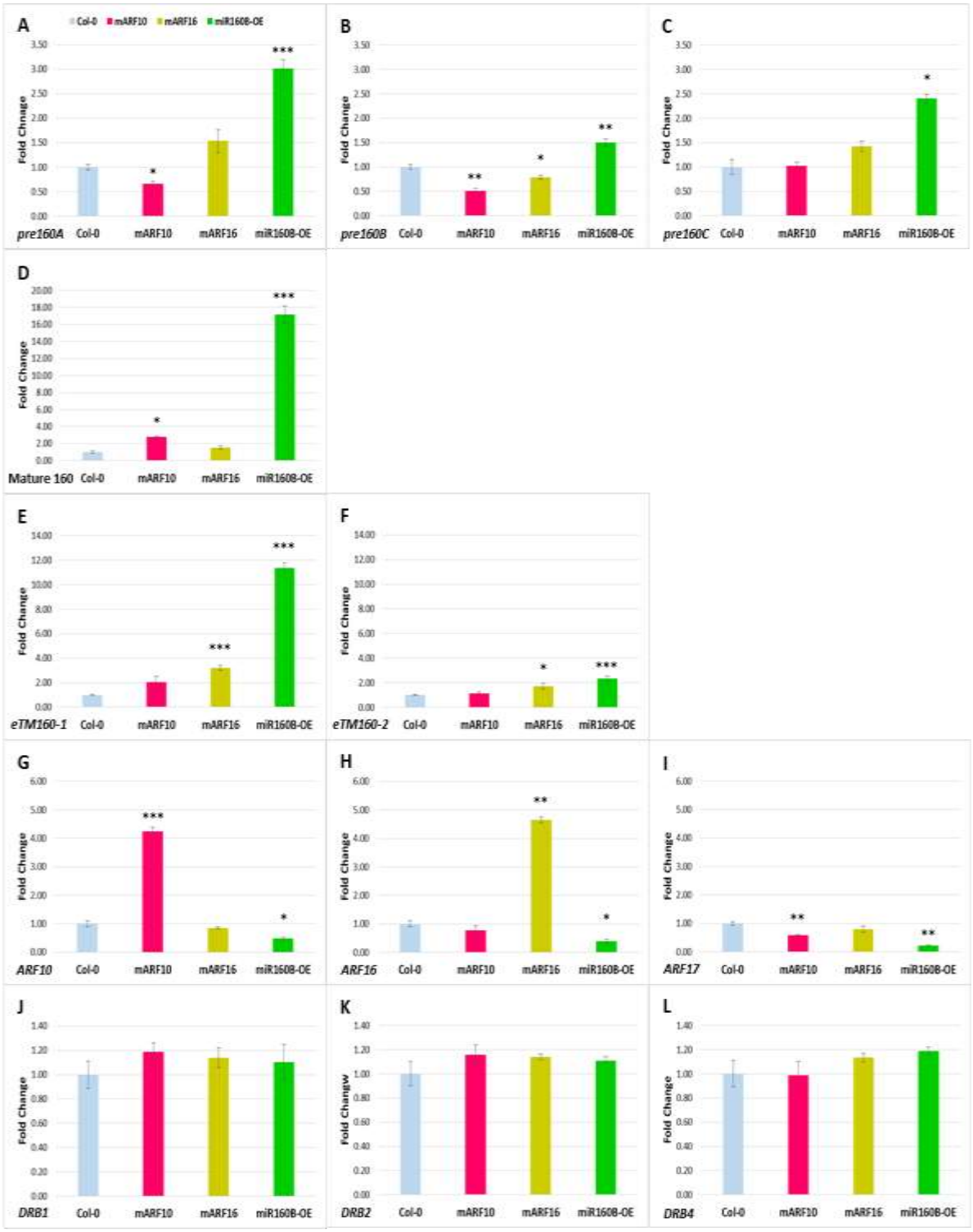

Figure 5.8. RT-qPCR analysis of the miR160/*ARF10*/*ARF16*/*ARF17* expression module in root tissue of Col-0, Col-0/m*ARF10*, Col-0/m*ARF16* expression, and Col-0/*MIR160B* genetic backgrounds. Analysed in root tissue of Col-0 (blue), Col-0/m*ARF10* (pink), Col-0/m*ARF16* (yellow), and Col-0/*MIR160B* (green) transformant lines were *PRI-MIR160A/B/C* precursor genes (A,B, and C), *eTM160-1* and *eTM160-2* miR160 endogenous target mimic (E and F), *ARF10/16/17* miR160 target genes (G, H, and I), and *DRB1* (J), *DRB2* (K), and *DRB4* (L) expression, and STL-qPCR analysis of miR160 accumulation (D). Fold changes were determined by the ΔΔCt method, with three biological replicates, and normalised to Col-0. Averages of expression fold change in the transformant lines were compared to Col-0 by a standard two-tailed t-test. Error bars represent SEM. *** $p \leq 0.001$, ** $p- \leq 0.01$, * $p \leq 0.05$.

PRI-MIR160A and *PRI-MIR160B* both showed a decrease in transcript abundance in the Col-0 plants expressing the m*ARF10* transgene (**Figure 5.8A** and **B**), indicative of more efficient precursor processing. Only *PRI-MIR160B* showed a similar trend in the Col-0/m*ARF16* transformant line (**Figure 5.8B**). All three miR160 encoding genes showed an increase in expression in the *PRI-MIR160B* overexpression transformant line (**Figure 5.8A-C**), suggesting that *PRI-MIR160A* and *PRI-MIR160C* expression increases in response to elevated *PRI-MIR160B* expression. It appeared that *PRI-MIR160A* and *PRI-MIR160B* were more efficiently processed by either DRB1 or DRB2 in Col-0/m*ARF10* plants, evidenced by an increase in mature miR160 abundance, while no change in Col-0/m*ARF16* plants was observed (**Figure 5.8D**). Mature miR160 abundance showed a dramatic increase in the Col-0/*MIR160B* transformant line (**Figure 5.8D**), presumably due to the large increase in precursor gene expression.

The expression of *eTM160-1* and *eTM160-2* increased most significantly in Col-0/*MIR160B* plants (**Figure 5.8E** and **F**), presumably in response to the dramatic increase in mature miR160 abundance to attempt to sequester the additional levels of miR160 present in Col-0/*MIR160B* plants. The abundance of *eTM160-1* and *eTM160-2* also increased in Col-0/m*ARF16* plants, potentially to buffer any alteration in miR160 abundance that may have occurred in this transformant line.

As expected, *ARF10* and *ARF16* expression increased ~4.0 and ~4.5-fold, respectively (**Figure 5.8G** and **H**), a result of miR160 resistance introduced by expression of m*ARF10* and m*ARF16* transgenes in Col-0/m*ARF10* and Col-0/m*ARF16* plants. Interestingly, neither *ARF10* nor *ARF16* expression changed in the reciprocal Col-0/m*ARF16* and Col-0/m*ARF10* transformant lines (**Figure 5.8G** and **H**). This observation indicates that increased mature miR160 abundance induced by m*ARF* transgene expression does not result in increased miR160-directed transcript cleavage of either endogenous *ARF10* or *ARF16* transcript. However, *ARF17* transcript levels decreased in the Col-0/m*ARF10* transformant line (**Figure 5.8I**). Overexpression of the *PRI-MIR160B* precursor transcript did result in decreased expression of *ARF10*, *ARF16*, and *ARF17* in Col-0/*MIR160B* plants (**Figure 5.8G-I**). This finding indicates that miR160-directed *ARF* target gene mRNA cleavage was increased in this plant line. Despite increased *PRI-MIR160* precursor transcript levels, no change in *DRB1*, *DRB2*, or *DRB4* expression was observed (**Figure 5.8J-L**), leading to the conclusion that all observed increases in miR160 abundance were a direct result of elevated precursor processing efficiency by the existing activity of the DRB protein pool.

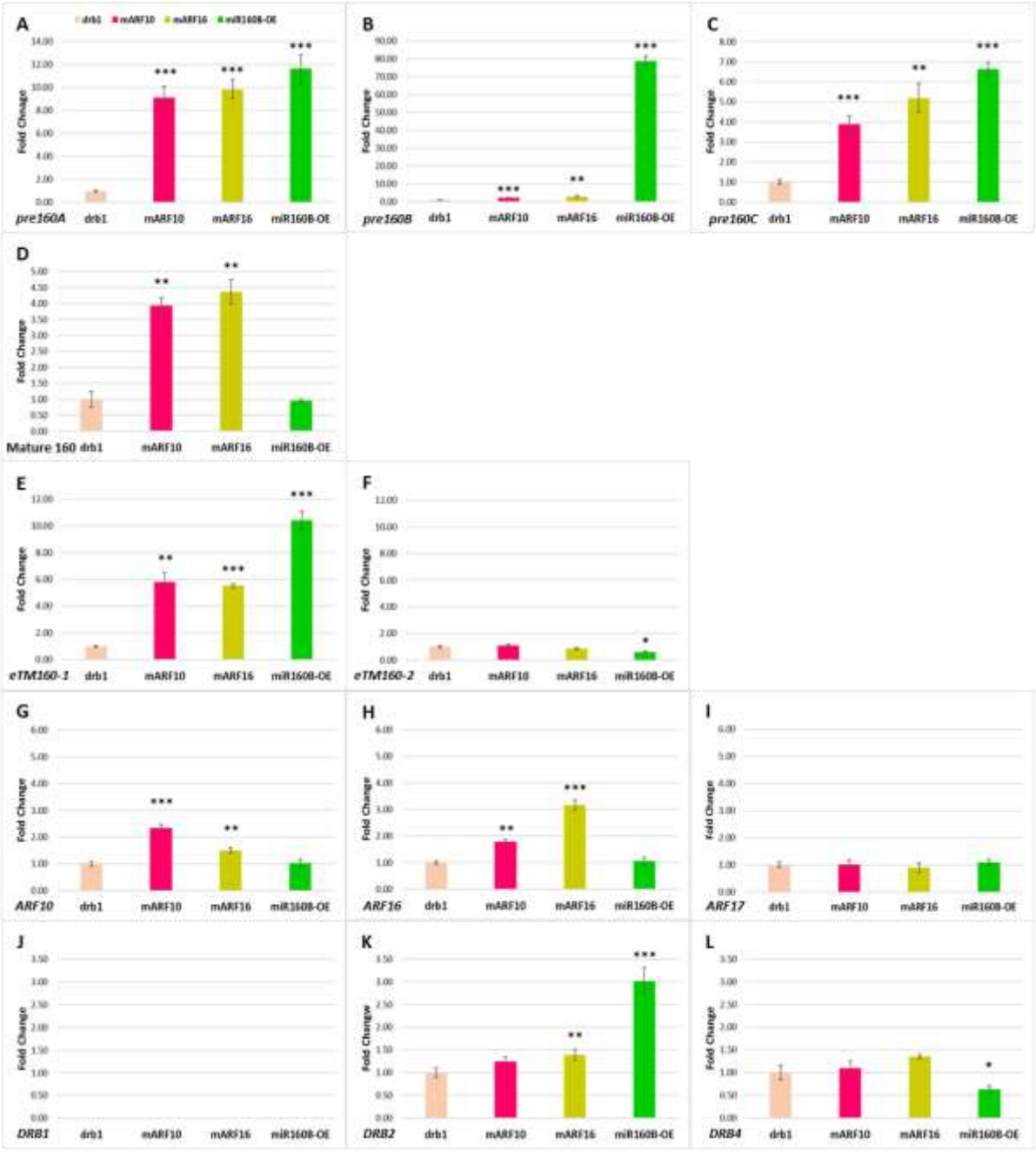

Figure 5.9. RT-qPCR analysis of the miR160/*ARF10*/*ARF16*/*ARF17* expression module in root tissue of *drb1*, *drb1*/m*ARF10*, *drb1*/m*ARF16* expression, and *drb1*/*MIR160B* genetic backgrounds. Analysed in root tissue of *drb1* (orange), *drb1*/m*ARF10* (pink), *drb1*/m*ARF16* (yellow), and *drb1*/*MIR160B* (green) transformant lines were *PRI-MIR160A/B/C* precursor genes (A,B, and C), *eTM160-1* and *eTM160-2* miR160 endogenous target mimic (E and F), *ARF10/16/17* miR160 target genes (G, H, and I), and *DRB1* (J), *DRB2* (K), and *DRB4* (L) expression, and STL-qPCR analysis of miR160 accumulation (D). Fold changes were determined by the ΔΔCt method, with three biological replicates, and normalised to *drb1*. Averages of expression fold change in the transformant lines were compared to *drb1* by a standard two-tailed t-test. Error bars represent SEM. *** $p \leq 0.001$, ** $p \leq 0.01$, * $p \leq 0.05$.

Expression of m*ARF10*, m*ARF16*, and *MIR160B* transgenes in the *drb1* background caused different molecular changes compared to expression of these same transgenes in Col-0 plants. Increased accumulation of all three miR160 precursor transcripts was observed in each *drb1* transformant line (**Figure 5.9A-C**), with the most dramatic increase in *PRI-MIR160B* expression observed in *drb1*/*MIR160B* plants, a finding that shows that this precursor transcripts significantly over-accumulates in the absence of DRB1 activity. However, mature miR160 abundance increased in both the *drb1*/m*ARF10* and *drb1*/m*ARF16* transformant lines, while no change in miR160 abundance was observed in *drb1*/*MIR160B* plants (**Figure 5.9D**). Taken together, quantification of precursor transcript expression and miR160 abundance across *drb1*/m*ARF10*, *drb1*/m*ARF16*, and *drb1*/*MIR160B* plants, strongly suggests that in the absence of DRB1 activity, miR160 regulates ARF10 and ARF16 transcript abundance via a translational repression mode of RNA silencing.

Only the endogenous target mimic, *eTM160-1*, showed dramatic changes in transcript abundance in the *drb1* background, with increases observed in all three transformant lines (**Figure 5.9E**). Previous molecular examinations (**Chapter 4**) indicated that in the absence of DRB1 and DRB4, *eTM160-1* may be acting as a target for miR160-directed translational repression, an argument further supported by these molecular analyses.

As in Col-0, *ARF10*, and *ARF16* expression increased in the *drb1*/m*ARF10* and *drb1*/m*ARF16* transformant lines, respectively, compared to unmodified *drb1* plants. In addition, *ARF10* and *ARF16* expression was also observed to increase in the reciprocal *drb1*/m*ARF16* and *drb1*/m*ARF10* transformant lines (**Figure 5.9G** and **H**). Considering that mature miR160 levels were elevated in both of these lines, the argument for miR160-directed translational repression of *ARF10* and *ARF16* in the absence of functional DRB1 is again further supported. Interestingly, *ARF17* expression remained unchanged in all three assessed *drb1* transformant lines (**Figure 5.9I**). This finding strongly indicated that the observed elevation in miR160 abundance in *drb1*/m*ARF10* and *drb1*/m*ARF16* plants was a direct response to elevated *ARF10* and *ARF16* abundance in these plants directing posttranscriptional gene silencing via translational repression. It also indicates that *ARF17* is not a target for miR160-directed translational repression in *Arabidopsis* roots.

The expression of *DRB2* was most significantly altered in *drb1*/*MIR160B* plants (**Figure 5.9J**), presumably in response to the similar significant increase in *PRI-MIR160* precursor transcript accumulation in this transformant line. Such a dramatic increase in *DBR2* expression also seemed to cause a small decrease in *DRB4* expression (**Figure 5.9L**), probably

a convergent effect facilitating DRB2-mediated processing of *PRI-MIR160* precursor transcripts. This finding again adds weight to the newly proposed role for DRB2 in the miRNA pathway in *Arabidopsis* roots, this role being that DRB2 is required for miR160 production and to mediate translational repression of *ARF10* and *ARF16* directed by miR160-directed RNA silencing.

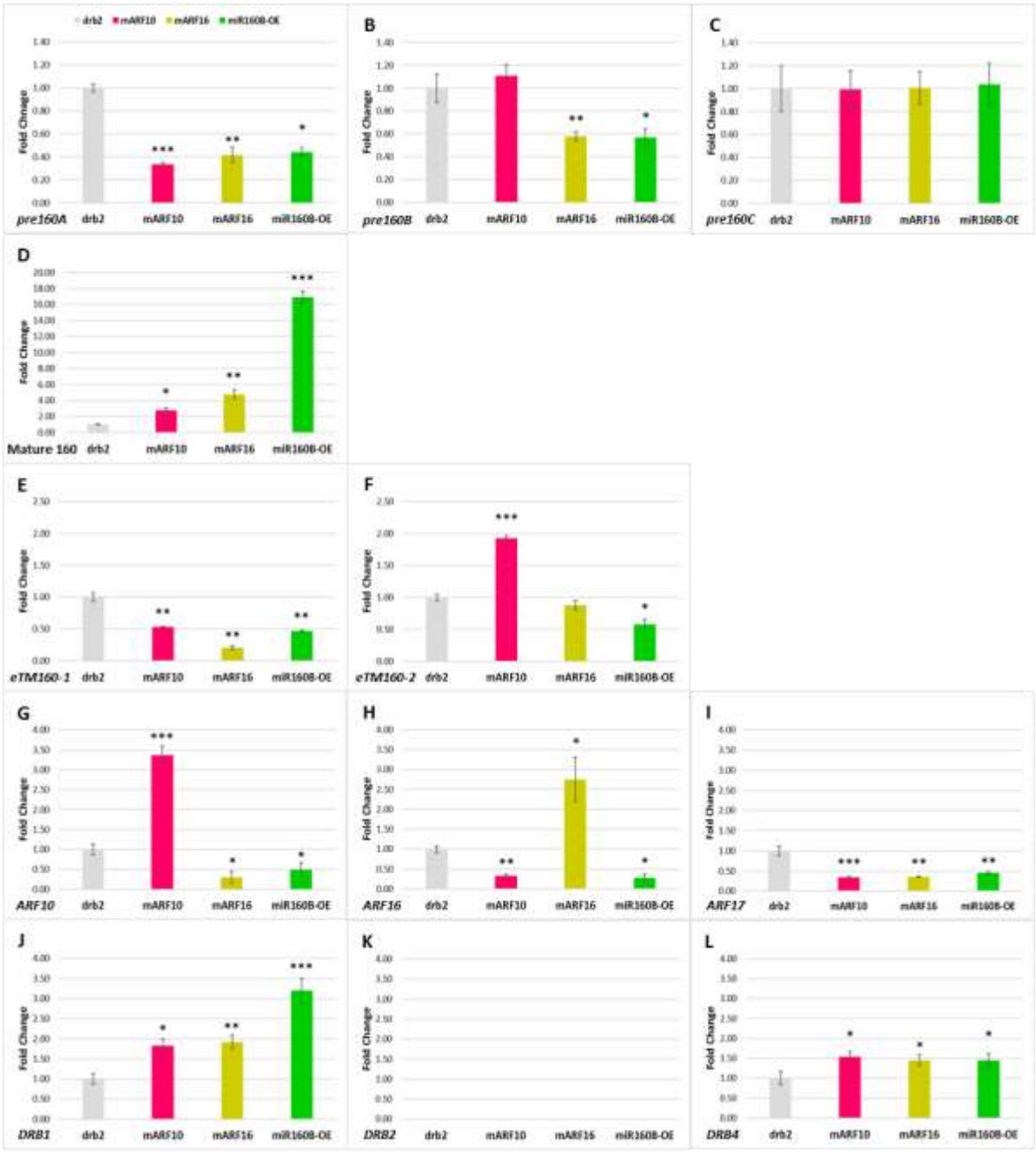

Figure 5.10. RT-qPCR analysis of the miR160/*ARF10*/*ARF16*/*ARF17* expression module in root tissue of *drb2*, *drb2*/m*ARF10*, *drb2*/m*ARF16* expression, and *drb2*/*MIR160B* genetic backgrounds. Analysed in root tissue of *drb2* (grey), *drb2*/m*ARF10* (pink), *drb2*/m*ARF16* (yellow), and *drb2*/*MIR160B* (green) transformant lines were *PRI-MIR160A/B/C* precursor genes (A,B, and C), *eTM160-1* and *eTM160-2* miR160 endogenous target mimic (E and F), *ARF10/16/17* miR160 target genes (G, H, and I), and *DRB1* (J), *DRB2* (K), and *DRB4* (L) expression, and STL-qPCR analysis of miR160 accumulation (D). Fold changes were determined by the ΔΔCt method, with three biological replicates, and normalised to *drb2*. Averages of expression fold change in the transformant lines were compared to *drb2* by a standard two-tailed t-test. Error bars represent SEM. *** $p \leq 0.001$, ** $p \leq 0.01$, * $p \leq 0.05$.

In *drb2* plants, expression of the m*ARF10*, m*ARF16*, and *MIR160B* transgenes also resulted in different molecular modifications to those seen in either the Col-0 or *drb1* backgrounds. *PRI-MIR160A* and *PRI-MIR160B* precursor transcripts showed decreased accumulation in all three transformant lines except for the *drb2*/m*ARF10* plant line, where *PRI-MIR160B* abundance did not change. Interestingly, compared to unmodified *drb2* plants, no change in *PRI-MIR160C* expression was observed in any of the three *drb2* lines where molecular modifications had been introduced to the miR160/*ARF10*/*ARF16*/*ARF17* expression module (**Figure 5.10A-C**). Observed decreases in *PRI-MIR160A* and *PRI-MIR160B* transcript abundance were presumably due to increased processing efficiency of these precursor transcripts by DRB1 in the absence of DRB2 antagonism, as evidenced by the enhanced accumulation of miR160 in *drb2*/m*ARF10*, *drb2*/m*ARF16*, and *drb2*/*MIR160B* plants (**Figure 5.10D**).

The expression of *eTM160-1* decreased in all three *drb2* transformant lines (**Figure 5.10E**), likely due to enhanced miR160-directed transcript cleavage, the only functional mechanism of miR160-directed posttranscriptional regulation active in the absence of DRB2. Surprisingly, *eTM160-2* expression significantly increased in *drb2*/m*ARF10* transformants (**Figure 5.10F**), possibly in response to increased processing efficiency of the *PRI-MIR160A* precursor transcript, and elevated miR160 abundance.

Again, *ARF10* and *ARF16* expression increased in *drb2/*m*ARF10* and *drb2*/m*ARF16* transformant lines, respectively (**Figure 5.10G** and **H**). Interestingly, in their reciprocal transformant lines, *drb2*/m*ARF16* and *drb2*/m*ARF10* plants, respectively, *ARF10* and *ARF16* expression decreased (**Figure 5.10G** and **H**). The observed reduction in *ARF* gene expression in these lines was likely due to transcript abundance being regulated via a mRNA cleavage mode of RNA silencing in the absence of DRB2 activity. Exclusive DRB1-mediated, miR160-directed mRNA cleavage also accounts for the observed reductions to *ARF10*, *ARF16*, and *ARF17* gene expression in the *drb2*/*MIR160B* transformant line (**Figure 5.10G-I**).

As in *drb1* plants, DRB1 expression in the absence of DRB2 increased in all three transformant lines (**Figure 5.10J** and **K**). In this case, however, *PRI-MIR160* precursor transcript processing was more efficient to accommodate potential increases in precursor expression. *DRB4* also showed small expression increases (**Figure 5.10L**), a result likely due to the absence of DRB2, reducing antagonism between DRB2 and DRB4. This result also supports the argument that DRB1 and DRB4 may cooperate in modifying the sRNA environment controlling aspects of *Arabidopsis* root architecture.

5.3 Discussion

5.3.1 Manipulating miR160-directed posttranscriptional regulation affects *Arabidopsis* root development

The impact of disrupted sRNA production and transcript targeting is a well-documented phenomenon, particularly in lateral and adventitious root development (Couzigou and Combier 2016; Gifford et al. 2008; Gutierrez et al. 2009; Mallory et al. 2005; Rademacher et al. 2011; Wang et al. 2005). In this study, the introduction of m*ARF10*, m*ARF16*, and *MIR160B* transgenes also induced significant modifications in primary, lateral, and adventitious root development, with the phenotypic consequences of *in planta* expression of these three transgenes extending into aerial tissues.

Observation of an altered primary root morphology was most pronounced in Col-0 plants harbouring the m*ARF10*, m*ARF16*, and *MIR160B* transgenes (**Figure 5.5A**), as all three transformant lines showed a significant increase in primary root length. This was a surprising result, as decoupling *ARF10* and *ARF16* posttranscriptional regulation was expected to have the opposite phenotypic effect to the enhancement of miR160-directed *ARF* gene expression repression in Col-0/*MIR160B* plants. Even more curious was that molecular changes in these transformant lines were not uniform (**Figure 5.8**), despite the collective increase in primary root length.

In adventitious roots, a previous report indicates that *ARF6* and *ARF8* expression is negatively regulated by ARF17 activity (Gutierrez et al. 2009). While no direct relationship between *ARF6* and *ARF8* was observed for either *ARF10* or *ARF16*, phenotypic consequences of modified *ARF10* and/or *ARF16* expression were observed in *ARF6/ARF8* regulated pathways (Gutierrez et al. 2009). The negative regulation of *ARF6/ARF8* by ARF17 was only observed in adventitious roots. However, *ARF6* has high expression in the cells of the root tip, where it has been shown to function redundantly with ARF5 in regulating primary root development (Rademacher et al. 2011). Therefore, the potential exists for regulation of *ARF6* by ARF10 and/or ARF16 in the primary root tip, leading to the observed root phenotypic changes in transformant lines with higher *ARF10* and *ARF16* expression.

ARF10 and ARF16 both regulate expression of *WOX* genes controlling stem cell population maintenance in the quiescent centre of the root tip, independent of ARF5 or ARF6 (Ding and Friml 2010). In plants overproducing miR160, the observed phenotypic consequences to primary root development were, therefore, unsurprising. The largely

unchanged primary root phenotypes when the m*ARF10* and m*ARF16* transgenes were expressed in either the *drb1* or *drb2* mutant lines suggests that both DRB1 and DRB2 are required for maintaining the sRNA environment, including miR160, necessary for normal primary root development.

Lateral root phenotypic changes were observed in the Col-0, *drb1*, and *drb2* transformant lines expressing the m*ARF10*, m*ARF16*, and *MIR160B* transgenes. In the Col-0 background, this appeared to be a direct relationship, as lateral root number only increased in Col-0/*MIR160B* plants (**Figure 5.5B**). In this transformant line, miR160 abundance increased dramatically (**Figure 5.8D**), while the expression of *ARF17*, a known negative regulator of lateral root development (Couzigou and Combier 2016; Mallory et al. 2005; Wang et al. 2005), decreased (**Figure 5.8I**).

All three *drb1* transformant lines showed increased lateral root number (**Figure 5.6B**), a significant observation considering that unmodified *drb1* plants have a reduced number of lateral roots (**Figure 3.5B**). Even though ARF10 and ARF16 play opposing roles in lateral root initiation (Wang et al. 2005), they both promote lateral root growth after lateral root initials have emerged through the root epidermis (Roychoudhry et al. 2013). Considering that *ARF10* and *ARF16* expression increased in their reciprocal *drb1*/m*ARF16* and *drb1*/m*ARF10* transformant lines (**Figure 5.9G** and **H**), it is apparent that both the m*ARF10* and m*ARF16* transgenes can rescue the deleterious effects of disrupted DRB1 function on lateral root development. However, lateral root number also increased in *drb2*/m*ARF10* and *drb2*/m*ARF16* plants (**Figure 5.7B**), plant lines with reduced *ARF16* and *ARF10* expression, respectively (**Figure 5.10G** and **H**). Taken together, these results suggest that ARF10 and ARF16 can promote lateral root development independent of each other.

Expression of the *PRI-MIR160B* encoding transgene also resulted in an increase in lateral root number in *drb1*/*MIR160B* plants (**Figure 5.6B**). In this transformant line, *ARF10*, *ARF16*, and *ARF17* expression all remain unchanged compared to their respective expression in unmodified *drb1* plants (**Figure 5.9G-I**), an expected result considering that mature miR160 abundance also remained unchanged (**Figure 5.9D**), presumably due to increased sequestration of miR160 by *eTM160-1* (**Figure 5.9E**). Further, as miR160 abundance has scaled to *ARF10*, *ARF16*, and *ARF17* transcript abundance, translational repression of any of these miR160 target transcripts could contribute to modified ARF activity resulting in the proliferation of lateral roots.

As with lateral roots, adventitious rooting in the Col-0 background appears to be directly proportional to miR160 abundance as an increase in adventitious root number was only observed in Col-0/*MIR160B* plants (**Figure 5.5C**). This transformant line also showed a reduction in *ARF17* expression (**Figure 5.8I**), a known repressor of adventitious root formation (Couzigou and Combier 2016; Gutierrez et al. 2009; Mallory et al. 2005). It is, therefore, likely that adventitious root number increased in this plant line as a result of decreased *ARF17* expression due to enhanced miR160-directed posttranscriptional regulation via mRNA transcript cleavage.

Adventitious rooting also increased in *drb1*/m*ARF10* plants transgene (**Figure 5.6C**). Considering that *ARF17* showed no change in expression in this transformant line, the potential for ARF16 to act as a negative regulator of *ARF6* and/or *ARF8* expression is again presented. In *drb1*/m*ARF10* plants, *ARF16* expression increased (**Figure 5.9H**), apparently counterintuitive to this proposed role in *ARF6/ARF8* expression regulation. However, miR160 abundance also increased in *drb1*/m*ARF10* plants, indicating an increase in posttranscriptional regulation via translational repression (**Figure 5.6D**), supported by a similar increase in *eTM160-1* expression (**Figure 5.6E**), providing further evidence that *eTM160-1* acts as a sequestration target for miR160-directed expression regulation. Taken together, this evidence points towards a decrease in ARF16 activity potentially causing an increase in ARF6 and/or ARF8 activity, known promoters of adventitious root growth and development (Gutierrez et al. 2009).

In *drb2*/m*ARF10* plants, an increase in adventitious root number was also observed. However, no change in adventitious rooting was observed in either *drb2*/m*ARF16* or *drb2*/*MIR160B* plants (**Figure 5.7C**). Further, *ARF16* and *ARF17* expression was reduced in *drb2*/m*ARF10* plants (**Figure 5.10H**), an expression profile that was readily accounted for by the elevated abundance of miR160 (**Figure 5.10D**). Given the proposed role for ARF16, and the confirmed role for ARF17 (Couzigou and Combier 2016; Gutierrez et al. 2009), in negatively regulating the activity of ARF6 and/or ARF8, it is unsurprising that an increase in adventitious root formation was observed in *drb2*/m*ARF10*.

In summary, when DRB1 is functional (Col-0 and *drb2* plants), increased repression of *ARF17* expression by miR160-directed target transcript cleavage directly promotes an increase in lateral and adventitious root growth and development. *ARF10* and *ARF16* are also targeted by this mechanism, leading to increased primary root growth. However, only *ARF10* and *ARF16* appear to be posttranscriptionally regulated by miR160-directed translational

repression in primary and lateral roots. Additionally, evidence has been presented suggesting a novel role for ARF16 negatively regulating, most likely, ARF6 function, in both primary and adventitious roots.

5.3.2 DRB2-mediated production of miR160 likely directs translational repression adding to the regulation of *ARF* target gene expression

Phenotypic changes in root architecture induced by introduction of the m*ARF10*, m*ARF16*, and *MIR160B* transgenes into the *drb1* mutant background clearly revealed that miR160 production can be directed by DRB proteins other than DRB1. DRB2 is known to process miRNA precursor transcripts to produce mature miRNAs (Eamens et al. 2012a). Specific examples of this exist in the literature, as miR164 and miR168 have been shown to be overproduced, and miR169 to be produced less efficiently in plants deficient in DRB2 activity (Eamens et al. 2012a). This demonstrates that DRB1 and DRB2 compete for access to the miR164 and miR168 precursor transcripts, while showing in parallel that DRB2 is also required for miR169 precursor transcript processing.

Regarding miR160, a clear hierarchy in transcript preference for processing by either DRB1 or DRB2 is evident. When both DRB1 and DRB2 are functional, in Col-0 roots, miR160 abundance increased significantly when the *PRI-MIR160B* precursor transcript was overexpressed (**Figure 5.8D**). Examination of *PRI-MIR160A*, *PRI-MIR160B*, and *PRI-MIR160C* precursor transcript abundance showed that DRB-mediated processing favours the most abundant precursor transcript, *PRI-MIR160B* in this instance (**Figure 5.8A-C**). There was also evidence for a positive expression regulatory relationship between each of the three *PRI-MIR160* precursors, as both *PRI-MIR160A* and *PRI-MIR160C* expression increased when only *PRI-MIR160B* was targeted for *in planta* overexpression. miR160 produced via this '*wild-type*' pathway regulated the expression of *ARF10*, *ARF16*, and *ARF17* via a mRNA cleavage mode of RNA silencing, as demonstrated by the observed decrease in target *ARF* expression (**Figure 5.8G-I**).

Decoupling *ARF10* expression from miR160-directed posttranscriptional regulation via expression of the m*ARF10* transgene resulted in the *PRI-MIR160A* and *PRI-MIR160B* precursor transcripts being more efficiently processed, as evidenced by increased miR160 accumulation (**Figure 5.8A**, **B**, and **D**). This provides direct molecular evidence that both *MIR160* gene expression, and the efficiency of *PRI-*/*PRE-MIR160* processing, respond to

fluctuations in the abundance of the miR160 *ARF* target transcripts. It also demonstrates that this response is possible by increasing DRB1- and/or DRB2-mediated processing efficiency, as neither *DRB1* nor *DRB2* expression changed in Col-0/m*ARF10*, Col-0/m*ARF16*, or Col-0/*MIR160B* plant lines (**Figure 5.8J** and **K**).

The requirement for DRB1 to process *PRI-MIR160* precursor transcripts was confirmed upon examination of precursor transcript abundance in all three transformant lines generated in the *drb1* background. However, mature miR160 abundance increased in *drb1*/m*ARF10* and *drb1*/m*ARF16* transformant lines even in the absence of functional DRB1 (**Figure 5.9D**). This exciting finding strongly indicated that another DRB protein must be able to mediate miR160 production in the absence of functional DRB1. DRB2 is the most likely candidate to facilitate *PRI-MIR160* precursor transcript processing in the absence of DRB1, as DRB2 has been shown previously to be able to act upon the same precursor transcripts as DRB1 (Eamens et al. 2012a), and that this study showed that *DRB2* expression increased in response to increased *PRI-MIR160B* precursor transcript expression (**Figure 5.9K**). DRB2 is known to mediate miRNA biogenesis leading to posttranscriptional regulation of target gene expression via a translational repression mode of RNA silencing rather than the 'traditional' mRNA cleavage mechanism (Reis et al. 2015). In the *drb1* background, miR160 abundance increased, presumably due to enhanced precursor transcript processing efficiency mediated by DRB2. Examination of *ARF10* and *ARF16* expression in the *drb1*/m*ARF10* and *drb1*/m*ARF16* transformant lines supports this conclusion, as *ARF10* and *ARF16* expression increased in their reciprocal m*ARF* transformant lines (**Figure 5.9G** and **H**), a pattern of expression indicative of posttranscriptional regulation via translational repression as miR160 abundance scaled to match target *ARF* gene expression.

The proposal that *ARF10* and *ARF16* are under posttranscriptional regulation via translational repression is supported by examination of their expression under the same molecular conditions but in the absence of functional DRB2. In *drb2* plants, *ARF10*, *ARF16*, and *ARF17* expression all decreased, except when either *ARF10* or *ARF16* was decoupled from miR160 posttranscriptional regulation in the *drb2*/m*ARF10* and *drb2*/m*ARF16* plant lines (**Figure 5.10G-I**). These observed decreases in expression all confirm that miR160 directs posttranscriptional regulation via mRNA transcript cleavage when DRB1 is functional. The observed increase in *DRB1* expression in *drb2*/m*ARF10*, *drb2*/m*ARF16*, or *drb2*/*MIR160B* plant lines also suggests that *DRB1* expression responds to increased *PRI-MIR160* precursor and *ARF* transcript levels (**Figure 5.10J**). The intermediate expression of *ARF10* and *ARF16*

transcripts in Col-0 plants, coupled with the observation of *ARF10* and *ARF16* expression increases along with miR160 abundance in *drb1* plants, and the decrease in expression in *drb2* plants, is highly indicative that *ARF10* and *ARF16* are under posttranscriptional regulation directed by both mRNA transcript cleavage and translational repression, requiring both DRB1 and DRB2, respectively.

In the miR160/*ARF10*/*ARF16*/*ARF17* expression module, there is an additional molecular mechanism to consider. *Endogenous target mimics* (*eTM*s) were previously identified for miR160 and have been demonstrated to relieve miR160-directed posttranscriptional regulation of *ARF10*, *ARF16*, and *ARF17* (Wu et al. 2013). Further, overexpression of *eTM160-1* can rescue the abnormal phenotype of *PRI-MIR160C* overexpression in *Arabidopsis* (Wu et al. 2013). Examination of *eTM160-2* showed little change in expression in any of the three transformant lines in either the Col-0 or *drb1* backgrounds (**Figure 5.8F** and **5.8F**). However, *eTM160-1* expression dramatically increased in Col-0/m*ARF16*, Col-0/*MIR160B*, *drb1*/m*ARF10*, *drb1*/m*ARF16*, and *drb1*/*MIR160B* plant lines, particularly in response to increased *PRI-MIR160* precursor transcript abundance (**Figure 5.8E** and **5.8E**).

Opposing expression responses of *eTM160-1* and *eTM160-2* when DRB2 is functional suggests that *eTM160-1* acts as a miR160 sequestration target of translational repression when miR160 is produced through a DRB2 dependent pathway. Conversely, *eTM160-2* expression increased, while *eTM160-1* expression decreased, when miR160 was produced through only a DRB1 dependent pathway (**Figure 5.10E** and **F**), supporting the argument that *eTM160-1* acts as a sequester of miR160 directing translational repression, while suggesting that *eTM160-2* sequesters miR160 directing mRNA transcript cleavage. Secondary structural differences are suspected to exist between *eTM160-1* and *eTM160-2* (Wu et al. 2013), allowing the possibility that these differences in secondary structure determine the mechanism by which *eTM160*s sequester miR160. Overexpression of an *Oryza sativa* (rice) *eTM160* (*Osa-eTM160-3*) in *Arabidopsis* demonstrated a superior ability to release *ARF10*, *ARF16*, and *ARF17* from miR160-directed posttranscriptional regulation (Wu et al. 2013). This provides additional evidence to suggest that structural differences in *eTM160* transcripts affects whether they sequester miR160 acting as targets for mRNA transcript cleavage or translational repression.

5.3.3 Conclusions

These findings confirm that DRB1-mediated production of miR160 leads to posttranscriptional regulation via mRNA transcript cleavage as previously reported (Mallory et al. 2005), while providing highly indicative evidence that DRB2 can process *PRI-MIR160* precursor transcripts resulting in miR160-directed translational repression. Moreover, that miR160-directed translational repression could mediate RNA silencing of *ARF10* and *ARF16* expression, but not *ARF17*, throughout the root in the absence of DRB1. Molecular examination of *eTM160-1* and *eTM160-2* expression led to the proposal that *eTM160-1* sequesters miR160 via translational repression, while *eTM160-2* does so acting as a target for mRNA transcript cleavage.

It was apparent from molecular examinations made in Col-0, *drb1*, *drb2*, and *drb12* genetic backgrounds that the miR160/*ARF10*/*ARF16*/*ARF17* is not the only expression module affected by changes in the sRNA environment leading to changes in root architecture. However, phenotypic and molecular analyses presented in this chapter suggest that a close relationship between the miR160/*ARF10*/*ARF16*/*ARF17* and the miR167/*ARF6*/*ARF8* expression modules exists. There is also evidence which suggests that alternate posttranscriptional regulatory pathways, affecting the miR160/*ARF10*/*ARF16*/*ARF17* expression module, also affect the miR167/*ARF6*/*ARF8* expression module.

Chapter 6

General Discussion

6.1 Overview of sRNA-directed posttranscriptional regulation and auxin signalling in root development

Auxin regulates many different aspects of *Arabidopsis* root growth and development, including primary, lateral, and adventitious root architecture (Overvoorde et al., 2010). In these root tissues, auxin regulates development by controlling the expression of genes from the *AUXIN RESPONSE FACTOR* (*ARF*) and *AUXIN/INDOLE-3-ACETICE ACID* (*Aux/IAA*) gene families (Guilfoyle and Hagen 2007). Ultimately, controlled activation of ARF transcription factors, responding to increased local auxin concentrations, leads to the differential expression of *AUXIN RESPONSE GENE*s (*ARG*s) (Chapman and Estelle 2009), inducing cellular changes in root tissues.

Small RNA (sRNA)-directed posttranscriptional regulation of the expression of auxin pathway genes is also well documented (Hrtyan et al. 2015). sRNA production in *Arabidopsis* is mediated by functional partnerships formed between DICER-LIKE (DCL) endonucleases and DOUBLE-STRANDED RNA BINDING (DRB) proteins to process structurally distinct double-stranded RNA (dsRNA) precursors (Eamens et al. 2012a; Mallory and Vaucheret 2006; Pelissier et al. 2011; Rajagopalan et al. 2006). The DRB1/DCL1 functional partnership is required to facilitate the production of microRNAs (miRNAs) (Dong et al. 2008; Szarzynska et al. 2009), while the DRB4/DCL4 functional partnership is required for the production of a number of sub-classes of small-interfering RNA (siRNA), including the *trans*-acting siRNAs (tasiRNAs) (Rajagopalan et al. 2006; Zhang et al. 2010). DRB2 can form functional partnerships with either DCL1 or DCL4 and, as such, is involved in regulating the production of both miRNA and siRNA sRNA species (Eamens et al. 2012a; Eamens et al. 2012b; Pelissier et al. 2011).

Specific examples of auxin responsive, sRNA-regulated pathways have been examined in *Arabidopsis*. tasiRNA target genes *ARF2*, *ARF3*, and *ARF4*, have a demonstrated role in repressing lateral root formation and growth (Marin et al. 2010), while *ARF6* and *ARF8*, targets of miR167, are involved in adventitious root growth and development, and are also expressed in the root tip (Kinoshita et al. 2012; Rademacher et al. 2011). *ARF10*, *ARF16*, and *ARF17* are targets of miR160 and function in primary, lateral, and adventitious root growth and development (Gutierrez et al. 2009; Mallory et al. 2005; Wang et al. 2005). Each of these clades of closely phylogenetically related *ARF* genes are posttranscriptionally regulated by a single sRNA species, to form what is referred to as a unique expression module.

Expression modules provide an excellent opportunity to study the effects of both auxin- and sRNA-directed regulation of developmentally critical morphological processes. The miR160/*ARF10*/*ARF16*/*ARF17* expression module is known to occupy different molecular niches in primary, lateral, and adventitious roots. In primary roots, ARF10 and ARF16 have the strongest influence as they repress *WUSCHEL-RELATED HOMEOBOX 5* (*WOX5*) gene transcription in distal stem cells at the root tip (Ding and Friml 2010). Studies which examined the phenotypic consequences of reducing *ARF10* and *ARF16* expression, by increasing miR160-directed posttranscriptional silencing, showed that without ARF10 and ARF16 activity, primary roots lost the ability to sense gravity (Wang et al. 2005). *ARF10*, *ARF16*, and *ARF17* are all expressed in lateral roots (Mallory et al. 2005; Wang et al. 2005). Here, ARF10 facilitates the formation of local auxin maxima in lateral root initials, promoting lateral root formation (Wang et al. 2005). Conversely, ARF16 and ARF17 have been shown to repress lateral root formation (Couzigou and Combier 2016; Mallory et al. 2005; Wang et al. 2005). In later development, ARF10 and ARF16 control the gravitropic setpoint angle (GSA) in formed lateral roots (Roychoudhry et al. 2013), essentially acting as promoters of lateral root growth following lateral root emergence. Only ARF17 has an experimentally validated role in adventitious root development, negatively regulating ARF6 and ARF8 activity which are known promoters of adventitious root growth (Gutierrez et al. 2009).

Posttranscriptional regulation of *ARF10*, *ARF16*, and *ARF17* is elicited by miR160 (Mallory et al. 2005). Tighter control of this expression module is achieved by *endogenous target mimics* (*eTM*s), non-protein-coding RNAs that act by sequestering miR160 before it silences the expression of its targeted genes (Wu et al. 2013). Initially, all miR160 production was thought to be solely mediated by the DRB1/DCL1 functional partnership leading to the classic mode of posttranscriptional regulation via target mRNA transcript cleavage (Eamens et al. 2009). However, miRNA biogenesis mediated by DRB2 is thought to regulate the expression of target transcripts via translational repression, rather than the classic transcript cleavage mechanism of miRNA-directed expression repression in *Arabidopsis* (Reis et al. 2015). Alternative posttranscriptional regulatory mechanisms could, therefore, lead to differentially regulated expression of miRNA target genes, resulting in different molecular changes and, ultimately, developmental consequences in different tissue types.

6.2 DRB1- and DRB2-mediated production of miR160 regulating *ARF10*/*ARF16*/*ARF17* expression in root development

The overall objectives of this research study were to identify an appropriate auxin responsive expression module, and to characterise the phenotypic and molecular consequences of manipulating this expression module in *Arabidopsis* roots via several different experimental strategies. Ultimately, this deconstruction of an expression module was aimed to provide a greater understanding of the relationship between sRNA-directed posttranscriptional regulation and auxin signalling, as well as to further define the role of sRNA processing machinery in *Arabidopsis* root growth and development.

Bioinformatic analyses presented in this study confirmed that several auxin responsive expression modules are under sRNA-directed posttranscriptional regulation, namely; the miR160/*ARF10*/*ARF16*/*ARF17*, miR167/*ARF6*/*ARF8*, and tasiRNA/*ARF3*/*ARF4* expression modules. The posttranscriptional regulation of each of these expression modules by distinct sRNA species has been demonstrated previously (Kinoshita et al. 2012; Mallory et al. 2005; Williams et al. 2005). Further, the role of the sRNA precursor processing protein DRB1, has been reported for both miR160 and miR167 (Eamens et al. 2009), while DRB4 is involved in tasiRNA production (Nakazawa et al. 2007). However, the sRNA sequence mapping analysis conducted in this study identified a potentially novel role for DRB2 in possibly processing the precursor transcripts for both the miR160 and miR167 sRNAs in *Arabidopsis*. The ability for DRB2 to mediate miRNA production was previously known, as miR164, miR168, and miR169 abundance, and target gene expression, have all been shown to be modified in mutant backgrounds deficient in DRB2 function (Eamens et al. 2012a). Furthermore, this study also used semi-quantitative RT-PCR assessment of the abundance of the miR160 target genes, *ARF10*, *ARF16*, and *ARF17* along with the miR167 target genes, *ARF6* and *ARF8*, to demonstrate differential accumulation of these target gene transcripts in inflorescence tissue of mutant lines deficient in DRB1 and DRB2 activity. This result indicated that miR160 and/or miR167 production may be mediated by DRB2, acting either synergistically or antagonistically to the functional interaction between DRB1 with DCL1.

The miR160/*ARF10*/*ARF16*/*ARF17* expression module was selected for further analysis based on previously reported findings showing a significant role for this expression module in *Arabidopsis* root growth and development (Gutierrez et al. 2009; Mallory et al. 2005; Wang et al. 2005). Additionally, these earlier studies showed that molecular modifications

made to the miR160/*ARF10*/*ARF16*/*ARF17* expression module, by modifying *ARF* function through T-DNA insertional mutagenesis, or by overexpressing miR160 precursor transcripts, and/or via the expression of miR160-resistant versions of *ARF10*, *ARF16*, and *ARF17* transcripts (m*ARF*s), led to direct phenotypic consequences in *Arabidopsis* roots (Gutierrez et al. 2009; Mallory et al. 2005; Wang et al., 2005). These findings focused the subsequent research undertaken in this study to only the miR160/*ARF10*/*ARF16*/*ARF17* expression module in *Arabidopsis* roots.

Arabidopsis roots can, essentially, be classified with three broad structural categories, primary, lateral, and adventitious root structures. In the tip of the primary root, *ARF17* is not expressed (Mallory et al. 2005; Wang et al. 2005), while ARF10 and ARF16 regulate the maintenance of a population of undifferentiated stem cells in and near the quiescent centre (Ding and Friml 2010). Phenotypic examination of the consequences of manipulating the miR160/*ARF10*/*ARF16*/*ARF17* expression module in different *drb* mutant backgrounds showed that in the absence of DRB1 activity, in both *drb1* single mutants, and *drb12* and *drb14* double mutants, led to a decrease in primary root elongation. However, the absence of DRB2 activity led to an increase in primary root length, but not when in conjunction with the absence of either functional DRB1 or DRB4. From this basic phenotypic observation, it was surmised that increased *ARF10* and/or *ARF16* expression inhibited primary root length, a result that is counterintuitive to the documented role of ARF10 and ARF16 as promoters of primary root elongation. However, *ARF16* expression also increased in *drb2* roots. When m*ARF10* and m*ARF16* transgenes were expressed in *drb1* and *drb2* mutant backgrounds only the *drb2/*m*ARF10* plant line showed an increase in primary root length.

As there is preliminary evidence (**Chapter 4**) to suggest that *MIR160A/B/C* and *DRB* gene expression, particularly *DRB4* expression, is directly influenced by auxin, *drb1* and *drb2* mutant plants were expected to show a decreased sensitivity to auxin. However, this was not the case. The exogenous treatment of these plant lines with a synthetic auxin could not fully rescue the abnormal phenotypes displayed by the individual *drb* mutant plant lines assessed in this experiment, although when DRB1 and DRB2 were both non-functional, phenotypic and molecular sensitivity to auxin treatment was reduced. This suggests that functional DRB1 and DRB2 are required in the root tip, mediating miR160 production and subsequent miR160-directed targeting of the *ARF10* and *ARF16* transcripts for normal primary root development. The main findings of this study on how the miR160/*ARF10*/*ARF16*/*ARF17* expression module influences primary root growth and development is graphically illustrated in **Figure 6.1**.

Further, it suggests that the phenotypic consequences of manipulating DRB1 and DRB2 function cannot be wholly explained by regarding only the miR160/*ARF10*/*ARF16*/*ARF17* expression module.

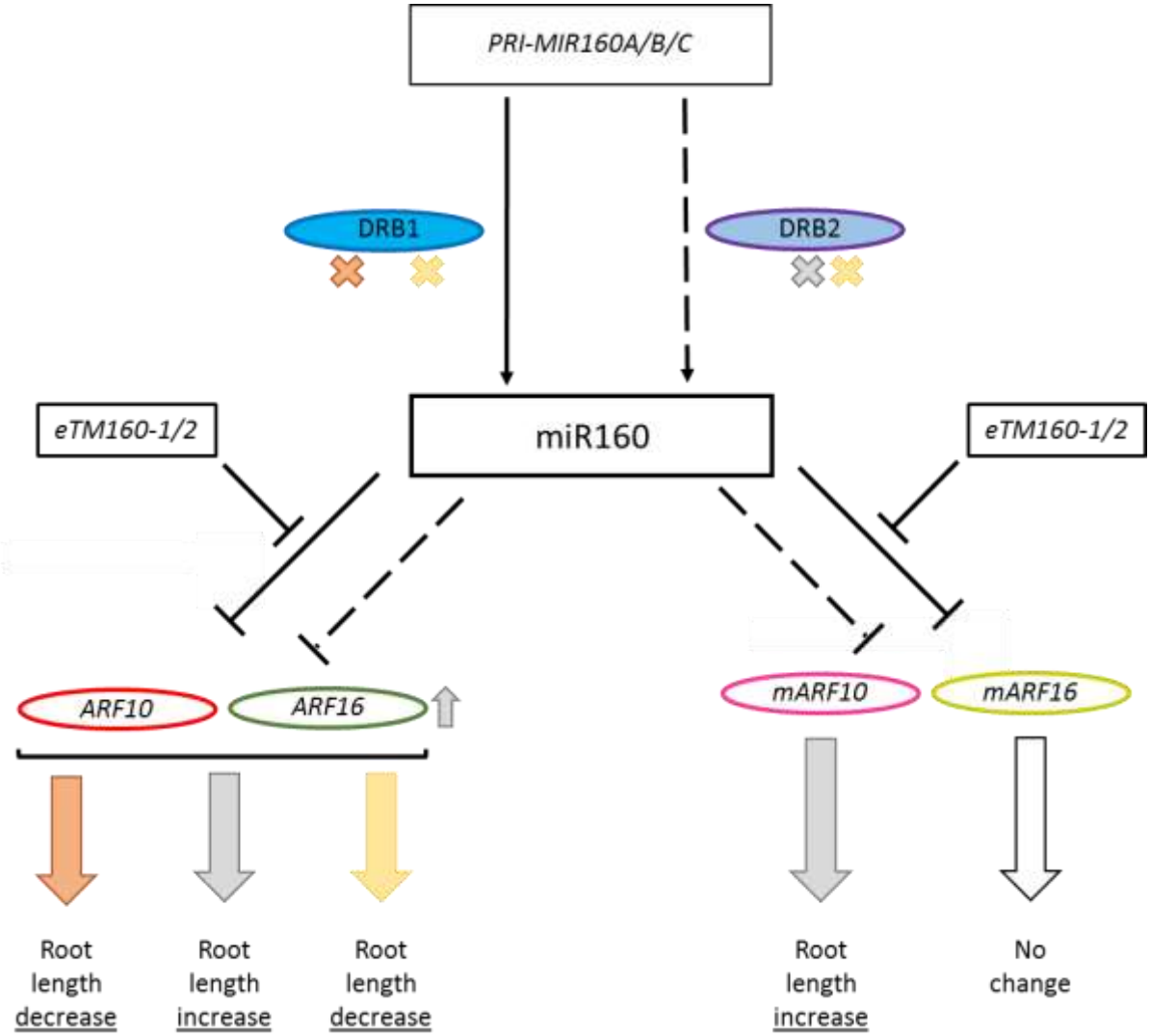

Figure 6.1. Summary schematic illustrating the main effects of manipulating the miR160/*ARF10*/*ARF16*/*ARF17* expression module on primary root development. miR160 precursor structures, transcribed from *PRI-MIR160A*/*B*/*C*, are processed into mature miR160 by either DRB1 (blue) or DRB2 (purple) directing posttranscriptional silencing by either transcript cleavage (solid arrow) or translational repression (broken arrow), respectively. *drb1* (orange cross), *drb2* (grey cross), and *drb12* (yellow cross) knockout mutant lines were used to assess the phenotypic consequences of miR160/*ARF10*/*ARF16*/*ARF17* expression module manipulation. Prior to *ARF10* (red ellipse) and/or *ARF16* (green ellipse) miR160-directed posttranscriptional silencing, *eTM160-1* and/or *eTM160-2* may sequester miR160 enabling finer control of *ARF10* and *ARF16* expression. In the primary root tip only *ARF16* expression increased in *drb2* (upwards grey arrow) plants. Primary root length decreased in *drb1* (downwards orange arrow) and *drb12* (downwards yellow arrow) plants, whilst primary root length increased in *drb2* (downwards grey arrow) and *drb2*/*mARF10* (downwards grey arrow) plants.

ARF10, *ARF16*, and *ARF17* are all expressed in *Arabidopsis* lateral roots (Mallory et al. 2005; Wang et al. 2005). *ARF10* is expressed in lateral root primordial cells as part of a molecular network defining the cell specific locations of auxin maxima within the pericycle (Wang et al. 2005). Conversely, ARF16 and ARF17 are known repressors of the formation of lateral root primordia (Mallory et al. 2005; Wang et al. 2005). Later in lateral root growth, ARF10 and ARF16 mediate the antigravitropic response, determining gravitropic setpoint angle (Roychoudhry et al. 2013), essentially acting as promoters of lateral root growth following lateral root initiation. Lateral root number also decreased in the *drb1*, *drb12*, and *drb14* mutant backgrounds, while lateral number increased in the *drb2*, *drb4*, and *drb24* mutants. As *ARF16* and *ARF17* expression also increased in DRB1 deficient backgrounds, but not in DRB2 deficient backgrounds, it suggests that repression of lateral root formation is dominant over promotion of lateral root formation by ARF10. More evidence for this exists, as overexpression of the *PRI-MIR160B* precursor transcript dramatically increased lateral root number in both wild-type and *drb1* genetic backgrounds, with a simultaneous decrease in *ARF16* and *ARF17* expression.

Considering the roles of ARF10, ARF16, and ARF17 in lateral root development, it is unsurprising that ARF10 influences lateral root formation to a lesser extent. Any expression change in *ARF10* would likely lead to negative phenotypic consequences in lateral root formation, as local auxin concentration is a highly sensitive signal for lateral primordia formation (Parry et al. 2009). Indeed, exogenous auxin treatment significantly increased the number of lateral roots at lower concentrations of wild-type, *drb1*, and *drb2* plants, but, the *drb12* mutant yet again, proved insensitive to auxin. However, when m*ARF10* transgenes were expressed in the *drb1* genetic background, the deleterious lateral root phenotype was able to be partially rescued, indicating that when *ARF10* expression is upregulated compared to *ARF16* and *ARF17* expression, the repression resulting from ARF16 and ARF17 activity can be overcome. This highlights the requirement of both DRB1 and DRB2 contributing to homeostatic maintenance of the sRNA environment in lateral roots. The main findings of this study on how the miR160/*ARF10*/*ARF16*/*ARF17* expression module influences lateral root growth and development is graphically illustrated in **Figure 6.2**.

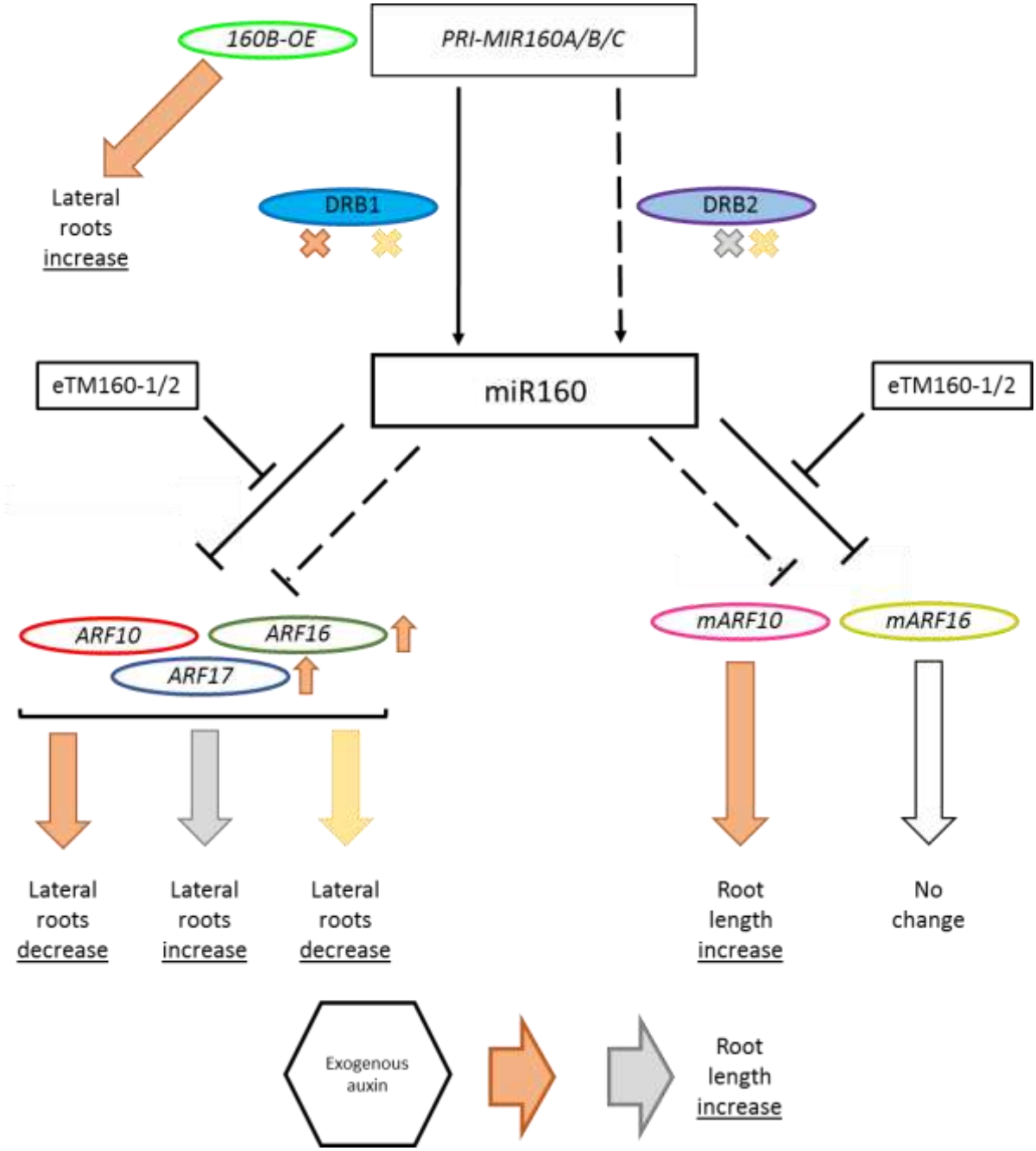

Figure 6.2. Summary schematic illustrating the main effects of manipulating the miR160/*ARF10*/*ARF16*/*ARF17* expression module on lateral root development. miR160 precursor structures, transcribed from *PRI-MIR160A*/*B*/*C*, are processed into mature miR160 by either DRB1 (blue) or DRB2 (purple) directing posttranscriptional silencing by either transcript cleavage (solid arrow) or translational repression (broken arrow), respectively. *drb1* (orange cross), *drb2* (grey cross), and *drb12* (yellow cross) knockout mutant lines were used to assess the phenotypic consequences of miR160/*ARF10*/*ARF16*/*ARF17* expression module manipulation. Prior to *ARF10* (red ellipse), *ARF16* (dark green ellipse), and/or *ARF17* (blue ellipse) miR160-directed posttranscriptional silencing, *eTM160-1* and/or *eTM160-2* may sequester miR160 enabling finer control of *ARF10*, *ARF16*, and *ARF17* expression. In lateral roots *ARF16* and *ARF17* expression increased in *drb1* (upwards orange arrows) plants. Lateral root number decreased in *drb1* (downwards orange arrow) and *drb12* (downwards yellow arrow) plants, whilst lateral root number increased in *drb2* (downwards grey arrow), *drb1*/*mARF10* (downwards orange arrow) and *drb1*/*PRI-MIR160B-OE* (diagonal downwards orange arrow) plants. Exogenous auxin treatment of *drb1* (sideways orange arrow) and *drb2* (sideways grey arrow) plants also resulted in increased lateral root number.

Only ARF17 is known to directly repress the formation of adventitious roots, by repressing ARF6 and ARF8 activity, themselves promoters of adventitious root growth (Gutierrez et al. 2009). However, mutant lines harbouring the *drb1* mutation showed an increase in adventitious root growth and development, and also showed increased *ARF17* expression. Further, exogenous auxin treatments did not alter this phenotype in the *drb1* single mutant. However, in *drb2* and *drb12* plants treated with 1.0 µM 2,4-D, adventitious rooting increased, although unexposed mutant lines harbouring the *drb2* mutation did not show large changes in adventitious rooting. This suggests that antagonism between DRB1 and DRB2, mediating miR160 production, is also required to maintain the sRNA environment in *Arabidopsis* adventitious roots. *ARF10* and *ARF16* both showed increased expression in their reciprocal m*ARF* transformant lines in the *drb1* background, supporting the conclusion that both DRB1 and DRB2 are required. The main findings of this study on how the miR160/*ARF10*/*ARF16*/*ARF17* expression module influences adventitious root growth and development is graphically illustrated in **Figure 6.3**. Although the absence of DRB1 would also disrupt the production of miR167, which in turn, would lead to increased *ARF6* and *ARF8* expression. Therefore, an additional normalising molecular mechanism must exist to account for the changes in *ARF17* expression in adventitious roots.

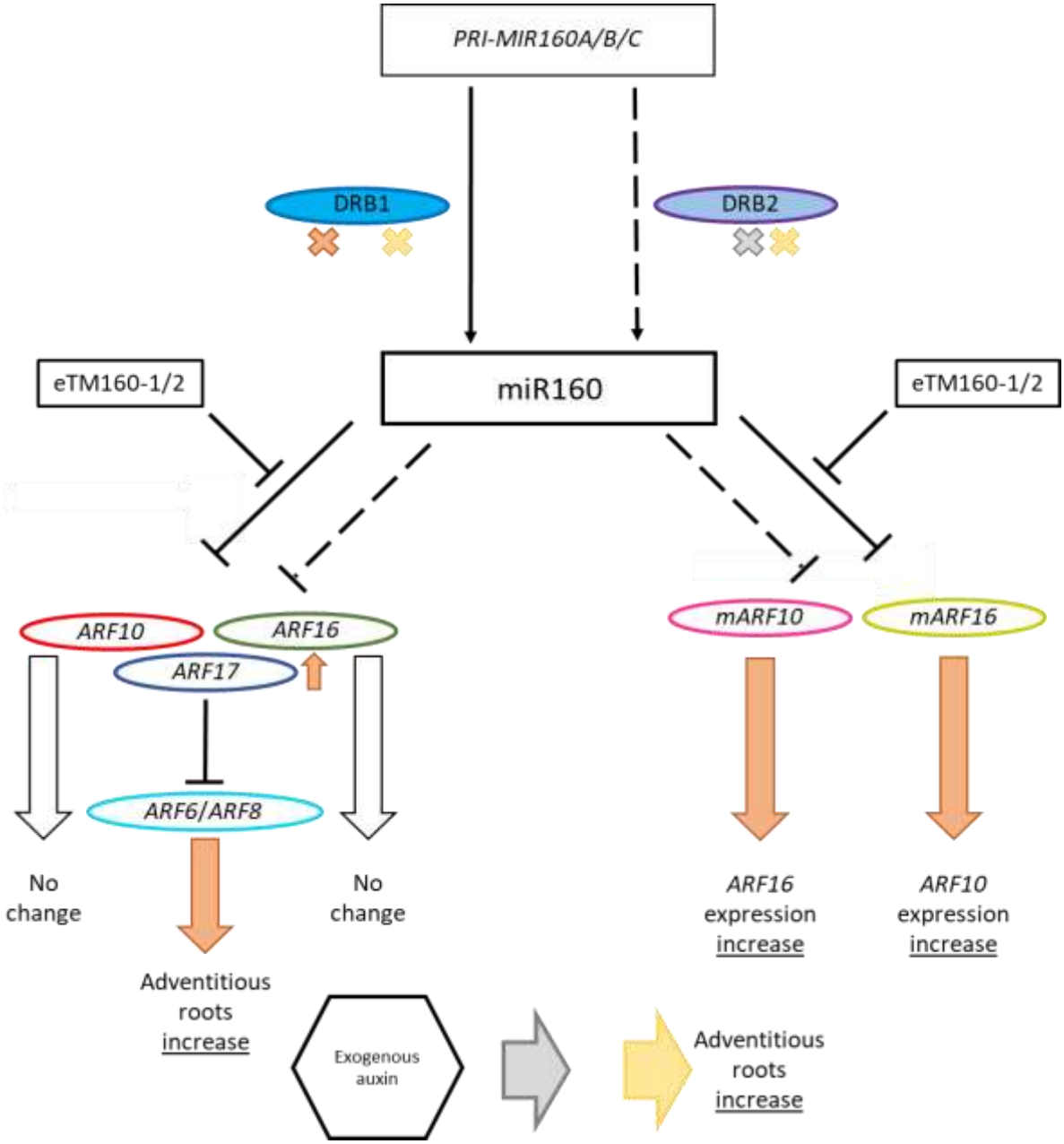

Figure 6.3. Summary schematic illustrating the main effects of manipulating the miR160/*ARF10*/*ARF16*/*ARF17* expression module on adventitious root development. miR160 precursor structures, transcribed from *PRI-MIR160A*/*B*/*C*, are processed into mature miR160 by either DRB1 (blue) or DRB2 (purple) directing posttranscriptional silencing by either transcript cleavage (solid arrow) or translational repression (broken arrow), respectively. *drb1* (orange cross), *drb2* (grey cross), and *drb12* (yellow cross) knockout mutant lines were used to assess the phenotypic consequences of miR160/*ARF10*/*ARF16*/*ARF17* expression module manipulation. Prior to *ARF10* (red ellipse), *ARF16* (green ellipse), and/or *ARF17* (blue ellipse) miR160-directed posttranscriptional silencing, *eTM160-1* and/or *eTM160-2* may sequester miR160 enabling finer control of *ARF10*, *ARF16*, and *ARF17* expression. In adventitious roots only *ARF17* expression increased in *drb1* (upwards orange arrows) plants. Adventitious root number also increased in *drb1* (downwards orange arrow) plants, most likely an indirect result on modified *ARF17* expression affecting *ARF6* and/or *ARF8* (cyan ellipse) expression. No effect on adventitious root number was observed in *mARF10* or *mARF16* plants. However, *ARF16* expression increased in *drb1*/*mARF10* (downwards orange arrow) and *ARF10* expression increased in *drb1*/*mARF16* (downwards orange arrow) plants. Exogenous auxin treatment of *drb2* (sideways grey arrow) and *drb12* (sideways yellow arrow) plants also resulted in increased adventitious root number.

Fluctuations in *PRI-MIR160* precursor transcript abundance, and miR160 accumulation, leading to changes in *ARF10*, *ARF16*, and *ARF17* expression, have been apparent throughout the experiments presented in this body of research. There also exists conflict with the established roles of this expression module and the phenotypes observed in the assessed *drb* mutant backgrounds. The apparent ability for DRB2 to process *PRI-MIR160* precursor transcripts increases the number of posttranscriptional regulatory mechanisms that miR160 may direct. miRNA precursor transcripts processed through a DRB2-dependent pathway are known to direct posttranscriptional regulation via translational repression rather than mRNA transcript cleavage (Reis et al. 2015).

For the miR160/*ARF10*/*ARF16*/*ARF17* expression module, this would mean that two competing posttranscriptional regulatory mechanisms would exist, allowing finer control of target gene expression and differentiating the roles of *ARF10*, *ARF16*, and *ARF17* in different *Arabidopsis* root tissue types. miR160 abundance scales with *ARF10* and *ARF16* expression, but not *ARF17*, in the absence of DRB1, an indication that miR160 is potentially directing the translational repression mechanism of posttranscriptional silencing of these two target transcripts. Further, the abundance of the *eTM160-1* transcript also scales in accordance with miR160 abundance when miR160 appears to be directing posttranscriptional silencing via translational repression. The existence of a specific regulator of miR160 in tissues where *ARF10* and *ARF16* are expressed provides further support for translational repression as a likely mechanism of posttranscriptional regulation. Translational repression would allow differential posttranscriptional regulation of *ARF10* and *ARF16* in primary, lateral, and adventitious roots, providing a pathway, whereby, apparently conflicting phenotypic consequences of molecularly manipulating the miR160/*ARF10*/*ARF16*/*ARF17* expression module may be resolved. The resemblance of the *drb12* phenotype to that of *drb1* plants does strongly indicate that DRB1-mediated production miRNAs that direct cleavage of their targeted transcripts, is the predominant silencing mechanism in *Arabidopsis* roots.

6.3 Future directions

While this program of research has expanded our understanding of the relationship between posttranscriptional regulation and auxin signalling, and the influence that this relationship has on root growth and development in *Arabidopsis*, it has also raised a number of further questions regarding the contribution of, and interaction between, individual miRNA/target gene expression modules in determining root developmental phenotypes. It has also not yet provided definitive, only indicative, evidence of DRB2-dependent, miR160-directed posttranscriptional silencing via translational repression.

Examination of the abundance of the ARF10 and ARF16 proteins is still required when miR160 is suspected to be directing translational repression to regulate the expression of its targeted genes in *Arabidopsis* roots. Only miR160 target gene assessment at the protein level will provide conclusive evidence as to whether or not, DRB2-dependent production of miR160 is directing the posttranscriptional silencing of *ARF10* and *ARF16* via translational repression in this tissue. Western blot hybridization analysis using polyclonal antibodies for ARF10 and ARF16 in root tissue of *drb* mutant backgrounds would provide insight into whether DRB2-mediated production of miR160 affects *ARF10* and *ARF16* translation.

For a comprehensive analysis of the effects of molecularly manipulating the miR160/*ARF10*/*ARF16*/*ARF17* expression module, phenotypic and molecular assessment of m*ARF* and *MIR160* overexpression transgenes in a range of *drb* mutant backgrounds need to be conducted. This study touched on such an assessment, by examining the phenotypic and molecular consequences of expressing the m*ARF10*, m*ARF16*, and *MIR160B* transgenes in Col-0, *drb1*, and *drb2* plants. However, for completeness, m*ARF17* expression, and *MIR160A* and *MIR160C* overexpression transgenes also need to be included in this assessment. Additionally, these transgenes could be expressed in the *drb4*, *drb12*, *drb14*, and *drb24* genetic backgrounds. Furthermore, the generation of *eTM160-1* and *eTM160-2* overexpression transgenes, and their introduction into the same suite of *drb* mutant backgrounds, would deepen our understanding of how these *eTM*s regulate miR160 levels in *Arabidopsis* roots.

Molecular analysis conducted in this study has focused on the whole root structure. However, the miR160/*ARF10*/*ARF16*/*ARF17* expression module has a variety of roles in different root tissue types. To aid the deconstruction of this expression module further it will be advantageous to assess the expression of the miR160/*ARF10*/*ARF16*/*ARF17* genes in specific root tissue types where they are active. Spatial analysis of *ARF10*, *ARF16*, and *ARF17*

expression, utilising GUS and GFP reporter systems, has already been conducted, identifying the specific cell populations where *ARF10*, *ARF16*, and *ARF17* are active. However, no such analysis has been performed in the suite of *drb* mutants assessed is this study. Performing similar spatial and temporal analysis of *ARF10*, *ARF16*, and *ARF17* expression in these *drb* mutant backgrounds, including m*ARF* and *MIR160* overexpression transgenes exogenous auxin treatments, could provide further insight into the exact role that ARF10, ARF16, and ARF17 are playing in the development of these root structures.

This study has also outlined the potential for a closely interlinked regulatory relationship between the miR160/*ARF10*/*ARF16*/*ARF17* and the miR167/*ARF6*/*ARF8* expression modules in primary and adventitious root development. Considering that *ARF6* and *ARF8* are also under posttranscriptional regulation directed by a miRNA, miR167, modifications in miRNA processing machinery present in the *drb* mutant backgrounds also influences the miR167/*ARF6*/*ARF8* expression module. Further, preliminary semi-quantitative RT-PCR analysis of *ARF6* and *ARF8* transcript abundance in *drb1*, *drb2*, and *drb12* inflorescence tissue, indicated a role for DRB2 in processing the *MIR167* precursor transcripts. The interconnected nature of this relationship cannot be ignored, therefore, similar molecular analyses to those presented here for the miR160/*ARF10*/*ARF16*/*ARF17* expression module should be performed for the miR167/ *ARF6*/*ARF8* expression module, to determine the extent of the molecular contribution of this expression module to the observed root phenotypes. If significant molecular changes were observed, then further deconstruction of the miR167/*ARF6*/*ARF8* expression module would be warranted. Generation of m*ARF6*, m*ARF8* and *MIR167* transgenes, and their expression in *drb* mutant backgrounds, would provide a comprehensive set of molecular analyses aimed to determine the role each of these expression modules makes to *Arabidopsis* root development. Such analyses would also enhance our understanding of the contributions made by DRB1 and DRB2 in controlling the sRNA environment governing root development in *Arabidopsis*.

6.4 Overall conclusions

The overall goal of this research thesis was to investigate the posttranscriptional regulatory pathways affecting miR160 production in *Arabidopsis* roots. The molecular consequences of altered posttranscriptional regulation by miR160 of auxin responsive target genes, *ARF10*, *ARF16*, and *ARF17*, and the resulting phenotypes, were of particular interest, as deconstructing such a complex regulatory module has broadened our understanding of these critical regulatory pathways in *Arabidopsis* development.

Taken together, the research described in this thesis confirms that *ARF10*, *ARF16*, and *ARF17* are under DRB1-dependent, miR160-directed posttranscriptional regulation via mRNA transcript cleavage in primary, lateral, and adventitious roots in *Arabidopsis*. Further, it provides highly indicative evidence that *ARF10* and *ARF16* are under additional posttranscriptional regulation via translational repression directed by miR160 produced through a DRB2-dependent biogenesis pathway, and that *eTM160-1* acts as a miR160 sequestration target in this alternate miR160-directed silencing pathway. It also provides preliminary evidence that a relationship between the miR160/*ARF10*/*ARF16*/*ARF17* and miR167/*ARF6*/*ARF8* expression modules is closer than previously thought, and further speculates that ARF16 may directly influence *ARF6*/ARF6 and/or *ARF8*/ARF8 expression/activity in primary and adventitious roots of *Arabidopsis*.

References

Abel S, Nguyen MD, Theologis A (1995) The PS-IAA4/5-LIKE family of early auxin-inducible mRNAs in *Arabidopsis thaliana*. *Journal of Moecular Biology* **251**:533-549.

Addo-Quaye C, Eshoo TW, Bartel DP, Axtell MJ (2008) Endogenous siRNA and miRNA targets identified by sequencing of the Arabidopsis degradome. *Current Biology* **18**:758-762.

Addo-Quaye C, Miller W, Axtell MJ (2009) CleaveLand: a pipeline for using degradome data to find cleaved small RNA targets. *Bioinformatics* **25**:130-131.

Adenot X, Elmayan T, Lauressergues D, Boutet S, Bouche N, Gasciolli V, Vaucheret H (2006) DRB4-dependent TAS3 trans-acting siRNAs control leaf morphology through AGO7. *Current Biology* **16**:927-932.

Aida M, Tasaka M (2006) Morphogenesis and patterning at the organ boundaries in the higher plant shoot apex. *Plant Molecular Biology* **60**:915-928.

Allen E, Xie Z, Gustafson AM, Carrington JC (2005) microRNA-directed phasing during trans-acting siRNA biogenesis in plants. *Cell* **121**:207-221.

Alonso JM, Stepanova AN, Leisse TJ, Kim CJ, Chen H, Shinn P, Stevenson DK, Zimmerman J, Barajas P, Cheuk R, Gadrinab C, Heller C, Jeske A, Koesema E, Meyers CC, Parker H, Prednis L, Ansari Y, Choy N, Deen H, Geralt M, Hazari N, Hom E, Karnes M, Mulholland C, Ndubaku R, Schmidt I, Guzman P, Aguilar-Henonin L, Schmid M, Weigel D, Carter DE, Marchand T, Risseeuw E, Brogden D, Zeko A, Crosby WL, Berry CC, Ecker JR (2003) Genome-wide insertional mutagenesis of *Arabidopsis thaliana*. *Science* **301**:653-657.

Arabidopsis Genome Initiative (2000) Analysis of the genome sequence of the flowering plant *Arabidopsis thaliana*. *Nature* **408**:796-815.

Axtell MJ (2013) Classification and comparison of small RNAs from plants. *Annual Review of Plant Biology* **64**:137-159.

Bainbridge K, Guyomarc'h S, Bayer E, Swarup R, Bennett M, Mandel T, Kuhlemeier C (2008) Auxin influx carriers stabilize phyllotactic patterning. *Genes & Development* **22**:810-823.

Baulcombe D (2004) RNA silencing in plants. *Nature* **431**:356-363.

Beauclair L, Yu A, Bouche N (2010) microRNA-directed cleavage and translational repression of the copper chaperone for superoxide dismutase mRNA in Arabidopsis. *Plant Journal* **62**:454-462.

Ben Amor B, Wirth S, Merchan F, Laporte P, d'Aubenton-Carafa Y, Hirsch J, Maizel A, Mallory AC, Lucas A, Deragon JM, Vaucheret H, Thermes C, Crespi M (2009) Novel long non-protein coding RNAs involved in Arabidopsis differentiation and stress responses. *Genome Research* **19**:57-69.

Bengough AG, McKenzie BM (1997) Sloughing of root cap cells decreases the frictional resistance to maize (*Zea mays* L.) root growth. *Journal of Experimental Botany* **48**:885-893.

Benjamins R, Quint A, Weijers D, Hooykaas P, Offringa R (2001) The PINOID protein kinase regulates organ development in Arabidopsis by enhancing polar auxin transport. *Development* **128**:4057-4067.

Bienvenut WV, Sumpton D, Martinez A, Lilla S, Espagne C, Meinnel T, Giglione C (2012) Comparative large scale characterization of plant versus mammal proteins reveals similar and idiosyncratic N-alpha-acetylation features. *Molecular Cell Proteomics* **11**:M111 015131.

Bishop CL (2003) JAW miRNAs regulate plant development. *Genome Biology* **4**:spotlight-20030820-20030802.

Boer DR, Freire-Rios A, van den Berg WA, Saaki T, Manfield IW, Kepinski S, Lopez-Vidrieo I, Franco-Zorrilla JM, de Vries SC, Solano R, Weijers D, Coll M (2014) Structural basis for DNA binding specificity by the auxin-dependent ARF transcription factors. *Cell* **156**:577-589.

Borsani O, Zhu J, Verslues PE, Sunkar R, Zhu JK (2005) Endogenous siRNAs derived from a pair of natural *cis*-antisense transcripts regulate salt tolerance in Arabidopsis. *Cell* **123**:1279-1291.

Bouguyon E, Gojon A, Nacry P (2012) Nitrate sensing and signaling in plants. *Seminars in Cell & Developmental Biology* **23**:648-654.

Bousios A, Gaut BS, Darzentas N (2017) Considerations and complications of mapping small RNA high-throughput data to transposable elements. *Mobile DNA* **8**:3.

Boutet S, Vazquez F, Liu J, Beclin C, Fagard M, Gratias A, Morel JB, Crete P, Chen X, Vaucheret H (2003) Arabidopsis HEN1: a genetic link between endogenous miRNA controlling development and siRNA controlling transgene silencing and virus resistance. *Current Biology* **13**:843-848.

Brand U, Fletcher JC, Hobe M, Meyerowitz EM, Simon R (2000) Dependence of stem cell fate in Arabidopsis on a feedback loop regulated by CLV3 activity. *Science* **289**:617-619.

Branscheid A, Marchais A, Schott G, Lange H, Gagliardi D, Andersen SU, Voinnet O, Brodersen P (2015) SKI2 mediates degradation of RISC 5'-cleavage fragments and prevents secondary siRNA production from miRNA targets in Arabidopsis. *Nucleic Acids Research* **43**:10975-10988.

Brodersen P, Sakvarelidze-Achard L, Bruun-Rasmussen M, Dunoyer P, Yamamoto YY, Sieburth L, Voinnet O (2008) Widespread translational inhibition by plant miRNAs and siRNAs. *Science* **320**:1185-1190.

Calderon-Villalobos LI, Tan X, Zheng N, Estelle M (2010) Auxin perception--structural insights. *Cold Spring Harbor Perspectives in Biology* **2**:a005546.

Carbonell A, Fahlgren N, Garcia-Ruiz H, Gilbert KB, Montgomery TA, Nguyen T, Cuperus JT, Carrington JC (2012) Functional analysis of three Arabidopsis ARGONAUTES using slicer-defective mutants. *Plant Cell* **24**:3613-3629.

Carrington JC, Ambros V (2003) Role of microRNAs in plant and animal development. *Science* **301**:336-338.

Casamitjana-Martinez E, Hofhuis HF, Xu J, Liu CM, Heidstra R, Scheres B (2003) Root-specific *CLE19* overexpression and the sol1/ 2 suppressors implicate a CLV-LIKE pathway in the control of Arabidopsis root meristem maintenance. *Current Biology* **13**:1435-1441.

Casimiro I, Marchant A, Bhalerao RP, Beeckman T, Dhooge S, Swarup R, Graham N, Inze D, Sandberg G, Casero PJ, Bennett M (2001) Auxin transport promotes Arabidopsis lateral root initiation. *Plant Cell* **13**:843-852.

Chapman EJ, Estelle M (2009) Mechanism of auxin-regulated gene expression in plants. *Annual Review of Genetics* **43**:265-285.

Chen JG, Shimomura S, Sitbon F, Sandberg G, Jones AM (2001) The role of auxin-binding protein 1 in the expansion of tobacco leaf cells. *Plant Journal* **28**:607-617.

Cho H, Ryu H, Rho S, Hill K, Smith S, Audenaert D, Park J, Han S, Beeckman T, Bennett MJ, Hwang D, De Smet I, Hwang I (2014) A secreted peptide acts on BIN2-mediated phosphorylation of ARFs to potentiate auxin response during lateral root development. *Nature Cell Biology* **16**:66-76.

Ckurshumova W, Krogan NT, Marcos D, Caragea AE, Berleth T (2012) Irrepressible, truncated auxin response factors: natural roles and applications in dissecting auxin gene regulation pathways. *Plant Signaling & Behavior* **7**:1027-1030.

Coutu C, Brandle J, Brown D, Brown K, Miki B, Simmonds J, Hegedus DD (2007) pORE: a modular binary vector series suited for both monocot and dicot plant transformation. *Transgenic Research* **16**:771-778.

Couzigou JM, Combier JP (2016) Plant microRNAs: key regulators of root architecture and biotic interactions. *New Phytologist* **212**:22-35.

Curtin SJ, Watson JM, Smith NA, Eamens AL, Blanchard CL, Waterhouse PM (2008) The roles of plant dsRNA-binding proteins in RNAi-like pathways. *FEBS Letters* **582**:2753-2760.

Davuluri RV, Sun H, Palaniswamy SK, Matthews N, Molina C, Kurtz M, Grotewold E (2003) AGRIS: Arabidopsis gene regulatory information server, an information resource of Arabidopsis cis-regulatory elements and transcription factors. *BMC Bioinformatics* **4**:25.

Dharmasiri N, Dharmasiri S, Weijers D, Lechner E, Yamada M, Hobbie L, Ehrismann JS, Jürgens G, Estelle M (2005) Plant development is regulated by a family of auxin receptor F box proteins. *Developmental Cell* **9**:109-119.

Dharmasiri S, Swarup R, Mockaitis K, Dharmasiri N, Singh SK, Kowalchyk M, Marchant A, Mills S, Sandberg G, Bennett MJ, Estelle M (2006) AXR4 is required for localization of the auxin influx facilitator AUX1. *Science* **312**:1218-1220.

Ding Z, Friml J (2010) Auxin regulates distal stem cell differentiation in Arabidopsis roots. *Proceedings of the National Academy of Sciences of the United States of America* **107**:12046-12051.

Dolan L, Janmaat K, Willemsen V, Linstead P, Poethig S, Roberts K, Scheres B (1993) Cellular organisation of the *Arabidopsis thaliana* root. *Development* **119**:71-84.

Dong Z, Han MH, Fedoroff N (2008) The RNA-binding proteins HYL1 and SE promote accurate in vitro processing of pri-miRNA by DCL1. *Proceedings of the National Academy of Sciences of the United States of America* **105**:9970-9975.

Eamens AL, Kim KW, Curtin SJ, Waterhouse PM (2012a) DRB2 is required for microRNA biogenesis in *Arabidopsis thaliana*. *PloS One* **7**:e35933.

Eamens AL, Smith NA, Curtin SJ, Wang MB, Waterhouse PM (2009) The *Arabidopsis thaliana* double-stranded RNA binding protein DRB1 directs guide strand selection from microRNA duplexes. *RNA* **15**:2219-2235.

Eamens AL, Wook Kim K, Waterhouse PM (2012b) DRB2, DRB3 and DRB5 function in a non-canonical microRNA pathway in *Arabidopsis thaliana*. *Plant Signaling & Behavior* **7**:1224-1229.

Ellis CM, Nagpal P, Young JC, Hagen G, Guilfoyle TJ, Reed JW (2005) AUXIN RESPONSE FACTOR1 and AUXIN RESPONSE FACTOR2 regulate senescence and floral organ abscission in *Arabidopsis thaliana*. *Development* **132**:4563-4574.

Engstrom EM (2012) HAM proteins promote organ indeterminacy: but how? *Plant Signaling & Behavior* **7**:227-234.

Fahlgren N, Montgomery TA, Howell MD, Allen E, Dvorak SK, Alexander AL, Carrington JC (2006) Regulation of AUXIN RESPONSE FACTOR3 by TAS3 ta-siRNA affects developmental timing and patterning in Arabidopsis. *Current Biology* **16**:939-944.

Fahlgren N, Sullivan CM, Kasschau KD, Chapman EJ, Cumbie JS, Montgomery TA, Gilbert SD, Dasenko M, Backman TW, Givan SA, Carrington JC (2009) Computational and analytical framework for small RNA profiling by high-throughput sequencing. *RNA* **15**:992-1002.

Fang Y, Spector DL (2007) Identification of nuclear dicing bodies containing proteins for microRNA biogenesis in living Arabidopsis plants. *Current Biology* **17**:818-823.

Fei Q, Xia R, Meyers BC (2013) Phased, secondary, small interfering RNAs in posttranscriptional regulatory networks. *Plant Cell* **25**:2400-2415.

Finet C, Fourquin C, Vinauger M, Berne-Dedieu A, Chambrier P, Paindavoine S, Scutt CP (2010) Parallel structural evolution of auxin response factors in the angiosperms. *Plant Journal* **63**:952-959.

Fletcher JC, Brand U, Running MP, Simon R, Meyerowitz EM (1999) Signaling of cell fate decisions by CLAVATA3 in Arabidopsis shoot meristems. *Science* **283**:1911-1914.

Friml J, Palme K (2002) Polar auxin transport - old questions and new concepts? *Plant Molecular Biology* **49**:273-284.

Galweiler L, Guan C, Muller A, Wisman E, Mendgen K, Yephremov A, Palme K (1998) Regulation of polar auxin transport by AtPIN1 in Arabidopsis vascular tissue. *Science* **282**:2226-2230.

Gao Y, Zhang Y, Zhang D, Dai X, Estelle M, Zhao Y (2015) Auxin binding protein 1 (ABP1) is not required for either auxin signaling or Arabidopsis development. *Proceedings of the National Academy of Sciences of the United States of America* **112**:2275-2280.

Ghanashyam C, Jain M (2009) Role of auxin-responsive genes in biotic stress responses. *Plant Signaling & Behavior* **4**:846-848.

Gifford ML, Dean A, Gutierrez RA, Coruzzi GM, Birnbaum KD (2008) Cell-specific nitrogen responses mediate developmental plasticity. *Proceedings of the National Academy of Sciences of the United States of America* **105**:803-808.

Gil P, Dewey E, Friml J, Zhao Y, Snowden KC, Putterill J, Palme K, Estelle M, Chory J (2001) BIG: a calossin-like protein required for polar auxin transport in Arabidopsis. *Genes & Development* **15**:1985-1997.

Gleave AP (1992) A versatile binary vector system with a T-DNA organisational structure conducive to efficient integration of cloned DNA into the plant genome. *Plant Molecular Biology* **20**:1203-1207.

Gojon A, Krouk G, Perrine-Walker F, Laugier E (2011) Nitrate transceptor(s) in plants. *Journal of Experimental Botany* **62**:2299-2308.

Goldsmith MH, Cataldo DA, Karn J, Brenneman T, Trip P (1974) The rapid non-polar transport of auxin in the phloem of intact Coleus plants. *Planta* **116**:301-317.

Gordon SP, Chickarmane VS, Ohno C, Meyerowitz EM (2009) Multiple feedback loops through cytokinin signaling control stem cell number within the Arabidopsis shoot meristem. *Proceedings of the National Academy of Sciences of the United States of America* **106**:16529-16534.

Gray WM, del Pozo JC, Walker L, Hobbie L, Risseeuw E, Banks T, Crosby WL, Yang M, Ma H, Estelle M (1999) Identification of an SCF ubiquitin-ligase complex required for auxin response in *Arabidopsis thaliana*. *Genes & Development* **13**:1678-1691.

Gray WM, Kepinski S, Rouse D, Leyser O, Estelle M (2001) Auxin regulates SCF(TIR1)-dependent degradation of AUX/IAA proteins. *Nature* **414**:271-276.

Gregory RI, Chendrimada TP, Cooch N, Shiekhattar R (2005) Human RISC couples microRNA biogenesis and posttranscriptional gene silencing. *Cell* **123**:631-640.

Guilfoyle TJ, Hagen G (2007) Auxin response factors. *Current Opinion in Plant Biology* **10**:453-460.

Guilfoyle TJ, Hagen G. (2001) Auxin response factors. *Journal of Plant Growth Regulation* **10**:281-291.

Guo HS, Xie Q, Fei JF, Chua NH (2005) MicroRNA directs mRNA cleavage of the transcription factor *NAC1* to downregulate auxin signals for Arabidopsis lateral root development. *Plant Cell* **17**:1376-1386.

Gutierrez L, Bussell JD, Pacurar DI, Schwambach J, Pacurar M, Bellini C (2009) Phenotypic plasticity of adventitious rooting in Arabidopsis is controlled by complex regulation of AUXIN RESPONSE FACTOR transcripts and microRNA abundance. *Plant Cell* **21**:3119-3132.

Hagen G, Guilfoyle TJ (2002) Auxin-responsive gene expression: genes, promoters and regulatory factors. *Plant Molecular Biology* **49**:373-385.

Hamann T, Benkova E, Baurle I, Kientz M, Jurgens G (2002) The Arabidopsis *BODENLOS* gene encodes an auxin response protein inhibiting MONOPTEROS-mediated embryo patterning. *Genes & Development* **16**:1610-1615.

Hamilton AJ, Baulcombe DC (1999) A species of small antisense RNA in posttranscriptional gene silencing in plants. *Science* **286**:950-952.

Han MH, Goud S, Song L, Fedoroff N (2004) The Arabidopsis double-stranded RNA-binding protein HYL1 plays a role in microRNA-mediated gene regulation. *Proceedings of the National Academy of Sciences of the United States of America* **101**:1093-1098.

Hardtke CS, Berleth T (1998) The Arabidopsis gene *MONOPTEROS* encodes a transcription factor mediating embryo axis formation and vascular development. *EMBO Journal* **17**:1405-1411.

Hawker NP, Bowman JL (2004) Roles for Class III HD-Zip and *KANADI* genes in Arabidopsis root development. *Plant Physiology* **135**:2261-2270.

Heidstra R, Welch D, Scheres B (2004) Mosaic analyses using marked activation and deletion clones dissect Arabidopsis SCARECROW action in asymmetric cell division. *Genes & Development* **18**:1964-1969.

Hemmati M, Hammati H, Conroy C, Xing T (2017) Knockout of ATMKK1 reduces Arabidopsis response to 2, 3, 5-Triiodobenzoic acid in leaves. *Journal of Plant Development* **24**:23-31.

Higo K, Ugawa Y, Iwamoto M, Korenaga T (1999) Plant *cis*-acting regulatory DNA elements (PLACE) database. *Nucleic Acids Research* **27**:297-300.

Hiraguri A, Itoh R, Kondo N, Nomura Y, Aizawa D, Murai Y, Koiwa H, Seki M, Shinozaki K, Fukuhara T (2005) Specific interactions between DICER-LIKE proteins and HYL1/DRB-family dsRNA-binding proteins in *Arabidopsis thaliana*. *Plant Molecular Biology* **57**:173-188.

Hobe M, Muller R, Grunewald M, Brand U, Simon R (2003) Loss of CLE40, a protein functionally equivalent to the stem cell restricting signal CLV3, enhances root waving in Arabidopsis. *Development Genes and Evolution* **213**:371-381.

Hrtyan M, Slikova E, Hejatko J, Ruzicka K. (2015) RNA processing in auxin and cytokinin pathways. *Journal of Experimental Botany* **66**:4897-4912.

Hunter C, Willmann MR, Wu G, Yoshikawa M, de la Luz Gutierrez-Nava M, Poethig SR (2006) Trans-acting siRNA-mediated repression of *ETTIN* and *ARF4* regulates heteroblasty in Arabidopsis. *Development* **133**:2973-2981.

Iwata Y, Takahashi M, Fedoroff NV, Hamdan SM (2013) Dissecting the interactions of SERRATE with RNA and DICER-LIKE 1 in Arabidopsis microRNA precursor processing. *Nucleic Acids Research* **41**:9129-9140.

Jeong, D.H., S. Park, J. Zhai, S.G. Gurazada, E. De Paoli, B.C. Meyers, and P.J. Green. (2011) Massive analysis of rice small RNAs: mechanistic implications of regulated microRNAs and variants for differential target RNA cleavage. *Plant Cell* **23**:4185-4207.

Johnson NR, Yeoh JM, Coruh C, Axtell MJ (2016) Improved placement of multi-mapping small RNAs. *G3* **6**:2103-2111.

Jones-Rhoades MW, Bartel DP (2004) Computational identification of plant microRNAs and their targets, including a stress-induced miRNA. *Molecular Cell* **14**:787-799.

Jones B, Gunneras SA, Petersson SV, Tarkowski P, Graham N, May S, Dolezal K, Sandberg G, Ljung K (2010) Cytokinin regulation of auxin synthesis in Arabidopsis involves a homeostatic feedback loop regulated via auxin and cytokinin signal transduction. *Plant Cell* **22**:2956-2969.

Kazan K (2013) Auxin and the integration of environmental signals into plant root development. *Annals of Botany* **112**:1655-1665.

Kazan K, Manners JM (2009) Linking development to defense: auxin in plant-pathogen interactions. *Trends in Plant Science* **14**:373-382.

Kelley DR, Arreola A, Gallagher TL, Gasser CS (2012) ETTIN (ARF3) physically interacts with KANADI proteins to form a functional complex essential for integument development and polarity determination in Arabidopsis. *Development* **139**:1105-1109.

Kepinski S, Leyser O (2004) Auxin-induced SCFTIR1-Aux/IAA interaction involves stable modification of the SCFTIR1 complex. *Proceedings of the National Academy of Sciences of the United States of America* **101**:12381-12386.

Kinoshita N, Wang H, Kasahara H, Liu J, Macpherson C, Machida Y, Kamiya Y, Hannah MA, Chua NH (2012) *IAA-Ala Resistant3*, an evolutionarily conserved target of miR167, mediates Arabidopsis root architecture changes during high osmotic stress. *Plant Cell* **24**:3590-3602.

Krizek BA (2011) Auxin regulation of Arabidopsis flower development involves members of the AINTEGUMENTA-LIKE/PLETHORA (AIL/PLT) family. *Journal of Experimental Botany* **62**:3311-3319.

Krouk G, Lacombe B, Bielach A, Perrine-Walker F, Malinska K, Mounier E, Hoyerova K, Tillard P, Leon S, Ljung K, Zazimalova E, Benkova E, Nacry P, Gojon A (2010) Nitrate-regulated auxin transport by NRT1.1 defines a mechanism for nutrient sensing in plants. *Developmental Cell* **18**:927-937.

Kurihara Y, Watanabe Y (2004) Arabidopsis micro-RNA biogenesis through DICER-LIKE 1 protein functions. *Proceedings of the National Academy of Sciences of the United States of America* **101**:12753-12758.

Lanet E, Delannoy E, Sormani R, Floris M, Brodersen P, Crete P, Voinnet O, Robaglia C (2009) Biochemical evidence for translational repression by Arabidopsis microRNAs. *Plant Cell* **21**:1762-1768.

Laskowski MJ, Williams ME, Nusbaum C, Sussex IM (1995) Formation of lateral root meristems is a two-stage process. *Development* **121**:3303-3310.

Lavagi I, Estelle M, Weckwerth W, Beynon J, Bastow RM (2012) From bench to bountiful harvests: a road map for the next decade of Arabidopsis research. *Plant Cell* **24**:2240-2247.

Leblanc N, Perrot-Rechenmann C, Barbier-Brygoo H (1999) The auxin-binding protein Nt-ERabp1 alone activates an auxin-like transduction pathway. *FEBS Letters* **449**:57-60.

Lee DJ, Park JW, Lee HW, Kim J (2009) Genome-wide analysis of the auxin-responsive transcriptome downstream of *iaa1* and its expression analysis reveal the diversity and complexity of auxin-regulated gene expression. *Journal of Experimental Botany* **60**:3935-3957.

Lescot M, Dehais P, Thijs G, Marchal K, Moreau Y, Van de Peer Y, Rouze P, Rombauts S (2002) PlantCARE, a database of plant *cis*-acting regulatory elements and a portal to tools for in silico analysis of promoter sequences. *Nucleic Acids Research* **30**:325-327.

Leyser O (2002) Molecular genetics of auxin signaling. *Annual Review of Plant Biology* **53**:377-398.

Li F, Orban R, Baker B (2012) SoMART: a web server for plant miRNA, tasiRNA and target gene analysis. *Plant Journal* **70**:891-901.

Li J, Yang Z, Yu B, Liu J, Chen X (2005) Methylation protects miRNAs and siRNAs from a 3'-end uridylation activity in Arabidopsis. *Current Biology* **15**:1501-1507.

Liu X, Zhang H, Zhao Y, Feng Z, Li Q, Yang HQ, Luan S, Li J, He ZH (2013) Auxin controls seed dormancy through stimulation of abscisic acid signaling by inducing ARF-mediated ABI3 activation in Arabidopsis. *Proceedings of the National Academy of Sciences of the United States of America* **110**:15485-15490.

Llave C, Xie Z, Kasschau KD, Carrington JC (2002) Cleavage of SCARECROW-LIKE mRNA targets directed by a class of Arabidopsis miRNA. *Science* **297**:2053-2056.

Lopez-Bucio J, Hernandez-Abreu E, Sanchez-Calderon L, Nieto-Jacobo MF, Simpson J, Herrera-Estrella L (2002) Phosphate availability alters architecture and causes changes in hormone sensitivity in the Arabidopsis root system. *Plant Physiology* **129**:244-256.

Lopez-Bucio J, Hernandez-Abreu E, Sanchez-Calderon L, Perez-Torres A, Rampey RA, Bartel B, Herrera-Estrella L (2005) An auxin transport independent pathway is involved in phosphate stress-induced root architectural alterations in Arabidopsis. Identification of BIG as a mediator of auxin in pericycle cell activation. *Plant Physiology* **137**:681-691.

Mallory AC, Bartel DP, Bartel B (2005) MicroRNA-directed regulation of Arabidopsis AUXIN RESPONSE FACTOR17 is essential for proper development and modulates expression of early auxin response genes. *Plant Cell* **17**:1360-1375.

Mallory AC, Bouche N (2008) MicroRNA-directed regulation: to cleave or not to cleave. *Trends in Plant Science* **13**:359-367.

Mallory AC, Dugas DV, Bartel DP, Bartel B (2004) MicroRNA regulation of NAC-domain targets is required for proper formation and separation of adjacent embryonic, vegetative, and floral organs. *Current Biology* **14**:1035-1046.

Mallory AC, Vaucheret H (2006) Functions of microRNAs and related small RNAs in plants. *Nature Genetics* **38**:S31-36.

Marin E, Jouannet V, Herz A, Lokerse AS, Weijers D, Vaucheret H, Nussaume L, Crespi MD, Maizel A (2010) miR390, Arabidopsis TAS3 tasiRNAs, and their AUXIN RESPONSE FACTOR targets define an autoregulatory network quantitatively regulating lateral root growth. *Plant Cell* **22**:1104-1117.

Martinez de Alba AE, Jauvion V, Mallory AC, Bouteiller N, Vaucheret H (2011) The miRNA pathway limits AGO1 availability during siRNA-mediated PTGS defense against exogenous RNA. *Nucleic Acids Research* **39**:9339-9344.

Matsui A, Nguyen AH, Nakaminami K, Seki M (2013) Arabidopsis non-coding RNA regulation in abiotic stress responses. *International Journal of Molecular Sciences* **14**:22642-22654.

Mayer KF, Schoof H, Haecker A, Lenhard M, Jurgens G, Laux T (1998) Role of WUSCHEL in regulating stem cell fate in the Arabidopsis shoot meristem. *Cell* **95**:805-815.

Meinke DW, Cherry JM, Dean C, Rounsley SD, Koornneef M (1998) *Arabidopsis thaliana*: a model plant for genome analysis. *Science* **282**:662, 679-682.

Meng Y, Ma X, Chen D, Wu P, Chen M (2010) MicroRNA-mediated signaling involved in plant root development. *Biochemical & Biophysical Research Communications* **393**:345-349.

Montgomery TA, Howell MD, Cuperus JT, Li D, Hansen JE, Alexander AL, Chapman EJ, Fahlgren N, Allen E, Carrington JC (2008) Specificity of ARGONAUTE7-miR390 interaction and dual functionality in TAS3 *trans*-acting siRNA formation. *Cell* **133**:128-141.

Mosher RA, Schwach F, Studholme D, Baulcombe DC (2008) PolIVb influences RNA-directed DNA methylation independently of its role in siRNA biogenesis. *Proceedings of the National Academy of Sciences of the United States of America* **105**:3145-3150.

Muller P, Schier AF (2011) Extracellular movement of signaling molecules. *Developmental Cell* **21**:145-158.

Muller R, Bleckmann A, Simon R (2008) The receptor kinase CORYNE of Arabidopsis transmits the stem cell-limiting signal CLAVATA3 independently of CLAVATA1. *Plant Cell* **20**:934-946.

Nakazawa M, Yabe N, Ichikawa T, Yamamoto YY, Yoshizumi T, Hasunuma K, Matsui M (2001) *DFL1*, an auxin-responsive *GH3* gene homologue, negatively regulates shoot cell elongation and lateral root formation, and positively regulates the light response of hypocotyl length. *Plant Journal* **25**:213-221.

Nakazawa Y, Hiraguri A, Moriyama H, Fukuhara T (2007) The dsRNA-binding protein DRB4 interacts with the DICER-LIKE protein DCL4 in vivo and functions in the *trans*-acting siRNA pathway. *Plant Molecular Biology* **63**:777-785.

Navarro L, Dunoyer P, Jay F, Arnold B, Dharmasiri N, Estelle M, Voinnet O, Jones JD (2006) A plant miRNA contributes to antibacterial resistance by repressing auxin signaling. *Science* **312**:436-439.

Nikovics K, Blein T, Peaucelle A, Ishida T, Morin H, Aida M, Laufs P (2006) The balance between the MIR164A and CUC2 genes controls leaf margin serration in Arabidopsis. *Plant Cell* **18**:2929-2945.

Oh E, Zhu JY, Bai MY, Arenhart RA, Sun Y, Wang ZY (2014) Cell elongation is regulated through a central circuit of interacting transcription factors in the Arabidopsis hypocotyl. *Elife* **3**.

Okushima Y, Overvoorde PJ, Arima K, Alonso JM, Chan A, Chang C, Ecker JR, Hughes B, Lui A, Nguyen D, Onodera C, Quach H, Smith A, Yu G, Theologis A (2005) Functional genomic analysis of the *AUXIN RESPONSE FACTOR* gene family members in *Arabidopsis thaliana*: unique and overlapping functions of ARF7 and ARF19. *Plant Cell* **17**:444-463.

Overvoorde P, Fukaki H, Beeckman T (2010) Auxin control of root development. *Cold Spring Harbor Perspectives in Biology* **2**:a001537.

Overvoorde PJ, Okushima Y, Alonso JM, Chan A, Chang C, Ecker JR, Hughes B, Liu A, Onodera C, Quach H, Smith A, Yu G, Theologis A (2005) Functional genomic analysis of the *AUXIN/INDOLE-3-ACETIC ACID* gene family members in *Arabidopsis thaliana*. *Plant Cell* **17**:3282-3300.

Palme K, Galweiler L (1999) PIN-pointing the molecular basis of auxin transport. *Current Opinion in Plant Biology* **2**:375-381.

Pandey B, Gupta OP, Pandey DM, Sharma I, Sharma P (2013) Identification of new stress-induced microRNA and their targets in wheat using computational approach. *Plant Signaling & Behavior* **8**:e23932.

Parent JS, Jauvion V, Bouche N, Beclin C, Hachet M, Zytnicki M, Vaucheret H (2015) Post-transcriptional gene silencing triggered by sense transgenes involves uncapped antisense RNA and differs from silencing intentionally triggered by antisense transgenes. *Nucleic Acids Research* **43**:8464-8475.

Park J, Kim YS, Kim SG, Jung JH, Woo JC, Park CM (2011) Integration of auxin and salt signals by the NAC transcription factor NTM2 during seed germination in Arabidopsis. *Plant Physiology* **156**:537-549.

Park JY, Kim HJ, Kim J (2002a) Mutation in domain II of IAA1 confers diverse auxin-related phenotypes and represses auxin-activated expression of Aux/IAA genes in steroid regulator-inducible system. *Plant Journal* **32**:669-683.

Park MY, Wu G, Gonzalez-Sulser A, Vaucheret H, Poethig RS (2005) Nuclear processing and export of microRNAs in Arabidopsis. *Proceedings of the National Academy of Sciences of the United States of America* **102**:3691-3696.

Park W, Li J, Song R, Messing J, Chen X (2002b) CARPEL FACTORY, a DICER homolog, and HEN1, a novel protein, act in microRNA metabolism in *Arabidopsis thaliana*. *Current Biology* **12**:1484-1495.

Parry G, Calderon-Villalobos LI, Prigge M, Peret B, Dharmasiri S, Itoh H, Lechner E, Gray WM, Bennett M, Estelle M (2009) Complex regulation of the TIR1/AFB family of auxin receptors. *Proceedings of the National Academy of Sciences of the United States of America* **106**:22540-22545.

Pelissier T, Clavel M, Chaparro C, Pouch-Pelissier MN, Vaucheret H, Deragon JM (2011) Double-stranded RNA binding proteins DRB2 and DRB4 have an antagonistic impact on polymerase IV-dependent siRNA levels in Arabidopsis. *RNA* **17**:1502-1510.

Peret, B, De Rybel M, Casimiro E, Benkova E, Swarup R, Laplaze L, Beeckman T, Bennett MJ. (2009). Arabidopsis lateral root development an emerginf story. *Trends in Plant Science* **14**:399.408.

Perez-Torres CA, Lopez-Bucio J, Cruz-Ramirez A, Ibarra-Laclette E, Dharmasiri S, Estelle M, Herrera-Estrella L (2008) Phosphate availability alters lateral root development in Arabidopsis by modulating auxin sensitivity via a mechanism involving the TIR1 auxin receptor. *Plant Cell* **20**:3258-3272.

Piya S, Shrestha SK, Binder B, Stewart CN, Jr., Hewezi T (2014) Protein-protein interaction and gene co-expression maps of *ARF*s and *Aux/IAA*s in Arabidopsis. *Frontiers in Plant Science* **5**:744.

Ploense SE, Wu MF, Nagpal P, Reed JW (2009) A gain-of-function mutation in IAA18 alters Arabidopsis embryonic apical patterning. *Development* **136**:1509-1517.

Prigge MJ, Greenham K, Zhang Y, Santner A, Castillejo C, Mutka AM, O'Malley RC, Ecker JR, Kunkel BN, Estelle M (2016) The Arabidopsis auxin receptor F-Box proteins AFB4 and AFB5 are required for response to the synthetic auxin Picloram. *G3* **6**:1383-1390.

Prufer K, Stenzel U, Dannemann M, Green RE, Lachmann M, Kelso J (2008) PatMaN: rapid alignment of short sequences to large databases. *Bioinformatics* **24**:1530-1531.

Qin H, Chen F, Huan X, Machida S, Song J, Yuan YA (2010) Structure of the *Arabidopsis thaliana* DCL4 DUF283 domain reveals a noncanonical double-stranded RNA-binding fold for protein-protein interaction. *RNA* **16**:474-481.

Qu F, Ye X, Morris TJ (2008) Arabidopsis DRB4, AGO1, AGO7, and RDR6 participate in a DCL4-initiated antiviral RNA silencing pathway negatively regulated by DCL1. *Proceedings of the National Academy of Sciences of the United States of America* **105**:14732-14737.

Rademacher EH, Moller B, Lokerse AS, Llavata-Peris CI, van den Berg W, Weijers D (2011) A cellular expression map of the Arabidopsis *AUXIN RESPONSE FACTOR* gene family. *Plant Journal* **68**:597-606.

Rajagopalan R, Vaucheret H, Trejo J, Bartel DP (2006) A diverse and evolutionarily fluid set of microRNAs in *Arabidopsis thaliana*. *Genes & Development* **20**:3407-3425.

Raman S, Greb T, Peaucelle A, Blein T, Laufs P, Theres K (2008) Interplay of miR164, *CUP-SHAPED COTYLEDON* genes and LATERAL SUPPRESSOR controls axillary meristem formation in *Arabidopsis thaliana*. *Plant Journal* **55**:65-76.

Rand TA, Petersen S, Du F, Wang X (2005) ARGONAUTE2 cleaves the anti-guide strand of siRNA during RISC activation. *Cell* **123**:621-629.

Rashotte AM, Brady SR, Reed RC, Ante SJ, Muday GK (2000) Basipetal auxin transport is required for gravitropism in roots of Arabidopsis. *Plant Physiology* **122**:481-490.

Reed JW (2001) Roles and activities of Aux/IAA proteins in Arabidopsis. *Trends in Plant Science* **6**:420-425.

Reinhardt D, Mandel T, Kuhlemeier C (2000) Auxin regulates the initiation and radial position of plant lateral organs. *Plant Cell* **12**:507-518.

Reinhardt D, Pesce ER, Stieger P, Mandel T, Baltensperger K, Bennett M, Traas J, Friml J, Kuhlemeier C (2003) Regulation of phyllotaxis by polar auxin transport. *Nature* **426**:255-260.

Reis RS, Hart-Smith G, Eamens AL, Wilkins MR, Waterhouse PM (2015) Gene regulation by translational inhibition is determined by DICER partnering proteins. *Nature Plants* **1**:14027.

Rinaldi MA, Liu J, Enders TA, Bartel B, Strader LC (2012) A gain-of-function mutation in IAA16 confers reduced responses to auxin and abscisic acid and impedes plant growth and fertility. *Plant Molecular Biology* **79**:359-373.

Robert-Seilaniantz A, MacLean D, Jikumaru Y, Hill L, Yamaguchi S, Kamiya Y, Jones JD (2011) The microRNA miR393 re-directs secondary metabolite biosynthesis away from camalexin and towards glucosinolates. *Plant Journal* **67**:218-231.

Rodriguez-Serrano M, Pazmino DM, Sparkes I, Rochetti A, Hawes C, Romero-Puertas MC, Sandalio LM (2014) 2,4-Dichlorophenoxyacetic acid promotes S-nitrosylation and oxidation of actin affecting cytoskeleton and peroxisomal dynamics. *Journal of Experimental Botany* **65**:4783-4793.

Rojo E, Sharma VK, Kolaleva V, Raikhel NV, Fletcher JC (2002) CLV3 is localized to the extracellular space, where it activates the Arabidopsis CLAVATA stem cell signaling pathway. *Plant Cell* **14**:969-977.

Roychoudhry S, Del Bianco M, Kieffer M, Kepinski S (2013) Auxin controls gravitropic setpoint angle in higher plant lateral branches. *Current Biology* **23**:1497-1504.

Sabatini S, Beis D, Wolkenfelt H, Murfett J, Guilfoyle TJ, Malamy J, Benfey P, Leyser O, Bechtold N, Weisbeek P, Scheres B (1999) An auxin-dependent distal organizer of pattern and polarity in the Arabidopsis root. *Cell* **99**:463-472.

Sablowski R (2007) Flowering and determinacy in Arabidopsis. *Journal of Experimental Botany* **58**:899-907.

Sato A, Yamamoto KT (2008) What's the physiological role of domain II-less Aux/IAA proteins? *Plant Signaling & Behavior* **3**:496-497.

Schauer SE, Jacobsen SE, Meinke DW, Ray A (2002) DICER-LIKE1: blind men and elephants in Arabidopsis development. *Trends in Plant Science* **7**:487-491.

Schoof H, Lenhard M, Haecker A, Mayer KF, Jurgens G, Laux T (2000) The stem cell population of Arabidopsis shoot meristems in maintained by a regulatory loop between the CLAVATA and WUSCHEL genes. *Cell* **100**:635-644.

Smith AE (1989) Degradation, fate, and persistence of phenoxyalkanoic acid herbicides in soil. *Reviews of Weed Science* **4**:1-24.

Song L, Axtell MJ, Fedoroff NV (2010) RNA secondary structural determinants of miRNA precursor processing in Arabidopsis. *Current Biology* **20**:37-41.

Souer E, van Houwelingen A, Kloos D, Mol J, Koes R (1996) The no apical meristem gene of Petunia is required for pattern formation in embryos and flowers and is expressed at meristem and primordia boundaries. *Cell* **85**:159-170.

Stowe-Evans EL, Harper RM, Motchoulski AV, Liscum E (1998) NPH4, a conditional modulator of auxin-dependent differential growth responses in Arabidopsis. *Plant Physiology* **118**:1265-1275.

Stowe-Evans EL, Luesse DR, Liscum E (2001) The enhancement of phototropin-induced phototropic curvature in Arabidopsis occurs via a photoreversible phytochrome A-dependent modulation of auxin responsiveness. *Plant Physiology* **126**:826-834.

Strader LC, Monroe-Augustus M, Bartel B (2008) The IBR5 phosphatase promotes Arabidopsis auxin responses through a novel mechanism distinct from TIR1-mediated repressor degradation. *BMC Plant Biology* **8**:41.

Svistoonoff S, Creff A, Reymond M, Sigoillot-Claude C, Ricaud L, Blanchet A, Nussaume L, Desnos T (2007) Root tip contact with low-phosphate media reprograms plant root architecture. *Nature Genetics* **39**:792-796.

Szarzynska B, Sobkowiak L, Pant BD, Balazadeh S, Scheible WR, Mueller-Roeber B, Jarmolowski A, Szweykowska-Kulinska Z (2009) Gene structures and processing of *Arabidopsis thaliana* HYL1-dependent pri-miRNAs. *Nucleic Acids Research* **37**:3083-3093.

Tagami Y, Inaba N, Kutsuna N, Kurihara Y, Watanabe Y (2007) Specific enrichment of miRNAs in *Arabidopsis thaliana* infected with Tobacco mosaic virus. *DNA Research* **14**:227-233.

Takase T, Nakazawa M, Ishikawa A, Kawashima M, Ichikawa T, Takahashi N, Shimada H, Manabe K, Matsui M (2004) ydk1-D, an auxin-responsive GH3 mutant that is involved in hypocotyl and root elongation. *Plant Journal* **37**:471-483.

Tao Y, Ferrer JL, Ljung K, Pojer F, Hong F, Long JA, Li L, Moreno JE, Bowman ME, Ivans LJ, Cheng Y, Lim J, Zhao Y, Ballare CL, Sandberg G, Noel JP, Chory J (2008) Rapid synthesis of auxin via a new tryptophan-dependent pathway is required for shade avoidance in plants. *Cell* **133**:164-176.

Tiwari SB, Hagen G, Guilfoyle TJ (2003) The roles of auxin response factor domains in auxin-responsive transcription. *Plant Cell* **15**:533-543.

Traas J, Doonan JH (2001) Cellular basis of shoot apical meristem development. *International Review of Cytology* **208**:161-206.

Tsuzuki M, Takeda A, Watanabe Y (2014) Recovery of dicer-like 1-late flowering phenotype by miR172 expressed by the noncanonical DCL4-dependent biogenesis pathway. *RNA* **20**:1320-1327.

Ulmasov T, Hagen G, Guilfoyle TJ (1999) Activation and repression of transcription by auxin-response factors. *Proceedings of the National Academy of Sciences of the United States of America* **96**:5844-5849.

Ulmasov T, Murfett J, Hagen G, Guilfoyle TJ (1997) Aux/IAA proteins repress expression of reporter genes containing natural and highly active synthetic auxin response elements. *Plant Cell* **9**:1963-1971.

van den Berg CW, V. , Hendriks G, Weisbeek P, Scheres B (1997) Short-range control of cell differentiation in the Arabidopsis root meristem. *Nature* **390**:287-289.

Vanderhoef LN, Stahl CA (1975) Separation of two responses to auxin by means of cytokinin inhibition. *Proceedings of the National Academy of Sciences of the United States of America* **72**:1822-1825.

Vanneste S, De Rybel B, Beemster GT, Ljung K, De Smet I, Van Isterdael G, Naudts M, Iida R, Gruissem W, Tasaka M, Inze D, Fukaki H, Beeckman T (2005) Cell cycle progression in the pericycle is not sufficient for SOLITARY ROOT/IAA14-mediated lateral root initiation in *Arabidopsis thaliana*. *Plant Cell* **17**:3035-3050.

Vaucheret H (2006) Post-transcriptional small RNA pathways in plants: mechanisms and regulations. *Genes & Development* **20**:759-771.

Vazquez F (2006) Arabidopsis endogenous small RNAs: highways and byways. *Trends in Plant Science* **11**:1360-1385.

Vazquez F, Gasciolli V, Crete P, Vaucheret H (2004a) The nuclear dsRNA binding protein HYL1 is required for microRNA accumulation and plant development, but not posttranscriptional transgene silencing. *Current Biology* **14**:346-351.

Vazquez F, Vaucheret H, Rajagopalan R, Lepers C, Gasciolli V, Mallory AC, Hilbert JL, Bartel DP, Crete P (2004b) Endogenous *trans*-acting siRNAs regulate the accumulation of Arabidopsis mRNAs. *Molecular Cell* **16**:69-79.

Vernoux T, Besnard F, Traas J (2010) Auxin at the shoot apical meristem. *Cold Spring Harbor Perspectives in Biology* **2**:a001487.

Vernoux T, Kronenberger J, Grandjean O, Laufs P, Traas J (2000) PIN-FORMED 1 regulates cell fate at the periphery of the shoot apical meristem. *Development* **127**:5157-5165.

Vidal EA, Araus V, Lu C, Parry G, Green PJ, Coruzzi GM, Gutierrez RA (2010) Nitrate-responsive miR393/AFB3 regulatory module controls root system architecture in *Arabidopsis thaliana*. *Proceedings of the National Academy of Sciences of the United States of America* **107**:4477-4482.

Walsh TA, Neal R, Merlo AO, Honma M, Hicks GR, Wolff K, Matsumura W, Davies JP (2006) Mutations in an auxin receptor homolog AFB5 and in SGT1b confer resistance to synthetic picolinate auxins and not to 2,4-dichlorophenoxyacetic acid or indole-3-acetic acid in Arabidopsis. *Plant Physiology* **142**:542-552.

Wang JW, Wang LJ, Mao YB, Cai WJ, Xue HW, Chen XY (2005) Control of root cap formation by microRNA-targeted auxin response factors in Arabidopsis. *Plant Cell* **17**:2204-2216.

Wang Y, Li K, Li X (2009) Auxin redistribution modulates plastic development of root system architecture under salt stress in *Arabidopsis thaliana*. *Journal of Plant Physiology* **166**:1637-1645.

Williams L, Carles CC, Osmont KS, Fletcher JC (2005) A database analysis method identifies an endogenous *trans*-acting short-interfering RNA that targets the Arabidopsis *ARF2*, *ARF3*, and *ARF4* genes. *Proceedings of the National Academy of Sciences of the United States of America* **102**:9703-9708.

Williamson LC, Ribrioux SP, Fitter AH, Leyser HM (2001) Phosphate availability regulates root system architecture in Arabidopsis. *Plant Physiology* **126**:875-882.

Windels D, Bielewicz D, Ebneter M, Jarmolowski A, Szweykowska-Kulinska Z, Vazquez F (2014) miR393 is required for production of proper auxin signalling outputs. *PloS One* **9**:e95972.

Windels D, Vazquez F (2011) miR393: integrator of environmental cues in auxin signaling? *Plant Signaling & Behavior* **6**:1672-1675.

Wojcik AM, Gaj MD (2016) miR393 contributes to the embryogenic transition induced *in vitro* in Arabidopsis via the modification of the tissue sensitivity to auxin treatment. *Planta* **244**:231-243.

Worley CK, Zenser N, Ramos J, Rouse D, Leyser O, Theologis A, Callis J (2000) Degradation of Aux/IAA proteins is essential for normal auxin signalling. *Plant Journal* **21**:553-562.

Wu F, Yu L, Cao W, Mao Y, Liu Z, He Y (2007) The N-terminal double-stranded RNA binding domains of Arabidopsis HYPONASTIC LEAVES1 are sufficient for pre-microRNA processing. *Plant Cell* **19**:914-925.

Wu HJ, Wang ZM, Wang M, Wang XJ (2013) Widespread long noncoding RNAs as endogenous target mimics for microRNAs in plants. *Plant Physiology* **161**:1875-1884.

Wu MF, Tian Q, Reed JW (2006) Arabidopsis microRNA167 controls patterns of *ARF6* and *ARF8* expression, and regulates both female and male reproduction. *Development* **133**:4211-4218.

Xie Q, Frugis G, Colgan D, Chua NH (2000) Arabidopsis NAC1 transduces auxin signal downstream of TIR1 to promote lateral root development. *Genes & Development* **14**:3024-3036.

Yang L, Wu G, Poethig RS (2012) Mutations in the GW-repeat protein SUO reveal a developmental function for microRNA-mediated translational repression in Arabidopsis. *Proceedings of the National Academy of Sciences of the United States of America* **109**:315-320.

Yang X, Lee S, So JH, Dharmasiri S, Dharmasiri N, Ge L, Jensen C, Hangarter R, Hobbie L, Estelle M (2004) The IAA1 protein is encoded by AXR5 and is a substrate of SCF(TIR1). *Plant Journal* **40**:772-782.

Yang Z, Ebright YW, Yu B, Chen X (2006) HEN1 recognizes 21-24 nt small RNA duplexes and deposits a methyl group onto the 2' OH of the 3' terminal nucleotide. *Nucleic Acids Research* **34**:667-675.

Yoon EK, Yang JH, Lim J, Kim SH, Kim SK, Lee WS (2010) Auxin regulation of the microRNA390-dependent transacting small interfering RNA pathway in Arabidopsis lateral root development. *Nucleic Acids Research* **38**:1382-1391.

Yu B, Yang Z, Li J, Minakhina S, Yang M, Padgett RW, Steward R, Chen X (2005) Methylation as a crucial step in plant microRNA biogenesis. *Science* **307**:932-935.

Yu LP, Miller AK, Clark SE (2003) POLTERGEIST encodes a protein phosphatase 2C that regulates CLAVATA pathways controlling stem cell identity at Arabidopsis shoot and flower meristems. *Current Biology* **13**:179-188.

Zhang C, Li G, Zhu S, Zhang S, Fang J (2014) tasiRNAdb: a database of ta-siRNA regulatory pathways. *Bioinformatics* **30**:1045-1046.

Zhang W, Gao S, Zhou X, Xia J, Chellappan P, Zhou X, Zhang X, Jin H (2010) Multiple distinct small RNAs originate from the same microRNA precursors. *Genome Biology* **11**:R81.

Zhao Y (2010) Auxin biosynthesis and its role in plant development. *Annual Review of Plant Biology* **61**:49-64.

Zheng Q, Zheng Y, Ji H, Burnie W, Perry SE (2016) Gene regulation by the AGL15 transcription hactor reveals hormone interactions in somatic embryogenesis. *Plant Physiology* **172**:2374-2387.

Zhu QH, Stephen S, Kazan K, Jin G, Fan L, Taylor J, Dennis ES, Helliwell CA, Wang MB (2013a) Characterization of the defense transcriptome responsive to *Fusarium oxysporum*-infection in Arabidopsis using RNA-seq. *Gene* **512**:259-266.

Zhu QH, Stephen S, Taylor J, Helliwell CA, Wang MB (2013b) Long noncoding RNAs responsive to *Fusarium oxysporum* infection in *Arabidopsis thaliana*. *New Phytologist* **201**:574-587.

Zolla G, Heimer YM, Barak S (2010) Mild salinity stimulates a stress-induced morphogenic response in *Arabidopsis thaliana* roots. *Journal of Experimental Botany* **61**:211-224.

Appendices

Appendix 1 – Primers

Table S1.1. Primers used in this study.

Primer Name	Primer Sequence
Cloning primers	
prom*ARF10* FOR (XhoI)	TCACTCGAGAATGCAAGACAACCCACCAA
prom*ARF10* REV (BamHI)	TCAGGATCCCTAGACGAAGTTGTGTAACC
prom*ARF16* FOR (XbaI)	TCACTCGAGTGGATTCATCACATTTATCAT
prom*ARF16* REV (XhoI)	TCATCTAGAACATGCGGAAATTTATTGAGC
PRI-MIR160B-OE FOR (XhoI)	TCACTCGAGGCACGCTGTGTCTGTCTCTTT
PRI-MIR160B-OE REV (BamHI)	TCAGGATCCTGCCTTGATTGGAAGATCTGA
pORE1 genotype FOR	GCTGATATGGCCGCTGTTTGT
pORE1 genotype REV	CAATGTACCCCTGGCTGTGT
pBART genotype FOR	CATCGAGACAAGCACGGTCA
pBART genotype FOR	AAACCCACGTCATGCCAGTT
Semi-quantitative RT-PCR primers	
ABP1 RT FOR	TCCGAGGCTAAAAGCAAGCA
ABP1 RT REV	TCGCAAATGCAATCAAGATGT
ARF3 RT FOR	CAACTGGTCCCAAGAGAAGC
ARF3 RT REV	TGCAAGACCTTATGGAAACCA
ARF4 RT FOR	GGGAATGATTTAAGCGAGCA
ARF4 RT REV	ATACTACCCCACCCGGAAAC
ARF6 RT FOR	CAGAGACAGCTTGGATGGC
ARF6 RT REV	CAGGGTCTTTTGGAAGATCG
ARF8 RT FOR	GGTTGGGCGTTCATTAGACA
ARF8 RT REV	ATGTACCAAACGTTATTCACAAATG
TIR1 RT FOR	CGATGACTTCCACATTCAGC
TIR1 RT REV	TGTCAAGCTTCTTTGTCAATGC
BIG RT FOR	TCACTGTTGGCATCTTCTTCA
BIG RT REV	ACTGCAACAGGTCCTTTGGT
IAA1 RT FOR	AAGCGCAAGAACAACGACTC

IAA1 RT REV	AGTGCTTTGAGAAGCTCTGGA
IAA14 RT FOR	CCCTTGTGCTCCATAACTCC
IAA14 RT REV	GGATGGAGCTCCTTATCTTCG
ARF10 RT FOR	CGGTACTAAATTCCCGATTTTCT
ARF10 RT REV	GAATGTAACTTGTTGTTACCGGTGT
ARF16 RT FOR	CAGTACCTTCATTCCCAAGCA
ARF16 RT REV	GATGTTTCGGAGACCGAGAG
ARF17 RT FOR	AGCAGCACCTGATCCAAGTC
ARF17 RT REV	GTCGACACTTTTCCCAAATCA
ACTIN2 RT FOR	TCTTCCGTCTTTCTTTCCA
ACTIN2 RT REV	GAGAGAACAGCTTGGATGGC
RT-qPCR primers	
EF1-α FOR	TGAGCACGCTCTTCTTGCTTTCA
EF1-α REV	GGTGGTGGCATCCATCTTGTTACA
PRI-MIR160A FOR	ATATGCTGAGCCCATCGAGTATCG
PRI-MIR160A REV	ATGCATGGCTCCTCATACGCC
PRI-MIR160B FOR	GCCACAAGAAAACATCGATTTAGTTTC
PRI-MIR160B REV	TGCTTGACTACTCTGTACGCCA
PRI-MIR160C FOR	CCACGAGTGGATACCGATTTTG
PRI-MIR160C REV	GCTTGACTCCTTGTACGCCAC
eTM160-1 FOR	TCTTCAGAGATGGCCTGACGA
eTM160-1 REV	AATCGTAATCCTAATCAGTGTT
eTM160-2 FOR	ACCGGACTGTCAGTGCTTGAT
eTM160-2 REV	TTCGCAAATGTCACTCCAAAA
ARF10 FOR	CGGTTTTTGGAAGAAGAGGCGG
ARF10 REV	GCGTCCAACATCCTCAGATTCCAT
ARF16 FOR	AACTTTCTCCTTCTCTCGGTCTCCG
ARF16 REV	AGCTTGCCGAACAATACAATATGGG
ARF17 FOR	CGAGTCAAGATGGCTATGGA
ARF17 REV	CATCCCATGTGATCTGAAGC
DRB1 FOR	ATGACCTCCACTGATGTTTCC
DRB1 REV	TGCTAATTCCCGGAGAGC
DRB2 FOR	ATGTATAAGAACCAGCTACAAGAGTTG
DRB2 REV	CAGCAGCAGAGTGTTCAGC
DRB4 FOR	AAATGGGAACTCGAACCAGA
DRB4 REV	CCACCTTGGAAGAAGGTTGA

Stem-loop RT-qPCR primers	
sno101 FOR	CTTCACAGGTAAGTTCGCTTG
sno101 REV	AGCATCAGCAGACCAGTAGTT
miR160 REV (synthesis)	GTCGTATCCAGTGCAGGGTCCGAGGTATTCGCACTGGATACG ACTGGCAT
miR160 FOR	GCTGCCTGGCTCCCTGT
Generic STL	CCAGTGCAGGGTCCGAGGTA

Appendix 2 – Materials

MS Stock Solutions

MS Macro (g/L)	Ammonium nitrate (NH_4NO_3)	= 33.0
	Potassium nitrate (KNO_3)	= 38.0
	Monobasic potassium phosphate (KH_2PO_4)	= 3.4
	Magnesium sulfate heptahydrate ($MgSO_4.7H_2O$)	= 7.4
	Calcium chloride dehydrate ($CaCl_2.2H_2O$)	= 8.8
MS Micro (g/500 mL)	Manganese sulfate tetrahydrate ($MnSO_4.4H_2O$)	= 11.15
	Sodium molybdate dehydrate ($Na_2MoO_4.2H_2O$)	= 0.125
	Boric acid (H_3BO_3)	= 3.11
	Zinc sulfate heptahydrate ($ZnSO_4.7H_2O$)	= 4.3
	Copper sulfate pentahydrate ($CuSO_4.5H_2O$)	= 0.0125
	Cobalt chloride hexahydrate ($CoCl_2.6H_2O$)	= 0.0125
	Potassium iodide (KI)	= 0.115
MS Vitamins (mg/L)	Nicotinic acid ($C_6H_5NO_2$)	= 50.0
	Pyridoxine HCl ($C_8H_{12}ClNO_3$)	= 50.0
	Thiamine HCl ($C_{12}H_{17}N_4OS^+$)	= 10.0
	Glycine ($C_2H_5NO_2$)	= 200
MS Iron (g/500 mL)	EDTA ($C_{10}H_{14}N_2Na_2O_8$)	= 3.35
	Iron chloride hexahydrate ($FeCl_3.6H_2O$)	= 2.70

Murashige and Skoog (MS) agar plant growth media

To prepare 1.0 L of MS agar growth media, the following was used:

- MS Macro 50.0 mL
- MS Micro 0.25 mL
- MS Vitamins 2.5 mL
- MS Iron 1.25 mL
- Sucrose 7.5 g
- Myoinositiol 25 mg

Made to 1.0 L with MQ H_2O

pH adjusted to 5.7 with 1M KOH

8.0 g Bacto Agar added.

Autoclaved

Cetyltrimethylammonium Bromide (CTAB) Buffer

To prepare 50 mL of CTAB genomic DNA extraction buffer the following solution was made:

- 1.5 g CTAB
- 14.0 mL 5M NaCl
- 5.0 mL 1M *Tris*-HCl, pH 8.0
- 2.0 mL 0.5M EDTA, pH 8.0
- 29.0 mL MQ H_2O

***Tris*/Borate/EDTA (TBE) Buffer**

To prepare 1.0 L of 10X TBE buffer, the following solution was made:

- 108 g *Tris*-HCl
- 55.0 g H_3BO_3
- 40.0 mL 0.5 EDTA, pH 8.0

Solution made to 1.0 L with MQ H_2O

Autoclaved

Appendix 3 – m*ARF10* and m*ARF16* synthesised sequences

Figure S3.1. Synthesised m*ARF10* sequence. Full length coding domain sequence of the miR160-resistant *ARF10* transcript. Eight base pairings (red) in the miR160 binding site (bold) were changed to introduce mismatches in this sequence without changing the amino acid sequence, remaining sequences in the binding site were left unchanged (green), and no other base pairings were changed throughout the remainder of the transcript (black). Restriction sites *SalI* and *BamHI* (purple) were introduced for cloning purposes at the 5' and 3' ends of the transcript, respectively.

Figure S3.2. Synthesised m*ARF16* sequence. Full length coding domain sequence of the miR160-resistant *ARF16* transcript. Eight base pairings (red) in the miR160 binding site (bold) were changed to introduce mismatches in this sequence without changing the amino acid sequence, except where an appropriate mismatch could be made with a substituted amino acid (yellow). The remaining sequences in the binding site were left unchanged (green), and no other base pairings were changed throughout the remainder of the transcript (black). Restriction sites *EcoRI* and *SalI* (purple) were introduced for cloning purposes at the 5' and 3' ends of the transcript, respectively.

Appendix 4 – Degradome Analyses

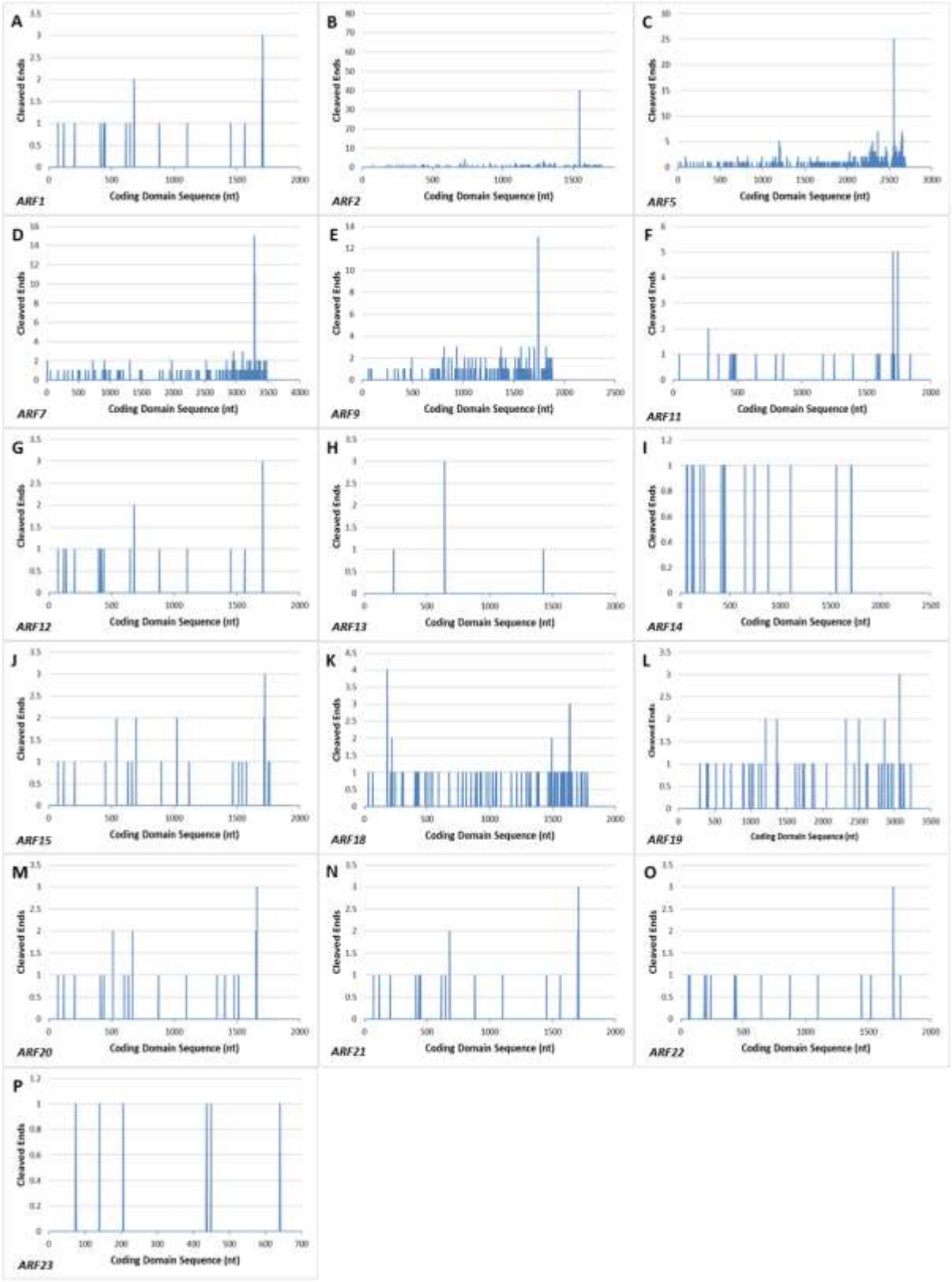

Figure S4.1. Degradome analysis of potential sRNA-targeted auxin responsive gene transcripts. Col-0 (blue) coding domain sequences of auxin responsive genes *ARF1* (A), *ARF2* (B), *ARF5* (C), *ARF7* (D), *ARF9* (E), *ARF11-15* (F-J), and *ARF19-23* (K-P), were analysed in floral tissue for degradome cleaved end products, excluding those presented in **Figure 3.1**.

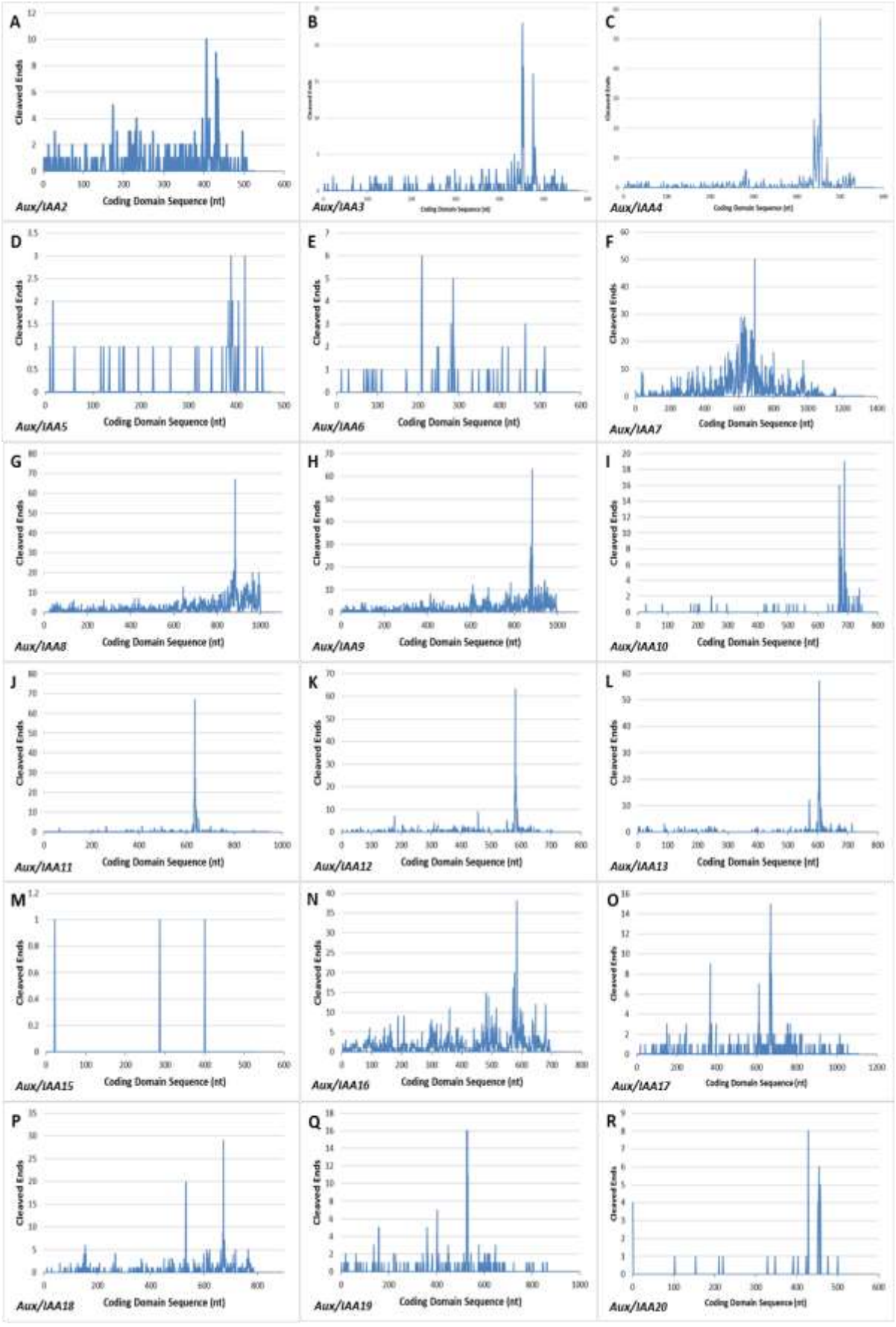
A
Cleaved Ends
Coding Domain Sequence (nt)
Aux/IAA2
B
Aux/IAA3
C
Aux/IAA4
D
Aux/IAA5
E
Aux/IAA6
F
Aux/IAA7
G
Aux/IAA8
H
Aux/IAA9
I
Aux/IAA10
J
Aux/IAA11
K
Aux/IAA12
L
Aux/IAA13
M
Aux/IAA15
N
Aux/IAA16
O
Aux/IAA17
P
Aux/IAA18
Q
Aux/IAA19
R
Aux/IAA20

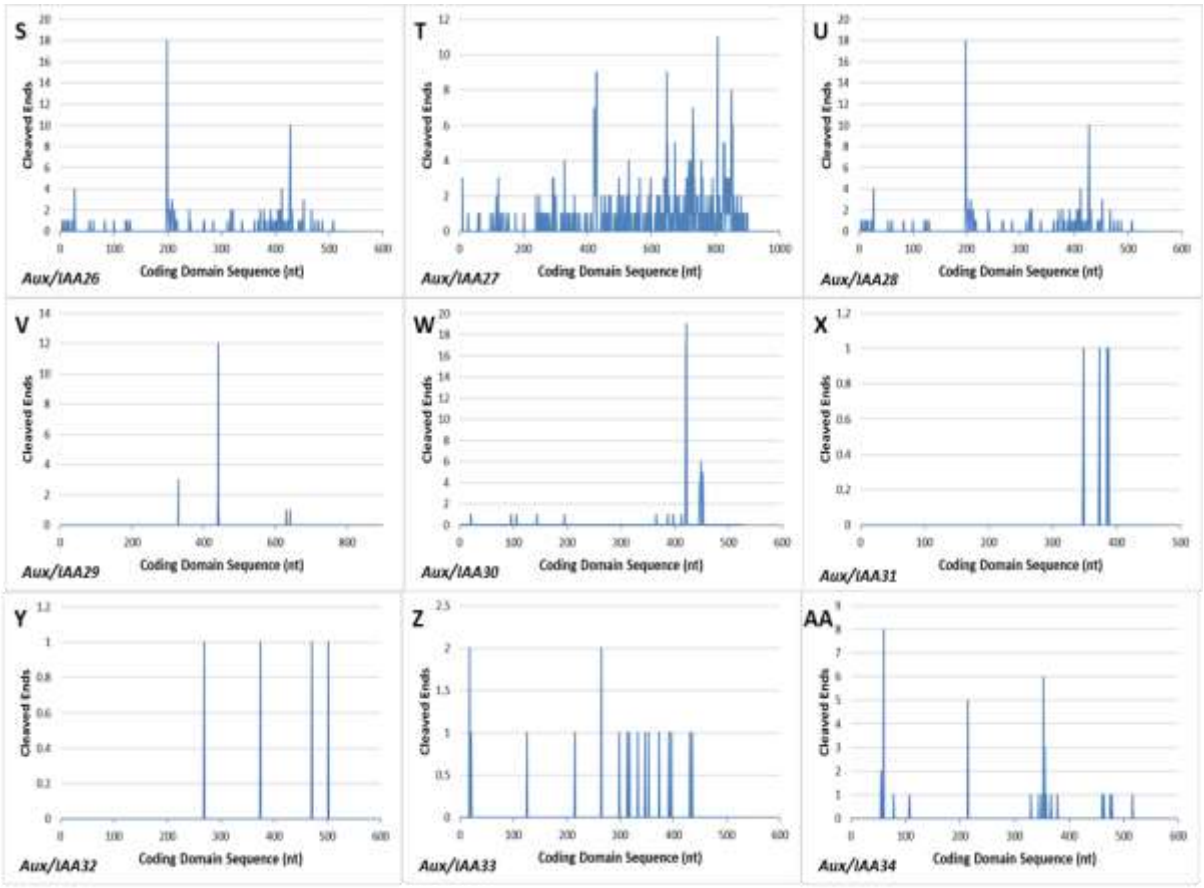

Figure S4.2. Degradome analysis of potential sRNA-targeted auxin responsive gene transcripts. Col-0 (blue) coding domain sequences of auxin responsive genes *Aux/IAA2-13* (A-L), *Aux/IAA15-20* (M-R), and *Aux/IAA26-34* (S-AA), were analysed in floral tissue for degradome cleaved end products, these analyses are in addition to those presented in **Figure 3.1**.

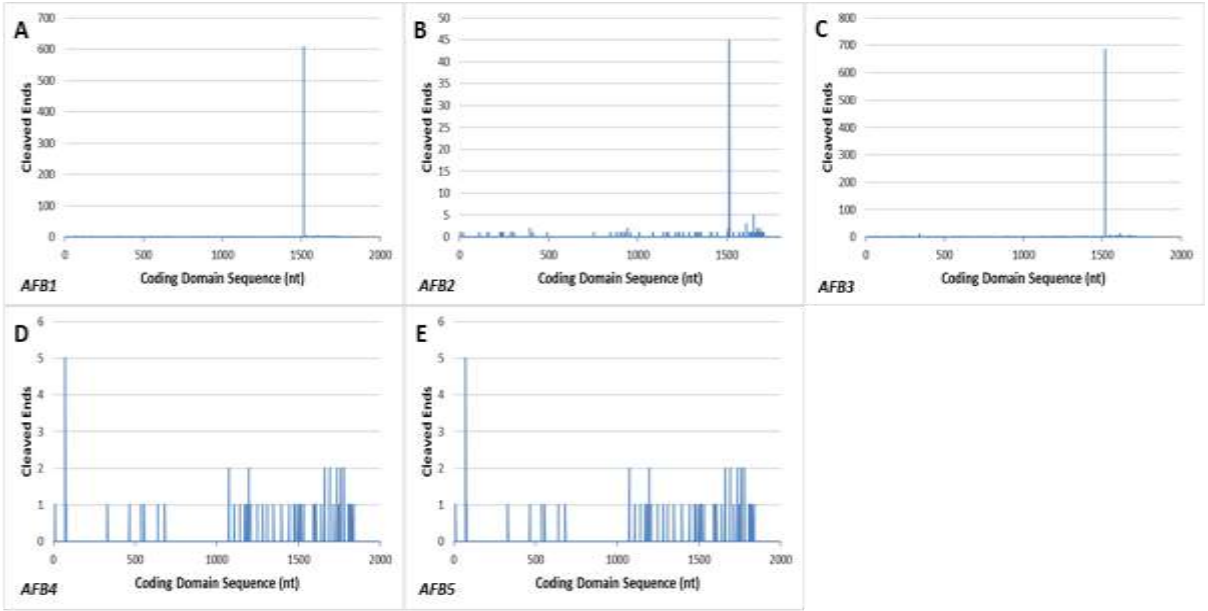

Figure S4.3. Degradome analysis of potential sRNA-targeted auxin responsive gene transcripts. Col-0 (blue) coding domain sequences of auxin responsive genes *AFB1-5* (A-E), were analysed in floral tissue for degradome cleaved end products, these analyses are in addition to those presented in **Figure 3.1**.

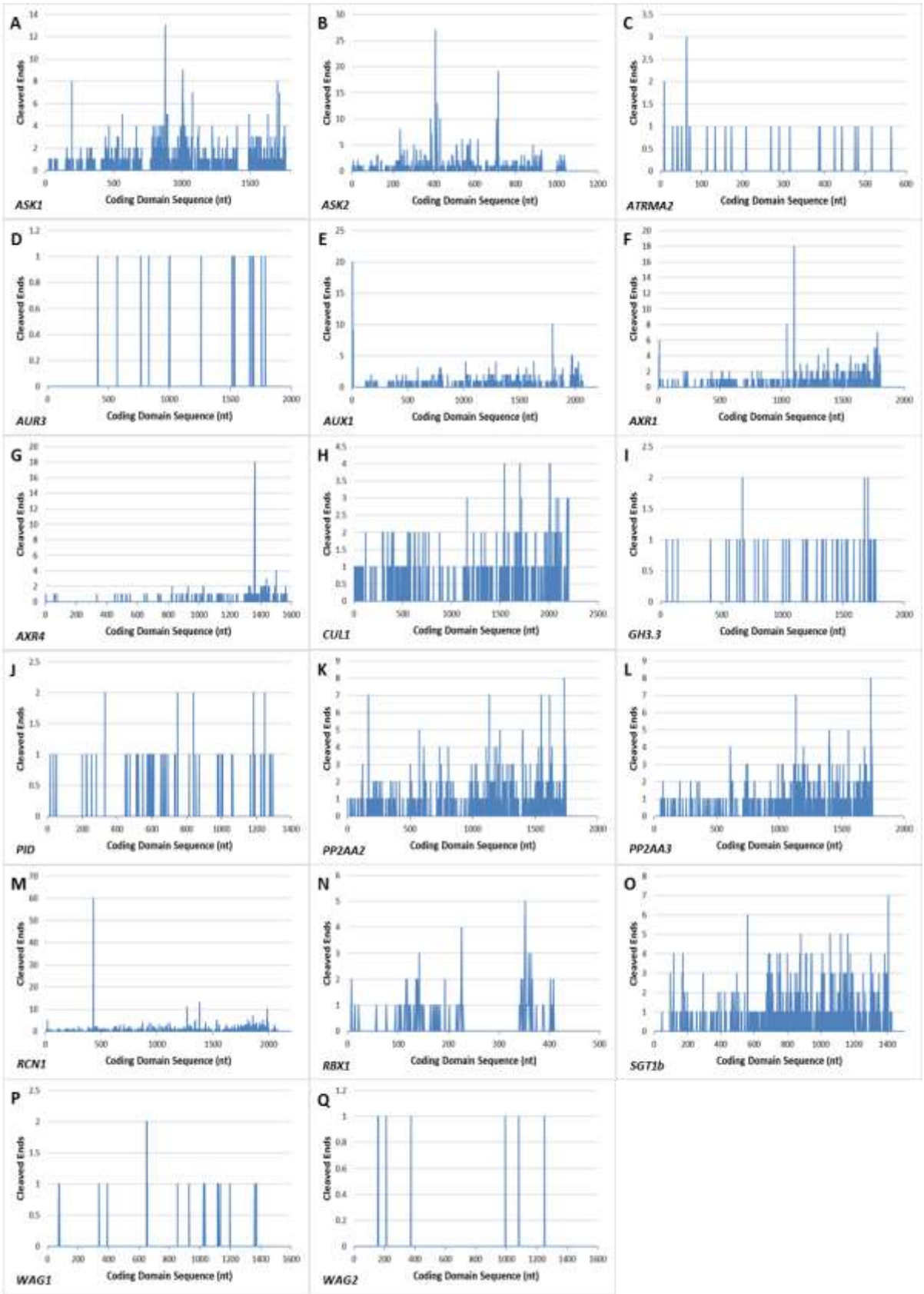

Figure S4.4. Degradome analysis of potential sRNA-targeted auxin responsive gene transcripts. Col-0 (blue) coding domain sequences of auxin responsive genes *ASK1* (A), *ASK2* (B), *ATRMA2* (C), *AUR3* (D), *AUX1* (E), *AXR1* (F), *AXR4* (G), *CUL1* (H), *GH3.3* (I), *PID* (J), *PP2AA2* (K), *PP2AA3* (L), *RCN1* (M), *RBX1* (N), *SGT1b* (O), *WAG1*, (P), and *WAG2* (Q), were analysed in floral tissue for degradome cleaved end products, these analyses are in addition to those presented in **Figure 3.1**.

Appendix 5 – sRNA Sequence Alignment Analyses

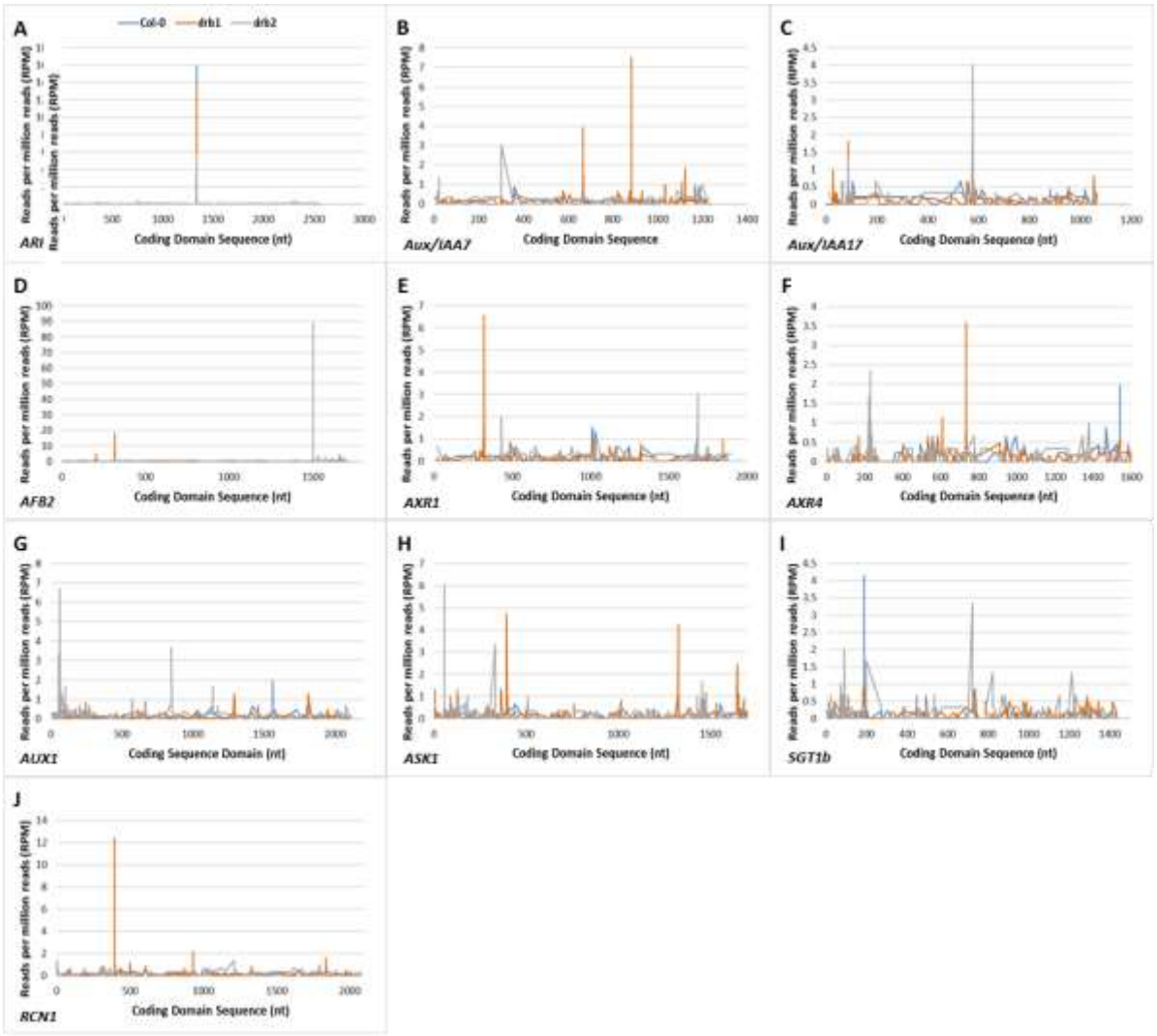

Figure S5.1. sRNA mapping analysis of potential sRNA-targeted auxin responsive gene transcripts. Coding domain sequences of auxin responsive genes *ARF2* (A)*, Aux/IAA7* (B), *Aux/IAA17* (C), *AFB2* (D), *AXR1* (E), *AXR4* (F), *AUX1* (G), *ASK1* (H), *SGT1b* (I), and *RCN1* (J) were mapped against the three available sRNA libraries from Col-0 (blue), *drb1* (orange), and *drb2* (grey) floral tissue. Peaks indicate proportion of sRNA sequence identities mapping to complementary target transcript sequences, with the sRNA cleavage position at the transcript nucleotide shown. These analyses are in addition to those presented in **Figure 3.2**.

Appendix 6 – T1 phenotypes of the expression m*ARF10*, m*ARF16*, and *MIR160B* transgenes in Col-0, *drb1*, and *drb2*

Agrobacterium-mediated transformation of Col-0, *drb1*, and *drb2* plants with the m*ARF10*, m*ARF16*, and *MIR160B* transgenes was performed in this study. T_3 generation plants were used for the final analysis, however, phenotypic and genotypic assessment of the putative transformants was necessary before the final phenotypic and molecular analysis could be undertaken. To this end, the phenotypes of Col-0, *drb1*, and *drb2* plants potentially expressing the m*ARF10*, m*ARF16*, and *MIR160B* transgenes is documented here. Resulting phenotypes were given a score of 1-3, with 1 being mild and 3 being severe, based on the number of phenotypic abnormalities observed throughout the development of these plants, the degree to which these phenotypic modifications were displayed was also accounted for in this scoring system.

Figure S6.1. Phenotypes of T1 Col-0/m*ARF10* plants. The m*ARF10* transgene was introduced into Col-0 plants, T_0, via standard *Agrobacterium*-mediated transformation. Putative Col-0/m*ARF10* transformants were numbered arbitrarily 1-30 (A-AD) for progeny tracking. Col-0/m*ARF10* putative transformants were scored, 1-3 (lower right), based on severity of displayed phenotypes.

Figure S6.2. Phenotypes of T1 Col-0/m*ARF16* plants. The m*ARF16* transgene was introduced into Col-0 plants, T_0, via standard *Agrobacterium*-mediated transformation. Putative Col-0/m*ARF16* transformants were numbered arbitrarily 1-20 (A-T) for progeny tracking. Col-0/m*ARF16* putative transformants were scored, 1-3 (lower right), based on severity of displayed phenotypes.

Figure S6.3. Phenotypes of T1 Col-0/*MIR160B* plants. The *MIR160B* transgene was introduced into Col-0 plants, T_0, via standard *Agrobacterium*-mediated transformation. Putative Col-0/*MIR160B*transformants were numbered arbitrarily 1-20 (A-T) for progeny tracking. Col-0/*MIR160B* putative transformants were scored, 1-3 (lower right), based on severity of displayed phenotypes.

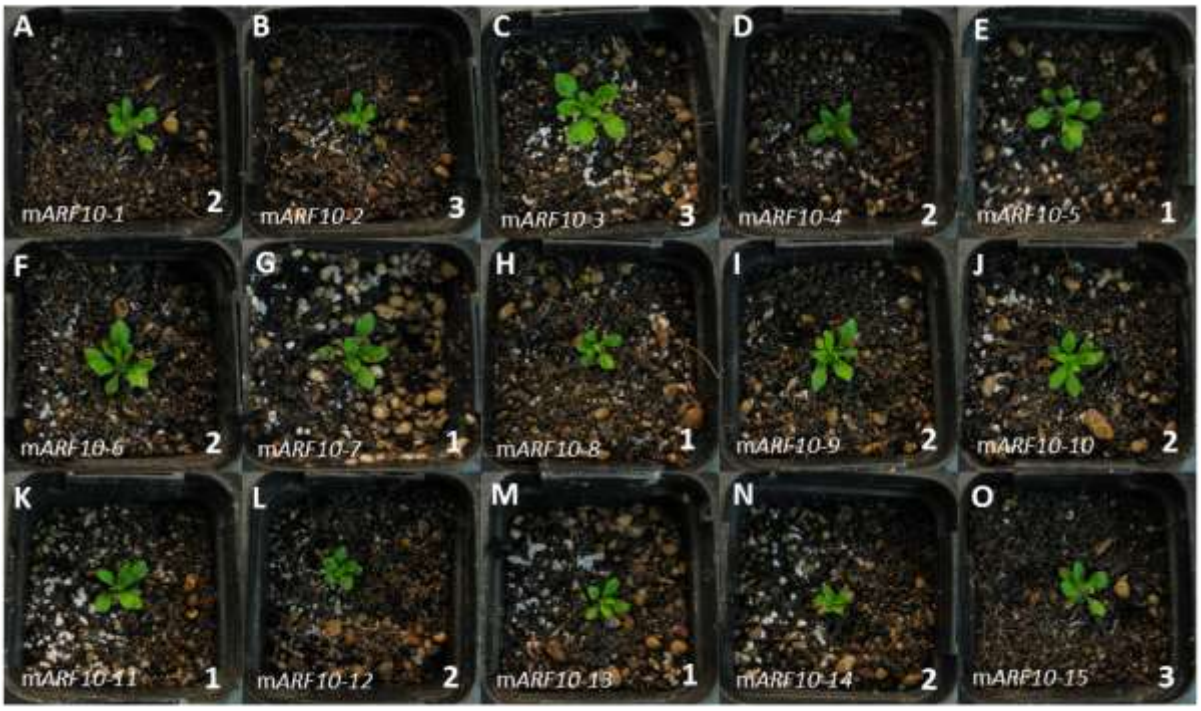

Figure S6.4. Phenotypes of T1 *drb1*/m*ARF10* plants. The m*ARF10* transgene was introduced into *drb1* plants, T_0, via standard *Agrobacterium*-mediated transformation. Putative *drb1*/m*ARF10* transformants were numbered arbitrarily 1-15 (A-O) for progeny tracking. *drb1*/m*ARF10* putative transformants were scored, 1-3 (lower right), based on severity of displayed phenotypes.

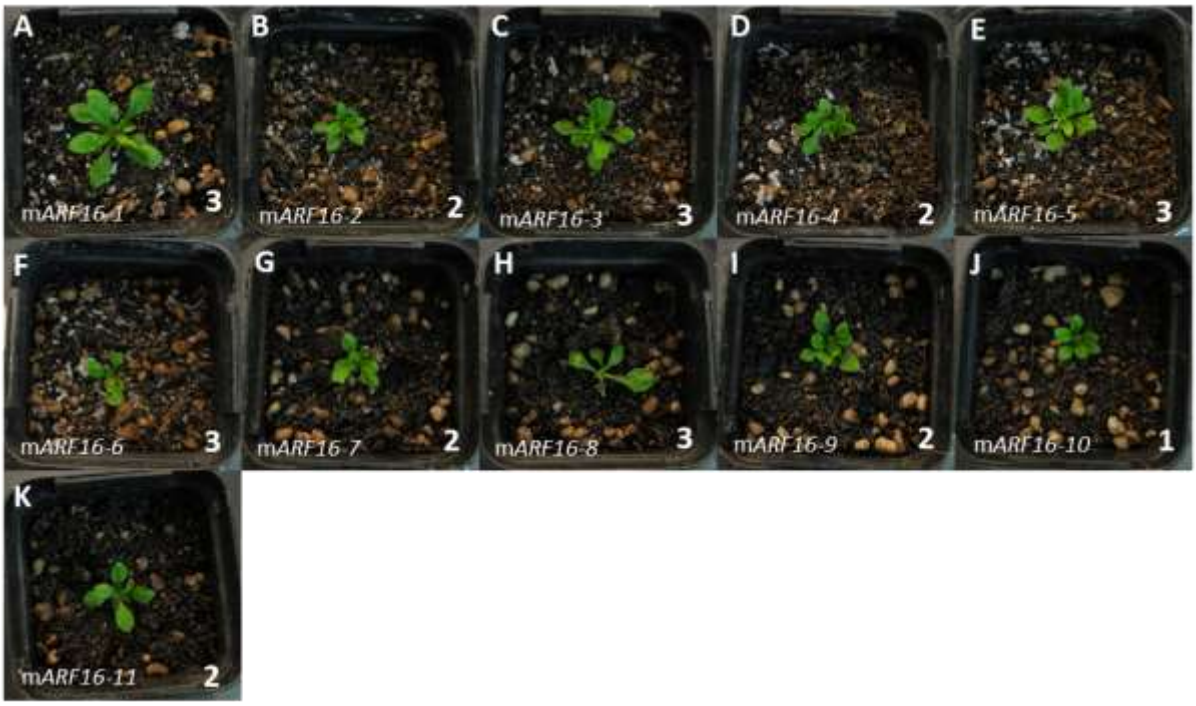

Figure S6.5. Phenotypes of T1 *drb1*/m*ARF16* plants. The m*ARF16* transgene was introduced into *drb1* plants, T_0, via standard *Agrobacterium*-mediated transformation. Putative *drb1*/m*ARF16* transformants were numbered arbitrarily 1-11 (A-K) for progeny tracking. *drb1*/m*ARF16* putative transformants were scored, 1-3 (lower right), based on severity of displayed phenotypes.

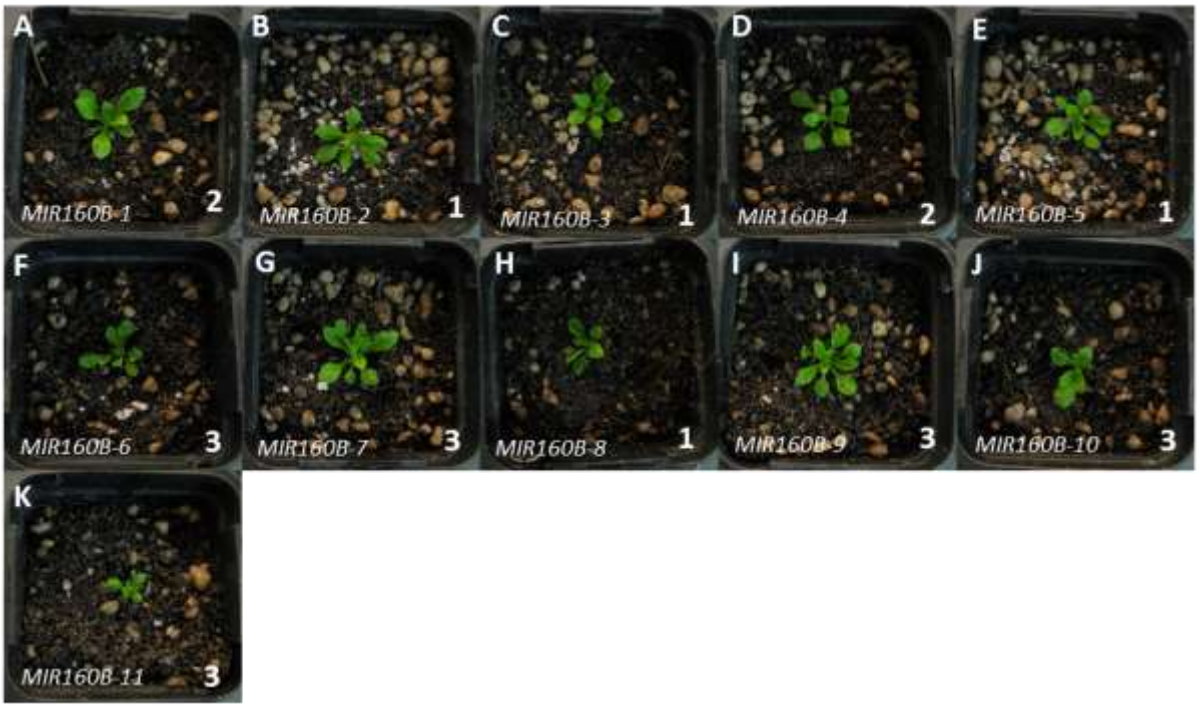

Figure S6.6. Phenotypes of T1 *drb1*/*MIR160B* plants. The *MIR160B* transgene was introduced into *drb1* plants, T_0, via standard *Agrobacterium*-mediated transformation. Putative *drb1*/*MIR160B* transformants were numbered arbitrarily 1-11 (A-K) for progeny tracking. *drb1*/*MIR160B* putative transformants were scored, 1-3 (lower right), based on severity of displayed phenotypes.

Figure S6.7. Phenotypes of T1 *drb2*/m*ARF10* plants. The m*ARF10* transgene was introduced into *drb2* plants, T_0, via standard *Agrobacterium*-mediated transformation. Putative *drb2*/m*ARF10* transformants were numbered arbitrarily 1-10 (A-J) for progeny tracking. *drb2*/m*ARF10* putative transformants were scored, 1-3 (lower right), based on severity of displayed phenotypes.

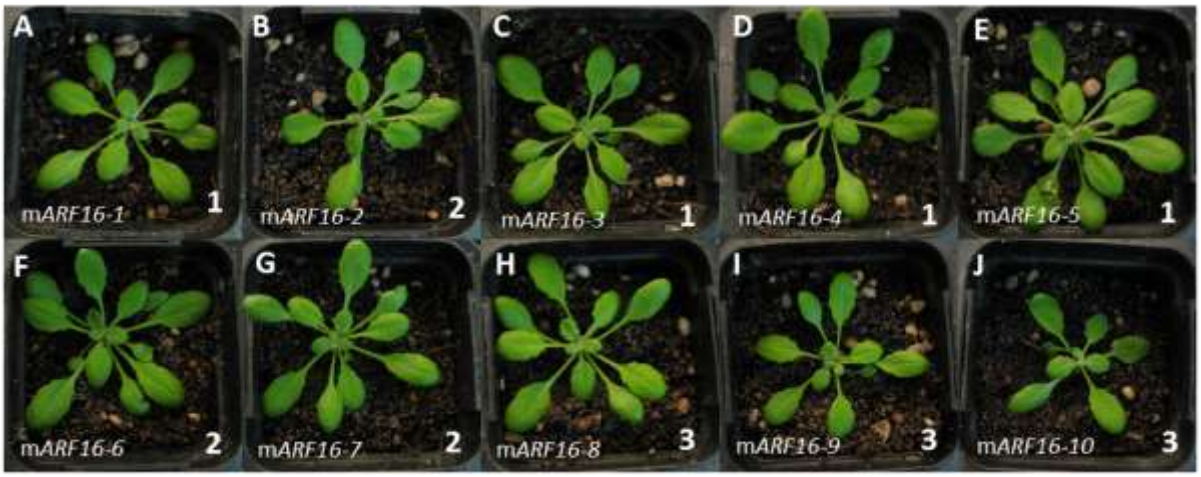

Figure S6.8. Phenotypes of T1 *drb2*/m*ARF16* plants. The m*ARF16* transgene was introduced into *drb2* plants, T_0, via standard *Agrobacterium*-mediated transformation. Putative *drb2*/m*ARF16* transformants were numbered arbitrarily 1-10 (A-J) for progeny tracking. *drb2*/m*ARF16* putative transformants were scored, 1-3 (lower right), based on severity of displayed phenotypes.

Figure S6.9. Phenotypes of T1 *drb2*/*MIR160B* plants. The *MIR160B* transgene was introduced into *drb2* plants, T_0, via standard *Agrobacterium*-mediated transformation. Putative *drb2*/*MIR160B* transformants were numbered arbitrarily 1-12 (A-L) for progeny tracking. *drb2*/*MIR160B* putative transformants were scored, 1-3 (lower right), based on severity of displayed phenotypes.

Several plants displaying mild, intermediate, and severe phenotypes were selected for each background/transgene combination for propagation into the T_2 generation (**Appendix 7**).

Appendix 7 – T2 phenotypes of the expression m*ARF10*, m*ARF16*, and *MIR160B* transgenes in Col-0, *drb1*, and *drb2*

Progeny of T_1 Col-0, *drb1*, and *drb2* transformed with the m*ARF10*, m*ARF16*, and *MIR160B* transgenes selected for prorogation into T_2 are presented here. As with T_1, T_2 transformants have been given a score representing the phenotype displayed by these plants. This score represents the extent and severity of displayed phenotypic abnormalities compared with untransformed plants of the same genetic background. Additionally, the phenotypic score in the T_2 represents penetrance of the phenotype displayed by the T_1 progenitor.

Figure S7.1. Phenotypes of T2 Col-0/m*ARF10* plants. The progeny of putative Col-0/m*ARF10* transformants Col-0/m*ARF10-3-4* (A), Col-0/m*ARF10-17-1* (B), Col-0/m*ARF10-17-2* (C), Col-0/m*ARF10-17-3* (D), and Col-0/m*ARF10-21-1* (E) were scored, 1-3 (lower right), based on penetrance and severity of displayed phenotypes.

Figure S7.2. Phenotypes of T2 Col-0/m*ARF16* plants. The progeny of putative Col-0/m*ARF16* transformants Col-0/m*ARF16-5-1* (A), Col-0/m*ARF16-5-1* (B), Col-0/m*ARF16-5-3* (C), Col-0/m*ARF16-5-4* (D), Col-0/m*ARF16-5-5* (E), Col-0/m*ARF16-11-2* (F), Col-0/m*ARF16-11-5* (G), Col-0/m*ARF16-11-7* (H), Col-0/m*ARF16-11-8* (I), and Col-0/m*ARF16-19-1* (J) were scored, 1-3 (lower right), based on penetrance and severity of displayed phenotypes.

Figure S7.3. Phenotypes of T2 Col-0/*MIR160B* plants. The progeny of putative Col-0/*MIR160B* transformants Col-0/*MIR160B-11-1* (A), Col-0/*MIR160B-15-1* (B), Col-0/*MIR160B-15-2* (C), Col-0/*MIR160B-15-3* (D), and Col-0/*MIR160B-19-1* (E) were scored, 1-3 (lower right), based on penetrance and severity of displayed phenotypes.

Figure S7.4. Phenotypes of T2 *drb1*/m*ARF10* plants. The progeny of putative *drb1*/m*ARF10* transformants *drb1*/m*ARF10-3-1* (A), *drb1*/m*ARF10-3-2* (B), *drb1*/m*ARF10-3-3* (C), *drb1*/m*ARF10-8-1* (D), *drb1*/m*ARF10-12-1* (E), *drb1*/m*ARF10-12-2* (F), and *drb1*/m*ARF10-12-3* (G) were scored, 1-3 (lower right), based on penetrance and severity of displayed phenotypes.

Figure S7.5. Phenotypes of T2 *drb1*/m*ARF16* plants. The progeny of putative *drb1*/m*ARF16* transformants *drb1*/m*ARF16-4-1* (A), *drb1*/m*ARF16-4-2* (B), *drb1*/m*ARF16-4-3* (C), *drb1*/m*ARF16-4-4* (D), *drb1*/m*ARF16-7-1* (E), *drb1*/m*ARF16-7-2* (F), and *drb1*/m*ARF16-11-5* (G) were scored, 1-3 (lower right), based on penetrance and severity of displayed phenotypes.

Figure S7.6. Phenotypes of T2 *drb1*/*MIR160B* plants. The progeny of putative *drb1*/*MIR160B* transformants *drb1*/*MIR160B-7-1* (A), *drb1*/*MIR160B-7-2* (B), *drb1*/*MIR160B-7-3* (C), *drb1*/*MIR160B-9-4* (D), and *drb1*/*MIR160B-10-2* (E) were scored, 1-3 (lower right), based on penetrance and severity of displayed phenotypes.

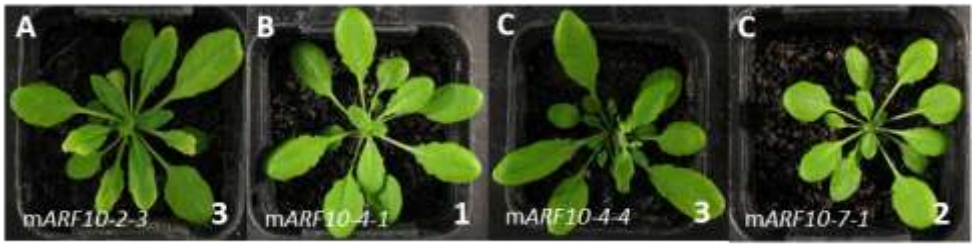

Figure S7.7. Phenotypes of T2 *drb2*/m*ARF10* plants. The progeny of putative *drb2*/m*ARF10* transformants *drb2*/m*ARF10-2-3* (A), *drb2*/m*ARF10-4-1* (B), *drb2*/m*ARF10-4-4* (C), and *drb2*/m*ARF10-7-1* (D) were scored, 1-3 (lower right), based on penetrance and severity of displayed phenotypes.

Figure S7.8. Phenotypes of T2 *drb2*/m*ARF16* plants. The progeny of putative *drb2*/m*ARF16* transformants *drb2*/m*ARF16-1-1* (A), *drb2*/m*ARF16-3-1* (B), *drb2*/m*ARF16-3-3* (C), *drb2*/m*ARF16-3-4* (D), *drb1*/m*ARF16-5-1* (E), *drb2*/m*ARF16-5-4* (F), *drb2*/m*ARF16-6-1* (G), *drb2*/m*ARF16-6-2* (H), *drb2*/m*ARF16-10-1* (I), and *drb2*/m*ARF16-10-2* (J) were scored, 1-3 (lower right), based on penetrance and severity of displayed phenotypes.

Figure S7.9. Phenotypes of T2 *drb2*/*MIR160B* plants. The progeny of putative *drb2*/*MIR160B6* transformants *drb2*/*MIR160B-2-1* (A), *drb2*/*MIR160B-2-2* (B), *drb2*/*MIR160B-3-2* (C), *drb2*/*MIR160B-8-2* (D), and *drb2*/*MIR160B-11-1* (E) were scored, 1-3 (lower right), based on penetrance and severity of displayed phenotypes.

Three representative plants, which the displayed the greatest degree of phenotype penetrance and severity across both the T_1 and T_2 generations from each background/transgene combination, were selected for propagation into the T_3 generation. T_3 plants were genotyped before molecular analysis was performed (**Appendix 8**).

Appendix 8 – Col-0, *drb1*, and *drb2 -mARF10*, *-mARF16*, and *PRI-MIR160B-OE* Genotyping

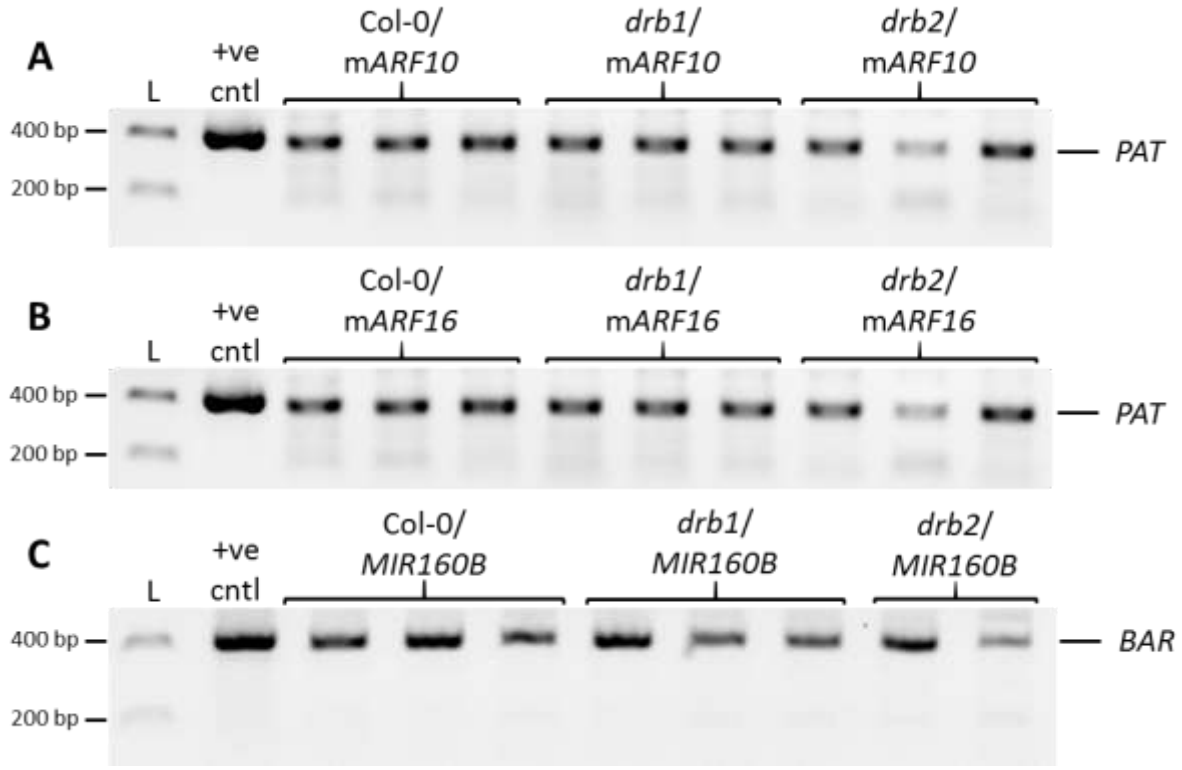

Figure S8.1. Genotyping PCR confirming expression of the m*ARF10*, m*ARF16*, and *MIR160B* transgenes in Col-0, *drb1*, and *drb2* backgrounds. PCR analysis was conducted to determine the expression of the m*ARF10*, m*ARF16*, and *MIR160B* transgenes in Col-0, *drb1*, *drb2* plants, with three biological replicates per transgene per background. Primers for the *PHOSPHINOTHRICIN ACETYLTRANSFERASE* (*PAT*) were used to assess the expression of the m*ARF10* (A) and m*ARF16* (B) transgenes. Primers for the *BASTA* (*BAR*) gene were used to assess the expression of the *MIR160B* (C) transgenes. Empty pORE1 (A and B) and pBART (C) were used as positive (+ve) controls (cntl).